The Climate Change Impact on Power Grid Transmission Capacity

Sergio Montaña Salas

PSL UNIVERSITÉ PARIS

THÈSE DE DOCTORAT
DE L'UNIVERSITÉ PSL

Préparée à Mines Paris - PSL

The Climate Change Impact on Power Grid Transmission Capacity

L'impact du changement climatique sur la capacité de transport des réseaux électriques

Soutenue par

Sergio Montaña-Salas

Le 12 Decembre 2025

École doctorale n°621

Ingénierie des Systèmes, Matériaux, Mécanique, Energétique

Spécialité

Energétique et procédés

Composition du jury :

Robin GIRARD Full Professor Mines Paris-PSL	*Président du jury* *Examinateur*
Fabrizio PILO Full Professor & Vice-Rector for Territory University of Cagliari	Rapporteur
Zita VALE Full Professor & Director of Research Polytechnic of Porto ISEP, GECAD	Rapporteuse
Lyons PADRAIG Director of Research International Energy Research	*Examinateur*
Valentina SESSA Associate Professor Mines Paris-PSL	*Examinatrice*
Andrea MICHIORRI Professor & Research Mines Paris-PSL	*Directeur de thèse*

MINES PARIS | PSL

Remerciements

Firstly, I would like to thank my supervisor, Andrea Michiorri, whose extensive knowledge, constant support, and guidance ensured that this research continually evolved.

The love and support of my wife and daughter made the development of my thesis even more exciting. To my father and sister, who were always close despite the distance, and without whom I would not have come this far.

I am very grateful to all my colleagues, my office mates, and, of course, all the researchers at the school and other European universities who collaborated. Without all of them, this thesis would not have been possible.

Contents

Remerciements i

List of Figures v

List of Tables ix

List of Symbols xiv

Definitions xv

Acronyms xvii

1 Introduction 1
- 1.1 Context . . . 2
- 1.2 Chapter Outline . . . 5
- 1.3 State of the Art . . . 6
  - 1.3.1 Weather impacts on Power System Network Component . . . 6
  - 1.3.2 Heat Transfer in Network Power Systems Components . . . 6
  - 1.3.3 Network Planning . . . 16
  - 1.3.4 Aging . . . 18
  - 1.3.5 Climate Projection Models . . . 19
- 1.4 Motivation and Challenges . . . 22
- 1.5 Contributions and Structure of the Thesis . . . 24
- 1.6 List of publications . . . 26
- 1.7 Outline of the Thesis . . . 28

2 Long-Term Thermal Rating 29
- 2.1 Introduction . . . 30
- 2.2 Methodology . . . 31
  - 2.2.1 Thermal Models Methodologies . . . 32
  - 2.2.2 Quasi-Dynamic Thermal Ratings . . . 44
  - 2.2.3 Databases and Data Overview . . . 49
- 2.3 Results . . . 50
  - 2.3.1 qDTR: Analyzed at the component level . . . 50
  - 2.3.2 quasi-Dynamic Thermal Rating (qDTR): Analyzed at the Regional Level 56
- 2.4 Conclusion . . . 59
- 2.5 Limitations . . . 61

3 Network Planning with Probabilistic Long-Term Thermal Ratings 63

3.1 Introduction . . . 64
3.2 Methodology . . . 65
3.3 Network Expansion Planning . . . 66
3.3.1 Transmission Expansion Planning . . . 68
3.3.2 Optimal Power Flow . . . 70
3.3.3 Transmission Expansion Planning influenced by the Climate . . . 72
3.4 Risk Management with Quasi Dynamic Thermal Ratings . . . 76
3.4.1 qDTR Risk Management Under Climatic Scenarios . . . 78
3.5 Aging Evaluation . . . 85
3.5.1 Aging Modelling . . . 85
3.6 Databases and Data Overview . . . 87
3.7 Results . . . 88
3.7.1 Network Planning under qDTR with Fixed-Probability Constraints . . . 90
3.7.2 Regional Power System Expansion Under Climate Influence: Integrating Generation, Demand, and Transmission Capacity . . . 95
3.7.3 IEEE 24-bus reliability test system Transmission Expansion Plan . . . 103
3.7.4 Network Planning with Stochastic Risk-Aware . . . 110
3.8 Conclusion . . . 120
3.9 Limitations . . . 123

4 Impact of climate change on transmission systems 125
4.1 Introduction . . . 126
4.2 Methodology . . . 128
4.3 Impact of climate change on transmission systems . . . 129
4.3.1 Integrating qDTR and Climate Models in Transmission Planning . . . 130
4.4 Databases and Data Overview . . . 132
4.5 Results . . . 133
4.5.1 Impact of climate change on network transmission capacity . . . 133
4.5.2 Impact of climate change on network costs . . . 138
4.6 Conclusion . . . 152
4.7 Limitations . . . 155

5 Findings, Discussion and Perspectives 156
5.1 Conclusions . . . 156
5.2 Methodological Contributions . . . 156
5.2.1 Integrating qDTR into Network Planning . . . 158
5.3 Summary of Research Contributions Across Chapters and Case Studies . . . 159
5.3.1 Long-Term Thermal Rating Method . . . 159
5.3.2 Integration of Thermal Ratings into Network Planning: . . . 160
5.3.3 Impact of Climate Change on Transmission Capacity and Economics: . . . 161
5.4 Broader Implications and Future Directions . . . 164

A Annex A : Mathematical Formulation of Thermal Models 166
A.1 Overhead Lines . . . 166
A.1.1 Parameters . . . 166
A.1.2 Heat Solar Power Gain . . . 167
A.1.3 Radiative Power Loss . . . 167
A.1.4 Convective Power Loss . . . 167
A.1.5 DC Current Calculation . . . 168
A.2 Power Transformers . . . 168

A.2.1 Parameters . . . 168
A.2.2 Power Loss Calculations . . . 169
A.2.3 Temperature Correction Factors [127] . . . 169
A.2.4 Newton's Method for Transformer Loading Factor . . . 169
A.2.5 Transformer Rated Power and Current . . . 170
A.3 Underground Lines . . . 170
A.3.1 Parameters . . . 170
A.3.2 Thermal Resistance Calculation . . . 171
A.3.3 Thermal Model Equations . . . 172
A.3.4 Electrical Resistance Calculation . . . 172
A.3.5 Dielectric Losses . . . 172
A.3.6 Current Calculation Using IEC 60287 . . . 172

B Annex B : Power System Components Description 173
B.1 Power System Components Parameters . . . 173
B.1.1 Paper B . . . 173
B.1.2 Paper A . . . 174
B.2 Demand Projections by Trajectory [180] . . . 174
B.3 Installed capacity projections by Trajectory [180] . . . 174
B.4 Published Papers: Paper A . . . 175
B.5 Published Papers: Paper B . . . 202
B.6 Submitted Papers: Paper G . . . 232
B.7 Published Papers: Conference A . . . 256
B.8 Published Papers: Conference B . . . 261

Bibliography 266

List of Figures

1.1 Projected Long-term Changes in Global Temperature and Radiative Forcing, referred to the Representative Concentration Pathways (RCP) 1850-2300, from [11]. Higher Representative Concentration Pathways (RCP) scenarios correspond to stronger warming pathways, directly impacting thermal ratings. 2
1.2 Comparison of dynamic capacity versus Static Thermal Rating (STR) over time for a Overhead Lines (OHL) line: the shaded risk area highlights periods where dynamic capacity falls below the STR, indicating potential component risk under adverse thermal conditions. Derived from [23] 4
1.3 The relationship between climate change and transmission power system planning 4
1.4 Map of the Transmission System Network in Europe [28] 7
1.5 Rating categorization related to temperature limits. Derived from [58] 11
1.6 Thermal Rating Methodologies adapted from [10] 12
1.7 Overview of Dynamic Thermal Line Rating Concept. Derived and modified from [57] 13
1.8 Quasi Dynamic Thermal Rating Method. From [79] 15
1.9 Graphical abstract of the thesis. For each contribution, the corresponding research questions are listed. 25
1.10 Graphical structure of the thesis illustrating the mapping of research questions across domains. 28

2.1 Heat Transfer Process for Overhead Lines. Based on and extended from [29] . . . 33
2.2 Overhead conductor 225 kV line - Lingostiere - Roumoules - Valderoure. From [115] 34
2.3 Heat Transfer Process for Underground Cable (UGL)s 35
2.4 Data processed from the International Soil Moisture Network 41
2.5 Performance Comparison of Machine Learning Models for Soil Moisture Estimation 42
2.6 Thermal model of oil-to-air heat transfer. Based and Derived from [126] 43
2.7 Annual Comparison of Rating Methodologies for the OHL - 225 kV line - Lingostiere - Roumoules - Valderoure [115], also analyzed in Fig. 2.2. Here, the Dynamic Thermal Rating (DTR) represent the ampacity of the component, during the evaluated period and using the thermal model described in Section 2.2.1.1. 45
2.8 Details the four-step process of qDTR, using the OHL evaluated is a 225 kV line - Lingostiere - Roumoules - Valderoure [115] as an example, also analyzed in Fig. 2.2 47
2.9 Evaluation of qDTR temporal resolutions selection strategies compared to DTR in year 2003, calculated at annual, day/night, and month/hour time scales, and using historical meteorological data described in Table 2.3. 51

2.10 Performance Steady State Thermal Model evaluated in Long-term Horizon, evaluated on a 400/225kV 1190 MVA Oil-immersed Power Transformer (PT) at a node in southern France. 52
2.11 Performance of qDTR in the PT evaluated in Long-term Horizon vs Seasonal traditional ratings, for a 400/225kV 1190 MVA PT at a node in southern France. 53
2.12 Daily time series of estimated soil moisture with (a) XGBoost at Soil 5 and (b) LASSO (green) at Soil 2 compared to $ERA5$ data (red) and test values (black dashed). 54
2.13 Assessment of qDTR ($X_R = 0.1\%$) Performance Across Extended temporal resolutions, Seasonal, Monthly, and Annual Applied to the UGL Specified in Annex B 55
2.14 qDTR calculated for each month/hour combination for OHL, PT, and UGL calculated in the node of Tavel (southeast France). Colours represent months from the coldest (blue) to the warmest (red). A dashed black line represents STR . . . 56
2.15 Geographical distribution of the mean qDTR difference at the country level over fifty years for the historical reference. The analysis is performed for the main power components: OHL, PT, and UGL, and illustrates the difference in the variation of the historical average for each region. 57
2.16 Percentage difference between $\text{qDTR}_{\text{month/hour}}$ and $\text{qDTR}_{\text{yearly}}$ in some European countries for: (a) PT, (b) OHL, (c) UGL 58

3.1 Functional block structure of a typical network planning methodology, adapted from [132]. 67
3.2 Thermal-electric linkage between Direct Current Optimal Power Flow (DCOPF) and Thermal Ratings 71
3.3 Illustration of temperature risk assessment for an OHL conductor. Subfigure (a) shows meteorological parameter distributions with lower quantiles in red; (b)–(c) show scatter plots highlighting the combined effect of wind and solar radiation; (d) presents the rating probability density with the lower capacity threshold (red dashed lines). 77
3.4 Temporal Risk Assessment Analysis for a component, showing the risk area caused when the power flow exceeds the component capacity 78
3.5 Temporal Risk (red zone) Assessment Analysis for the Line 27 of of the test network [145], where is represented the steady-state (80 C°) and contingency ratings (95)C° 79
3.6 Overview Thermal Risk Management into long-term transmission expansion planning 80
3.7 Temporal Risk Assessment Analysis for a component, showing the risk area caused when the power flow exceeds the component capacity, mainly limited by the maximum temperature and the low probability rating selected by the operator. . 81
3.8 kernel density estimates (KDE) estimation for a line. Power flow and conductor temperature, incorporating congestion probabilities 82
3.9 Visual representation of the procedure, the integration of the qDTR methodology is highlighted in yellow 90
3.10 Rating Difference on transmission capacity in European Transmission, the difference in capacity for qDTR (Percentage Change $\Delta_{\%} \frac{qDTR_{Month/Hour}}{qDTR_{year}}$) in June at 14 h for Summer and October at 22 h for Winter 91
3.11 Visual representation of the procedure, the integration of the Generation, Demand, and Ratings Approach influenced by the climate, is highlighted in yellow. 96

3.12 Overview of Spatial and Temporal Demand: Regional Mapping and Demand Profiles . . . 98
3.13 Demand Projection performance . . . 101
3.14 Temporal Resolution Analysis of qDTR: month/hour vs year $\frac{qDTR_{year}-qDTR_{hour}}{qDTR_{year}}$ Impacts on Generation Expansion and Transmission . . . 102
3.15 Visual representation of the transmission expansion procedure. . . . 103
3.16 MMDA Selection Days Results Example . . . 106
3.18 Comparison of generation production and network investment requirements under two planning scenarios. . . . 108
3.19 Visual representation of the procedure for risk-aware transmission planning. . . . 110
3.20 Scenario input flowchart showing historical demand and RES profiles . . . 111
3.21 IEEE RTS 24-Bus Test System Overview: 11 existing conventional units, 17 loads, 38 existing lines with 32 candidates and new Renewable Energy Sources (RES) Power Plants . . . 113
3.22 Cumulative Distribution Function (CDF) of Line 22 rating as a function of X_R, evaluated across multiple temporal resolution, using historical climate datasets. The curves illustrate how rating estimates vary with increasing X_R, highlighting the influence of temporal resolution on thermal rating assessments. The dashed green line represents the standard rating with STR for comparison. . . . 114
3.23 Flowchart of overload risk assessment using Monte Carlo with out-of-sample as the outcome evaluation method . . . 115
3.24 KDE estimation for the Line 26. Power flow and conductor temperature during the fourth epoch in yearly time resolution, incorporating congestion probabilities 116
3.25 Power flow in Line 18 using Historical information . . . 117
3.26 Power flow in Line 22 using Historical information . . . 118
3.27 Power flow in Line 32 using Historical information . . . 118

4.1 Climate Change: RCP Scenarios Consequences. Updated from [181] . . . 127
4.2 Changes in the distribution of daily mean air and soil (1.8 mts) temperature in Sardinia over the decades (from 1970 to 2010), based on the reanalysis. The curves illustrate a progressive shift towards higher mean temperatures over time. The shaded color areas represent thresholds for cold, warm, and extreme events, defined using the percentile limits from [2] and calculated on the last period 2010-2020 as a reference. . . . 129
4.3 Conceptual Framework Linking qDTR and Climate Modeling for Enhanced Transmission Planning . . . 130
4.4 Geographical distribution of the mean qDTR difference at the country level over fifty years for the RCPs and the historical. This is performed for the main power components (OHL - PT and UGC), described in Tables B.1,B.2, B.3. The first row reflects the difference in the variation of the historical average for the region, and the subsequent rows illustrate the variation in the average for each RCP. . . . 135
4.5 Difference in the calculated $qDTR_{month/hour}$ between historical values and RCP projections 2.6, 4.5, 8.5. Performed for (OHL - PT, and UGL) in a node located in Tavel, southeast France. . . . 136
4.6 Geographical distribution of annual $qDTR_{8.5}$ across France for Cable 2. The second panel shows the yearly evolution of $qDTR_{week}$ for historical $qDTR_{H}$ and projected $qDTR_{RCP}$ in the Île-de-France region. The red zone indicates overload risk if $qDTR_{RCP\text{-}year}$ is applied. This figure is reproduced from **Paper A**. . . . 138

4.7 Climate impacts on transmission capacity, the difference in capacity for qDTR (Percentage Change $\Delta_{\%} \frac{qDTR_{RCP}}{qDTR_H}$) for summer day (June) at 14 h RCP 2,6, 4.5 and 8.5 scenarios for OHL. This figure is reproduced from **Paper B**. 139
4.8 Visual representation of the procedure, mainly showing the inclusion of different climate scenarios and risk assessment. 143
4.9 Scenario input flow diagram for network planning: Integrating RCP-based demand projections, renewable energy generation, and transmission capacity 145
4.10 Power flow in Line 12: Heatmap of $|P_f|$ normalized by the thermal limit with $qDTR_{year,RCP}$. The results indicates. 146
4.11 Power flow in Line 22: Heatmap of $|P_f|$ normalized by the thermal limit with $qDTR_{year,RCP}$. The plot a 147
4.12 Power flow in Line 32: Heatmap of $|P_f|$ normalized by the thermal limit with $qDTR_{year,RCP}$. The figure shows no restriction caused by the thermal limit. . . . 148
4.13 Thermal ratings and utilization under historical and RCP 4.5 climate scenario in Line 22. The yellow triangle highlights ratings that fall below historical benchmark areas, indicating that the monthly/hourly performance does not underestimate the associated risk. 150
4.14 Thermal ratings and utilization under historical and RCP 8.5 climate scenario in Line 22. 150

List of Tables

1.1 Static Time Resolution Models. Modified from [60] . . . 16
1.2 Summary of RCPs, based on [111]. The term "representative" emphasises that each RCP is just one of many scenarios leading to a specific radiative forcing, while "pathway" highlights the importance of both concentration levels and the trajectory to reach them. . . . 19
1.3 Classification of literature by thermal rating methodology, risk modelling, and planning horizon relevant to this thesis. . . . 21
1.4 Mapping of Publications to Thesis Contributions and Chapters . . . 26

2.1 Dependency of the rated current versus the thermal resistance T_4. From [8] . . . 36
2.2 Empirical coefficients for estimating thermal conductivity of soil . . . 39
2.3 Data Overview in Long-term Thermal Ratings . . . 49
2.4 Model Performance - Moisture and Temperature evaluated according to the procedure described in subsection. 2.2.1.2 . . . 54

3.1 Input Data Overview for Long-term Transmission Expansion Planning . . . 87
3.2 Capabilities of Selected Open-Source Power System Modeling Tools (Python-Based) 89
3.3 Variation (in %) for Generation and Transmission Expansion Planning (G&TEP) Cases . . . 94
3.4 Case Specifications Parameters . . . 101
3.5 Reduction percentages $\frac{qDTR_{year}-qDTR_{hour}}{qDTR_{year}} \times 100$ by Generation Technology . . . 102
3.6 Results for the two scenarios concerning investment and costs, the scenarios covering historical and projected static $qDTR_{year}$, and $\text{qDTR}_{\text{Hour}}$ . . . 106
3.7 Input Parameters . . . 112
3.8 Geographical coordinates of the 24 buses in southern France . . . 113
3.9 Percentage Change ($\Delta\%$) Across Historical Scenario . . . 119

4.1 Input Data Overview for Long-Term Thermal Ratings and Transmission Expansion Planning under Climate Change . . . 132
4.2 Variation for the three scenarios concerning historical values for qDTR for the European region. . . . 134
4.3 Percentage Change $\Delta_{\%}$) in Seasonal Mean qDTR Capacity Over Fifty Years Under $\text{RCP}_{2.6,\ 4.5,\ 8.5}$ Scenarios (month/hour Resolution) . . . 137
4.4 Variation in system costs . . . 140
4.5 $\Delta_{\%}$ Variation for the three scenarios concerning investment and costs, the scenarios covering historical and projected static (STR), historical (qDTR_{H}), and projected (qDTR_{RCP}). From **Paper A**. . . . 141

4.6 Variation (in %) for the three scenarios concerning yearly fixed rating and costs. In this table the STR is calculated using the $qDTR_{year}$ and RCP with $qDTR_{month/hour}$ 142
4.7 Input Parameters 143
4.8 Comparative Analysis of Climate Scenarios: Operational, Capital, and Economic Impacts. The percentage change is calculated using the formula: $(Scenario_A - Scenario_B)/Scenario_B \times 100$. 148

A.1 Empirical coefficients for estimating thermal conductivity of soil 171

B.1 Overhead Line Characteristic Data 173
B.2 Underground Cable Characteristic Data [184] 173
B.3 Power Transformer Characteristic Data [185] 174
B.4 Underground Cable Characteristic Data Cable 1 [184] 174
B.5 Underground Cable Characteristic Data Cable 2 [186] 174
B.6 Electricity demand projections by trajectory (in TWh), used in the case studies of sections 3.7.4 and 4.5.2. 174
B.7 Installed capacity projections by trajectory and technology (in GW), used in the case studies of sections 3.7.4 and 4.5.2 174

List of Symbols

Chapter 1

Symbol	Description	Units
Q_J	Heat generated from power losses (Joule heating and core losses)	W
$Q_{s/int}$	Environmental heat influence (solar radiation or nearby cables)	W
Q_c	Convective heat exchange with surrounding air (e.g., wind)	W
Q_R	Radiative heat exchange	W
Q_{cd}	Conductive heat exchange	W
θ	Ambient temperature	°C
H_s	Solar radiation intensity	W/m^2
w_s	Wind speed	m/s
Q_{cd}	Conductive heat exchange through soil, depending on soil temperature, moisture, thermal conductivity, and conductor loss factors	W
θ_s	Soil temperature	°K
ψ_s	Soil moisture	m^3/m^3
δ_s	Soil thermal conductivity	$W/(m \cdot K°)$
λ	Conductor loss factor (geometry and material dependent)	-

Chapter 2

Symbol	Description	Units
	Cables	
n_l	Number of conductors in the cable	-
L	Cable burial depth	mm
S_l	Spacing between conductors of the same circuit	mm
R_{UGL}, R_{OHL}	AC resistance per unit length at maximum operating temperature	Ω/m
D^*	External diameter of cable	m
T_1	Thermal resistance of insulation	$K \cdot m/W$
T_2	Thermal resistance of sheath	$K \cdot m/W$

T_3	Thermal resistance of armor	K · m/W
T_4	Thermal resistance of surrounding medium	K · m/W
σ	Surface absorption coefficient	dimensionless
Power Transformers		
x_r	Exponent for oil temperature rise due to total losses	-
R_{ll}	Ratio of load losses to no-load losses at rated conditions	-
K	Load factor (load current / rated current)	pu
θ_o	Top-oil temperature	K
$\Delta\theta_{or}$	Top-oil temperature rise at rated losses	K
$\Delta\theta_h$	Hot-spot gradient rise	K
$\Delta\theta_{hr}$	Hot-spot gradient at rated load	K
θ_h	Hot-spot temperature	K
P_{LL}	Load losses	W
P_{NL}	No-load losses	W
Surrounding Medium		
p_s	Thermal resistivity of soil	K · m/W
H_s	Solar radiation intensity	W/m^2
w_s	Wind speed	m/s
θ	Ambient air temperature	°C
θ_c	Maximum conductor temperature	°C
S_r	Total precipitation	m
Thermal Balance		
Q_M	Magnetic heating losses	W/m
Q_s	Solar heat gains	W/m
Q_i	Corona heat losses	W/m
Q_R	Radiative cooling losses	W/m
Q_E	Evaporative cooling losses	W/m
Soil Moisture and Temperature Model		
$\hat{\theta_s}$	Projected soil temperature vector	°C
Φ_i	Input feature matrix (e.g., θ, H_s)	-
κ	Model coefficient vector (Lasso)	-
$\hat{\psi}_i$	Projected soil moisture for i-th sample	m^3/m^3
ϕ_i	Feature vector for i-th sample	-
f_k	k-th regression tree in XGBoost model	-
$\mathcal{F}$	Space of all possible regression trees	-
K_t	Number of trees in ensemble model	-
quasi Dynamic Thermal Model		
A_f and α	Power Law normalization constant and Scaling parameter	A ,dimensionless
c	the zero-probability offset term	A

Chapter 3: Optimization Planning Model

Symbol	Description	Units
Sets and Indexes		
Ep	Set of planning epochs (expansion periods)	-
$\mathcal{N}$	Set of buses (nodes)	-
T	Set of time periods within a representative year or Horizon	-
$\mathcal{G}$	Set of generating units	unit
RES $\subset \mathcal{G}$	Subset of renewable generators (PV and Wind)	unit
$\mathcal{L}$	Set of existing transmission lines	-
$\mathcal{NL}$	Set of candidate (new) transmission corridors/lines	-
$\text{Max}_{k,l}$	Maximum number of circuits that can be added on corridor l	-
tangents	Number of segments used to linearize quadratic losses	-
$y \in$ Ep	year in the Expanded period (Epoch)	years
$t \in$ T	Time period index	-
$n \in$ N	Bus index	-
$g \in \mathcal{G}$	Generator index	-
$l \in \mathcal{L}$	Line index	-
$k \in_{\{1.\text{Max}_{k,l}\}}$	Parallel line or component index on l	-
Scalars / Weights		
N_y	Number of (representative) years	years
w_t	Time-weighting factor of period t	Hours
Decision Variables		
$P_{g,t,y}$	Active power output of generator unit g at time t in year y	MW
$P_{\text{Ls},n,t,y}$	Load shedding at node n, time t, year y	MW
$P_{\text{Cur},g,t,y}$	Curtailed renewable power of generator g, time t, year y	MW
$P_{l,y,t}$	Active power flow on (existing) line l at time t in year y	MW
$P_{l,y,k,t}$	Active power flow on new parallel k of line l at time t	MW
$P_{\text{loss},l,y,t}$	Active power losses on (existing) line l at time t in year y	MW
$P_{\text{loss},l,y,k,t}$	Active power losses on new parallel k of line l at time t in year y	MW
$\theta_{n,y,t}$, $\theta_{m,y,t}$	Voltage phase angles at the *from*- and *to*-bus of a line, year y, time t	rad
$\theta_{k,y,t}$	Phase-shifting (or tap-induced) angle of circuit/transformer k, year y, time t	rad
$Z_{l,k,y}$	Binary status: 1 if parallel k of line l is build in year y, 0 otherwise	-
$C_{z,l,k,y}$	Binary investment decision: 1 if circuit k of corridor l is *built* in year y	-
$P_{\text{inj},n,t}$	Active net power injection at node n and time t	MW
Network and Electrical Parameters		

$F_{qdtr,l,t}$	Thermal Rating calculated with qDTR of line l at time t	MVA
$F_{qdtr,l,k,t}$	Thermal Rating calculated with qDTR of new parallel k on line l at time t	MVA
x_n	Reactance of transmission line k	Ω
τ_n	Tap ratio (magnitude) of transformer/controlled branch	p.u.
Losses Aproximation		
r_ℓ	Series resistance of line ℓ (used for losses)	Ω
p	Index of tangent point for loss linearization	-
tan	Number of intervals for loss tangents	-
m_p	Slope of tangent at interval p	-
a_p	Offset of loss tangent at interval p	-
$s \in \{-1, 1\}$	Sign index for absolute-value linearization of losses	-
Cost Parameters		
C_g	Generation cost of unit g	€/MWh
Cost_{Ls}	Penalty cost of load shedding	€/MWh
CO2_p	Carbon price for CO_2 emissions	€/tCO_2
Curt_c	Penalty cost for renewable curtailment	€/MWh

Definitions

Climate: From [1], "The average state of the atmosphere during a period of time (weeks, decades, years, or millennia)".

Climate Change: From [2], "A change in the state of the climate that can be identified (e.g., by using statistical tests) by changes in the mean and/or the variability of its properties and that persists for an extended period, typically decades or longer".

Conservative or Worst Case Weather Condition: This refers to the practice of considering extreme or adverse weather conditions when assessing the performance and reliability of power system components. The specific criteria depend on the transmission owner's policies, industry standards, or engineering experience.

Extreme: An event that exceeds or does not reach a threshold close to the highest or lowest range typically observed for that variable.

Loading: From [3], the amount of current which is actually transported by the Power component.

Long-Term Planning From [4], extends beyond 15 years, addressing the comprehensive development of the power system infrastructure, including generation expansion, transmission upgrades, and the integration of emerging technologies to support future demand and decarbonization targets.

Maximum Temperatures: From [3], it's the temperature at loading capacity to prevent damage to insulation or conductor strength, ensuring safe operation and preventing irreversible degradation.

Medium-Term Planning From [4], encompasses a period of 10 to 15 years, assessing strategic adjustments driven by evolving market dynamics, economic conditions, and policy directives, ensuring network adequacy and cost-effective operation.

Network Expansion Planning From [5], is the process of identifying the necessary network infrastructure such as transmission lines, cables, and power transformers to ensure efficient and reliable power transfer from generation resources to load centers. Particularly, this thesis will be limited to a long-term.

Power System Network Components: In this thesis, it is related to Overhead Lines, Power Transformers, and Underground Cables. Sometimes is also referred to as **Power System Component**.

Rating: According to [3], is the maximum current that a power system component can safely carry and it is determined by transmission or utility owners.

Reanalysis: This term refers specifically to the ECMWF ERA5 weather reanalysis dataset, produced by the Copernicus Climate Change Service (C3S) [6].

Risk From [7], it is the product of the probability of a thermal overload and the resulting impact.

Sag: From [7], Thermal expansion due to increased temperature can cause a transmission line to drop below its minimum safety clearance, posing potential safety hazards.

Short Term Planning From [4], spans from a few hours up to three years and involves continuous operational analysis to address urgent energy supply requirements, ensuring system reliability and meeting immediate demand fluctuations.

Thermal Backfill: From [8], materials are specifically placed to surround underground cables, optimizing thermal conductivity and ensuring stable heat dissipation in varying soil conditions.

Transmission Companies: From [9], stakeholders that own transmission infrastructure, including overhead lines, underground cables, power transformers, and reactive compensation equipment. The operation of this infrastructure is carried out in accordance with directives from the independent Transmission System Operator (TSO).

Weather: From [1], 'Condition of the atmosphere at a particular time'.

Acronyms

ACSR Aluminum Conductor Steel Reinforced

CAPEX Capital expenditure

CDF Cumulative Distribution Function

DCOPF Direct Current Optimal Power Flow

DTR Dynamic Thermal Rating

G&TEP Generation and Transmission Expansion Planning

GDP Gross Domestic Product

GHG Greenhouse Gas

HotST Hot Spot Temperature

IPCC Intergovernmental Panel on Climate Change

ISMN International Soil Moisture Network

KDE kernel density estimates

LTER Long-Term Emergency rating

MCS Monte Carlo Simulations

MMDA Modified Maximum Dissimilarity Algorithm

NEP Network Expansion Planning

NUTS Nomenclature of Territorial Units for Statistics

NWP Numerical Weather Prediction

OHL Overhead Lines

OPEX Operational expenditure

OPF Optimal Power Flow

PDF Probability Density Function

PT Oil-immersed Power Transformer

PV Photovoltaic Plant

qDTR quasi-Dynamic Thermal Rating

RCP Representative Concentration Pathways

RES Renewable Energy Sources

SSPs Shared Socioeconomic Pathways

STR Static Thermal Rating

TEP Transmission Expansion Planning

TSO Transmission System Operator

UGL Underground Cable

Chapter 1

Introduction

Résumé en Français

Ce chapitre propose une vue d'ensemble des limites thermiques et de leur intégration dans la planification des systèmes électriques, en mettant l'accent sur les lignes aériennes, les câbles souterrains et les transformateurs de puissance. Il analyse l'influence des conditions météorologiques, de la variabilité climatique et des régimes d'exploitation sur la capacité et le vieillissement des composants. Les principales méthodologies sont présentées, telles que les limites thermiques statiques, saisonnières, en temps réel, dynamiques et quasi-dynamiques, ainsi que les approches probabilistes et déterministes pour la planification à court et à long terme. Le chapitre explore également l'évaluation des risques, le vieillissement des actifs et l'intégration des modèles de projection climatique, en soulignant l'importance des données spatiotemporelles pour une planification résiliente et efficace des réseaux de transport. Enfin, il passe en revue les principales questions de recherche, les défis et les contributions.

1.1 Context

The capacity assessment of *Power System Network Components* is fundamental to the operation and planning of networks [4]. Traditionally, transmission companies and operators have limited this capacity based on thermal limits[1] [10], influenced primarily by heat transfer processes between conservative weather conditions and the thermal losses caused by the current flowing. However, these limits do not always account for the climate's influence on weather factors, such as ambient temperature, soil moisture, and wind speed, which significantly affect the thermal behaviour of transmission power components by influencing their ability to dissipate Joule losses into the surrounding medium. For instance, lower ambient temperatures enhance heat dissipation and increase transmission capacity, while higher temperatures have the opposite effect.

Nevertheless, climate projections point to the emergence of unfavourable conditions (Fig. 1.1). By 2100, global temperatures could rise by 1.5–5°C, coupled with declining precipitation trends [11]. Such changes are expected to have a direct and negative impact on the electricity system [12], particularly by reducing transmission capacity. Failure to account for this variability may result in increased costs, decreased operational efficiency, and missed opportunities to enhance system reliability.

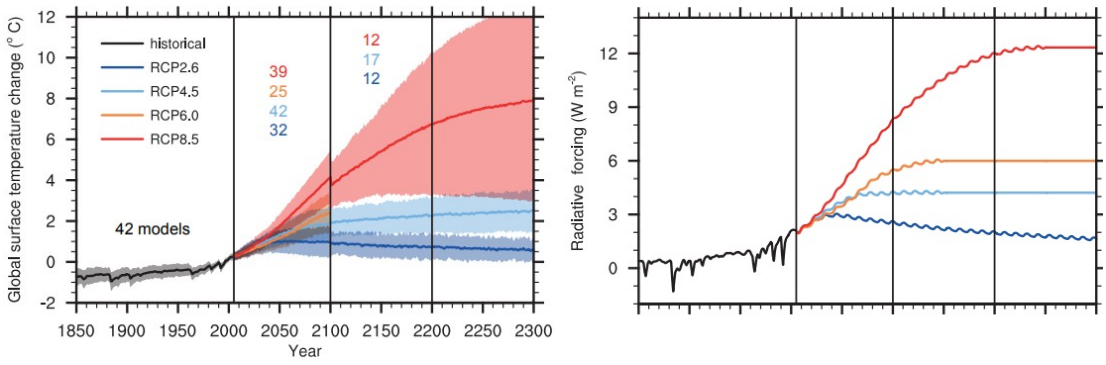

Figure 1.1: Projected Long-term Changes in Global Temperature and Radiative Forcing, referred to the Representative Concentration Pathways (RCP) 1850-2300, from [11]. Higher RCP scenarios correspond to stronger warming pathways, directly impacting thermal ratings.

On the other hand, these unfavourable climatic conditions, particularly elevated temperatures, also affect other sectors of the electricity system [13]. Beyond transmission power components, elevated temperatures also impact generation efficiency and electricity demand. For example, high temperatures reduce thermodynamic cycle efficiency of thermodynamic cycles and lower air density in fossil fuel generators, thereby decreasing their power output [14]. Simultaneously, electricity demand is expected to rise, especially in warmer regions, due to the increased use of air conditioning. Studies estimate that by 2050, peak per-capita electricity demand could increase by up to 9.5% in temperate cities [15], and even reach 21% on extremely

[1] While also subject to system stability and permissible voltage.

hot days in locations such as California [16], placing further stresses on the transmission power component. In response to and to mitigate these impacts, several climate policies have been implemented across Europe, with a clear focus on the electricity sector [17]. These strategies aim to accelerate the expansion of Renewable Energy Sources (RES) and facilitate the integration of electric vehicle charging stations [18].

However, the interrelationship between changes induced by climate in transmission capacity, seasonal load demand variations, and RES expansion is expected to place even more pressure on transmission power components and to intensify network congestion and curtailment [19, 20]. Addressing these challenges necessitates substantial increases in transmission capacity to ensure system reliability and efficiency. For instance, by 2050, the European Union's transmission and distribution systems are expected to expand with the addition or replacement of over 4 million kilometres of lines in the announced pledges scenario [21], while the United States, the effects of global warming are expected to reduce Overhead Lines (OHL) capacity by an average of 1.9% to 5.8% between 2040 and 2050, compared to the 1990–2010 period [22].

To address these issues, two primary strategies for increasing transmission capacity can be identified: uprating or enhancing existing network power system components and implementing straightforward solutions such as upgrades and rebuilds. The last two strategies are particularly suitable for networks facing issues related to the end of their economic service life or engineered serviceability, often requiring replacement or reinforcement. These strategies are typically associated with long lead times and are capital intensive. In contrast, the enhancing strategy presents a valuable opportunity to improve the overall utilization of transmission power systems, particularly in scenarios where the integration of RES is closely tied to temperature and influenced by environmental factors.

The rating enhancement strategy for transmission power component aims to increase power transfer capacity, taking into account the associated risks, as described in [23]. Among these strategies, described in [24], is increasing maximum thermal capacity based on climatic conditions, a concept that has been explored for decades through Dynamic Thermal Rating (DTR). This method addresses capacity constraints influenced by environmental factors, from real-time monitoring to short and medium-term (typically less than 15 years) network planning. However, while DTR presents notable advantages such as increased integration of RES, deferred investments and congestion cost [25], it is often overlooked in studies focused on long-term network expansion, where more comprehensive assessments of transmission infrastructure are often required to manage heat transfer variables beyond lines and cables [26]. Consequently, traditional solutions tend to dominate, often applying fixed capacity values for the entire year, such as Static Thermal Rating (STR), and seasonally adjusted ratings that are not influenced by future climatic changes. These approaches are often insufficient, with actual capacity falling short more than 80% of the time, and in some cases with the potential to underestimate risk, as detailed in Fig. 1.2. As a result, this leads to the construction of new transmission lines or extensive upgrading of existing ones, which involves long lead times, high costs and social challenges. Therefore, unlocking the potential of thermal ratings for long-term analysis represents a significant step toward integrating climate change considerations into transmission planning, en-

abling a more comprehensive assessment of its impacts on power grid components while ensuring system reliability and meeting future demand.

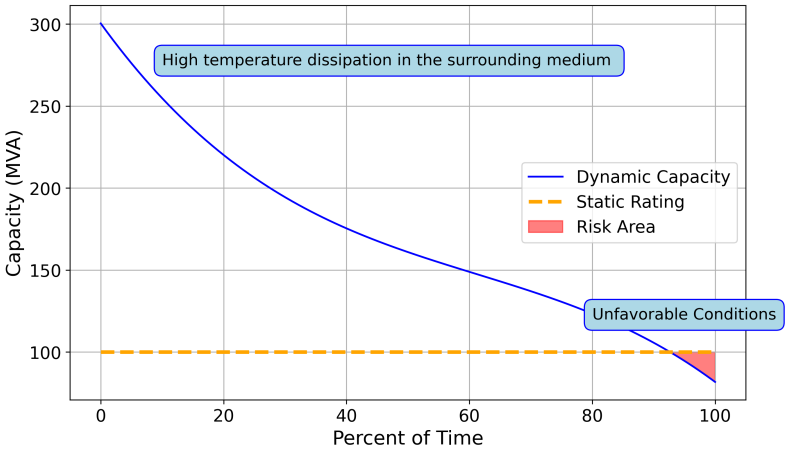

Figure 1.2: Comparison of dynamic capacity versus STR over time for a OHL line: the shaded risk area highlights periods where dynamic capacity falls below the STR, indicating potential component risk under adverse thermal conditions. Derived from [23]

In this context, Network Expansion Planning (NEP) faces challenges on three main fronts, better illustrated in Fig. 1.3. First, the thermal performance of network power system components is increasingly affected by local spatio-temporal weather conditions. Second, future demand and the deployment of RES must be aligned with policy assumptions for reducing greenhouse gas emissions, which are often analyzed using optimization models. Finally, the projected climate change is expected to affect both transmission capacity and demand profiles, adding further stress to the transmission power component and requiring adaptation measures during the transmission network planning process.

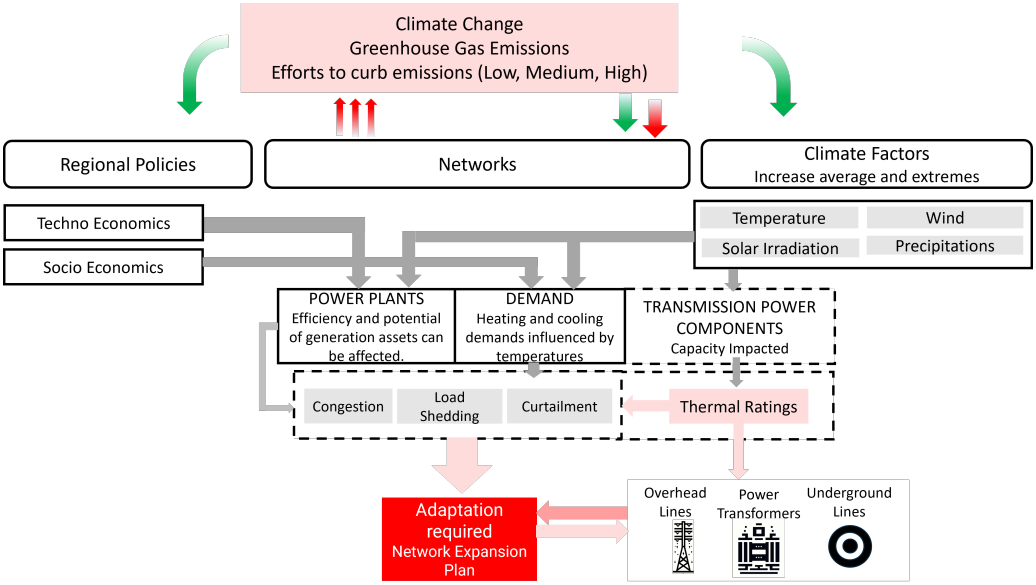

Figure 1.3: The relationship between climate change and transmission power system planning

1.2 Chapter Outline

In the face of these challenges, it is crucial to evaluate methodologies that incorporate and enable analysis of climate change impacts on power system component. The chapter begins by examining how weather affects transmission power system components through underlying heat transfer mechanisms (Sections 1.3.1–1.3.2). It then introduces the spectrum of rating methodologies, from static to dynamic and probabilistic approaches (Sections 1.3.2.4–1.3.2.5). Next, Section 1.3.3 discusses the role of ratings influenced by the climate in Network Expansion Planning (NEP), and Section 1.3.5 explores climate modelling approaches.

Section 1.5 provides an overview of the contributions made to this thesis. Additionally, a complete list of all publications, including those that were developed as second contributors, can be found in Section 1.6. Finally, Section 1.7 presents a structured outline of the thesis, guiding the reader through the subsequent chapters.

1.3 State of the Art

1.3.1 Weather impacts on Power System Network Component

In particular, the interaction between environmental or weather conditions and the thermal losses caused by the current flowing through the transmission power components can have both positive and negative effects. Favourable conditions, such as high wind speed, can enhance component cooling, improving the thermal performance in OHL. Conversely, adverse meteorological factors, as described in [27], such as low soil moisture and elevated soil temperatures, can reduce capacity by up to 50% and 15% in Underground Cable (UGL). Therefore, understanding these thermal limits and the influence of weather conditions is essential for improving network efficiency and the integration and expansion of RES, which are increasingly dependent on UGL and require optimized use of existing Oil-immersed Power Transformer (PT) infrastructure.

The main concern is that transmission networks in Europe span a wide range of climatic regions, from coastal to mountainous areas, each with distinct weather patterns and temperature variations, as shown in Fig.1.4. This geographical diversity complicates the assessment of thermal limits, as the influence of climatic conditions on transmission capacity can vary significantly across regions. Incorporating these diverse climatic factors into a unified framework for rating assessment is particularly challenging, as it requires a comprehensive understanding of how localized weather patterns, seasonal variations, and long-term climate change projections affect the thermal performance of transmission components.

For this purpose, the following paragraphs will examine the influence of each weather factor on the heat dissipation mechanisms of OHL, PT, and UGL, showing their impacts on power transmission capacity.

1.3.2 Heat Transfer in Network Power Systems Components

To determine the maximum tolerable thermal capacity in a transmission power component, one of the most important physical processes is the heat transfer mechanism from the component's surface to the surrounding environment, categorized as conduction, convection, and radiation. This relationship has been extensively studied over the decades, particularly in the contexts of OHL[29–31], UGL [27, 32], and PT [33–35]. These studies have led to a generalized formulation of the thermal behaviour, as captured by the heat balance in Eq. (1.1). This equation describes the thermal interaction between a transmission power component and its surrounding environment. Heat is generated internally through power losses (Q_J), primarily due to Joule heating and core losses. Meanwhile, external environmental factors influence heat transfer through solar radiation or proximity to other heat sources ($Q_{s/int}$), convection (Q_c) from the wind, radiation (Q_r), and conduction (Q_{cd}). As a result, in steady-state conditions, this equation forms the basis for the development of power system component thermal ratings.

$$Q_J + Q_{s/int} = Q_r + Q_c \ + Q_{cd} \tag{1.1}$$

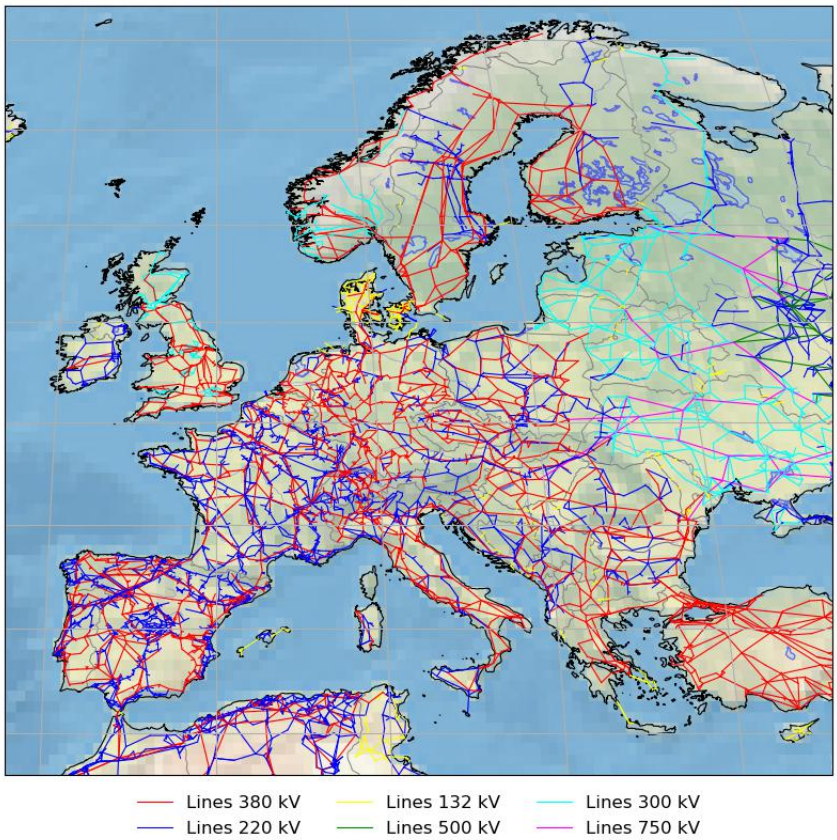

Figure 1.4: Map of the Transmission System Network in Europe [28]

1.3.2.1 Overhead Lines

In OHLs, the impact of heating generated by joule losses and solar radiation could cause loss of conductor strength due to annealing and can cause the conductor sag to increase [36], resulting in reduced conductor-to-ground clearance. To counteract this, the degree of convection depends directly on the relationship between air temperature and wind speed.

This thermal relationship is formally defined and applied through well-established standards and guidelines described in [29, 37], which provide analytical formulations to characterize the thermal performance of bare overhead conductors. These standards are generally used to estimate OHL capacity under varying environmental conditions and geographical locations. Some comparisons have been made between the two approaches, which reveal that, despite differences in their underlying assumptions, both adhere to a similar thermal relationship and exhibit only minor deviations at high conductor temperature conditions in [38, 39], which are usually associated with low wind speeds [40].

According to the analytical formulations referenced in the guidelines, specific sensitivity analyses can already be found in the literature, linking conductor rating to weather conditions and revealing the impacts of climatic conditions on capacity. As shown in [41], in the absence of wind, cooling occurs solely through radiation and natural convection, resulting in a conductor capacity up to 4.8 times lower than under high wind conditions ($\geq$10 fps), where the influence

of air temperature becomes negligible. However, this trend does not always hold during periods of elevated ambient temperatures and solar irradiation, typically occurring during the day. In fact, [42] shows that 80% of low-wind conditions (<1m/s) occur at night. This highlights the significant variability in heat transfer scenarios, which are strongly influenced by geographic location, temporal resolution, and seasonal patterns, as further explored in [36].

Similarly, the geographic distribution of the intensity of weather conditions within the same time period, on the same OHL, and not distant, enhances the available capacity headroom, which varies significantly, highlighting the need to include spatial and temporal variations [43]. Additionally, seasonal temperature variations affect capacity, with the difference between winter and summer leading to a reduction of 20% for specific conductor of stranded copper in the United Kingdom [44]. Intraday variability may also lead to notable differences; for instance, an Aluminum Conductor Steel Reinforced (ACSR) conductor located in northern Sweden may observe up to a 33% increase in rating compared to midday conditions with full and direct sunlight [30]. Finally, in [42], an extended analysis was conducted on the effects of various meteorological variables under steady-state conditions for an ACSR conductor. This study reaffirmed wind speed as the critical parameter influencing thermal performance. However, it also highlighted that at low wind speeds, radiative heat loss can account for up to 40% of the convective cooling term, whereas its significance diminishes considerably as wind speed increases [45].

A key insight from this analysis is that since OHL often span tens of kilometres, conductor ratings exhibit significant variability in response to changes in wind speed, air temperature, and seasonal and spatial conditions. This underscores the importance of incorporating better resolution meteorological and geographic data into capacity assessments. Generalizing thermal ratings for a given component, even within the same region, can lead to underestimates and suboptimal planning decisions. The following section focuses on PT, where similar climate-dependent mechanisms arise, but with different dynamics.

1.3.2.2 Power Transformers

Oil-cooled PT, unlike transmission lines, are assets fixed at a single geographical location, where heat transfer occurs mainly in the oil, winding and core. In these components, heat generated by current, winding, and core losses is dissipated through convection and radiation, through cooling influenced by oil and ambient temperatures. Like other transmission power components, the thermal behaviour of PT has been modelled using thermal-electrical analogies and heat transfer theory [33, 35, 46]. Mainly converging the general recommendations to estimate the steady-state method, with recognized limitations above rating, such as oil expansion, external mechanisms, voltage and frequency influences. In these, a critical parameter in evaluating both operational performance and loss of life (ageing) is the Hot Spot Temperature (HotST), due to its strong correlation with gas formation in the solid insulation and oil.

In fact, the determination of this variable is mainly influenced by the average ambient temperature and PT loading within the thermal model. For instance, [47] analyzes the steady-state relationship between these three variables using the IEC 60076-7 method [35], revealing that the

allowable PT loading (pu) for an HotST of 98 °C can vary significantly from more than 1.6 to less than 0.8 depending on weather conditions. This highlights the important role that ambient temperature plays in thermal evaluations. Although the effects of other climatic factors, such as wind and precipitation, on thermal performance have been analyzed [48], however in [35] makes it impractical to incorporate them directly into the methodology due to their significant variability.

Similar to OHL, seasonal temperature variations have a significant impact on PT thermal performance. In [49], a yearly analysis of a ground-mounted oil-natural air-natural PT demonstrates that lower ambient temperatures during winter improve operating conditions, whereas higher temperatures in summer result in more constrained capacity. Similar results could be realized for geographic location, where local climatic factors can positively affect the loading, and for two similar PTs with the same load profile by as much as 10 per cent.

The impact of solar radiation becomes important in regions with high ambient temperatures. In [25, 50], a new model is introduced that incorporates the effect of solar radiation in the thermal radiation process, showing a potential reduction in loading capacity ranging from 6.6% to 4%. On the other hand, PT are closely linked to RES, as they are part of the PT buses that are directly affected by temperature, solar radiation, and wind. Increased production driven by favourable weather conditions can raise power transfer demands, leading to higher thermal losses and accelerating ageing, thereby increasing the risk of a reduced lifetime.

1.3.2.3 Underground Lines

As PTs, UGLs are also affected by the increasing integration of RES, leading to thermal stresses due to joule losses and possible reductions in service life. On the other hand, like the OHLs, these cables typically span tens of kilometres, and heat dissipation depends primarily on soil properties and environmental factors. Considering that the UGL is buried in a homogeneous soil, heat transfer occurs mainly by conduction [27].

Similarly to previous transmission power components, an analytical formulation for this heat transfer equation has been proposed by applying thermal analogies [32, 51] or using finite element analysis, with comparative accuracy analyses presented in [52, 53]. Most of them assume static equilibrium, isotherm, and with and without moisture migration. In particular, significant differences can arise when variations in conductor construction, core configuration, and physical properties are considered.

However, soil properties and conditions can vary considerably in different geographical regions. As a result, the ability of the surrounding soil to dissipate heat from UGL depends primarily on the interaction between soil characteristics, environmental conditions, and moisture content. Among these factors, the thermal resistivity of the soil (^{o}Cm/W) turns out to be the most important determinant of heat transfer, accounting for 70% to 90% of the total thermal resistance of a 15 kV buried cable [8, 54]. Furthermore, thermal resistivity is very sensitive to moisture content [55], which itself fluctuates with seasonal variations. In arid conditions (low moisture content), the reduction in thermal conductivity significantly increases the risk of overheating in the conductor, underlining the importance of including these two factors within

the method [27]. Finally, in [56], the analysis is reinforced, highlighting the high dependence and correlation between temperature and humidity of the surrounding soil, among other factors, such as laying depth and physical properties.

The influence of soil thermal resistivity becomes particularly pronounced when expressed in terms of temperature. In [27], a 50% reduction in cable capacity was observed when the thermal resistivity of the soil is tripled, coupled with a 5 °C increase in ambient temperature.

To mitigate this effect, distribution systems commonly employ backfill materials that standardize soil properties, thereby minimizing thermal fluctuations and enhancing thermal stability and efficiency. In [8], a comprehensive review of the thermal performance of backfill materials underscores their susceptibility to long-term variations in surrounding soil properties and weather conditions, demonstrating the change and significance of the study of climatic conditions on these components.

Overall, transmission networks across Europe encounter diverse climatic conditions, ranging from coastal to mountainous regions, complicating the assessment of thermal limits in power system components such as OHL, PT, and UGL. These components exhibit distinct thermal behaviours due to different heat dissipation processes: convection in OHL, benefiting from wind cooling; oil circulation in PT, impacted by air temperature; and soil conduction in buried UGL, and primarily influenced by soil moisture and thermal resistivity. Where, as shifting weather patterns and seasonal variations amplify thermal stresses, a comprehensive framework for thermal capacity assessments that considers both spatial and temporal climate variability becomes increasingly essential.

1.3.2.4 Thermal Ratings

The sections analyzed above illustrate the impact of weather and climate conditions on thermal limits determined by thermal models. However, to protect the lifespan of transmission power system components, capacity limits are imposed to maintain safe operating temperatures [57], a practice encapsulated in the concept of thermal ratings. These ratings, determined through the network operator analysis, define the maximum allowable current based on thermal limits, ensuring that temperature thresholds are not exceeded, thus preventing accelerated ageing or potential failure. As discussed in [8, 37], these limits can be categorized as follows:

- **Transient rating:** Sudden loading changes with unchanging temperatures. Usually, in a short time during specified periods, without exceeding the maximum allowable conductor temperature, usually under defined load conditions during emergencies or contingency. For instance, in UGL/OHL, there are sub-designations associated with time, such as Long-Term Emergency rating (LTER) exceeding 24 hours (infrequent/ non-consecutive) and short-duration ratings ranging from 15 minutes to 4 hours (very infrequent, non-consecutive), typically considering thermal equilibrium and transient thermal limits [3].
- **Steady state or Continuous rating:** Maximum allowable constant loading that causes the conductor to reach its maximum allowable temperature under specified weather conditions and conductor characteristics, assuming thermal equilibrium and continuous load.

As a special condition, during a contingency event, the transmission power component is allowed to be overloaded above the continuous rating, but it is not expected to have a significant impact on the lifetime and loss of conductor strength, as is detailed in Fig. 1.5. However, the frequency and duration of these overloads should be low. Regarding this issue, various discussions and recommendations can be found in the literature for UGL [3], OHL [23], and PT [47], primarily aimed at preventing forced outages.

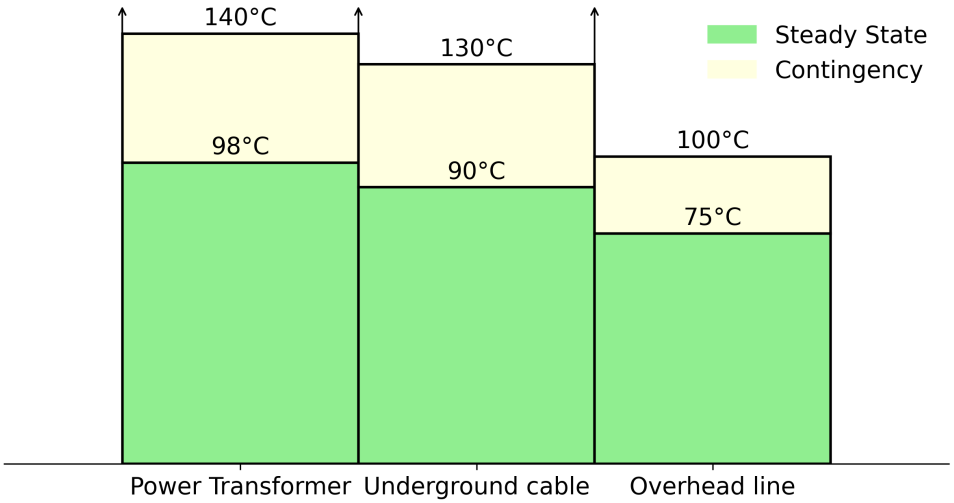

Figure 1.5: Rating categorization related to temperature limits. Derived from [58]

1.3.2.5 Long-Term Thermal Ratings

For decades, utilities and transmission operators have employed conservative worst-case condition rating assessments or STR, guided by standard fixed values of weather conditions criteria or historical data analysis [59]. However, nowadays, the range of rating estimation methodologies used by utilities has shifted towards dynamic methods that provide assessments in near real-time, offering data acquisition intervals as short as 15 minutes or less, as seen in real-time rating systems, illustrated in Fig. 1.6.

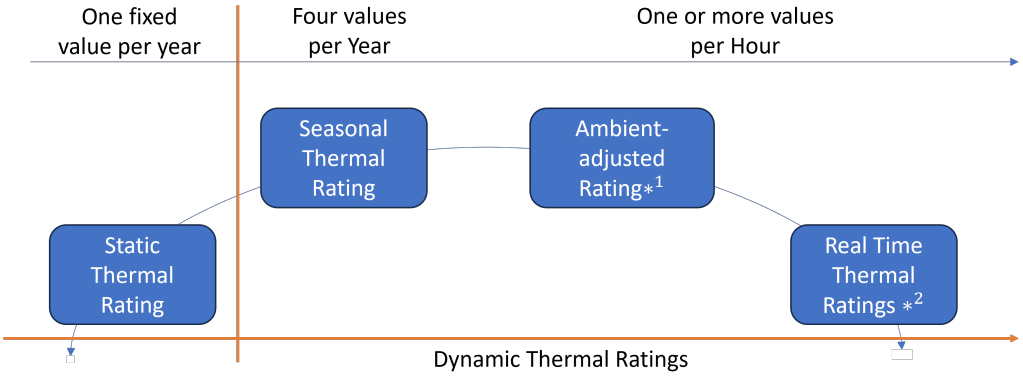

1. Adjusted by ambient air temperature (θ)
2. Influenced by ambient conditions such as local weather conditions, and/or the line's physical conditions

Figure 1.6: Thermal Rating Methodologies adapted from [10]

All these methodologies differ in their assumptions and the way environmental conditions are utilized. The most important differences are:

- **Static Ratings (STR) - Conservative baseline:** Determined using worst-case deterministic assumptions, based on past operating experience or time series of weather data, characterized by low probability of occurrence and associated with low-risk conditions [60]. These ratings have the potential to remain fixed for decades or change in response to the policies of transmission system operators or transmission companies.
- **Seasonal Ratings:** Determined by the maximum temperature limits based on seasonal static assumptions, usually derived from historical data. This rating is continuously extended throughout the season, distinguished by special climate conditions, i.e., summer.
- **Ambient-Adjusted Ratings:** A methodology similar to the static approach but with more frequent updates (typically every hour), but adjusted based on ambient air temperature measurements, enabling more responsive limits.
- **Real-Time Ratings - Fully dynamic:** A step forward in using real-time monitoring, whether meteorological or measurements of physical components such as tension or HotST, relies on the length of the component and the number of variables measured, integrating thermal models to determine the actual capacity. This methodology typically includes the deployment of remote sensing, measurement, communication, and thermal model analysis.

The common concept underlying these applications is the DTR, which has been extensively analyzed and validated over several decades. Originally introduced in [57, 61], with its fundamental algorithm described in [62] and illustrated in Fig. 1.7, the DTR integrates the influence of external factors, such as weather conditions, into thermal models to dynamically estimate component performance. To better understand its rationale, it is important to distinguish between ampacity and thermal rating, as discussed in [63]. *Ampacity* refers to the maximum current a conductor or equipment can carry continuously without exceeding its design temperature limit

from physical property determined by material and environmental characteristics. In contrast, the *thermal rating* represents the operational current limit established by the network operator (DSO or TSO) to ensure that the component remains within safe thermal and mechanical boundaries under given environmental conditions. When this limit is updated in real time, it becomes the *Real-Time Rating*, which represents the instantaneous ampacity of the component according to prevailing weather and loading conditions. In this sense, DTR acts as a bridge between the physical capacity of transmission assets and the operational limits set by networks operators. Numerous studies highlight the benefits of DTR [45, 64], including: i) reduced or deferred transmission capital expenditures [65, 66], ii) increased efficiency through alleviating transmission line congestion and enhancing RES integration [67, 68], and iii) minimized rating violations during $N-1$ contingency scenarios [69].

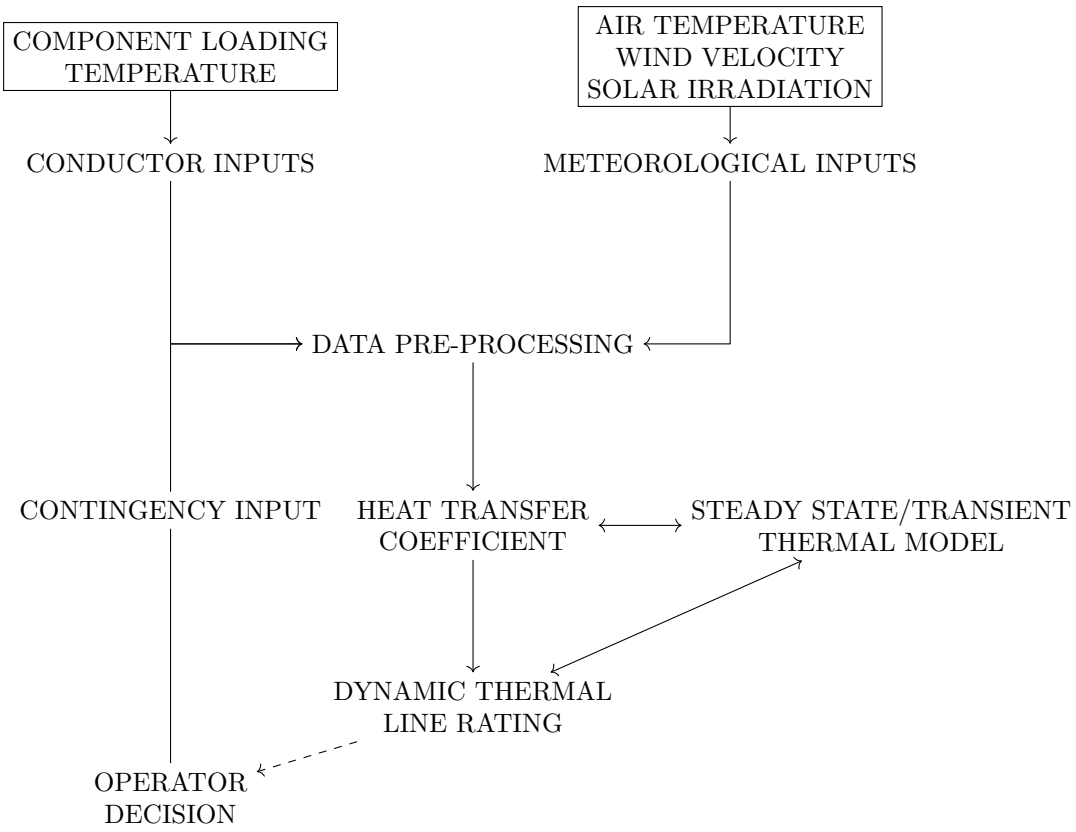

Figure 1.7: Overview of Dynamic Thermal Line Rating Concept. Derived and modified from [57]

As the component's temperature is the primary variable in DTR, weather and mechanical conditions can be determined using two methods: i) Real-time measurement equipment [70] from the component temperature or physical monitors like line tension [10, 71], known as direct measurement. Nowadays, this is typically performed for new circuits with embedded optical fibre, as described in [64], offering excellent accuracy and precision but with barriers such as high capital costs and non-applicability to already installed networks. ii) A thermal mathematical model based on information on the surrounding weather conditions, combined with steady and transient ratings using historical data, numerical weather predictions, or weather measurements

[72, 73]. This method increases capacity compared to static thermal rating but reduces the risk of overloading.

The DTR methodology is typically oriented toward decision-making for short-term operations, applying day-ahead and intraday forecasting methods [63, 74–76], often based on real-time equipment or Numerical Weather Prediction (NWP) models and incorporating techniques to manage uncertainties in environmental conditions and transmission power component behaviour [77]. In contrast, medium and long-term approaches to determining DTR apply deterministic or probabilistic methods to assess maximum capacity.

The **deterministic** method evaluates the transmission power component ratings based on worst-case conditions outlined in STR, ensuring safe operational limits across all transmission assets. While the approach significantly lowers the probability of exceeding safety and thermal thresholds, it does not completely remove the possibility of such violations, as evidenced by the red zone in Fig. 1.2. In contrast, the **probabilistic** method analyzes the changing and uncertain behaviour of surrounding weather conditions abstracted from local weather station observations datasets or from NWP. An approach to this method involves evaluating a Cumulative Distribution Function (CDF) of hourly steady-state ratings using historical weather data to represent the long-term climatic profile of the area [78]. A second approach involves analyzing the key climatic variables that affect the transmission power component rating, using probability distributions to assess the rating while accepting a specific level of risk.

Nevertheless, in practice, network planners require more stable thermal ratings over the analyzed frequency, reducing fluctuations associated with real-time DTR while leveraging the spatio-temporal advantages of ambient conditions and the capability to estimate them at varying time frequencies. To address these challenges, a method called quasi-Dynamic Thermal Rating (qDTR) has emerged, enabling more consistent capacity analysis of components over time.

1.3.2.6 Quasi-Dynamic Thermal Rating

This is a probabilistic method that assesses the stable thermal ratings of transmission components over a defined timescale with a specified thermal probability level, as initially introduced in [79]. The concept serves as a tradeoff between STR and DTR, integrating thermal dynamic analysis from the DTR method with statistical models to determine ratings over a period while considering conservative overload thresholds. Ultimately, this approach enables transmission operators to implement a rating that is more dynamic than traditional STR but less variable than real-time DTR.

The objective of this methodology, as visually illustrated in Fig. 1.8, is to increase power system capacity keeping component safe and allowing ratings to exceed traditional STR limits, as shown in Fig. 1.8a. The remaining subfigures in Fig. 1.8 present an example of statistical analysis applied to a series of OHL ratings calculated over a specific historical period. Fig. 1.8b shows rating estimates derived from historical climate data, calculated using two different temporal resolutions and at two different thermal boundary ranges, demonstrating the potential for improved capacity utilization. Figures 1.8c and 1.8d illustrate the CDF of the calculated ratings based on intraday variability, specifically differentiating between daytime and nighttime

operating windows.

This quasi-dynamic approach enables transmission operators and system planners to incorporate more stable and climate influenced ratings into their operational and planning optimization models. It offers a conservative yet flexible risk profile that better reflects climate variability than traditional STR, facilitating more efficient and reliable utilization of the transmission network over long-term horizons.

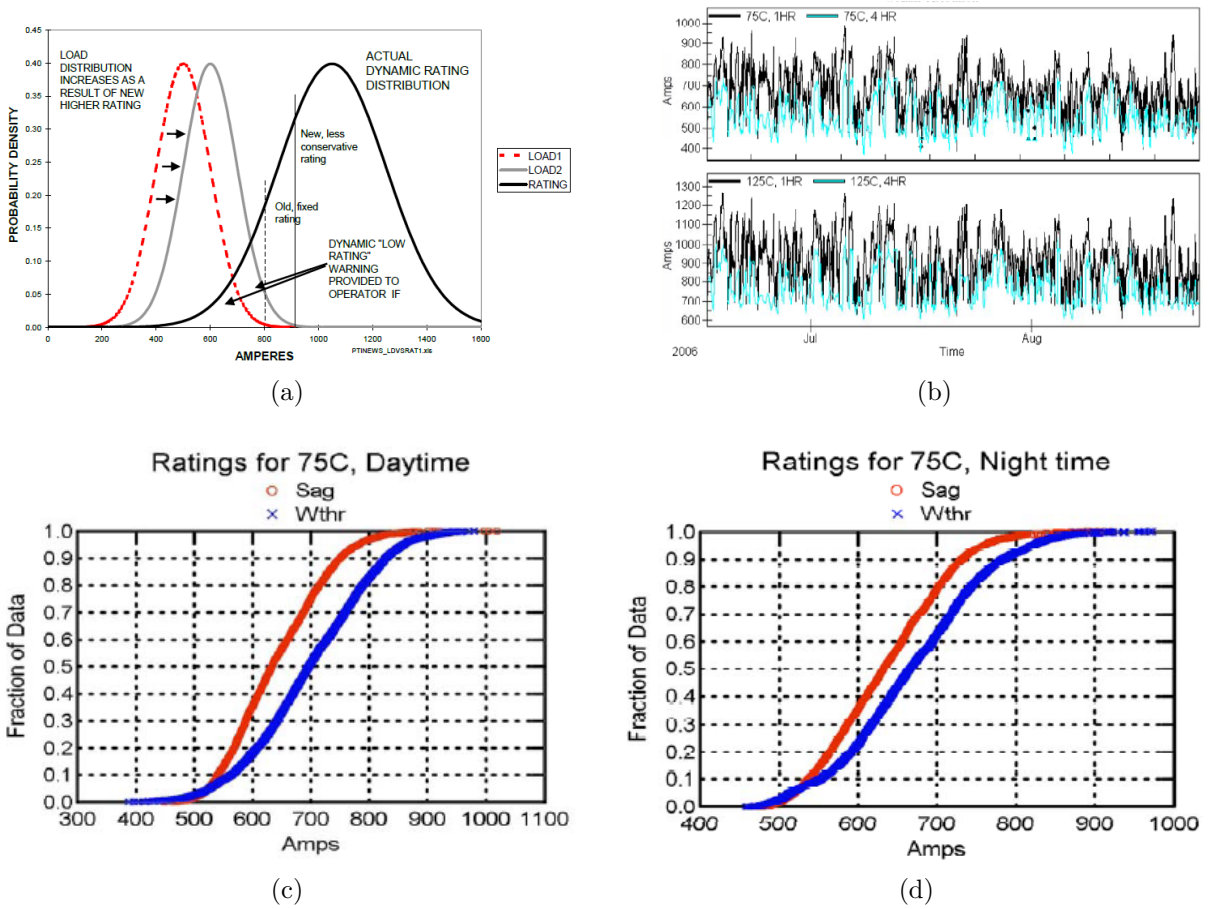

Figure 1.8: Quasi Dynamic Thermal Rating Method. From [79]

Although this method has not been extensively studied compared to direct or short-term probabilistic DTR methodologies, some methodological approaches exist, primarily focused on OHL [80, 81]. For instance, [82] presents a qDTR method that utilises a non-steady-state thermal equation to estimate LTER, aiming to optimise transmission congestion in competitive electricity markets for short-term planning. Conversely, [83] applies steady-state thermal ratings for various long-term frequencies (monthly, seasonal, yearly), using a fix confidence level in key meteorological thresholds for OHL, enhancing thermal limits to alleviate congestion.

1.3.2.7 Other Probabilistic Methods

Finally, there are also other approaches whose methodological basis is similar to qDTR and can be integrated under the same approach. In [84], an exponential probability density function is

presented and evaluated on a two year dataset to calculate the DTR and estimate the optimal generation investment. A similar approach introduces a probabilistic STR to assess varying thermal rating limits based on time of day or seasonal periods for OHL are outlined in [60, 85]. This method incorporates acceptable risk tolerance levels for steady-state rating assessments over extended periods and at various frequencies, enabling time-based analysis and assessment, as illustrated in Table 1.1.

Rating	**Ratings per year**	**Description**
Probabilistic STR	1	Constant fix value for whole year
Seasonal	4	The year is divided into: December–February: Winter June–August: Summer September–November: Autumn March–May: Spring
Monthly	12	The year is divided into calendar months
Season Day/night	8	The year is divided by seasons, and each season day is divided into daytime (6 am–6 pm) and night-time (6 pm–6 am)
Monthly Day/night	24	The year is divided into calendar months, and each month is divided into daytime and night-time

Table 1.1: Static Time Resolution Models. Modified from [60]

The main advantage of these methodologies is that they take advantage of the influence of the ability of the environment to provide additional capacity headroom network power system components, and as a tradeoff, it allows the detection of the risk of overrating in unfavourable conditions, as in the case of OHL, where in [86] it is observed that the STR value decreases up to 11%, not 1% as recommended by [87].

1.3.3 Network Planning

As previously explained, favourable and unfavourable climatic conditions surrounding transmission power components can significantly impact their capacity. Therefore, in the context of the network planning decision-making process, it is crucial to incorporate thermal ratings as decision variables within the steady-state power flow equations. The traditional approach to defining the power flows of existing and future transmission components is based on their rated capacities, typically using AC or DC power flow equations [88]. However, considering the influence of DTR requires a new approach within the power flow.

To address this, some alternative approaches have been proposed in the literature. One approach focuses on updating the hourly line ratings of each transmission power component in steady state based on the DTR model as a fix value [89, 90], applying Direct Current Optimal Power Flow (DCOPF) due to its rapid solution capability, which is crucial for long-term analysis and effectively manages active power constraints [89]. Another approach introduces the temperature as a decision variable, integrating heat balance equations and the resistance

influenced by the temperature effect within power flow equations as a nonlinear model in [91], primarily explored in short-term planning and medium-term distribution expansion planning in [66]. A further line of research implements algorithms that account for DTR uncertainty, applying probabilistic power flow constraints. In [76], a Chance-Constrained DCOPF introduces a CDF to define line rating bounds with a specified violation probability for analysing short-term day-ahead planning. A probabilistic N-1 secure dispatch applies a DCOPF Chance-constrained problem to include certain meteorological uncertainties, is presented in [92]. Other methods that include analysis of the overloading risk in transmission power component are introduced in [93–95]

However, long-term NEP in power systems must also consider future changes in loads, costs, and generator dispatch, ensuring that the system operates effectively under worst-case scenarios and withstands adverse weather conditions. This type of analysis involves both the analysis of the optimisation formulation and, secondly, the inclusion of the weather surrounding variable in the component for the future; for this part, more extensive details are described in 1.3.5.

Regarding the formulation of optimisation problems, the literature was analysed from two perspectives: (i) a deterministic approach from the point of rating estimation, in which transmission expansion decisions are made considering a future scenario. In [90], a mixed-integer linear DCOPF model is proposed, incorporating conservative line capacity increases when DTR technology is deployed, alongside uncertainties related to load growth rates and discount factors. Another approach is where demands and transmission power components' capacity must be met, even in the worst-case scenarios. ii) The second perspective is stochastic optimization, which considers uncertain parameters. In [96], a two-stage mixed-integer nonlinear programming model is proposed, incorporating the stochastic nature of DTR to assess both the economic benefits and the overload risk associated with its implementation.

1.3.3.1 Risk Management for Thermal Ratings

According to [23], "Uprating will increase the electrical capacity of the line and, therefore, based on risk, potentially increase the consequences of a failure." As discussed in previous sections on planning and thermal ratings, risk is inherently linked to the nature of DTR, emphasizing the need to understand the implications of exceeding transmission component temperature limits. To address this, [81] proposes a risk assessment approach in which the probability of surpassing the maximum allowable conductor temperature in OHL is quantified to determine an appropriate confidence level for safe operation. Similarly, [88] introduces a risk-averse stochastic DTR model for OHLs based on quantile and superquantile regression, capturing both conductor thermal dynamics and forecast uncertainty within operational constraints. In addition, [7] presents a probabilistic method for evaluating thermal capacity under temporary overload conditions, particularly for LTER and very LTER in OHLs, considering timeframes ranging from a few hours to 90 days.

Other short-term operational studies, such as [97, 98], further demonstrate the potential of integrating DTR into distributionally robust optimal power flow frameworks to manage overload risks under RES uncertainty. However, the implementation of these risk-based formulations

remains largely confined to short-term horizons. Extending them to long-term transmission expansion planning continues to pose challenges due to data limitations, computational complexity, and climatic uncertainty yet doing so is essential to ensure resilient grid development under increasing RES penetration.

1.3.4 Aging

Thermal ratings and ageing are closely interrelated, especially in the context of power system components. Thermal ratings methodologies provide a framework to define the safe continuous operating capacity of components at their thermal limits, accounting for both steady-state and contingency scenarios. Thermal ageing, in turn, refers to the degradation of materials (such as insulation and thermal stress) under cumulative service stress resulting from prolonged exposure to temperature or abnormal stress [99]. Exceeding the rated temperature accelerates the ageing process, reducing the component's lifespan and compromising its usefulness over a longer period of time. For example, as highlighted in the guide [100], the PT insulation is rated to withstand a continuous temperature of 110°C at its hottest point, which aligns with a standard expected lifespan of 180,000 hours (roughly 20 years). However, even short-term overloading beyond this threshold, as allowed for in emergency ratings, can result in accelerated ageing, where even short overloads can reduce years of expected insulation lifespan. Similarly, in UGL, the model in [101] details that high temperatures at hot spots drastically shorten cable life, sometimes by more than 35%. Therefore, thermal ratings are not just operational or planning limits; they are essential for life projection and management of ageing and asset replacement.

This relationship between ratings and ageing has been studied for OHL in [102] over a medium-term horizon. This study presents an approach that combines conductor temperature driven degradation, modelled by the Arrhenius formula [103], with statistical ageing behaviour, represented by the Weibull distribution. This highlights that probabilistic ageing models are essential for reliability assessments, rather than relying on deterministic lifetimes. A data-driven method for PT in long-term planning is proposed in [104], where the standard thermal ageing model [105] is used to calculate acceptable continuous overload limits for safety. A reliability focused approach, as described in [106], enhances traditional static PT sizing by incorporating thermal ageing models based on [105] and [35]. Lastly, [107] introduces a spatial and temporal framework to quantify thermal ageing in OHL, integrating detailed weather forecasting models.

Although ageing and thermal overload have been studied separately, combining both risks in long-term ratings has not been fully explored. In fact, the literature contains some temperature-related limits; for instance, [108] describes how aluminium conductors begin to lose mechanical strength when operated above 93°C, whereas copper conductors exhibit significant annealing effects above approximately 75°C. The degradation in strength is time-dependent, as illustrated by the annealing curves in [109], which show how extended exposure to high temperatures leads to a reduction in tensile strength. For instance, at 150°C, copper can lose a significant portion of its strength in just a few hours. To manage this, contingency ratings are designed with strict operational limits, as detailed before in Fig. 1.5; In [110], it is assumed that emergency operation above standard temperatures will not exceed 600 hours over the conductor's 30-year lifespan.

This restriction ensures that emergency loading represents less than 5% of total operating life, limiting long-term degradation. Thus, ratings are not only operational constraints but also life management that balances reliability and asset lifetime.

1.3.5 Climate Projection Models

Long-term climate projections are inherently uncertain, particularly when incorporating Greenhouse Gas (GHG) mitigation pathways, which are ultimately autocorrelated. Simultaneously, environmental factors associated with climate change, including extreme weather events such as storms, heat waves, droughts, and intense precipitation, pose substantial risks to transmission components, potentially compromising the capacity. These factors, mainly affected by climate change, will play a unique role in implementing active transition and network expansion planning. Therefore, establishing a framework of methodologies and tools for low-carbon energy is essential to this task.

Given these challenges, scenario analysis using climate model projections offers a suitable methodology for assessing the potential impacts of future energy transitions, climate variability, and mitigation strategies on power systems components through potential investments. The Intergovernmental Panel on Climate Change (IPCC) developed the scenarios RCP to examine the interplay between socioeconomic development and climate change identified by their approximate total radiative forcing in the year 2100 [16]. These scenarios serve as a framework for assessing the impact of various energy generation and transportation strategies on future climate outcomes, also detailed in Table 1.2 [111]. $RCP_{2.6}$ depicts the most intensive GHG reduction efforts, resulting in the smallest projected temperature rise, whereas $RCP_{8.5}$ represents a business-as-usual scenario with minimal mitigation efforts, leading to the most severe climate impacts.

Name	**Radiative forcing**	**Concentration (p.p.m.)**	**Pathway**
RCP8.5	$> 8.5\ W\ m^{-2}$ in 2100	$> 1370\ CO_2$-equiv. in 2100	Rising
RCP6.0	$\approx 6\ W\ m^{-2}$ at stabilization after 2100	$\approx 850\ CO_2$-equiv. (at stabilization after 2100)	Stabilization without overshoot
RCP4.5	$\approx 4.5\ W\ m^{-2}$ at stabilization after 2100	$\approx 650\ CO_2$-equiv. (at stabilization after 2100)	Stabilization without overshoot
RCP2.6	Peak at $\approx 3\ W\ m^{-2}$ before 2100 and then declines	Peak at $\approx 490\ CO_2$-equiv. before 2100 and then declines	Peak and decline

Table 1.2: Summary of RCPs, based on [111]. The term "representative" emphasises that each RCP is just one of many scenarios leading to a specific radiative forcing, while "pathway" highlights the importance of both concentration levels and the trajectory to reach them.

In addition to the RCP scenarios, which describe long-term temperature stabilization goals and their associated carbon emissions trajectories, Shared Socioeconomic Pathways (SSPs) are socioeconomic development trends that complement RCPs, enabling combined assessments of emissions, development, and climate impacts. Both sets of trajectories allow for a spatial assessment of regional climate change and its specific impacts on the energy sector. Understanding

these environmental impacts is vital to improving the resilience and reliability of electric systems under changing climate conditions. For example, in [22], a two-step methodology is proposed to estimate climate-induced capacity reductions in OHLs by combining thermal models and electricity demand projections in the United States. The study examines the interrelationship between future climate scenarios, electricity demand, and transmission capacity, utilizing historical data to estimate that load increases could reduce capacity by between 1.9% and 5.8% by mid-century. Notably, most climate impact analyses in the energy sector have traditionally focused on generation or demand aspects [13, 16, 112]. For example, [112] presents a stochastic-robust optimization approach to evaluate the influence of climate variability and extreme weather events on power systems, employing 13 distinct climate scenarios to capture a wide range of future conditions.

In summary, as outlined in the previous chapters, the modelling of thermal limits encompasses a broad spectrum from steady-state current ratings to advanced models that incorporate real-time, weather-dependent variations. While some methodologies address these dynamic influences, recent research has also introduced probabilistic approaches within steady-state thermal modelling frameworks, which assume thermal equilibrium across network components during the planning phase. This approach supports the integration of thermal ratings into long-term NEP while deliberately avoiding the added complexity of transient or time-varying simulations. Simultaneously, academic research has increasingly emphasized the critical role of environmental and climatic factors, which challenge the adequacy of static planning assumptions. Therefore, integrating climate projections into thermal rating methodologies is critical for resilient long-term NEP.

Finally, as can be observed, traditionally, long-term NEP has relied on static or seasonal ratings, designed around worst-case scenarios and guided by the (N-1) contingency criterion, which ensures system reliability under the loss of any single component [4, 10]. However, this conservative approach often overlooks the operational flexibility enabled by DTR, whether deterministic or probabilistic. It also tends to exclude considerations of overload risk within a probabilistic or optimization-based context. To situate the current study within the broader research, Table 1.3 summarises the key contributions that have informed this work. These studies are grouped by their relevance to the integration of thermal limits in long-term power system planning, particularly where they intersect with rating methodologies, planning strategies, and climate adaptation.

Reference	Type	Description
Long-Term Thermal Ratings / Thermal Models Methods		
[29, 32, 37, 38, 87]	OHL	
[3, 8, 27, 51, 52]	UGL	
[33–35, 46–48, 50, 105, 113]	PT	
Long-Term Thermal Ratings / Rating Methods		
[41, 57, 62, 70, 89–91]	OHL	Real Time
[30, 36, 44, 49]	Mixed	Real-Time + Seasonal/Static
[10]	OHL	Adjusted Ambient Rating
[79–83]	OHL	qDTR
[40, 43, 78]	OHL	Statistical Forecasting
[63, 68, 72, 73]	OHL	Probabilistic Forecasting
[65–67, 84, 85, 114]	OHL	Data-Driven
[30, 96]	OHL, PT	Stochastic
Temporal Horizon		
[10, 22, 68, 73, 78, 80, 96]	OHL	Long-Term
[40, 49, 66, 79, 114]	Mixed	Medium-Term
[41, 60, 63, 83]	OHL	Short-Term
Long Term Ratings / Risk Method		
[76, 77, 92, 94, 96]	OHL	Chance-Constrained / Overloading
[7]	OHL	Probabilistic Risk Density Functions for LTER
[60, 93]	OHL, PT	Thermal Overloading
Network Planning with Thermal Ratings		
[[30, 66, 74, 79, 82, 89, 91, 92, 94, 114]],[[4, 12, 13, 15, 65, 67, 84, 96]]	Mixed	Short-term, medium-term, long-term
Weather and Climatic Modeling		
[1, 55, 56]	UGL	Soil properties
[22]	OHL	RCP

Table 1.3: Classification of literature by thermal rating methodology, risk modelling, and planning horizon relevant to this thesis.

1.4 Motivation and Challenges

Weather and climatic conditions are known to significantly influence transmission capacity, as captured by standardized thermal models. However, the integration of these models embedded in rating methodologies into long-term planning frameworks under changing climate conditions remains, limiting the understanding of how climate change may affect the future capacity and reliability of transmission power system components. Standardized thermal models, such as those used in DTR, provide valuable insight into how ambient temperature, wind speed, solar radiation, and other environmental factors influence component ratings. However, most existing studies and implementations focus on short-term or operational timescales, often ignoring the complexities and uncertainties associated with longer planning horizons under changing climate conditions. Furthermore, these models are predominantly applied to OHL, where weather conditions can have more pronounced and immediate effects on thermal capacity. For UGL and PT, the thermal response can vary; however, the emphasis on long-term thermal analysis remains limited. Therefore, when accounting for climatic effects in long-term horizon analysis, the following challenge arises:

Challenge 1: Assessing Thermal Rating Methodology for Long-Term Analysis

Evaluating thermal ratings over long periods requires considering the impact of climate variability on transmission components. Traditional methods emphasize short-term or real-time conditions and rarely account for gradual shifts in seasonal averages, long-term warming trends, or increased frequency of extreme events on the thermal limits of assets in geographically diverse environments. Additionally, conventional STR approaches are typically fixed, relying on conservative or generalized values for all components. These are often preferred for their simplicity and their ability to constrain thermal limits within network planning frameworks. By contrast, modern DTR approaches provide high-resolution estimates but introduce variability and complexity that limit their applicability to long-term studies.

Balancing model complexity with practical usability is therefore essential for transmission planning under climate change and remains a challenging task. As network electricity needs evolve under increasing climate uncertainty, establishing accurate and operationally viable methodologies becomes essential to support climate-sensitive transmission planning.

Challenge 2: Integrating Thermal Ratings into Long-Term network Planning

Long-term transmission planning requires a spatio-temporal assessment of thermal limits of transmission power system components to ensure that network components can meet future generation and demand needs without violating operational constraints. Traditionally, thermal ratings are static and applied over decades, assuming stable climate conditions and ignoring intermediate variability. However, these static approaches are increasingly insufficient in the face of changing climate variability and uncertainty.

A key task lies in adapting existing methodologies to incorporate probabilistic assessments of thermal overload risk under future climate conditions. This requires integrating long-term thermal ratings with models that reflect environmental variability, moving beyond fixed assumptions and toward dynamic, risk-based planning. By quantifying overload risk, probabilistic approaches

enable more flexible asset use, reduce unnecessary conservatism, and improve system resilience. Achieving the right balance between safety margins and probabilistic risk assessments is critical to ensure both reliability and adaptability in future grid development.

Challenge 3: Assessing the Impact of Climate Change on Transmission Systems

Climate change introduces increased variability and uncertainty in environmental conditions, directly influencing the thermal capacity and operational reliability of transmission system components. However, current planning practices often ignore future climate constraints, limiting the potential for robust and adaptive grid development. Over extended planning horizons, these changing conditions undermine static ratings methods, which fail to capture gradual, nonlinear, or region-specific environmental changes. On the other hand, incorporating risk into the dynamic assessment of technical limits offers a more adaptable framework. Ultimately, combining climate-model uncertainty with thermal risk management requires methodological advances that go beyond current planning practices.

1.5 Contributions and Structure of the Thesis

The main objective of this thesis can be summarized as follows:

To develop a methodology for long-term power system planning that incorporates dynamic thermal ratings and accounts for climate change and local meteorological conditions.

To address the challenges outlined in Section 1.4, the thesis makes three main contributions:

Contribution 1: ***Methodology for Long-Term Thermal Rating Estimation:***

This contribution proposes a data-driven methodology for estimating long-term thermal ratings of network power system components that requires accounting for both temporal weather variability, including daily and seasonal cycles, and spatial variability, such as regional differences and topography. The objective is to balance the maximization of transmission capacity with risk management under environmental variability. The methodology is designed for integration into planning processes, providing reliable, forward-looking estimates over extended periods under changing environmental conditions.

Two research questions have been formulated to address the listed contribution:

RQ1: How can thermal ratings of power system components be defined in a manner that effectively incorporates both temporal and spatial variability?

RQ2: How can thermal ratings be defined to simultaneously maximize transmission capacity and limit operational risk?

Contribution 2: ***Integration of Thermal Ratings into Network Planning:***

This contribution formulates a NEP model that incorporates long-term thermal ratings as dynamic constraints. This enhances both cost effectiveness and operational reliability, bridging the gap between static planning and operationally dynamic approaches. In relation to planning, and following the identification of two key research questions, the following formulations have been developed:

RQ3: How can thermal ratings be integrated into long-term transmission expansion planning methodology?

RQ4: What are the operational and investment implications of incorporating thermal risk considerations into transmission planning?

Contribution 3: ***Impact of Climate Change on Transmission Capacity and Economics:***

This contribution evaluates the long-term economic and operational impacts of climate change on transmission capacity, to support the development of climate-aware expansion strategies that address projected risks under the energy transition.

The remaining two research questions to be addressed are:

RQ5: What is the impact of climate change on the thermal ratings of individual power system components, considering both temporal variations and regional climatic differences?

RQ6: What is the impact of climate change on network expansion planning, considering its influence on the thermal capacity of transmission power system components?

The following chapters address these research questions. Figure 1.9 summarizes the thesis framework, showing how contributions and research questions align with the overarching theme of integrating climate change into long-term transmission planning. The diagram illustrates the general framework of long-term thermal rating analysis and its integration into transmission network planning under climate change, emphasizing how the formulated research questions align with and address the key themes of the thesis. Each research question focuses on a specific challenge and methodological contribution, together forming an integrated framework for advancing capacity assessment under spatio-temporal climate variability.

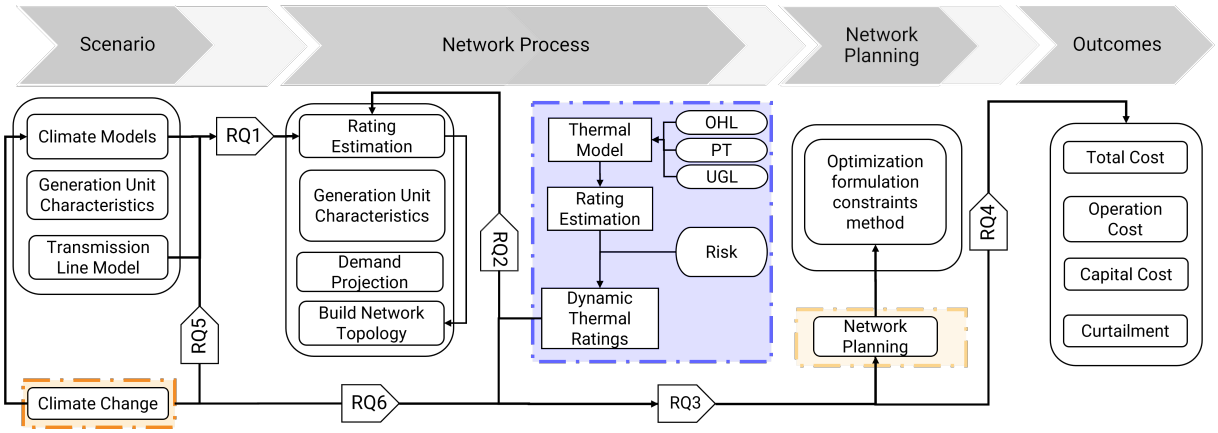

Figure 1.9: Graphical abstract of the thesis. For each contribution, the corresponding research questions are listed.

1.6 List of publications

The research presented in this thesis has resulted in the publication of articles in peer-reviewed journals and conferences. These publications reflect the development of the main research topics, particularly the integration of climate change considerations into power system planning using the probabilistic approach for thermal ratings.

The Table 1.4 provides a correspondence between each publication and the relevant chapters of the thesis, highlighting the author's contribution to the different phases of the study. This includes published, in preparation papers, and contributions to collaborative research projects.

	Chapter 2	**Chapter 3**	**Chapter 4**
Paper A	2.2.1.2, 2.3.2	3.7.3	
Paper B	2.2.1,2.3.2	3.7.1.1	-
Paper F	3.7.1.1	-	-
Paper G	-	3.7.3	4.5.2
Conf. D	2.3.2		3.7.2
Conf. E	2.3.2		-

Table 1.4: Mapping of Publications to Thesis Contributions and Chapters

Peer-reviewed journals:

- **A: Montana-Salas Sergio**, Michiorri Andrea. "Long-term climate-driven underground cable thermal ratings for network planning". *Electric Power Systems Research*, Volume 241, 2025, 111401, ISSN 0378-7796. https://doi.org/10.1016/j.epsr.2024.111401
- **B: Montana-Salas Sergio**, Michiorri Andrea. "Assessment of the influence of climate change on power grid transmission capacity." *Sustainable Energy, Grids and Networks*, Volume 42, 2025, 101695. https://doi.org/10.1016/j.segan.2025.101695
- **C:** A.I. Estanqueiro, H. Algarvio, A. Couto, A. Michiorri, **Montana-Salas Sergio**, D. Pudjianto, P. Hägglund, J. Dobschinski, R. Bolgaryn, T. Kanefendt, J. Gentle, S.M.S. Alam, Z.M. Priest, A.W. Abboud. "Dynamic Line Rating Models and Their Potential for a Cost-Effective Transition to Carbon-Neutral Power Systems." *WIREs Energy Environ*, Volume 14, 2025, e70002. https://doi.org/10.1002/wene.70002

International Conferences:

- **D: Montana-Salas Sergio**, Michiorri Andrea. "Assessing Regional Capacity Expansion: The Role of Quasi-Dynamic Thermal Ratings in a Changing Climate." *IEEE PES Innovative Smart Grid Technologies Europe*, ISGT EUROPE 2024, Conference paper. https://doi.org/10.1109/ISGTEUROPE62998.2024.10863802
- **E: Montana-Salas Sergio**, Michiorri Andrea. "Weather-Based Quasi-Dynamic Thermal Ratings for Power Transformers." *IEEE PES Innovative Smart Grid Technologies Con-*

ference Europe, Conference paper. https://doi.org/10.1109/ISGTEUROPE56780.2023.10408026

Articles in preparation:

- **F: Montana-Salas Sergio**, Michiorri Andrea. "Climate-Informed Risk Assessment in Transmission Expansion Planning: Integrating Climate Change Impacts into Decision Making." In progress.
- G: **Montana-Salas Sergio**, Ruggeri Simona, Soma Gian Giuseppe, Michiorri Andrea, and Celli Gianni. "Optimizing Distribution Planning with Long-Term Thermal Ratings in the Energy Transition." In progress.

1.7 Outline of the Thesis

This thesis presents an analysis of long-term thermal ratings and their implications for electricity transmission systems in the context of climate change. The study is structured around three main components, illustrated in Fig. 1.10 and mapping of research questions across domains.

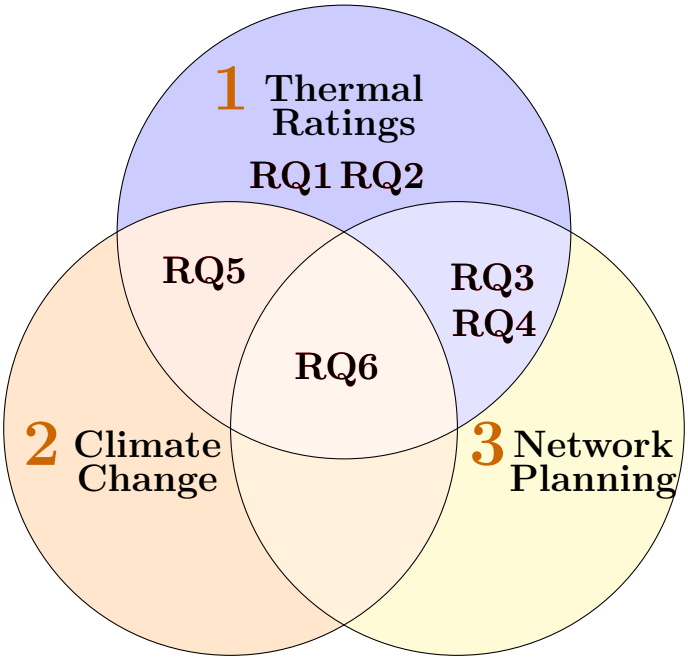

Figure 1.10: Graphical structure of the thesis illustrating the mapping of research questions across domains.

Chapter 2 begins with the estimation of ratings using thermal models, dynamic thermal rating techniques, and probabilistic functions. This chapter lays the groundwork for understanding how the ratings of transmission components can vary under different thermal conditions influenced by the space-time.

Following this, chapter 3 focuses on the integration of these ratings into power system planning. Thermal rating lower fix probabilistic threshold and stochastic approaches are examined, supported by simulation tools to assess system performance under various operating scenarios. This stage considers the topology of the network, including generation assets, load profiles, and transmission infrastructure.

Chapter 4 presents climate change as an essential consideration in long-term planning, exploring future projections and their impacts on thermal capacity and grid reliability. It highlights how climate variability can influence long-term planning decisions.

Each chapter begins with an introduction and data context, followed by a clearly defined methodology that describes each step of the process, as shown in the Fig. 1.9. Limitations are addressed to provide transparency and facilitate the interpretation of the results. The thesis concludes in Chapter 5 with key findings, broader implications, and future research directions.

Chapter 2

Long-Term Thermal Rating

Résumé en Français

Ce chapitre présente le développement et la validation d'une méthodologie de qDTR appliquée aux principaux composants des réseaux de transport d'électricité OHL, UGL et PT afin de réduire les limites des approches de capacités thermiques statiques face à la variabilité climatique. Des modèles thermiques en régime permanent, intégrant les effets de la température ambiante, du rayonnement solaire, du vent, des propriétés du sol et de l'humidité, sont élaborés pour estimer les capacités de transport et les limites opérationnelles des équipements. Pour les UGL, un modèle dynamique du sol, enrichi par des techniques d'apprentissage automatique, capture les variations spatio-temporelles de température et d'humidité, tandis que pour les PT, les pertes dépendantes de la charge et les températures d'huile sont prises en compte. En intégrant explicitement la variabilité climatique spatio-temporelle dans les modèles thermiques, cette approche comble le fossé entre les hypothèses statiques et la nécessité d'évaluations de capacité adaptatives, conciliant profondeur technique et applicabilité régionale pour la planification à long terme.

2.1 Introduction

Assessing the thermal rating of power system components is fundamental for evaluating long-term planning and reliability, particularly under changing climate conditions. In this regard, thermal models play a crucial role in determining safe operating limits based on ambient and load conditions. Traditionally, these models are used to assess the influence of environmental conditions, such as ambient temperature, wind speed, and humidity, in methodologies such as STR and all approaches related to DTR in transmission components, with defined time scales. However, for decades, they have usually been based on averaged or conservative assumptions, overlooking the full spectrum of spatio-temporal climate variability, especially for unmonitored assets.

These limitations create challenges for long-term planning, where investment and operational decisions must be made years in advance, and infrastructure improvements require long lead times. It is essential to emphasize that during the NEP process, the system must remain reliable under adverse, low-probability but critical scenarios, where unfavorable environmental conditions coincide to create the highest risk of thermal overload. Unlike operations, which allow short-term adjustments, planning must incorporate sufficient margins to guarantee reliability against extreme or prolonged climatic events.

To support reliable, climate influenced network planning, thermal models must be coupled with more dynamic and steady methodologies to incorporate the cumulative and geographically differentiated effects of weather variability over long time horizons. This includes considering gradual warming trends, changes in wind patterns, and the increased frequency of extreme weather events. In response to this need, this chapter develops a data-driven framework for estimating long-term thermal ratings of transmission system components, going beyond short-term operational models. By integrating spatio-temporal climate data into thermal modelling and applying a qDTR approach, the framework enables a nuanced, region specific assessment of thermal capacity under future environmental scenarios.

2.2 Methodology

The main objective of this chapter is to present a methodology that supports weather-aware capacity assessments, mindful of location, and suitable for long-term horizons. This forms the basis of *Contribution 1*: the development of a long-term thermal rating estimation method. To achieve this, the chapter describes a step-by-step approach for integrating climate-based thermal capacity models into long-term planning. The methodology is structured around three fundamental steps, each aligned with corresponding research questions:

Step 1: Detail the theory behind the estimation of thermal models PT, OHL, and UGL in Section 2.2.1. This forms the methodological basis for understanding how to estimate the specific thermal limits of the components under changing environmental conditions and given their geographical location, in order to address the research question **RQ1**.

Step 2: Introduce the qDTR methodology to capture the prolonged and changing impact of weather factors such as temperature trends, wind variability, and extreme weather events on thermal capacity, as detailed in Section 2.2.2. This step addresses the question **RQ2:** where the proposed method facilitates a more dynamic and flexible representation than the traditional STR concept and enables the analysis of asset performance.

Step 3: Conduct a spatially analysis of long-term thermal rating variability based on historical climate data, as described in Section 2.3.2. By applying the qDTR approach across diverse geographic regions on the continent, this step generalizes the findings from Step 1 and strengthens **RQ2**. It additionally enables capacity analysis by quantifying risks induced by the climate and regional disparities in asset performance, providing essential insights for adaptive and resilient network planning.

2.2.1 Thermal Models Methodologies

To evaluate the thermal behaviour of transmission system components under varying environmental conditions, it is necessary to establish reliable steady-state thermal models. This section presents the thermal-electric formulation for OHL, PT, and UGL. These models provide the analytical basis for estimating long-term thermal ratings and thus contribute to addressing research question RQ1, which focuses on the explicit integration of spatiotemporal variability into component rating methodologies.

While this section describes the main modelling equations and assumptions used, a complete and detailed mathematical implementation, and calculation steps, can be found in Annex A, in addition for more details regarding the nomenclature can be found in the List of Symbols table on page xi. This detailed implementation not only enables estimating component ratings under various climatic conditions but also facilitates exploring different electrical and physical configurations. By adjusting for conductor properties, material characteristics, and environmental surrounding scenarios, a flexible and extensible approach is provided.

2.2.1.1 Overhead Lines

OHLs are vital components in the electrical network, generally designed for a useful life of more than 50 years. Within this component, there are various electrical characteristics and configurations; however, it is also true that cables with ACSR are widely used due to their favourable mechanical and electrical properties.

These lines typically cover long distances, traversing diverse geographic regions and experiencing a wide range of climatic conditions. Consequently, their thermal performance is highly sensitive to environmental factors such as temperature, wind, and solar radiation, variables increasingly affected by the surrounding climatic conditions. To assess potential impacts on line capacity, standardized thermal models are used to calculate the current-carrying capacity (ampacity) of the conductors, as established in international guides and standards [29, 37, 87].

While these thermal models for OHLs share a common structure, they differ in the specific factors and assumptions used in the thermal balance calculations. However, the general form of the steady-state heat balance equation is given by:

$$Q_J + Q_M + Q_s + Q_i = Q_C + Q_R + Q_E \tag{2.1}$$

As shown in Eq. (2.1) and illustrated in Fig. 2.1 details that the total heat gained by the conductor (through Joule heating Q_J, magnetic heating Q_M, solar heating Q_s, and corona heating Q_i) must be balanced by the total heat lost (through convective cooling Q_c, radiative cooling Q_R, and evaporative cooling Q_E) without violating the temperature limit. In this thesis, the focus is placed on the most influential terms Q_J, Q_S, Q_C, and Q_R, as these are most directly affected by ambient temperature, solar irradiance, and wind conditions factors, which exhibit significant variability. Other terms, such as magnetic, corona, and evaporative cooling, are not considered due to either their minimal influence or the recommendation of the evaluation guide from which the thermal model is derived.

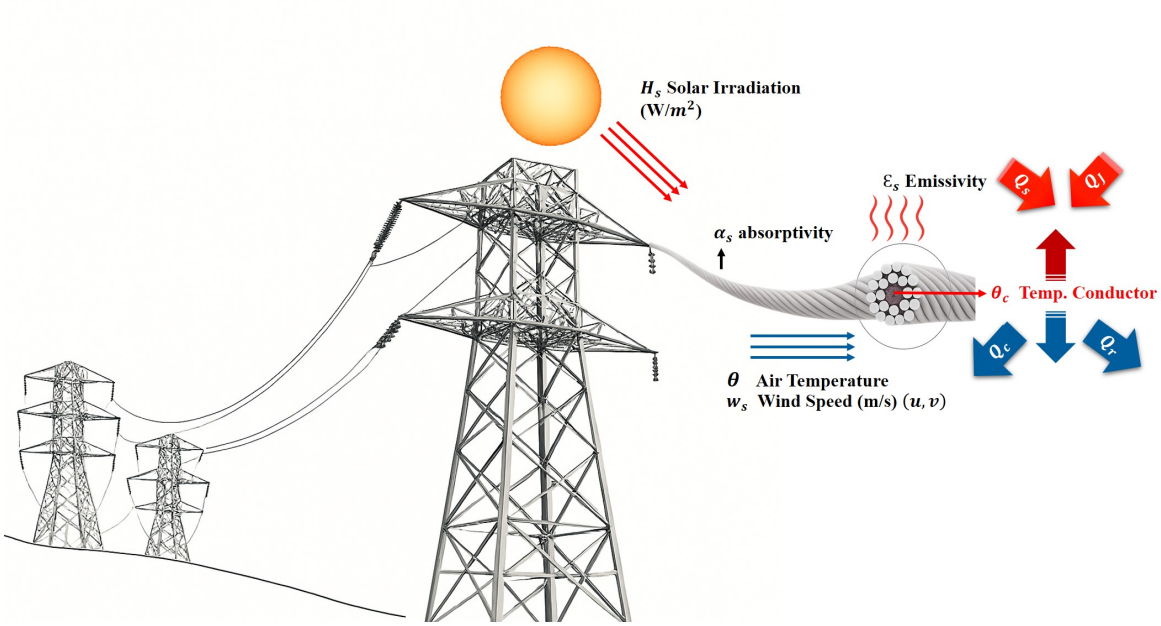

Figure 2.1: Heat Transfer Process for Overhead Lines. Based on and extended from [29]

A numerical model for calculating the line thermal rating, as outlined in [29], is as follows.

$$I = \left[\frac{(Q_r(\theta, \theta_c) + Q_c(\theta, w_s, \theta_c) - Q_s(H_s)}{R_{OHL}(\theta, \theta_c)}\right]^{(0.5)} \tag{2.2}$$

Where the parameters are influenced by: surface absorbivity for Q_s, surface emissivity, maximum allowable temperature (θ_c) and air temperature (θ) for Q_r. The parameter Q_s, depends on atmospheric values such as wind speed (w_s) and θ. For instance, applying Eq. 2.2 to a 225 kV line from [115] detailed in Fig. 2.2 reveals significant spatiotemporal variability in the line's thermal capacity. This figure helps us understand the ampacity profiles at two different times on the same component in the same year, capturing contrasting weather influences.

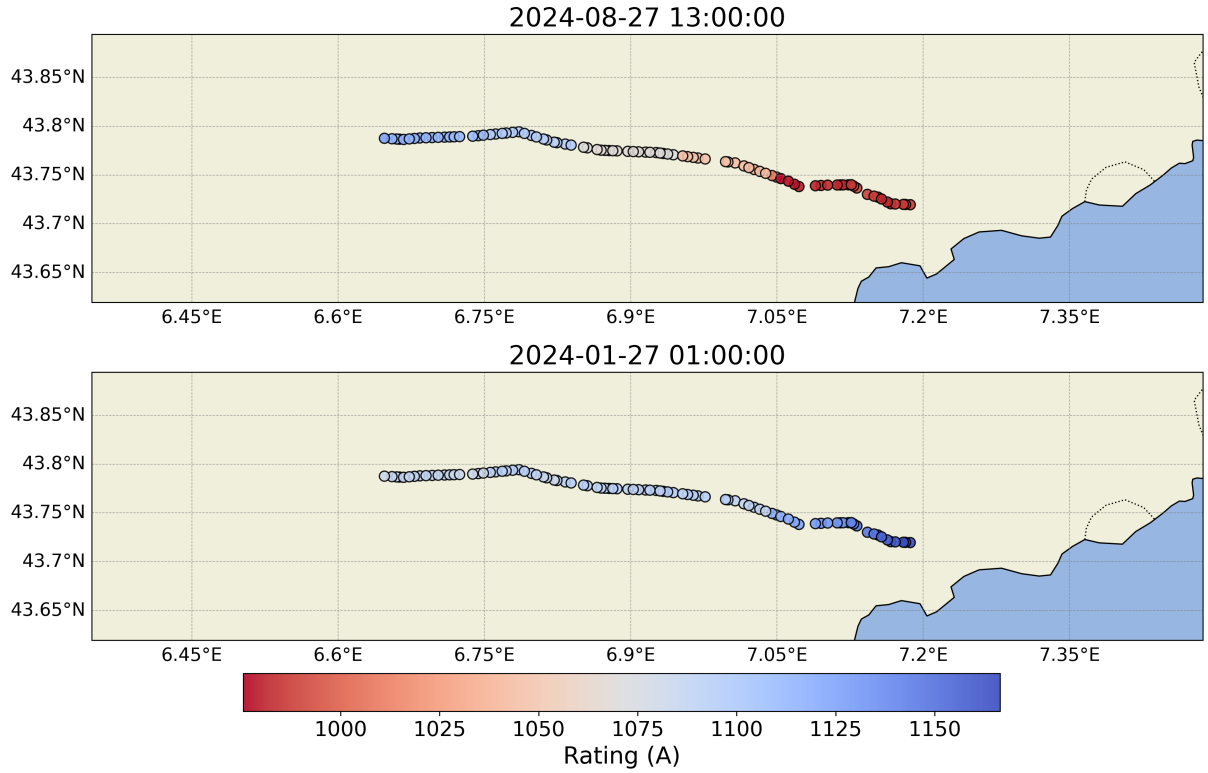

Figure 2.2: Overhead conductor 225 kV line - Lingostiere - Roumoules - Valderoure. From [115]

In particular, during the winter night (lower Fig. 2.2), conductor ampacity are generally higher (represented in cooler colours) due to lower ambient temperatures and potentially favourable wind conditions. In contrast, the summer daytime profile (upper Fig. 2.2) shows an overall reduction in current carrying capacity (represented by warmer hues) caused by increased solar radiation and higher ambient temperatures, which reduce the efficiency of convective and radiative cooling. This spatially distributed ampacity, which varies along the geographic length of the line, highlights how regional meteorological differences and diurnal effects directly influence the maximum allowable current. By integrating these variations into long-term planning through more dynamic models, grid operators can more accurately reflect environmental constraints and opportunities in transmission capacity assessments.

2.2.1.2 Underground Cables

Historically, there has been a significant disparity in the proportion of cable length installed as OHL compared to UGL on transmission [116]. This imbalance is primarily explained by the substantially higher construction costs of UGL, often several times that of OHL, as well as additional factors influencing NEP, such as public opposition and residents' risk perceptions, as detailed in [117]. However, the global demand for underground installations is steadily increasing, driven in part by the rapid expansion of RES, the need to enhance network resilience, and helps reduce public opposition to the expansion of the electricity network due to its visual impact [118]. UGLs offer a viable solution to reduce environmental-related disruptions com-

monly affecting OHL, such as wildfires and windstorms, making them an increasingly important component in modern power system planning.

As described in the previous section, OHL losses are primarily attributed to Joule heating. While UGL also experience heat generated by Joule losses (Q_j) flowing through the conductive components (Q_i) and the surrounding medium (Q_{cd}) illustrated in Fig. 2.3, is highly dependent on the soil temperature, humidity, thermal resistance (T_s), separation distance from other conductors and physical loss factors (λ) [32]. While solar irradiance, wind, and convection are usually considered negligible for buried cable, due to these factors predominantly influencing other heat transfer processes to the ground and water movement [1]; For insulated cables installed in air, convection and radiation are significant and must be taken into account [27]. A key difference lies in the surrounding environment: in OHL, ambient and wind contribute to convective cooling, providing natural electrical insulation from the ground. In contrast, UGL systems rely on synthetic insulating materials, which also act as thermal insulators, thus preventing heat dissipation from the conductor to the environment.

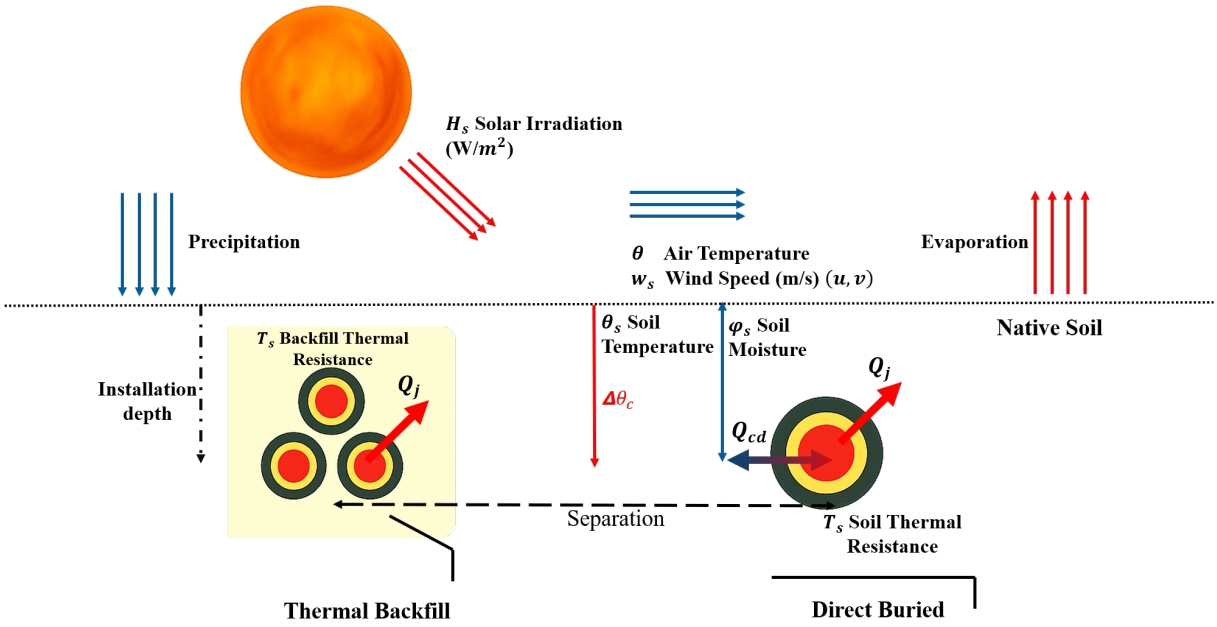

Figure 2.3: Heat Transfer Process for UGLs

Furthermore, the surrounding soil can act as a significant thermal barrier, which can have positive or negative effects, especially in dry conditions. To mitigate this, some installations incorporate specially selected fill materials designed to improve thermal conductivity and promote more efficient heat transfer. As a result, UGL typically face not only more complex heat generation sources but also more demanding cooling conditions compared to OHL. These thermal and electrical dynamics have been investigated and extended in **Paper A**.

To understand these correlations, a model is developed to quantify the long-term effect of climatic conditions on the capacity of UGL, summarized in the block diagram in Fig. 1.9. In the following subsections, the thermal models used will first be explained, mainly drawn from the

standard [51] and the research summarized in [27]. Secondly, the soil dynamics model will be explained, and finally, a supervised machine learning model will be presented to obtain all the necessary information from the previous two points. Although all these methods are applicable to buried cables, a special case is included for insulated cables in the air, given their prevalence in rural areas, as evaluated in Paper G.

A. Rating Model

To evaluate the rating of a buried cable under steady-state conditions, the thermal model specified in the IEC Standard 60287 [51] is implemented. This model takes into account the thermal interaction between the cable and its surrounding environment, such as soil type, moisture content, and installation configuration, where current capacity is calculated as a function of several influencing parameters, as shown in the generalized form Eq. (2.3). While the complete mathematical formulations of the method can be found in the Annex A, the key aspects relevant to this study are summarized below for clarity.

$$I_t = I(\theta_t, \psi_t, \text{cable construction, installation}) \tag{2.3}$$

Here, I_t represents the permissible thermal rating on time observation t, which depends on the temperature θ_t, soil thermal and moisture conditions ψ_t, design and installation characteristics of the cable. However, for buried UGL, heat flux can have an even greater influence, resulting in negative effects, where thermal conductivity can be reduced three times or more compared to the cable's conductivity. For instance, in [8], the impact of thermal resistivity in the surrounding medium (T_4 as defined in [51]) was examined for a 225 kV XLPE conductor. The results in Table 2.1 indicate that a 20% increase in thermal resistance resulted in a 15 °C increase in the conductor's temperature, necessitating a reduction in the cable's rating to maintain thermal limits. For this reason, a thermal model that accounts for this unfavorable condition, along with significant moisture migration, is also considered in this thesis.

	Parameter	**Reference**	**Increased T_4 (+20%)**
No drying out	Rated current for Θ_c = 90°C	1564 A	1453 A
	Conductor temperature for I = 1564 A	90°C	105°C
Drying out (2 zone Θ_{critical} = 60°C)	Rated current for Θ_c = 90°C	1470 A	1366 A
	Conductor temperature for I = 1470 A	90°C	119.5°C

Table 2.1: Dependency of the rated current versus the thermal resistance T_4. From [8]

According to [27, 51], the rating for UGL, considering the formation of a moisture zone around the cable, is given by:

$$
\begin{aligned}
I_t &= \sqrt{\frac{\Delta\theta_t - B + (v_t - 1)\Delta\theta_x}{R_{UGL_t}\mathrm{T1} + n_l \cdot R_{UGL_t}(1+\lambda_1)T_2 + C}} \quad \forall t \\
B &= W_d \left[\tfrac{1}{2}T_1 + n_l \cdot (T_2 + T_{3_t} + v_t T_{4_t})\right] \\
C &= n_l \cdot R_{UGL,t}\,(1 + \lambda_1 + \lambda_2)\,(T_2 + v_t T_{4_t})
\end{aligned}
\tag{2.4}
$$

This formulation emphasizes the influence of the *dry-wet thermal boundary* $\Delta\theta_x$ and the ratio v_t, which compares the thermal resistivities of the dry and wet zones in the surrounding soil. Other critical variables such as ambient temperature, precipitation, and soil moisture contribute indirectly to the values of ρ_{s_t}, $\lambda_{1,2}$, and thermal resistances $T_{1\text{–}4}$, which are determined based on the cable's construction and installation parameters.

A crucial component of this model is the thermal resistance of the surrounding medium, particularly for horizontally laid single-core cables, expressed as:

$$
T_{4_t} = \frac{\rho_{s_t}}{2\pi}\left[\ln\left(u + \sqrt{u^2 - 1}\right) + \ln\left(1 + \left(\frac{2L}{S_1}\right)^2\right)\right] \tag{2.5}
$$

In this equation, ρ_{s_t} is the thermal resistivity of the soil at t, S_1 is the distance between the axes of the cable, and $u = \frac{L}{D_e}$ is the ratio of the burial depth to the diameter. This resistivity varies according to soil conditions, such as moisture; therefore, it is essential to dynamically evaluate ρ_{s_t} to reflect the environment. This expression can be adapted for three-wire cables or installations that utilize thermal fill, as documented in [51].

Conversely, when the cable does not pass through a dry zone around the cable, Eq. 2.4 is redefined as:

$$
\begin{aligned}
I_t &= \sqrt{\frac{\Delta\theta_t - B}{R_{UGL_t}\mathrm{T1} + n_l \cdot R_{UGL_t}(1+\lambda_1)T_2 + C}} \quad \forall t \\
B &= W_d \left[\tfrac{1}{2}T_1 + n_l \cdot (T_2 + T_{3_i} + T_{4_i})\right] \\
C &= n_l \cdot R_{UGL_t}\,(1 + \lambda_1 + \lambda_2)\,(T_2 + T_{4_i})
\end{aligned}
\tag{2.6}
$$

When insulated conductors are installed outdoors, the external thermal resistance must be adjusted to account for both convective and radiative heat dissipation mechanisms. During the day, they would be directly exposed to solar radiation, which, similar to the OHL, presents an additional thermal influence on the cable's outer surface. This additional heat input is quantified from [27] by the term $\sigma D^* H$, where σ represents the surface absorption coefficient, D^* is the cable's external diameter, and H is the intensity of solar radiation in $\mathrm{W/m^2}$.

The rating expression presented is adapted in the B factor, and the results are as follows:

$$
B = W_d\left(0.5T_1 + n_l \cdot (T_2 + T_3 + T_{4_i}^*)\right) + \sigma D^* H_{s_i} T_{4_i}^* \tag{2.7}
$$

In this expression, T_4^* represents the adjusted thermal resistance of the external environment, which now includes the effect of solar exposure.

B. Soil Temperature and Moisture Dynamics for Thermal Analysis

Understanding the dynamic interaction between soil properties and atmospheric conditions is increasingly important, especially in variable climate scenarios. As highlighted in previous studies, soil temperature and moisture are key factors influencing the maximum current rating of UGL. Conventional approaches typically rely on static or fixed values of soil thermal properties to ensure their practical applicability. However, for long-distance applications, such as cables extending hundreds of kilometres, these static assumptions often lead to overly conservative estimates, reducing operational efficiency as soils are not homogeneous.

Among the parameters that affect cable thermal performance, soil thermal conductivity plays a significant role. In recent decades, various empirical and semi-empirical models have been proposed to estimate this property, incorporating factors such as soil moisture, texture, and organic matter. Notably, the model proposed in [119] integrates detailed soil physical and compositional characteristics, offering greater estimation accuracy under various environmental conditions and has demonstrated high predictive capacity ($R^2 = 0.98$) across ten different soil types. Given that climate datasets are used in this research to obtain long-term meteorological information, an important limitation becomes evident: climate projection datasets generally provide information on soil moisture (typically limited to the upper 10 cm) but lack sufficient data for deeper soil layers, where UGL are buried. Furthermore, the depth-projected soil temperature profiles tended to be overly smoothed, failing to capture the extreme conditions that significantly affect thermal ratings [120].

To address these challenges, this thesis searched for existing studies on soil moisture and temperature dynamics, focusing on models that incorporate multiple soil properties to more accurately reflect these complex processes. Leveraging these findings, an approach is proposed for estimating soil thermal properties at typical burial depths in UGL. This approach is scalable to regional applications by integrating publicly available soil datasets, as detailed in **Paper A**, and practically implemented in **Paper B**.

The core of the methodology consists of implementing a dynamic soil model enhanced by machine learning techniques (see Subsection 2.2.1.2), capable of capturing spatiotemporal variations in soil physical parameters. However, a crucial step in this process is the development of a mathematical relationship between the soil's physical-hydraulic characteristics and its thermal conductivity λ_s, which is inversely proportional to its thermal resistivity ρ_s.

To do this, we adopt an empirical formulation based on the work of [119, 121], which effectively models the behaviour of unsaturated soils. This model estimates λ_s by limiting it between the dry and saturated thermal conductivities (λ_{dry}, λ_{sat}) and using the Kersten number K_e, which captures the nonlinear effects of soil moisture:

$$\lambda_{s_t} = (\lambda_{sat_t} - \lambda_{dry_t})K_{e_t} + \lambda_{dry_t}, \quad \forall t \tag{2.8}$$

$$K_{e_t} = \exp\left(\alpha_s - \psi_t^{-\beta_s}\right) \tag{2.9}$$

In the above equations:

- ψ_t: Volumetric water content on observation t
- λ_{sat_t}, λ_{dry_t}: Saturated and dry thermal conductivity, respectively
- K_{e_t}: Kersten coefficient capturing moisture influence on thermal transfer

The shape parameters α_s and β_s govern the sensitivity of K_e to moisture content and are computed from the soil's particle size distribution and organic content:

$$\alpha_s = a_1 S_{\text{Sand}_\%} + a_2 S_{\text{Silt}_\%} + a_3 S_{\text{Org}_\%} + a_4 \tag{2.10}$$

$$\beta_s = b_1 S_{\text{Clay}_\%} + b_2 S_{\text{Org}_\%} + b_3 \tag{2.11}$$

The coefficients for these empirical relationships are listed in Table 2.2:

a_1	a_2	a_3	a_4	b_1	b_2	b_3
0.493	0.860	0.014	0.778	0.736	0.006	0.222

Table 2.2: Empirical coefficients for estimating thermal conductivity of soil

Using the above methodology and the features described in Table 2.3, it is estimated the thermal conductivity λ_s and its inverse, the daily soil thermal resistivity ρ_s, are estimated. These values are essential for calculating the υ-ratio (the dry-to-wet thermal resistivity ratio), which directly affects the thermal capacity of UGL operating under varying environmental conditions.

C. Estimating soil moisture and temperature

This module aims to enhance the estimation of soil moisture $(\hat{\psi})$ and temperature $(\hat{\theta_s})$ beyond what is offered by climate datasets. These variables are critical inputs to the UGL thermal model. The calculation is constrained by the input data described in Section 2.2.3, with a spatial resolution of 0.25°, a daily temporal resolution, and depth coverage from 0.8 to 1.2 meters. Feature selection was informed by a literature described in **Paper A**, focusing on relevant time series of meteorological variables, soil characteristics, and in situ measurements.

To prepare the data for modelling, the following preprocessing and transformation steps were performed:

a. Extraction of anomalies.

b. Removal of low-quality data, using intrinsic information, and including exclusion of stations with fewer than three months of valid data per year.

c. Interpolation to a consistent daily frequency.

d. Encoding of the cyclical day-of-year variable (t_c);

e. Min-max normalization of all input features.

f. Feature selection, optimized to maximize model prediction accuracy.

g. Encoding of soil types (S_{code}) based on the USDA soil texture classification system, as detailed in Table 1 of **Paper A**.

In this process, multiple machine learning algorithms were initially evaluated to identify the most appropriate modelling approach. These models were compared with in-situ data on soil moisture, temperature, and taxonomic classification from the International Soil Moisture Network (ISMN), covering depths from 0.05 m to 1.6 m, detailed in Fig. 2.4. These long-term, high-quality measurements are crucial for validating our model and for assessing the climate sensitivity of soil hydrological and thermal behaviour. It used the same training process, using a five-day rolling window of lagged observations previously determined via time series analysis using the partial autocorrelation function. The dataset is partitioned by both station and soil type. The training set comprises 70% of the total data, with 10% reserved for hyperparameter tuning using methods outlined in [122]. The remaining 30% is used for validation. To prevent overfitting, N-fold cross-validation is applied, ensuring that each fold maintains a representative distribution of soil types for robust performance evaluation.

The Selection criteria prioritized predictive accuracy measured by Root Mean Square Error (RMSE) and Mean Absolute Error (MAE), as well as computational efficiency, which is essential for the model's regional scalability in a continental domain. The results of this are illustrated in the following Fig. 2.5, where "ERA" refers to the historical data of moisture data from layer 4 (refer to Table 2.3). In this process, several machine learning algorithms were initially evaluated to determine the most suitable modelling approach. Models trained by the Extreme Gradient Boosting (XGBoost) [123] demonstrate notably strong performance, significantly reducing the error in soil-specific observations. Other models, such as Regression Trees (RT), K-Nearest Neighbors (k-NN), Random Forest (RF), Long Short-Term Memory Networks (LSTM), and Lasso Linear Regression, were also considered. The k-NN and LSTM models demonstrated moderate prediction accuracy, but they incurred higher computational costs and tended to overestimate moisture by approximately $+0.05\ m^3m^{-3}$ relative to observations.

Based on the analysis, XGBoost was selected as the model for soil moisture prediction due to its balance of accuracy and efficiency. For temperature estimation, Lasso Linear Regression yielded the most favourable results and was therefore adopted.

Only for a general representation of the procedure, the following mathematical formulation is provided. A more extensive and detailed description of the models can be found in [123, 124].

$$\hat{\kappa} = \arg\min_{\kappa \in \mathbb{R}^p} \frac{1}{2n} \|\theta_s - \Phi\kappa\|_2^2 \ + \ \alpha\|\kappa\|_1 \tag{2.12}$$

where:

$\theta_s \in \mathbb{R}^n$	observed soil temperature vector
$\Phi \in \mathbb{R}^{n \times p}$	input feature matrix (θ, H_s, S_r)
$\kappa \in \mathbb{R}^p$	vector of model coefficients
$\alpha \in \mathbb{R}_{\geq 0}$	regularization parameter

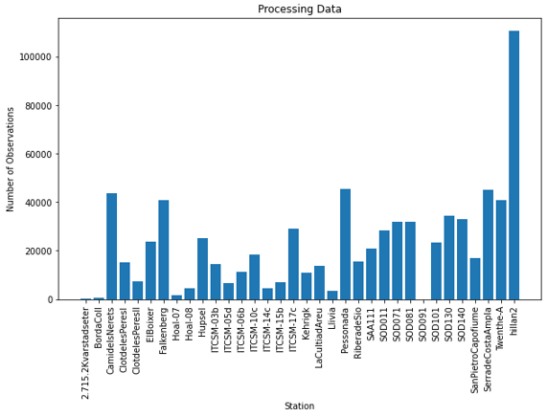

(a) Moisture Observation Density Across Stations

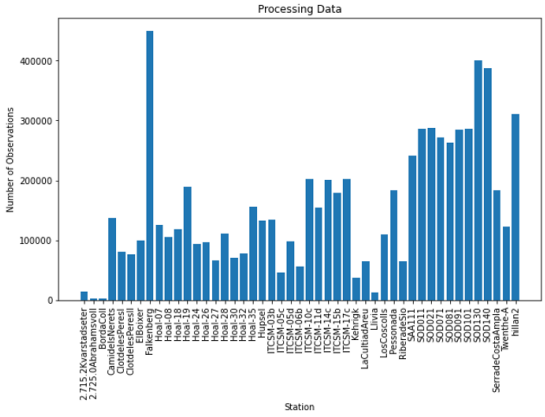

(b) Temperature Observation Density Across Stations

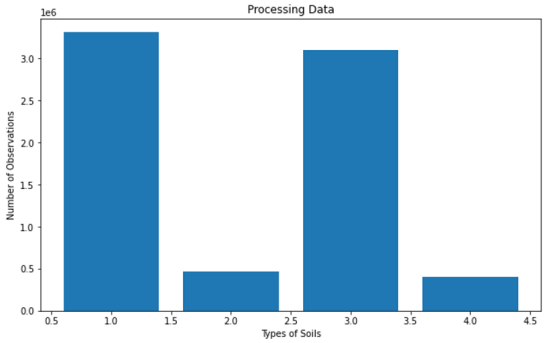

(c) Type of Soils Observation Density

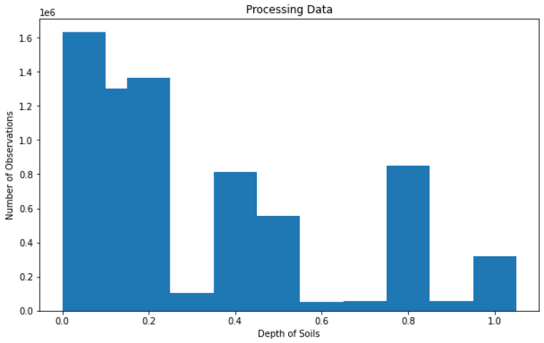

(d) Depth Observation Density

Figure 2.4: Data processed from the International Soil Moisture Network

The prediction for soil temperature is then:

$$\hat{\theta}_s = \Phi\hat{\kappa} \tag{2.13}$$

The general equation for the XGBoost Soil moisture Model is:

$$\hat{\psi}_t = \sum_{k=1}^{K_t} f_k(\phi_t), \quad f_k \in \mathcal{F} \tag{2.14}$$

where:

$\hat{\psi}_t \in \mathbb{R}$	predicted Soil Moisture for the i-th sample
$\Phi_t \in \mathbb{R}^p$	feature vector for the i-th sample
f_k	the k-th regression tree
$\mathcal{F}$	space of all possible regression trees
$K_t \in \mathbb{N}$	total number of trees in the ensemble by hyperparameters

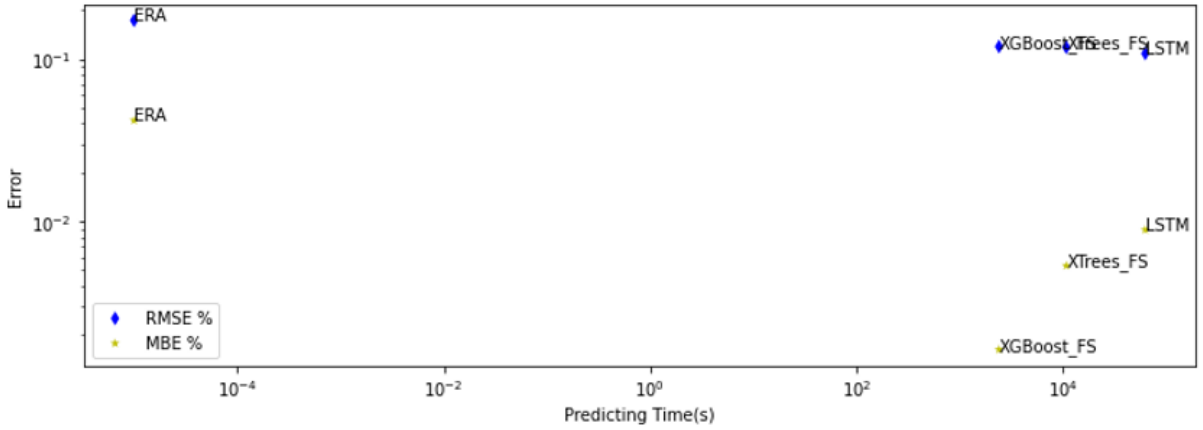

Figure 2.5: Performance Comparison of Machine Learning Models for Soil Moisture Estimation

2.2.1.3 Power Transformers

In this component, the main sources of heat generation (Q_j) are winding losses (q_{cu}), core losses (q_{fe}) and stray losses due to leakage flow, underlined in Eq.(2.15) and illustrated in Fig 2.6. In this process, the heat is initially transferred to the cooling medium by conduction (Q_c) and subsequently dissipated mainly by the dominant mechanism, along with radiation (Q_r) in transformer walls. This dissipation process is usually enhanced by natural or forced cooling systems and is governed by the oil and ambient temperatures (θ_{oil}, θ) [125].

$$Q_J(q_{cu}, q_{fe}) = Q_c(\theta_{oil}) + Q_r(\theta) - Q_s(\psi_r) \tag{2.15}$$

This continuous process achieves balance when the heat generated by the core and windings is equal to the heat dissipated by the cooling system [49]. Furthermore, since these transformers are not always housed indoors, solar radiation (Q_s) can influence their outdoor thermal behaviour, effectively reducing the net heat dissipation to the environment. An overview of cooling configurations and associated heat dissipation mechanisms is provided in [125], where the direct effect of adding auxiliary cooling equipment, which generates an increase in airflow, results in an impact on the rating of over 30 per cent.

To represent this, a thermally driven rating approach for PTs is employed, as detailed in the IEC 60076-7 loading guide [35], which is widely recognized in both industry and academia. In this approach, the rating of a PT is primarily constrained by the HotST, as defined by both the IEC and IEEE standards, since it directly influences insulation ageing, asset lifespan, and operational risk. Accurate HotST estimation is critical for enabling flexible loading strategies, predictive maintenance, and long-term asset planning.

The thermal model employed in this methodology integrates ambient temperature, predefined transformer-specific thermal gradients, and top-oil temperature, which is calculated using steady-state formulations. Specifically, the HotST (θ_h) is derived from the sum of the top-oil temperature (θ_o) and the hot-spot gradient rise ($\Delta\theta_h$). At the same time, θ_o itself is calculated using a load-dependent power loss expression that incorporates oil characteristics and exter-

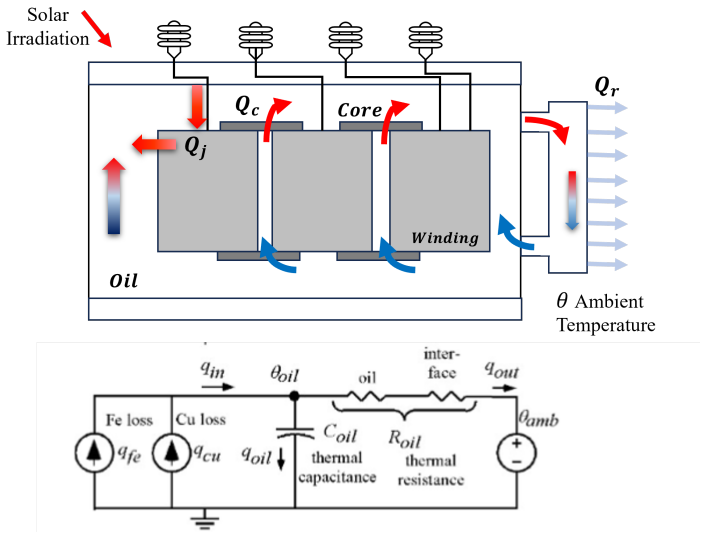

Figure 2.6: Thermal model of oil-to-air heat transfer. Based and Derived from [126]

nal factors. Enhancing the base IEC model, this approach includes correction factors for solar radiation, surface properties, and a dynamic representation of temperature-dependent losses, improving the impact under variable environmental conditions [127, 128].

$$\theta_o = \left[\frac{1 + K^2 R_{ll}}{1 + R_{ll}} + \frac{H_s}{P_{LL} + P_{NL}}\right]^{x_r} (\Delta\theta_{or}) + \theta \tag{2.16}$$

$$\theta_h = \theta_o + \Delta\theta_h \tag{2.17}$$

$$\theta_h = K^y \Delta\theta_{hr} + \left[\frac{1 + K^y R_{ll}}{1 + R_{ll}}\right]^{x_r} \Delta\theta_{or} + \theta_a \tag{2.18}$$

Here, $\Delta\theta_{or}$ (°C) denotes the steady-state temperature rise at rated losses; x_r represents the exponent associated with the oil temperature rise due to total losses, while R_{ll} denotes the ratio of load losses at rated current to no-load losses at rated voltage. The HotST serves as the central limiting parameter for the design and is instrumental in calculating the load factor K (per unit) per iteration. This load factor is defined as the ratio of the load current to the rated current. Additionally, from [113], the solar power is normalized into the load P_{LL} and the no-load losses P_{NL} in Eq. 2.16. Temperature correction due to ambient temperature changes is incorporated based on the methods outlined in [127, 128]. Finally, the capacity is calculated using the reverse calculation of the steady-state thermal model described in [129], described in Eq. 2.18, with a detailed explanation provided in Section A.2.1.

2.2.2 Quasi-Dynamic Thermal Ratings

In this thesis, the approach of Quasi-Dynamic Thermal Ratings is adopted as the principal methodology for conducting rating evaluation, which aims to establish a bridge between the traditionally used STR, commonly employed in long-term analysis and planning, and the highly variable real-time DTR, typically introduced in short-term planning studies. This difference in capacity over the year and the risk of overload during the summer months can be observed in the Fig. 2.7, where the two rating methodologies for the OHL in the example of Fig. 2.2 are quantified over the course of a year. As previously discussed in the literature, the qDTR method introduces a probabilistic framework that integrates thermal dynamics over defined time intervals, such as monthly or seasonal periods, while maintaining a conservative approach to risk decision-making. However, this model requires updates to facilitate the creation of a comprehensive data-driven methodology that accommodates both the temporal variability of climate and the regional differences in climate and topography, while effectively addressing related risks. This enhanced approach allows transmission operators to promote the dynamism and flexibility of their thermal ratings, avoiding the complexities and data or equipment requirements of real-time DTR, thereby mitigating the potential overload risks illustrated in Fig. 2.2.2 with red dots.

By applying statistical analysis and other probabilistic methodologies with defined confidence levels (e.g., 1% fixed-probability threshold), qDTR enables the estimation of thermal ratings that reflect environmental variability and operational uncertainties, thereby improving decision-making in long-term network planning and asset management. This method not only captures the capacity margin offered by favourable environmental conditions but also limit the risk of overloading under adverse scenarios, supporting a more adaptive operating strategy for transmission system operators.

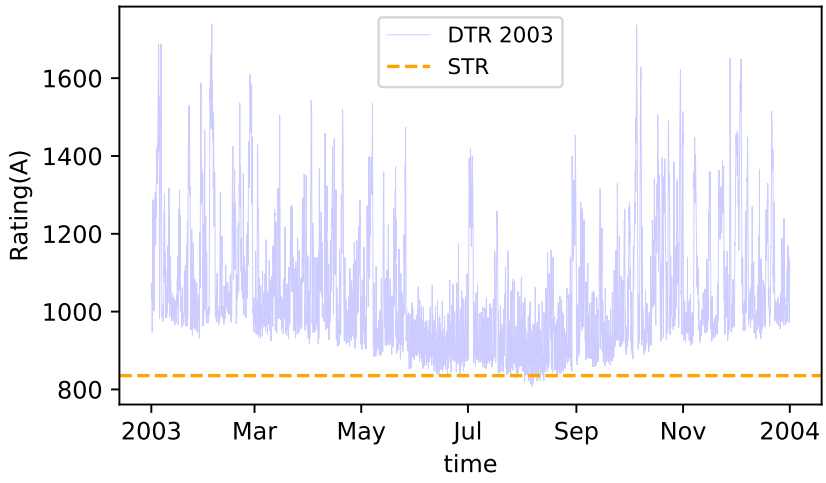

(a) DTR at steady state vs STR over the year 2003.

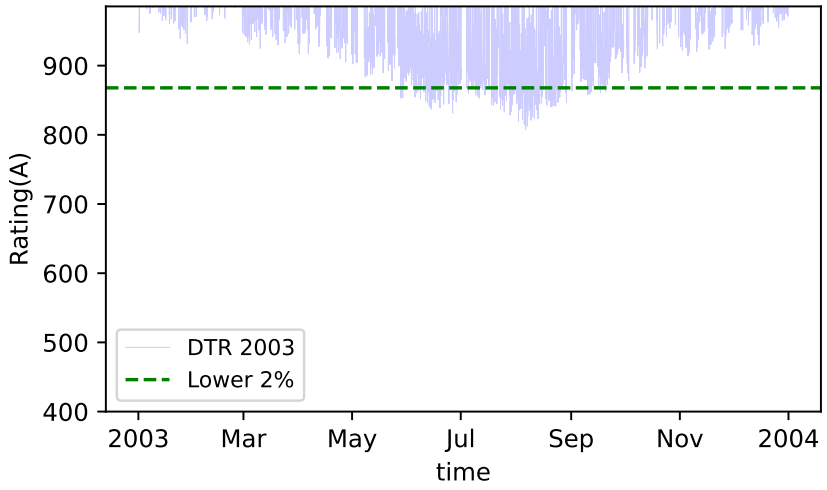

(b) Lower quantile threshold of DTR

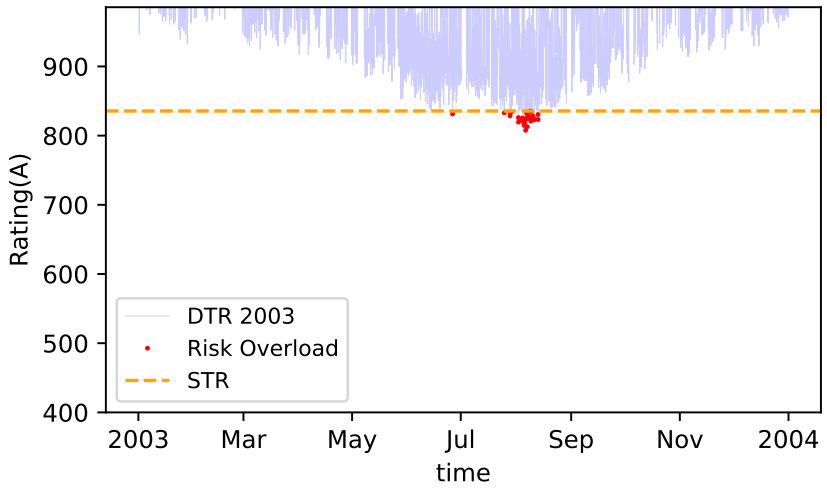

(c) Overload risk in 2003 when the STR method is selected.

Figure 2.7: Annual Comparison of Rating Methodologies for the OHL - 225 kV line - Lingostiere - Roumoules - Valderoure [115], also analyzed in Fig. 2.2. Here, the DTR represent the ampacity of the component, during the evaluated period and using the thermal model described in Section 2.2.1.1.

This methodological approach, originally introduced in [115], has since been implemented in other components and expanded across space and scenarios time domains specifically for UGL in papers **Paper B**, and for OHL and PT in **Paper A**, respectively, is graphically illustrated in Fig. 2.8 and algorithmically outlined in 2.2.2.1. It proceeds through the following five steps:

1. **Step 1:** At each spatial coordinate and for every hourly time step **(t)** within the defined time horizon scenario **(T)**, typically over a period of 50 years, the steady-state DTR is calculated by applying the appropriate thermal model corresponding to each type of power

system component. These include Eq. 2.2 for OHL, Eq. 2.4 for UGL, and Eq. 2.18 for power transformers. For OHL and UGL, which may span several kilometres, the minimum rating value across the entire length of the asset is selected for each time step to ensure robust estimation.

2. **Step 2:** The resulting DTR values are grouped into predefined temporal intervals **(TI)**, such as yearly, monthly, or monthly/hourly resolutions, according to the input selection in the analysis.

3. **Step 3:** For each temporal group, a power-law function is fitted to the lower tail of the DTR distribution. This predefined tail selection, set by the system operator, ensures a conservative assessment of extreme thermal loading scenarios.

4. **Step 4:** A probability threshold is defined (e.g., $x_R = 0.1\%$ in this example) to capture extreme conditions with low probability but potentially high impact. Assignment of this threshold can follow either a fixed selection to limit overload exposure, or risk-aware approach, as discussed in Section 3.4.

5. **Step 5:** Finally, the quasi-Dynamic Thermal Rating is derived in terms of current intensity $I(x_R)$, as expressed in Eq. 2.19, where A_f and α are the fitted parameters (normalization constant and Scaling parameter), and c is the zero-probability offset term.

$$I(x_R) = A_f x_R^{\alpha} + c, \tag{2.19}$$

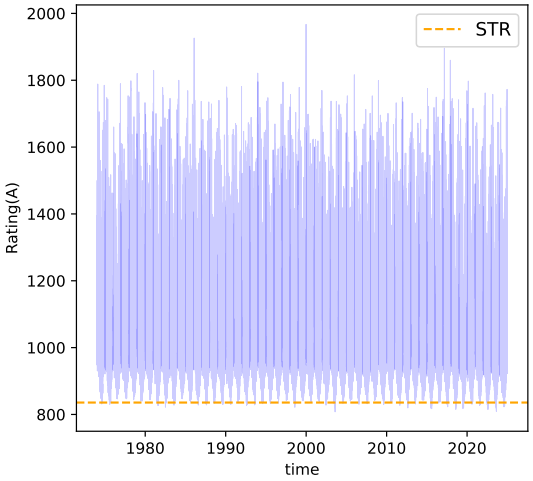

(a) **Step 1**: DTR Calculated over the 50 Year period, for the 225 kV line Lingostiere - Roumoules - Valderoure [115].

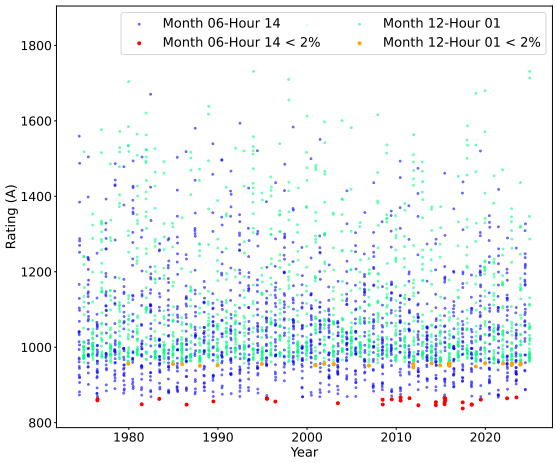

(b) **Step 2**: Grouping by month/hour temporal intervals, illustrated here for June at 14h and January at 12h.

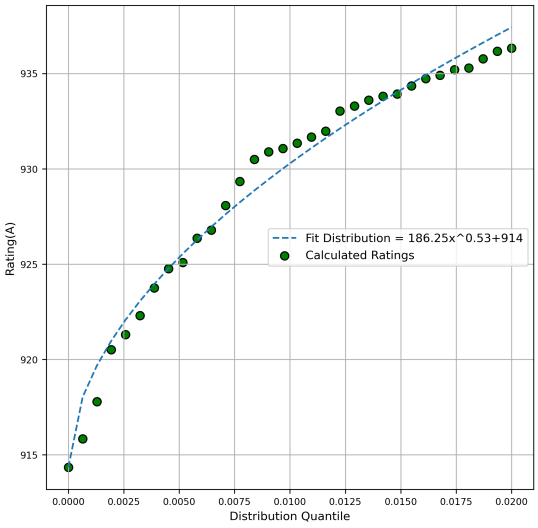

(c) **Step 3**: Power Law Fit at Lower 2 Percentile, in this case for Jan/01

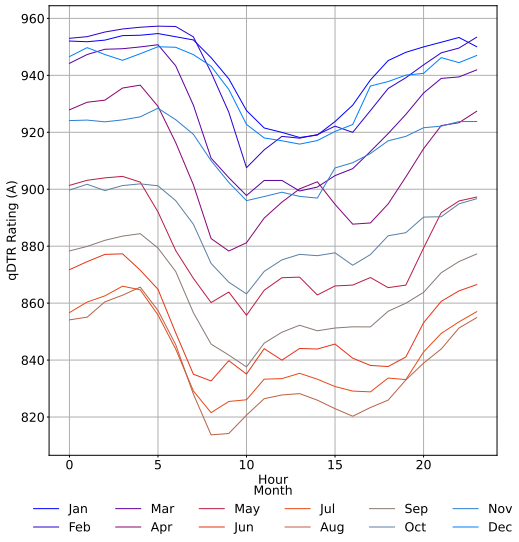

(d) **Step 4**: Month/Hour Representation of qDTR from Historical Data, estimated with a fixed-probability threshold of 0.1%

Figure 2.8: Details the four-step process of qDTR, using the OHL evaluated is a 225 kV line - Lingostiere - Roumoules - Valderoure [115] as an example, also analyzed in Fig. 2.2

This process allows the estimation of new long-term planning ratings that incorporate both the dynamic thermal behavior of the components and a quantifiable probability threshold to determine the risk profile, offering a practical alternative between traditional STR models and fully dynamic models.

2.2.2.1 General Algorithms for the qDTR Estimation

Algorithm 1: PT

Input:$(\theta_a, H_s, x_y, y, TI)\ \forall\ \mathbf{t} \in T$

Output: Rating $I_{\text{qDTR,TI}}$ at X_R

1. Define Thermal model for Iteration:
a. Losses correction due θ [127, 128]
b. Define Thermal Model In or Outdoor
$f(K) =$ 2.18

2.Calculate DTR :

Solve for $\forall\ t \in$ T
$K' = K - \frac{f(K)}{f'(K)}$
until $|K' - K| < 1e^{-3}$
$I_{\text{rated, K}} = I_{\text{rated},K'}$

$I_{\text{DTR,t}} = I_{\text{DTR,t}} \cup \{I_{\text{rated (K)}}\}$

3.Define Subgroups by $g(TI)$**:**

$I_{DTR,g} = \{i \mid i = g(TI),\ TI \in I_{DTR,t}(TI)\}$
$I_{\text{DTR,g},<2\%} = \{h \in I_{DTR,g} \mid h < q_{2\%}\}$
Where
$q_{2\%} = \{P(I_{\text{DTR,g,}} \leq h) \geq 2\%\}$

4.Compute Power Law Fitting from each $I_{\mathbf{DTR,g},<2\%}$:

$f(x) = Ax_R^{\alpha} + c$

5.Evaluate the qDTR for a thermal fixed-probability threshold $\mathbf{x_R}$**:**

$I_{qDTR}(0.1\%)_g \leftarrow \mathbf{A}(\mathbf{0.1}\%)^{\alpha} + c$

Algorithm 2: UGL

Input: $(\theta_a,\ H_s,\ Soil_{\%}, S_r,\ P_t, w_s,\ conductor,\ TI)\ \forall \mathbf{t} \in T$

Output: Rating $I_{\text{qDTR,TI}}$ at X_R

1. Define Thermal Model for Iteration:
a. Calculate $\hat{\theta_s}$ and $\hat{\psi}$ using Eq. 2.13, Eq. 2.14, Eq. A.27, and Eq. A.29
b. Define Thermal Model with or without Dryout
$f(I) =$ Eq. 2.4 or Eq. 2.6

2. Calculate DTR:

Solve for all $t \in T$:
$\Delta\theta_c = \theta_{c,max} - \theta_c$
$R = f(\text{cable}, \text{soil}, \theta)$
$I'_{\text{rated}} = f(I)$
until
$\Delta I < \varepsilon_I$ and $\Delta\theta < \varepsilon_T$
$I_{\text{DTR},t} = I_{\text{DTR},t} \cup \{I'_{\text{rated}}\}$

3.Define Subgroups by $g(TI)$**:**

$I_{DTR,g} = \{i \mid i = g(TI), TI \in I_{DTR,t}(TI)\}$
$I_{\text{DTR,g},<2\%} = \{h \in I_{DTR,g} \mid h < q_{2\%}\}$
Where
$q_{2\%} = \{P(I_{\text{DTR,g,}} \leq h) \geq 2\%\}$

4.Compute Power Law Fitting from each $I_{\mathbf{DTR,g},<2\%}$:

$f(x) = Ax_R^{\alpha} + c$

5.Evaluate the qDTR for a thermal fixed-probability threshold $\mathbf{x_R}$**:**

$I_{qDTR}(0.1\%)_g \leftarrow \mathbf{A}(\mathbf{0.1}\%)^{\alpha} + c$

Algorithm 3: OHL

Input:$(\theta_a, H_s, w, TI,\ conductor, \alpha, \beta, \gamma)\ \forall\ \mathbf{t} \in T$

Output: Rating $I_{\text{qDTR,TI}}$ at X_R

1. Define Thermal model for Iteration:
a. Calculate Qs, Qr and Qc:

using Eq.s in Sections A.1.2,A.1.4, A.1.3,A.1.4.4
c. Define rating functions:
$f(I) =$ 2.2 *or* 2.7 (for Insulated)

2.Calculate DTR :

Solve for $\forall\ t \in$ T
$\theta_c = \theta_{c,max}$
$I'_{\text{rated}} = f(I_{\theta_c})$
$I_{\text{DTR,t}} = I_{\text{DTR,t}} \cup \{I'_{\text{rated}}\}$

3.Define Subgroups by $g(TI)$**:**

$I_{DTR,g} = \{i \mid i = g(TI),\ TI \in I_{DTR,t}(TI)\}$
$I_{\text{DTR,g},<2\%} = \{h \in I_{DTR,g} \mid h < q_{2\%}\}$
Where
$q_{2\%} = \{P(I_{\text{DTR,g,}} \leq h) \geq 2\%\}$

4.Compute Power Law Fitting from each $I_{\mathbf{DTR,g},<2\%}$:

$f(x) = Ax_R^{\alpha} + c$

5.Evaluate the qDTR for a thermal fixed-probability threshold $\mathbf{x_R}$**:**

$I_{qDTR}(0.1\%)_g \leftarrow \mathbf{A}(\mathbf{0.1}\%)^{\alpha} + c$

2.2.3 Databases and Data Overview

Variable	Units	Section	Source	Process
Weather Reanalysis				
Temp. Air at 2 m (θ)	K	2.2.1.1, 2.2.1.2, 2.3.1	[6]	UGL, OHL, PT Thermal model
Total precipitation (S_r)	m	2.2.1.2, 2.3.1	[6]	UGL Thermal model ψ and θ_s Estimation
Net surface solar radiation (H_s)	J m^{-2}	2.2.1.1, 2.2.1.2, 2.3.1	[6]	UGL, OHL ,PT Thermal model
Wind u-v components at 10 m	m s^{-1}	2.2.1.1, 2.2.1.2,2.3.2	[6]	UGL, OHL Thermal model
Soil temperature at layer 4 (θ_{s4})	K	2.2.1.2, 2.2.1.2	[6]	UGL Thermal model Soil Heat Transfer
Soil moisture at layer 4 (ψ_{s4})	m^3 m^{-3}	2.2.1.2, 2.2.1.2	[6]	UGL Thermal model Soil Heat Transfer
Soil Properties				
Silt ($S_{silt\%}$)	%	2.2.1.2, 2.2.1.2	[130]	UGL Thermal model
Sand ($S_{sand\%}$)	%	2.2.1.2, 2.2.1.2	[130]	UGL Thermal model
Clay ($S_{clay\%}$)	%	2.2.1.2, 2.3.1	[130]	UGL Thermal model
Organic matter ($S_{org\%}$)	%	2.2.1.2, 2.3.1	[130]	UGL Thermal model
Texture Composition (S_{text})	-	2.2.1.2	[130]	UGL Thermal model
Bulk density (S_{bulk})	kg m^{-3}	2.2.1.2	[130]	UGL Thermal model
Soil Observations and Machine Learning Models				
Temperature (θ_s)	K	2.2.1.2, 2.3.1	[131]	UGL Thermal model LASSO Model
Moisture (ψ)	%	2.2.1.2, 2.3.1	[131]	UGL Thermal model XGBoost Model
Component Data				
Overhead Line	kV, A	2.3.1	Annex B	-
Power Transformer	MVA	2.3.1	Annex B	-
Underground Cable	kV, A	2.3.1	Annex B	-

Table 2.3: Data Overview in Long-term Thermal Ratings

2.3 Results

The following section explores how weather conditions affect the capacity of the transmission network. The objective is to evaluate the effectiveness of the proposed method to quantify the ratings (qDTRs), taking into account the heat transfer mechanisms of various terrains, locations and complexities introduced by climate-induced changes.

This analysis is conducted at both the component and regional scales, applying the methodology described in Section 2.2. The evaluation proceeds in two steps: (1) Assess how qDTR influences the allowed transmission capacity at the component level, and (2) Evaluate the impact of weather on network transmission capacity based on qDTR calculations at the regional scale.

For the sake of clarity, it should be noted that the data presented in the following sections were selected for their representative value, either as extreme cases, typical values, or for their relevance to the research objectives.

2.3.1 qDTR: Analyzed at the component level

This section uses data from papers **B** (OHL,PT), **A** (UGL), and **E** (OHL,PT).

(A). Overhead Lines

The advantage of qDTR lies in its ability to facilitate analysis at different temporal resolutions and risk thresholds associated with component overload. For instance, the Fig. 2.9 illustrates how various temporal resolution qDTR values can be obtained using the 225 kV OHL - Lingostiere - Roumoules - Valderoure analyzed in the previous figures and following the algorithm described in Section 2.2.2. These values serve as the basis for subsequent analysis over multiple long-term planning horizons. From Fig. 2.9a to Fig. 2.9d, a progressive assessment of the qDTR temporal resolutions applied to the year-horizon case. Fig. 2.9a shows the hourly rating profile for the whole year using the steady-state thermal model, overlaid with the annual qDTR threshold, mainly detailing a conservative result in selecting such a low rating. Fig. 2.9b introduces a day/night approach where thermal ratings are defined by month and time of day, distinguishing between day and night ratings. Fig. 2.9c adds a more refined approach using a month/hour-based rating that accounts for hourly variations across months, providing a more detailed envelope for the ratings curves. Finally, Fig. 2.9d compiles all approaches into a visual comparison, allowing direct observation of where the actual ampacity remains within or exceeds each threshold.

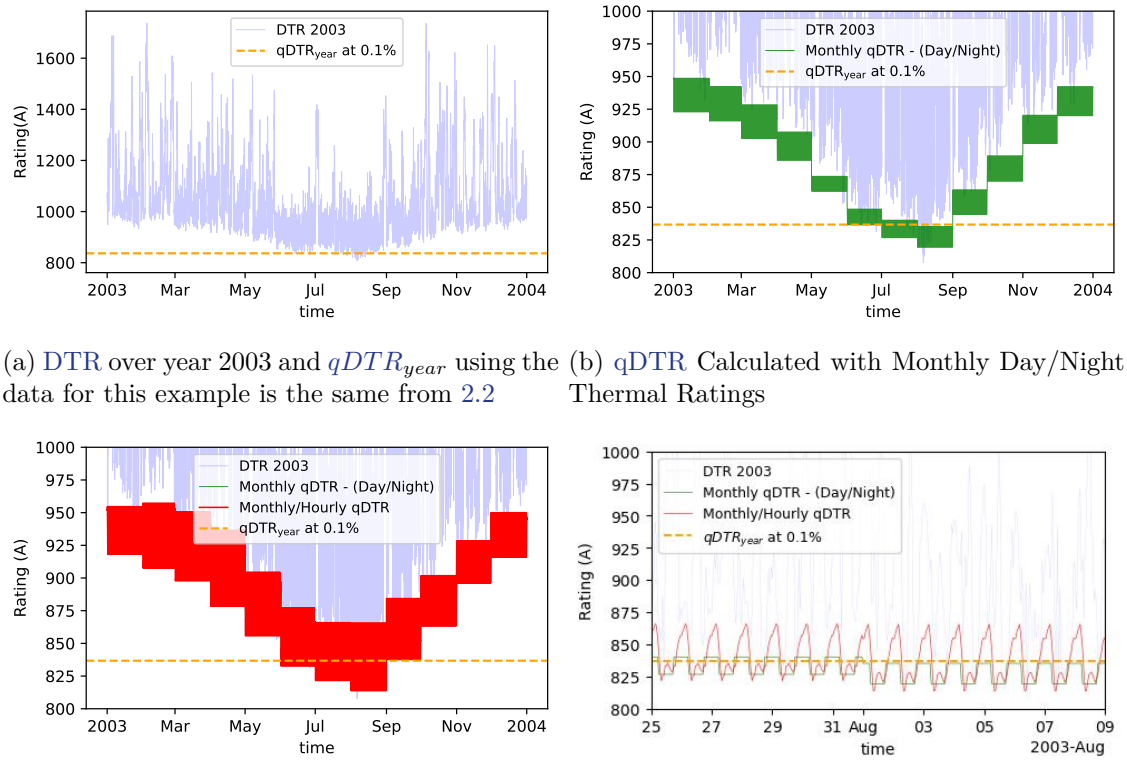

(a) DTR over year 2003 and $qDTR_{year}$ using the data for this example is the same from 2.2

(b) qDTR Calculated with Monthly Day/Night Thermal Ratings

(c) qDTR Calculated with Monthly/Hourly Thermal Ratings

(d) Comparative Plot of DTR and qDTR, Day/Night, and Month/Hour Curves

Figure 2.9: Evaluation of qDTR temporal resolutions selection strategies compared to DTR in year 2003, calculated at annual, day/night, and month/hour time scales, and using historical meteorological data described in Table 2.3.

The Fig. 2.9 shows the sensitivity and adaptability of the different qDTR temporal resolutions-strategies. Using $qDTR_{year}$ as a fixed threshold instead of the traditional STR results in 41 exceedances during the year, compared with the DTR. However, with the day/night approach, exceedances increase to 185 occurrences, indicating a more accurate and responsive thermal capacity model. The month/hour approach, which offers the finest temporal resolution, reduced these events to only 36 times, demonstrating better alignment with operational behaviour. Notably, the average capacity of the day/night and month/hour models exceeded $qDTR_{year}$ by 5.21% and 6.77%, respectively, with maximum gains of 12.61% and 14.44%. These results highlight the advantage of dynamic schemes, such as month/hourly qDTR, in maximizing asset utilization, with a trade-off between risk and operational efficiency. They also emphasize the importance of adopting customized steady state ratings, as finer temporal resolution offer not only improved performance but also a reduction of possible thermal limit violations, leading to more efficient network operation and planning.

(B). Power Transformers

The research presented at **paper E** allows for the analysis of long-term climatic influence and spatial variability on the performance of PTs. From this research, electrical and thermal

parameters, based on open-source data and those recommended in loading guides, are used to analyze the influence of long-term climatic conditions. In Fig. 2.10, the DTR values calculated using the thermal model described in Section 2.2.1.3 are presented for steady state, along with standard limits set by the transmission operator. When considering additional exposure to solar radiation, the results indicate a marked increase in thermal overload events, particularly during the summer months, where elevated ambient temperatures become a dominant influencing factor. Over the entire assessment period, the risk of thermal limit violations amounts to 9.8%, which represents a significant operational concern due to its high impact on asset reliability and system planning.

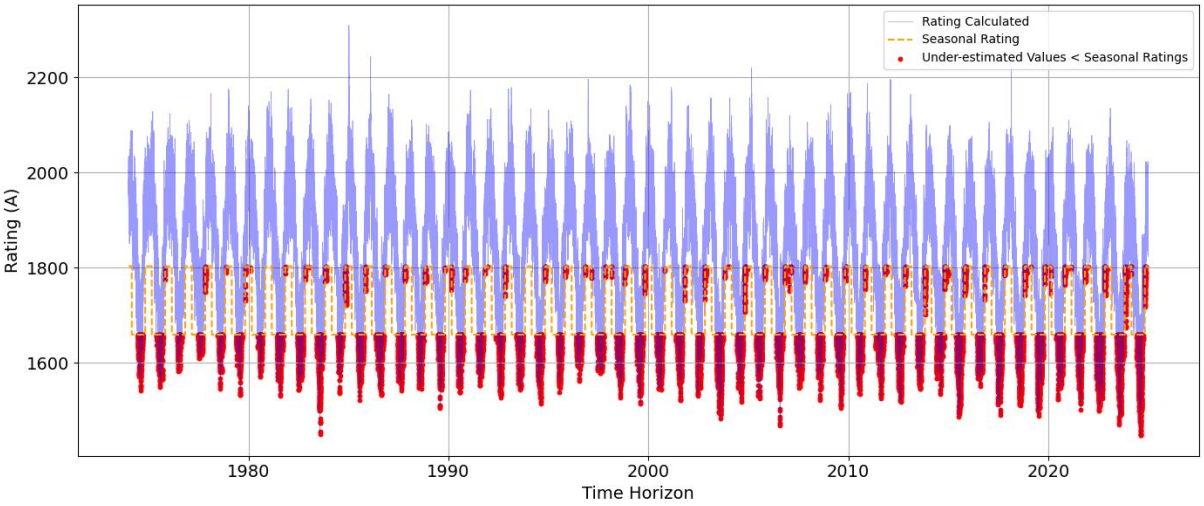

Figure 2.10: Performance Steady State Thermal Model evaluated in Long-term Horizon, evaluated on a 400/225kV 1190 MVA PT at a node in southern France.

Continuing with the evaluation of the same PT, but now excluding the influence of solar radiation (assuming that the ambient temperature surrounding the asset corresponds directly to the reanalysis data), the risk of thermal limit violation is slightly reduced to 9.7%. This marginal decrease of 0.1% reinforces the conclusion that ambient temperature is the primary factor influencing thermal performance in the model. At the same time, solar radiation plays a secondary, yet still significant, role in overload risk.

Using the qDTR methodology, we calculate transformer ratings under the same probability threshold criteria as in the previous analysis, employing the algorithm described in Section 2.2.2. As illustrated in Fig. 2.11, aligning the rating temporal resolution with with traditional seasonal rating results in a reduction in thermal overload risk during the summer while allowing for higher transformer capacity during colder periods. This demonstrates that incorporating weather factors, particularly by considering the lower end of the temperature probability distribution over the planning horizon, can improve both operational reliability and asset utilization in long-term planning frameworks.

(C). Underground Cables

The results presented in this section were previously introduced in papers **paper A**, where

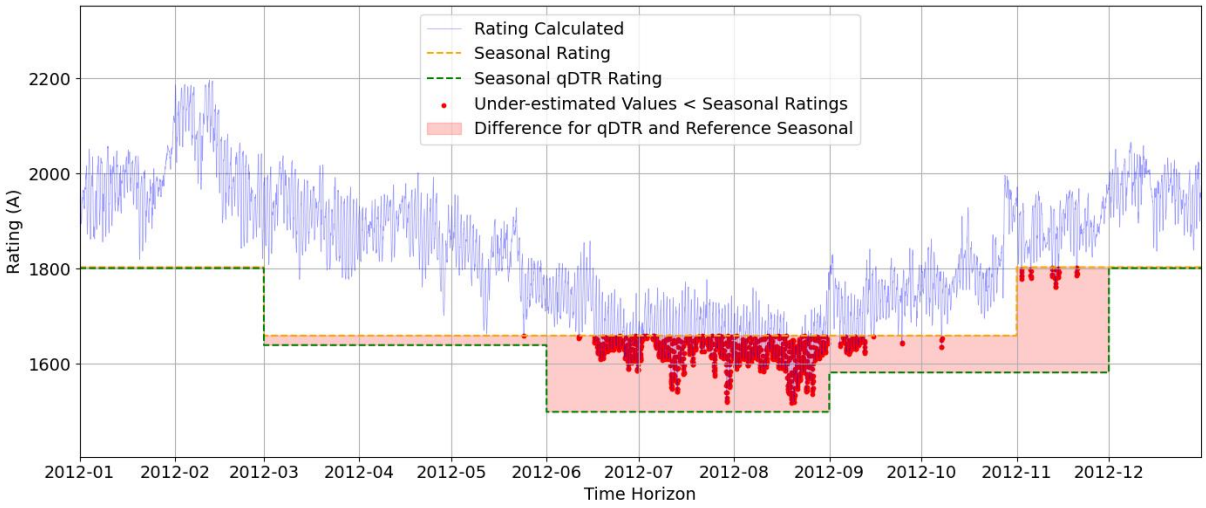

Figure 2.11: Performance of qDTR in the PT evaluated in Long-term Horizon vs Seasonal traditional ratings, for a 400/225kV 1190 MVA PT at a node in southern France.

a series of studies demonstrated the application of the qDTR methodology to UGL lines within the context of long-term power system planning, accounting for both direct burial and backfill configurations. The objective of that work was to assess the effectiveness of the proposed approach in quantifying qDTR, with particular attention to the heat transfer properties of various soil types and the added complexity arising from climate variability. As the methodology requires preprocessing to derive all necessary input parameters for the thermal calculations, the following section first presents the input models related to soil temperature and moisture. These results then serve as the basis for evaluating the performance of the qDTR methodology.

To estimate the parameters ψ_s and θ_s under various climate scenarios, the model described in Subsection 2.2.1.2 was trained, validated, and selected using daily resolution data. The performance of each candidate model was evaluated using historical data (detailed in Section 2.2.3), which served as a reference and are shown in Fig. 2.5. The final model selection was based on achieving the lowest error metrics across all models trained with different fold configurations, as summarized in Table 2.4.

The results are derived from diverse stations selected through cross-validation across the various soil codes considered and described previously in Fig. 2.4. For a graphical representation of model performance across different soil codes, refer to Fig. 2.12. At first glance, the XGBoost moisture model exhibits lower average error values compared to the $ERA5$ benchmark. Meanwhile, the Lasso temperature models show marginally superior performance, which highlights the robustness of $ERA5$ and supports its use as a reliable reference for historical analyses.

Soil moisture at the 20th percentile								Temperature at 80th Percentile							
	CV	Model					ERA_5		CV	Model					ERA_5
		0	1	2	3	4				0	1	2	3	4	
$RMSE_{20}$	0	0.29	0.07	0.13	0.08	0.14	0.22	$RMSE_{80}$	0	2.23	2.03	2.29	2.15	2.39	2.72
	1	0.05	0.21	0.08	0.09	0.08	0.15		1	2.69	2.43	2.73	2.63	2.83	3.64
	2	0.05	0.03	0.10	0.04	0.04	0.09		2	2.92	4.81	3.19	3.16	3.37	2.76
	3	0.05	0.06	0.06	0.16	0.05	0.07		3	2.02	1.85	2.25	1.90	2.14	2.90
	4	0.13	0.08	0.11	0.05	0.19	0.24		4	2.89	3.48	2.60	3.11	2.70	3.56
	Avg.	**0.11**	**0.09**	**0.10**	**0.08**	**0.10**	**0.16**		Avg.	**2.71**	**3.16**	**2.83**	**2.74**	**2.95**	**3.10**
MAE_{20}	0	0.29	0.06	0.11	0.07	0.13	0.22	MAE_{80}	0	2.23	2.03	2.29	2.15	2.39	2.72
	1	0.04	0.21	0.08	0.08	0.07	0.14		1	2.56	4.61	2.85	2.84	3.06	2.18
	2	0.04	0.03	0.11	0.03	0.04	0.08		2	1.71	1.55	1.95	1.61	1.87	2.32
	3	0.04	0.05	0.05	0.17	0.04	0.06		3	2.55	3.14	2.26	2.77	2.38	2.58
	4	0.12	0.07	0.10	0.04	0.19	0.24		4	2.64	2.96	3.03	2.56	3.41	2.21
	Avg.	**0.11**	**0.08**	**0.09**	**0.08**	**0.09**	**0.15**		Avg.	**2.34**	**2.86**	**2.48**	**2.39**	**2.62**	**2.40**

Table 2.4: Model Performance - Moisture and Temperature evaluated according to the procedure described in subsection. 2.2.1.2

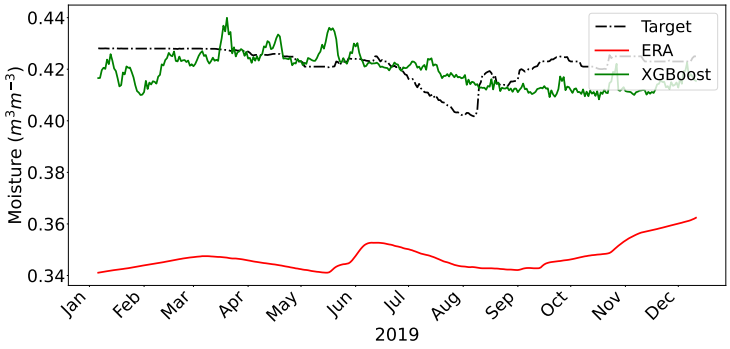

(a) Moisture

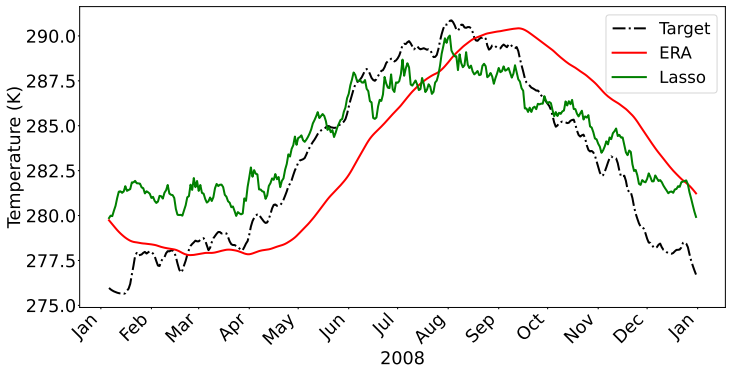

(b) Temperature

Figure 2.12: Daily time series of estimated soil moisture with (a) XGBoost at Soil 5 and (b) LASSO (green) at Soil 2 compared to $ERA5$ data (red) and test values (black dashed).

As explained above, the qDTR provides a probabilistic representation of the capacity during the analyzed period. By applying the methodology described in the algorithm presented in Section 2.2.2.1, an annual representation of the analyzed component is obtained with different temporal resolutions, and the effects of climate are estimated over the same time horizon as the

previous analysis on the UGL transmission capacity.

In Fig. 2.13, the thermal model first calculates the hourly calculated DTR over one year. The annual qDTR (black dashed line) is then calculated, and as in the traditional approach, a fixed value is applied throughout the year. Similarly, seasonal ratings (long and short dashed lines) are calculated for winter and summer, using a fixed overload probability of 0.1%. Using the same methodology, the monthly qDTR (green blue line) is calculated for each monthly combination.

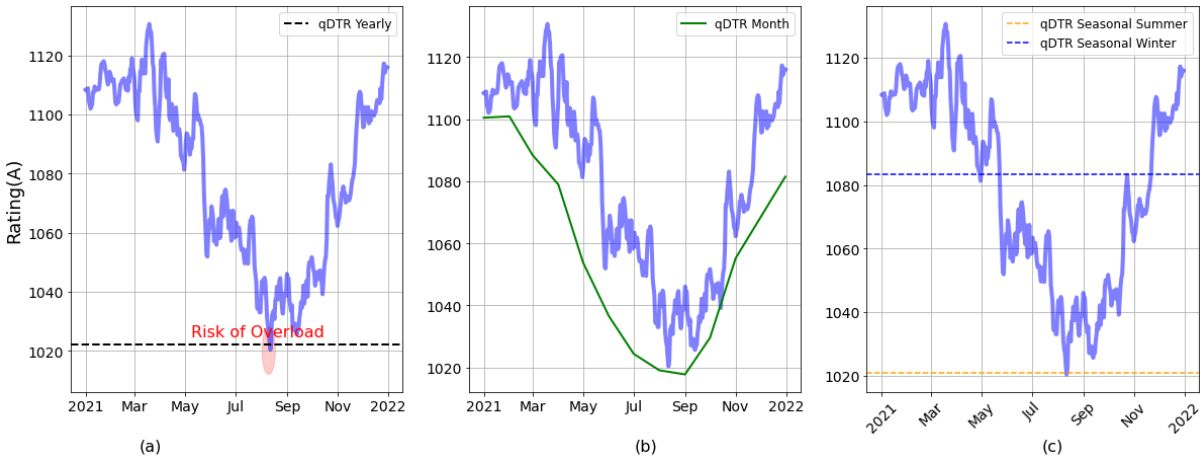

Figure 2.13: Assessment of qDTR ($X_R = 0.1\%$) Performance Across Extended temporal resolutions, Seasonal, Monthly, and Annual Applied to the UGL Specified in Annex B

A notable observation is that, for example, in 2021, selecting the traditional fixed annual method would have resulted in a risk of thermal overload. In contrast, the monthly methodology offers the possibility of reducing this risk while also taking full advantage of favourable climatic conditions during the rest of the year.

As a generalized approach to assessing the differences in behaviour resulting from the application of the qDTR methodology across the three power system components, we consider the node located in southeastern France and apply the qDTR to the historical data described in Table 2.3. This is illustrated in Fig. 2.14, which presents the annual and hourly variations of the three components at this location.

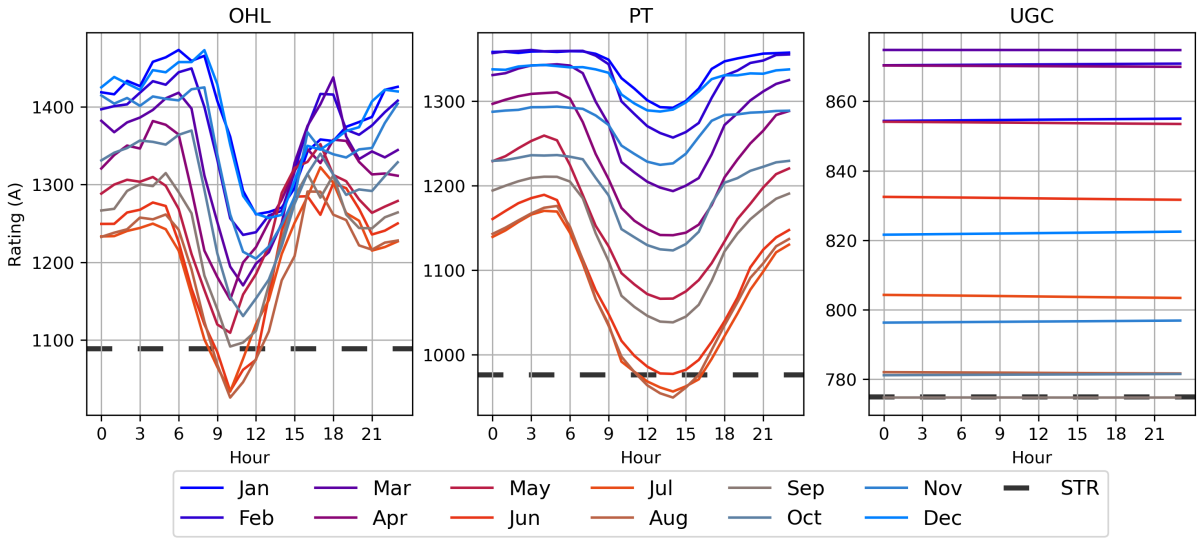

Figure 2.14: qDTR calculated for each month/hour combination for OHL, PT, and UGL calculated in the node of Tavel (southeast France). Colours represent months from the coldest (blue) to the warmest (red). A dashed black line represents STR

It is noteworthy that for OHL and PT, qDTR is lower than STR during summer daylight hours, thereby mitigating the risk of overload due to elevated temperatures. Conversely, during winter and nighttime periods, values increase significantly, resulting in greater overall transmission capacity. As expected, for UGL, the qDTR remains relatively constant throughout the day due to the high thermal inertia of the soil.

2.3.2 qDTR: Analyzed at the Regional Level

It is extended the analysis to a continental level across Europe, incorporating a comprehensive spatial assessment at a resolution of 0.25° over the same horizon. This extended approach enables a more detailed examination of variations between countries, capturing the influence of climatic and geographical factors on qDTR dynamics. These results have been analyzed previously in paper **B**.

The Fig. 2.15 illustrates the spatial variability of $\mathrm{qDTR_H}$ (where H denotes the historical horizon analyzed), expressed as the relative deviation of each location from the European average $qDTR_H/qDTR_{H_{\mathrm{Europe}}}$ (%). The variability reaches approximately 20%, 31%, and 87% for OHL, PT, and UGL, respectively. The lower variability of OHL is attributed to its dual dependence on wind speed and air temperature. In contrast, the high variability of UGL results from regional differences in soil properties, which significantly affect thermal diffusivity and moisture retention.

Previously, the relationship between the proposed methodology and the surrounding climatic conditions was examined by analyzing different transmission components under various scenarios. In this section, the emphasis shifts toward evaluating how the qDTR enhances rating estimation when applied to historical climatic data, with a fixed-probability thresholds. This enables a more consistent assessment of thermal capacity compared to traditional static methods. Furthermore, the regional analysis highlights the advantages of adopting finer temporal

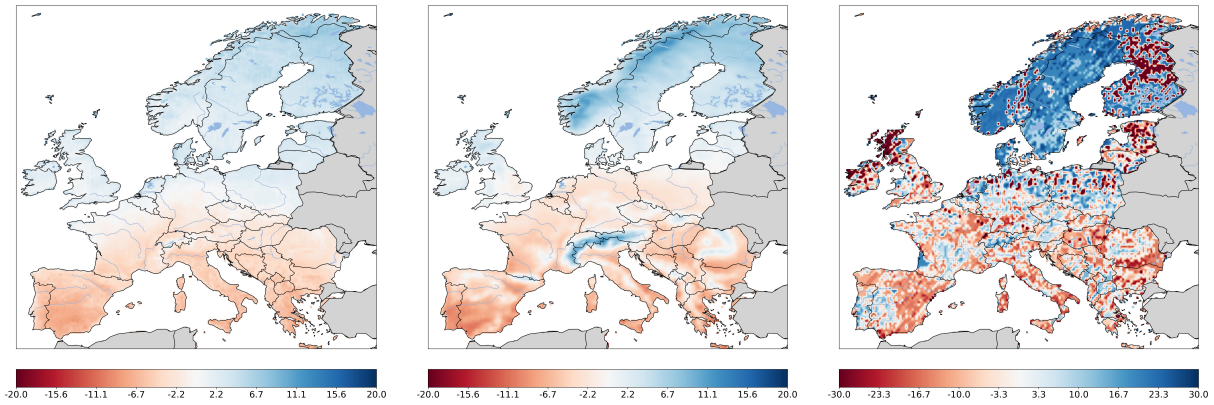

(a) OHL (b) PT (c) UGL

Figure 2.15: Geographical distribution of the mean qDTR difference at the country level over fifty years for the historical reference. The analysis is performed for the main power components: OHL, PT, and UGL, and illustrates the difference in the variation of the historical average for each region.

resolutions such as month/hour timescales over annual averages, capturing better the climatic variability that significantly influences component rating. These benefits are expressed through the relative difference, $\Delta_{\%} = \frac{qDTR_{\text{month/hour},H} - qDTR_{\text{year,H}}}{qDTR_{\text{year,H}}} \times 100\%$.

The results shown in Fig. 2.16 are obtained by evaluating the relative difference between $qDTR_{\text{month/hour},H}$ and $qDTR_{\text{year},H}$ at each coordinate and then analyzing these differences at the national level. To provide a comprehensive regional perspective, the mean, minimum, and maximum values were calculated by grouping the data into daytime (6:00-18:00) and nighttime periods for both winter and summer seasons.

The results suggest that incorporating regional climate effects using historical data improves the performance of $qDTR_{month/hour}$ relative to $\text{qDTR}_{\text{year}}$, especially during winter periods, with quantifiable positive impacts in several countries and components. This trend is particularly pronounced in the case of PT and OHL, as observed in Greece, where average improvements reach 22% and 24%, respectively. In contrast, the slower thermal response of deep soil in UGL constrains the improvement to approximately 6%.

Conversely, in correlation with the increased occurrence of warmer days, $qDTR_{\text{month/hour}}$ may fall below $qDTR_{\text{year}}$, with differences reaching a minimum of -12%, as observed in regions such as Spain for PTs. These deviations reflect the temperature deltas experienced by the components throughout the year; in areas where component temperatures remain relatively stable across seasons, the difference between $qDTR_{\text{month/hour}}$ and $qDTR_{\text{year}}$ tends to be smaller. For a more detailed analysis, the reader is referred to Tables 7–9 in the appendix of paper **B**.

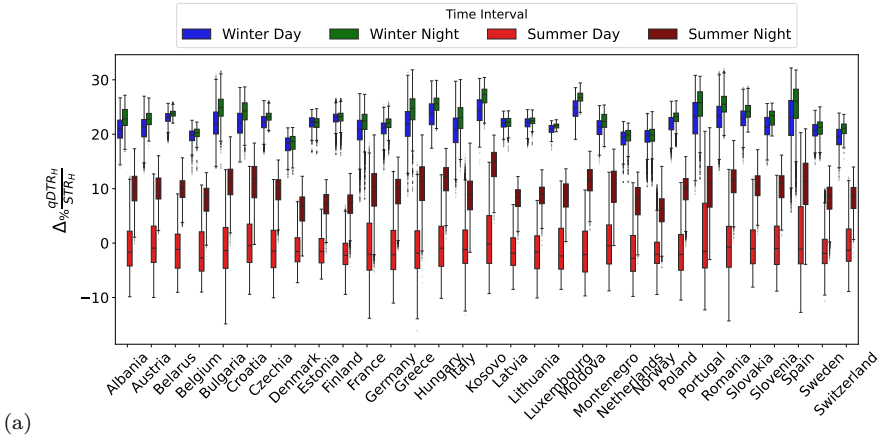

(a)

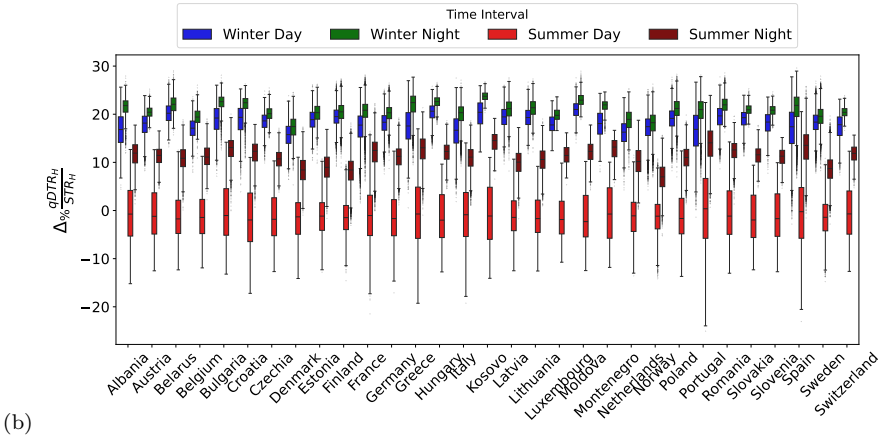

(b)

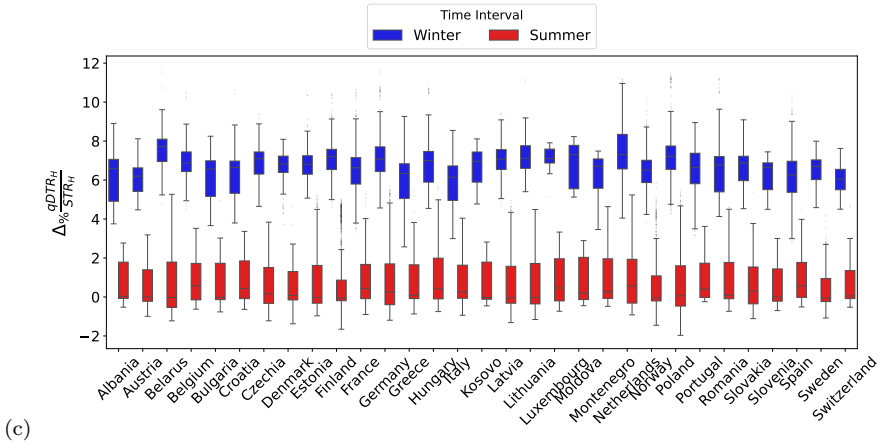

(c)

Figure 2.16: Percentage difference between $\text{qDTR}_{\text{month/hour}}$ and $\text{qDTR}_{\text{yearly}}$ in some European countries for: (a) PT, (b) OHL, (c) UGL

2.4 Conclusion

This chapter developed and validated qDTR methodology for transmission system components, addressing the limitations of static rating approaches on variable weather scenarios. By explicitly integrating spatio-temporal climate variability into thermal models, the framework bridges the gap between static thermal rating assumptions and the need for climate influenced and adaptive capacity assessments. The work combined component-level modelling with regional applications, thereby offering both technical depth and practical scalability for long-term planning.

The subsections 2.3.1 and 2.3.2 presented the results published in **Paper A** and **Paper B**, where the proposed models were applied to OHL, PT, and UGL. These studies demonstrated how the $qDTR_{month/hour}$ approach captures prolonged weather variability and enables more refined evaluation of available transmission capacity under different seasonal and climatic areas.

The results highlight three key outcomes that emerge from this chapter. First, the systematic adaptation of thermal models to long-term rating contexts was achieved. In the case of UGL, a soil analysis methodology introduced, explicitly accounting for moisture and temperature dynamics up 0.8 m depth. This approach delivered better accuracy, with mean absolute errors of 0.08 ($\pm$0.02) $m^3\,m^{-3}$ for soil moisture and 2.51 ($\pm$0.17) K for temperature, outperforming benchmark methods. The model substantially improved the reliability of underground cable rating estimates, which were shown to vary by up to 87% depending on soil and climate conditions.

Second, the qDTR methodology demonstrated the ability to maximise transmission capacity while maintaining conservative overload threshold. By focusing on the lower tail of the probability distribution (0.1% fixed-probability threshold), the approach ensured robustness to adverse conditions while preserving consistency across seasonal and long-term horizons. This enabled greater utilisation of the network during nights and colder periods while simultaneously reducing overload risks during hotter conditions. In practical terms, transmission capacity increased relative to the traditional static rating ($\Delta_{\%}\frac{qDTR_H}{STR_H}$), with gains of 17% for OHL, 22% for PT, and 6.8% for UGL in the Denmark regional analysis (see Subsection 2.3.2), all achieved while maintaining overload probabilities within the predefined risk thresholds.

Third, the spatio-temporal advantages of qDTR were demonstrated when compared with conventional STR, which rely on fixed annual or seasonal ratings and neglect the surrounding environment. The proposed method provided consistent results across multiple temporal resolutions, from month/hour to yearly, thereby capturing diurnal cycles, seasonal patterns, and geographical heterogeneity such as the differences between northern and southern climates. This flexibility reduced underutilisation of assets during favourable conditions while preventing risks during extreme climatic events.

Finally, by explicitly formulating fixed-probability threshold to limit overload exposure, and allowing planners to define risk tolerance levels, the qDTR approach established a bridge between short-term operational practices based on dynamic ratings and long-term planning methodologies traditionally constrained by conservative static assumptions. This integration demonstrates how overload risk, climate influenced methodologies can align operational and planning horizons,

ultimately leading to more resilient and cost-effective transmission systems.

Overall, the methods in this chapter demonstrated that static thermal assumptions systematically underestimate the climatic and temporal variability affecting transmission assets. By comparing conventional STR with quasi-dynamic methods based in probabilistic approach, it became evident that ratings must evolve beyond averages to adequately reflect both seasonal opportunities for increased capacity and the risks imposed by extreme conditions. In this context, the first contribution of the thesis introduces the qDTR methodology, a *methodology designed to estimate long-term thermal ratings in a probabilistic manner while explicitly connecting spatio-temporal dynamics with planning horizons*. This contribution is structured around two research questions: (i) incorporating climate variability into component ratings (RQ1), and (ii) balancing transmission capacity with risk selection (RQ2).

To address RQ1, the qDTR approach integrates thermal dynamics with probabilistic models at multiple temporal scales (hourly, daily, monthly, and annual), thus capturing seasonal cycles, diurnal fluctuations, and long-term climate changes. For example, high temperatures in summer limited component capacity, while winter conditions offered significant scope for additional capacity. In parallel, spatial heterogeneity was explicitly represented using high-resolution climate and soil datasets, capturing differences in topography, weather regimes, and soil properties. Continent-scale assessments confirmed substantial variability, with capacity differences of up to 20% for OHL, 31% for PT, and UGL with 87% due to soil differences, underscoring the importance of moving beyond uniform static ratings assumptions.

To resolve RQ2, the methodology adopts a probabilistic formulation that incorporates explicit thermal overload limit throughout fixed probability thresholds (e.g., 0.1%). This ensures that ratings are not only higher under favourable conditions but also robust to extreme adverse events. In Portugal, for instance, the application of the methodology enabled substantial capacity gains during winter nights compared to the traditional fixed yearly rating, reaching maximum increases of 28% for OHL, 31% for PT, and 8.9% for UGL (detailed in Subsection 2.3.2), all while maintaining overload probabilities within acceptable limits. By linking temporal and spatial variability with thermal overload risk-informed capacity margins, the methodology provides planners with a forward-looking, climate-adaptive method that balances the two objectives of maximising system capacity and reliability.

In conclusion, this chapter provides system planners with a method for assessing transmission ratings under varying climatic conditions. It moves beyond static and general ratings toward a climate-based probabilistic methodology that better reflects current variability. Nonetheless, an important gap remains: while this work demonstrated how to model the risk at the component and regional levels, the next step is to systematically embed these risk estimation into NEP models. This requires defining how risk tolerance can be included inside the investment decision-making and how qDTR can be extended to account for climate change projections over infrastructure lifetimes. Addressing this will be essential to ensure that electricity system planning remains reliable, cost-effective, and resilient under accelerating climate variability and extreme events.

2.5 Limitations

For this chapter, the following limitations apply:

- The thermal model used considers only steady-state conditions, assuming constant current flowing and ambient conditions at hourly intervals. This approximation is due to the use of data-driven methods based on reanalysis datasets and climate models, which typically provide long-term averages while excluding short-term or transient variability. Consequently, the method cannot capture dynamic thermal responses to rapid changes. While suitable for long-term planning, this approach limits its applicability to short- and medium-term scenarios, where transient effects can be crucial and require complementary analyses.

- This analysis does not consider climatic loads such as wind and ice, as it focuses solely on thermal behaviour. However, these loads can significantly influence strength, and their exclusion represents a limitation, especially in contexts where mechanical integrity is affected by extreme weather conditions caused by climate change.

- Thermal models for UGL installed in conduits, tubes, or pipes are not included in the current implementation. However, the model can be extended to incorporate these configurations if necessary. Furthermore, due to data limitations, the model homogenizes soil properties at the considered geographic resolution and depth; therefore, the results should be interpreted with caution. Transmission companies typically conduct detailed soil analyses during conductor installation to characterize the soil's structure. This model can be updated to incorporate such information when available. Another important consideration is that soil characteristics may present greater variability than represented in the database used, which assumes a spatial resolution of 1 km. Consequently, practical applications of this methodology may require one or more of the following actions: (i) selecting the worst-case scenario, (ii) performing a detailed soil survey, or (iii) using trench fill. For the latter case, calculations for controlled-fill facilities have already been integrated into the thermal model.

- The thermal model for PT focuses solely on the transformer winding hot-spot temperature without considering the thermal behaviour and operational constraints of critical subsystems such as bushings, core, tap changers, cooling systems, and cable end connections [129]. These components may impose additional thermal, dielectric, or mechanical limitations not reflected in the model.

- The method lies in its geographic focus on Europe, due primarily to the availability and density of in-situ measurements and harmonized datasets across the continent. While the architecture and methodology of the models presented in this thesis are scalable and adaptable, it is necessary to preserve the structure of the soil characteristics and climate information. Extending this approach globally would require access to similarly high-

resolution and accurate databases in other regions, whose quality, coverage, and rating standards may vary.

Chapter 3

Network Planning with Probabilistic Long-Term Thermal Ratings

Résumé en Français

Ce chapitre analyse l'intégration de la méthodologie quasi-dynamique pour l'estimation des limites thermiques des composants dans le cadre des plans d'expansion des réseaux. Cette intégration s'appuie sur diverses méthodologies ou outils de planification, en mobilisant soit une approche déterministe du risque de surcharge des composants, soit l'application de méthodes stochastiques pour son évaluation. Les études de cas comprennent des réseaux régionaux, continentaux et académiques. Les résultats obtenus mettent en évidence des gains spatio-temporels en matière de coûts d'exploitation, ainsi que le report ou l'évitement d'investissements dans les infrastructures.

3.1 Introduction

As detailed in Section 1.3.3, previous research on DTR methodologies has primarily concentrated on short-term operational applications, while long-term planning has continued to rely predominantly on traditional STR. However, as demonstrated by the results in Section 2.3, where transmission capacity gains of up to 22% for PT while overload risk remained limited by a lower quantile threshold, both favorable and unfavorable meteorological conditions can significantly influence the capacity of transmission power system components. Incorporating these weather effects as thermal rating decision variables in steady-state power flow equations is therefore essential for accurate and future resilient network planning.

Traditional fixed and static thermal rating constraint approaches assign uniform values to transmission components across long horizons and broad regions. As a result, they fail to capture the variability of environmental conditions. This simplification not only restricts operational flexibility in the management of optimal power flow but also underestimates the risk of thermal overload during increasingly frequent adverse weather events, which can jeopardize performance and accelerate asset aging. To address these limitations and enable the development of a reliable and weather influenced transmission network, thermal models must be integrated with dynamic and methodologies capable of capturing the geographically differentiated and cumulative impacts of climate variability over long-term planning horizons.

As shown in our previous results, the proposed qDTR methodology aims to bridge this gap. It introduces a data-driven methodology that captures long-term spatio-temporal climate variability and accounts for the prolonged effects of meteorological conditions, effectively linking the precision of short-term dynamic models with the strategic scope of long-term planning.

Nevertheless, integrating qDTR into the planning process presents non-trivial challenges. Alternative power flow formulations are required, as explored in recent literature, revealing a critical gap: the lack of established methods that incorporate qDTR into long-term transmission expansion planning. Furthermore, there remains limited analysis of the trade-offs and implications associated with embedding dynamic thermal constraints into investment and planning decisions. Closing these gaps is essential to advance qDTR from a conceptual framework to a practical planning tool enabling capacity assessments and supporting planning strategies that balance reliability, cost effectiveness, and system adaptability in the face of evolving weather and operational conditions.

The main objective of this chapter is to present conservative probabilistic with fixed-quantile and stochastic strategies for integrating qDTR into NEP and incorporating thermal overload risk into the decision-making process. More specifically, the contributions include the development of deterministic formulations that embed qDTR into transmission expansion planning models, along with the extension to stochastic approaches that explicitly take into account the risk of thermal overload under climate variability. Furthermore, the work evaluates investment and operational trade-offs using results that capture the cost, and reliability. To achieve this, the next section describes a step-by-step methodical approach.

3.2 Methodology

This section presents the proposed methodology, which introduces both deterministic and stochastic thermal overload risk strategies for integrating qDTR into transmission expansion planning. The objective is to provide a framework that supports investment and operational decision-making by capturing the dynamic and probabilistic nature of ratings. In doing so, the methodology directly addresses **RQ3** and **RQ4** by (i) demonstrating how qDTR can be systematically embedded into long-term planning models and (ii) evaluating its implications for network development strategies. The proposed methodology is structured into the following steps:

Step 1: Formulate a NEP framework that explicitly incorporates thermal ratings constraints into long-term expansion analysis, ensuring that transmission component ratings reflect spatiotemporal variability.

Step 2: Integrate deterministic formulations in which qDTR values are embedded as risk informed constraints, and evaluate their impact on planning outcomes, cost-effectiveness, and system reliability.

Step 3: Extend the formulation to a stochastic modeling approach that captures the probabilistic and risk-aware of qDTR, enabling planners to select acceptable capacity limits and to assess reliability under uncertainty.

Step 4: Conduct a comparative analysis between probabilistic and risk management results, highlighting trade-offs in investment decisions, operational flexibility, and overall system performance.

Step 5: Validate the methodology through case studies or numerical simulations, assessing its practical applicability and scalability in network planning scenarios.

3.3 Network Expansion Planning

Power system analyses span multiple time horizons, each serving distinct operational and planning purposes. It is therefore necessary to differentiate between them. *Very short-term* studies (ranging from milliseconds to minutes) focus on system dynamics, stability, protection, and automatic control responses to rapid events such as lightning strikes or load transients. *Operational planning* typically covers horizons of minutes to a week, including tasks such as economic dispatch, unit commitment, and maintenance scheduling [5]. In contrast, *short-term planning* (under 3 years) focuses on immediate operational needs, while *medium-term planning* (approximately 10–15 years) supports strategic decisions driven by evolving market, policy, and economic conditions. Finally, *Long-term planning* (over 15 years) takes a broader view, shaping the future structure of the power system by evaluating investment needs in generation, transmission, and emerging technologies [4]. While short-term studies prioritize real-time operation and system resilience, this chapter centers on long-term transmission system planning over a 15-year horizon. Its primary objective is to determine the optimal timing and selection of reinforcement on transmission network components required to ensure reliable and efficient power delivery, in the face of future challenges, such as addressing the increased electricity demand driven by climate change and large-scale electrification across transportation, heating, and industry. Within this planning horizon, it becomes feasible to incorporate the lifespan of transmission components, as it typically extends far beyond the scope of short and medium-term frameworks, making such considerations irrelevant for those planning stages.

To illustrate this process, Fig. 3.1 details the functional structure of a typical network system planning methodology, as commonly applied in transmission operator practices from [132]. This planning approach is typically applied over a long-term horizon, often 15 to 30 years, and may be repeated annually to reflect updated demand forecasts, generation scenarios, and, in this case, weather impacts, detailed in pink colour. The main objective is to minimize long-term investment and operating costs while ensuring adequate system reliability. This requires taking into account technical constraints on power flow and spatial factors, while accommodating both existing infrastructure and possible future extensions.

The process begins with demand projections, which may involve estimating peak demand across the system, in specific regions, or identifying representative (extreme or typical) load patterns. Next, system expansion alternatives capable of meeting future demand requirements are explored and evaluated. In parallel, it is increasingly necessary to take into account the deployment of RES, in line with regional or national policy objectives. To ensure reliable network operation, system behavior must be evaluated in both stationary and contingency situations. In this version of the process, thermal risks, such as power system component overload under emergency conditions, are explicitly included as part of the contingency analysis. While the main focus of this thesis is on thermal ratings, the logic represented in the diagram could be extended to include operational processes for identifying system inadequacies, such as equipment overloads or reliability standard violations.

Traditional approaches typically use power flow studies under normal and emergency condi-

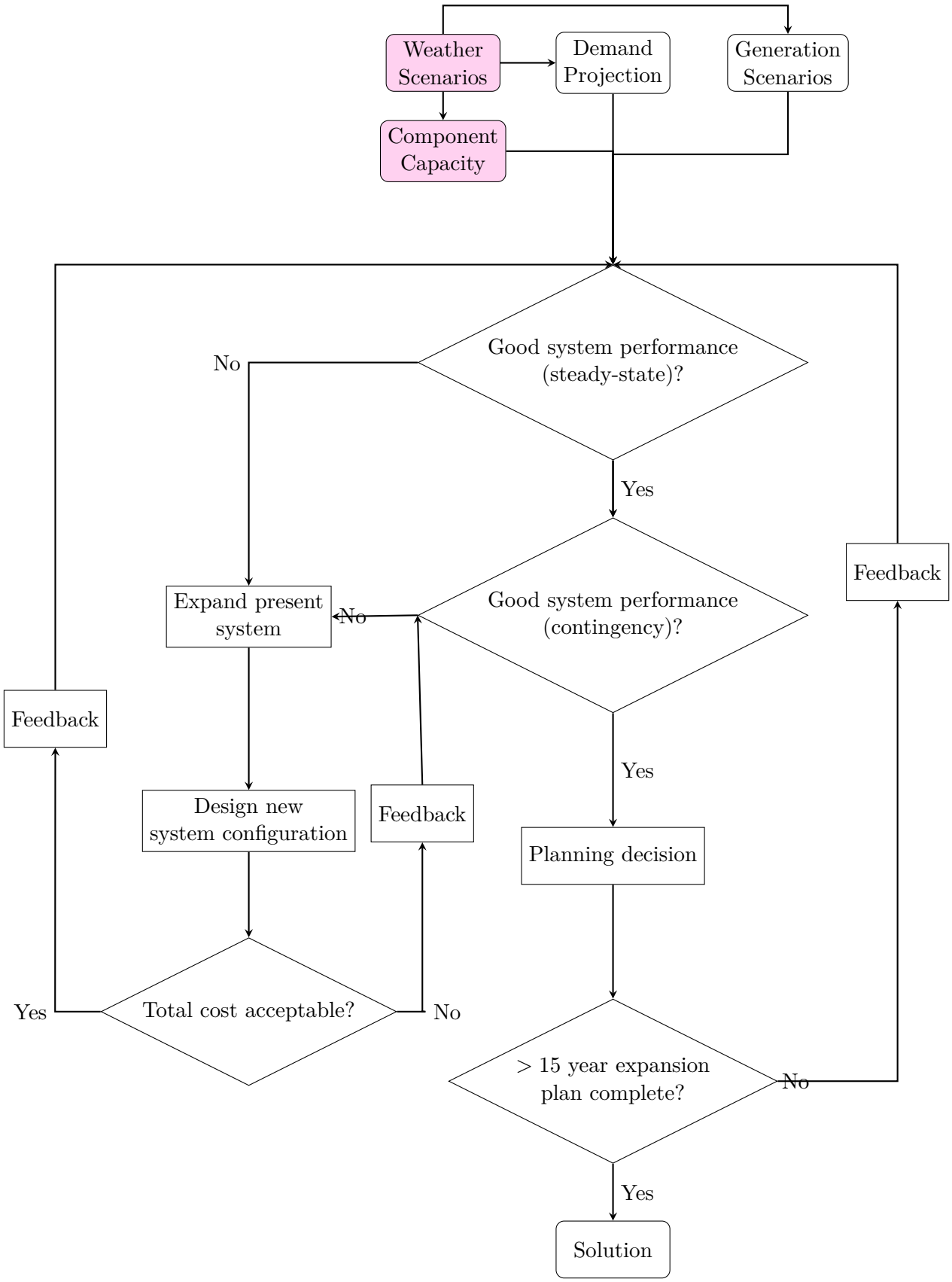

Figure 3.1: Functional block structure of a typical network planning methodology, adapted from [132].

tions to evaluate the effectiveness of proposed alternatives. These studies support the iterative formulation of network expansion plans to identify technically feasible and economically viable solutions.

Ultimately, this structured planning methodology enables the development of efficient and resilient transmission systems that meet long-term operational, regulatory, and environmental objectives. However, to drive the development of more climate-resilient and climate-influenced transmission networks (pink blocks in the block diagram), recent research has increasingly focused on integrating DTR into expansion planning frameworks.

As environmental conditions and generation/load patterns evolve, particularly due to decarbonization efforts and climate change, planning methodologies must adapt accordingly. Data-driven approaches to estimating continuous annual DTR, such as the method presented in [81], illustrate how historical ambient temperature and load data from the past five years can be used to derive thermal values for OHL. These methods are essential, as numerous studies have demonstrated the operational and economic advantages of DTR, including reducing congestion costs by minimizing generator redispatching and postponing or eliminating costly infrastructure upgrades.

To date, as described in section 1.3.3 and Table 1.3, most applications of DTR have focused on short and medium-term horizons, including day-ahead system operations, RES integration, real-time network management, and medium-term distribution planning. However, a significant gap remains in long-term NEP that considers future climate conditions and their effect on thermal capacity, particularly concerning the behavior of power system components under changing environmental scenarios.

This thesis seeks to address this gap by developing a long-term planning framework that incorporates qDTR and climate weather scenarios. To lay the groundwork for this methodology, it is first necessary to describe in detail the fundamental technical aspects of transmission NEP that are directly affected by the methodologies and findings presented in this chapter.

3.3.1 Transmission Expansion Planning

The Transmission Expansion Planning (TEP) problem seeks to determine the optimal configuration of the transmission network to support future system operation, ensuring efficient energy exchange between nodes. Its canonical mathematical formulation, as detailed in [132, 133], aims to minimize investment costs while satisfying operational constraints. The basic optimization structure is expressed as:

$$\min \quad \sum_{l \in \mathcal{L}} (\mathbf{Z}_l \, \tilde{\mathbf{i}}_l) \tag{3.1}$$

subject to:

$$\begin{aligned}
&\sum_{g \in \mathcal{G} \in n} P_g - \sum_{d \in \mathcal{D} \in n} P_d = \sum_{l \in \mathcal{N}} P_l, && \forall n \in \mathcal{N} \quad \text{(Power balance)} \\
&|P_l| \leq F_l^{\max} \mathbf{Z}_l, && \forall l \in \mathcal{L} \quad \text{(Branch flow limits)} \\
&P_{\min,g} \leq P_g \leq P_{\max,g}, && \forall g \in \mathcal{G} \quad \text{(Generator limits)} \\
&\mathbf{Z}_l \in \{0, 1\}, && \forall l \in \mathcal{L} \quad \text{(Investment decisions)}
\end{aligned} \tag{3.2}$$

Here, $\tilde{i}_l$ represents the investment cost of building or upgrading transmission line l, while Z_l is a binary decision variable indicating whether the investment is undertaken. In practice, TEP is subject to various sources of uncertainty, which can significantly influence long-term planning outcomes. Common uncertainties include projected demand growth, the availability and location of generation resources, climate dependent parameters (such as ambient temperature, wind speed, soil temperature, and volumetric water content), random outages of system components, and investment trends in new renewable energy sources.

The literature addresses these uncertainties using a range of modeling approaches [134], which can be broadly categorized as follows:

- Deterministic Models – Assume all inputs and future conditions are known with certainty. These models are typically formulated as Mixed-Integer Linear Programs (MILP) or Mixed-Integer Non-linear Programs (MINLP) [135, 136].
- Robust Optimization – Focuses on ensuring system feasibility under worst-case scenarios for uncertain parameters, such as demand or renewable generation availability [137].
- Stochastic Programming – Models sequential decision-making under uncertainty by incorporating multiple future scenarios, often formulated using Mixed-Integer Quadratic Programming (MIQP), as seen in [138].
- Adaptive Robust Optimization (ARO) – Combines flexibility and tractability by defining uncertainty sets and adapting decisions dynamically, as described in [136]

As outlined above, research questions **RQ3** and **RQ4** address the long-term implications of incorporating thermal ratings, particularly through the qDTR methodology into transmission expansion planning. In this chapter, the objective is not to propose new optimization algorithms, but rather to evaluate how existing planning frameworks and simulation tools respond when climate-aware branch thermal limits constraints are introduced. Most analyses are conducted using deterministic models to establish a clear reference for system performance under base conditions. Subsequently, stochastic approach will be introduced to account for thermal

risk assessment for transmission power components, particularly in scenarios involving climate variability.

This approach enables a focused investigation of how long-term thermal capacity impacted by the climate considerations influence network investment decisions, without adding unnecessary algorithmic complexity. To properly capture these effects, branch power flow constraints are reformulated to include qDTR thermal limits, extending the conventional steady-state representation to account for the probabilistic method of ratings.

3.3.2 Optimal Power Flow

In power system planning studies, Optimal Power Flow (OPF) plays a critical role in determining the most efficient operating conditions while meeting system constraints. However, solving the full AC-OPF model can be computationally intensive, especially in long-term planning scenarios. To address this, it is common practice, especially relevant in transmission planning contexts, to use simplified DCOPF equations, which linearize power flow as a function of voltage angle differences and ignore variations in reactive power and voltage magnitude. This DCOPF approximation significantly reduces the computational burden and ensures feasibility for large systems and extended time horizons, although at the expense of modeling accuracy [139]. In later stages of the analysis, AC-OPF is typically reintroduced to verify that acceptable voltage profiles are maintained under both normal and contingency conditions [5]. This thesis adopts a DCOPF formulation for its long-term investment planning optimization, in line with conventional practices in transmission system expansion.

The DC load flow equations are:

$$P_{L_{n,m}} = \frac{1}{X_{n,m}}(\theta_n - \theta_m) \tag{3.3}$$

$$\begin{aligned} P_{\text{inj},n} &= \sum_{g \in n} P_g - \sum_{d \in n} P_d \qquad \forall\, g, d \in n \\ P_{\text{inj},n} &= \sum_{k \in n} P_{L_k} - \sum_{k \in \text{m}} P_{L_k} \quad \forall\, L \in n \end{aligned} \tag{3.4}$$

$$P_{\min,g} \leq P_g \leq P_{\max,g} \quad \forall\, g \in n \tag{3.5}$$

$$\left|P_{L_{n,m}}\right| \leq F^{\max}_{L_{n,m}} \quad \forall\, L \in n \tag{3.6}$$

$$-\pi \leq \theta_n \leq \pi \tag{3.7}$$

Operational limits described in Eq. 3.6, with $F^{\max}_{L_{n,m}}$, enforce thermal capacity constraints on both existing and candidate transmission elements. For each transmission component, including OHL, UGL, and PT, power flow must remain within rated limits under both normal and contingency (N–1) conditions. With an objective function of the OPF as:

$$\min_{P_g} \quad \sum_{i \in \mathcal{G}} C_i(P_{g_i}) \tag{3.8}$$

It is important to note that, for now, it will retain the objective function detailed in Eq. 3.8 as an essential representation of the problem formulation. For simplicity, terms such as load shedding costs, environmental costs, operational storage costs, and aging, among others, are not included in multi-period investment scenarios. Some of these terms will be incorporated in subsequent formulations, which will be described in subsequent chapters.

In this context, the methodology adopted in this thesis focuses on the assessment of thermal ratings constraints as a key parameter for long-term expansion planning. It should be noted that these operational constraints are not considered static, but are influenced by the results of long-term thermal rating analyses and subsequently incorporate dynamic improvements through the qDTR methodology. This thermal-electric linkage between DCOPF and qDTR can be described in Fig. 3.2. This allows for an evaluation of transmission capabilities with a greater impact, also incorporating different time frequencies (hour, day, month, and year), the introduction of thermal risk, and consideration of future climate conditions. On the other hand, in order to analyze congestion, it is standard practice to perform an economic dispatch with N-1 security constraints to monitor flows through transmission components and prevent potential overloads in the event of a contingency.

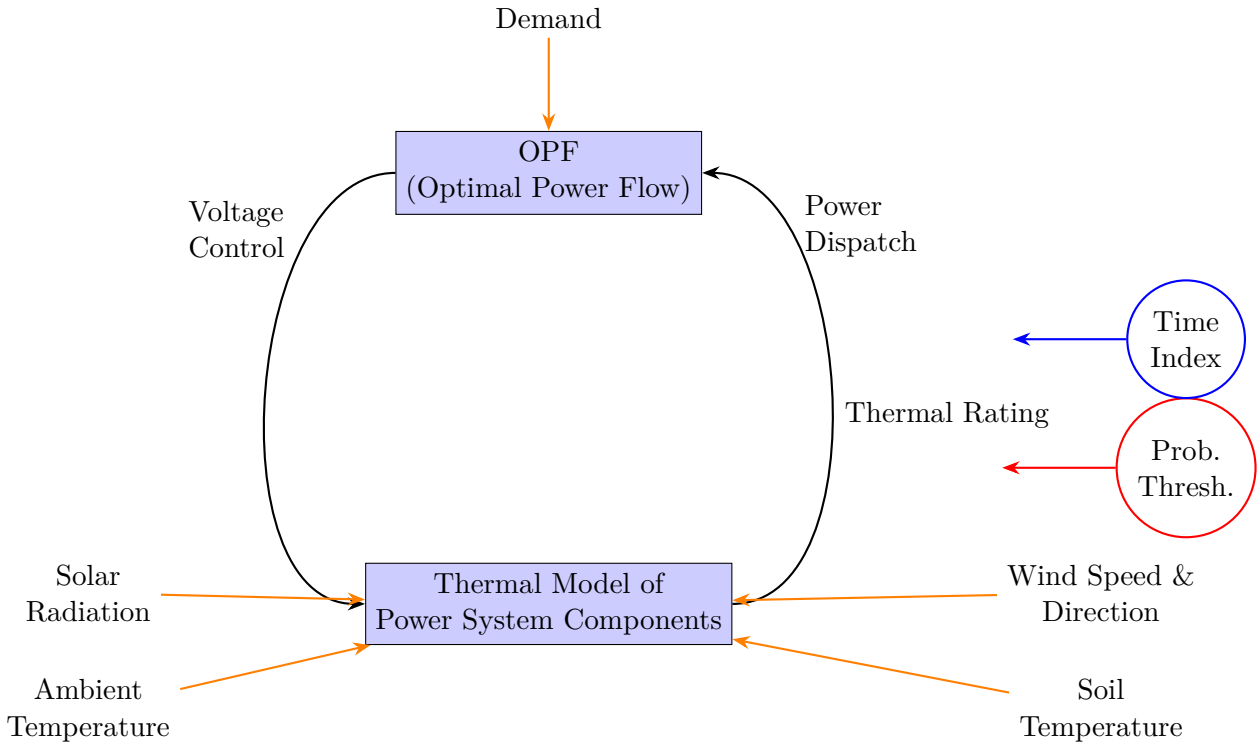

Figure 3.2: Thermal-electric linkage between DCOPF and Thermal Ratings

3.3.3 Transmission Expansion Planning influenced by the Climate

In this thesis, it is acknowledged that both electricity demand and generation are significantly influenced by weather conditions. However, our methodological approach focuses specifically on the thermal capacity of transmission power system components. Therefore, demand and generation are not represented in the main methodological framework or in the main illustrative figures. Nevertheless, with the intention to extend our methodology, certain applications or specific models presented in Section 3.3.1 also incorporate weather dependent demand and generation.

Accordingly, a more extensive optimisation formulation in Eq. 3.9 (based on Eq. 3.1) is described for a multi-period planning horizon, which includes generation costs, penalties for load shedding, carbon emission costs, penalties for renewable energy dispatch restrictions, and transmission investment costs, while ensuring the reliability and security of the electricity system. This extended formulation is especially suited for TEP studies that must balance technical feasibility, economic efficiency, and environmental impact in the capacity of transmission components.

Mathematically, based on the DCOPF formulation from [140] and extended, with the objective function is formulated as follows:

$$\min_{x_{var}} \quad \left(N_y(\text{Gen}_{cost} + \text{Load}_s + \text{CO2}_c + \text{Curtail}_c) + \text{Inv} \right) \tag{3.9}$$

Where:

- **Gen**$_{cost}$: Total generation cost from conventional and renewable generators.
- **Load**$_s$: Penalty cost associated with unserved demand (load shedding).
- **CO2**$_c$: Total cost of CO_2 emissions from non-renewable generators.
- **Curtail**$_c$: Penalty for curtailing renewable energy.
- **Inv**: Cost of investment in new transmission infrastructure, this includes OHL, UGL, PT.
- x_{var}: Variables to minimize such as $P_{g,t,y}$, $P_{\text{Ls},n,t,y}$, $P_{l,y,t}$, $Z_{l,k,y}$, $P_{\text{inj},n,t}$
- **Important note**: In these equations, when referring to a line using the symbol l or L, it may refer to an OHL, an UGL, or a PT modeled subsequently in the form of a line.
- **Note**: For more details regarding the nomenclature can be found in the List of Symbols table on page xi.

Objective Function Components

$$\text{Load}_s = \sum_{y\in\text{Ep}} \sum_{n\in\text{N}} \sum_{t\in\text{T}} P_{\text{Ls}n,t,y} \cdot \text{Cost}_{Ls} \cdot w_t \tag{3.10}$$

$$\text{CO2}_c = \sum_{y\in\text{Ep}} \sum_{g\in\text{G}} \sum_{t\in\text{T}} P_{g,t,y} \cdot \text{CO2}_p \cdot w_t, \quad \text{if } g \notin \{RES\} \tag{3.11}$$

$$\text{Curtail}_c = \sum_{y\in\text{Ep}} \sum_{g\in\text{G}} \sum_{t\in\text{T}} P_{\text{Cur},g,t,y} \cdot \text{Curt}_c \cdot w_t, \quad \text{if } g \in \{RES\} \tag{3.12}$$

$$\text{Gen}_{cost} = \sum_{y\in\text{Ep}} \sum_{g\in\text{G}} \sum_{t\in\text{T}} P_{g,t,y} \cdot C_g \cdot w_t \tag{3.13}$$

$$\text{Inv} = \sum_{y\in\text{Ep}} \sum_{l\in\text{NL}} \sum_{k=1}^{\text{Max}_{k,l}} C_{z,l,k,y} \cdot \text{Line}_c \tag{3.14}$$

Due to the fact that the selection of extreme and representative days arises from the maximum dissimilarity methodology described in [141] and also described in subsection 3.7.3, the weight w_t of each selected hour/day has been calculated by dividing the number of hours represented by the specific day weight.

Transmission Line Constraints

$$P_{l,y,t} + P_{\text{loss},l,y,t} \leq F_{qdtr,l,y,t}, \quad \forall l \in L,\ t \in T \tag{3.15}$$

$$P_{l,y,t} - P_{\text{loss},l,y,t} \geq -F_{qdtr,l,y,t}, \quad \forall l \in L,\ t \in T \tag{3.16}$$

These constraints ensure that the power flow $P_{l,y,t}$ on each transmission line l does not exceed its thermal limit with qDTR methodology $F_{qdtr,l,t}$ in either direction, including the effect of transmission losses $P_{\text{loss},l,y,t}$. It is important to note that $F_{qdtr,l,y,t}$ is of the form described in Eq. 2.19, where the selection of X_R depends on the risk approach used, as described in section 3.4 and calculated for the specific time t and y.

Power Flow Equations (DC Approximation)

$$P_{l,y,t} = \frac{1}{x_l \cdot \tau_l} (\theta_{n,y,t} - \theta_{m,y,t} - \phi_{l,y,t}) \quad \forall l \in L,\ t \in T \tag{3.17}$$

$$P_{l,y,t} = \frac{1}{x_l \cdot \tau_l} (\theta_{n,y,t} - \theta_{m,y,t} - \phi_{l,y,t}) \cdot Z_{l,k,y} \quad \forall l \in NL,\ t \in T \tag{3.18}$$

This DC power flow model links power flows to the difference in bus voltage angles $(\theta_n - \theta_m)$ across line l, where x_l is the line reactance and τ_l is the transformer tap ratio and ϕ_l is the angle (only meaningful to PT, but when is a cable or a line, $\phi_l = 0$ and τ_l equal to 1) [140]. For new lines the same constrain is used, but multiplied by $Z_{l,k,y}$.

New Line Investment Constraints

$$Z_{l,k+1} \leq Z_{l,k}, \quad \forall k \in \text{Max}_{k,l}, l \in \text{NL}, t \in T \tag{3.19}$$

$$\sum_{ny \leq y} C_{z,l,k,ny} \leq Z_{l,k,y}, \quad \forall y \in \text{Ep}, k \in \{1, \ldots, \text{Max}_{k,l}\} \tag{3.20}$$

$$C_{z,l,k,y} \geq Z_{l,k,y} - Z_{l,k,y-1}, \quad \forall y > 1, k \in \{1, \ldots, \text{Max}_{k,l}\} \tag{3.21}$$

$$C_{z,l,k,y} = Z_{l,y,k}, \quad \forall y = 1, k \in \{1, \ldots, \text{Max}_{k,l}\} \tag{3.22}$$

These constraints define the investment decision variables $Z_{l,k,y}$ for new transmission components, representing the investment of the k-th line or component of the new asset l in the period y in epoch Ep [142]. Through Eq. 3.20, it is ensured that the new line or component are installed sequentially across the periods; for instance, the second line or component cannot be built before the first, and the third before the second, which imposes an orderly progression of line investments. The Eq. 3.21 ensures that the accumulated investments up to period y do not exceed the indicator variable $Z_{l,k,y}$. Once a line or component is constructed in a prior period, it remains available in all subsequent periods. Finally, in Eq. 3.22, the first period is initialized. On the other hand, $Max_{k,l}$ represents the maximum number of new lines permitted for that asset, and NL represents the set of new lines.

Operational Limits for New Lines

$$-F_{qdtr,l,k,t} \cdot Z_{l,k} \leq P_{l,k,y,t} + P_{\text{loss},l,y,t} \leq F_{qdtr,l,k,t} \cdot Z_{l,k}, \quad \forall l \in \text{NL}, \ t \in T \tag{3.23}$$

This is to ensure that a new line only is constrained when it is expanded ($Z_{l,k} = 0$).

Transmission Loss Modeling

$$P_{\text{loss},p,\ell,y,t} \leq r_\ell \cdot \left(\frac{p}{\tan} \cdot F_{qdtr,\ell,t} \right)^2, \qquad \forall \ \ell \in L, \ t \in T \tag{3.24}$$

$$P_{\text{loss},p,\ell,y,t} \geq m_p \cdot (s \cdot P_{\ell,t}) + a_p, \qquad \forall \ p, \ s \in \{-1, 1\}, \ \ell \in L, \ t \in T \tag{3.25}$$

Here, $P_{\text{loss},l,t}$ represents ohmic losses in the line, where r_l is the resistance. Piecewise linearization (via m_p and a_p) approximates the quadratic loss curve $r_l P_l^2$, allowing the inclusion of losses in an efficient way. A more extensive description of this approximation could be found in [143].

Nodal Power Balance

$$\sum_{l \in n} P_{l,y,t} - \sum_{l \in (m)} P_{l,y,t} + \frac{1}{2} \sum_{l \in n} P_{\text{loss},l,y,t} + \frac{1}{2} \sum_{l \in m} P_{\text{loss},l,y,t} = P_{\text{inj},n,y,t} + P_{\text{Lsh},n,y,t}, \quad \forall n \in \mathcal{N}, \ t \in T \tag{3.26}$$

With this restriction, the balance of power at each node is limited: the total power that flows out minus the power that flows in, plus half of the associated losses, must equal the net power injection and any unmet demand. The losses are distributed between the sending and receiving buses.

Limitations

- DC-OPF apply only the active power balance equations, while reactive power balance equations are not modeled, and voltage magnitude is treated as a constant parameter rather than a decision variable.
- The formulation does not account for generator and cascade outages. This limits its applicability for secure planning under reliability standards.
- There is no modeling of ramping, startup/shutdown costs, minimum up/down times, or storage dynamics.
- Transmission losses are approximated. This can misrepresent actual losses during some scenarios.
- Due to the main objective to analyze the thermal ratings, this method could be greedy in terms of memory and computation. It could be solved with decomposition techniques.
- The model assumes a perfect forecast from climate models and does not include stochastic treatment of renewable energy variability, demand uncertainty, or equipment failures.
- Carbon pricing penalties and restrictions are implemented as static coefficients, while real-world implementations can vary dynamically or have limits on each region or country.

3.4 Risk Management with Quasi Dynamic Thermal Ratings

Special focus is placed on two distinct categories of risk considered in the estimation of long-term thermal ratings: (i) *Lower Capacity Threshold*, and (ii) the *Overtemperature Frequency*. These two risk dimensions are incorporated into the methodological basis of the proposed qDTR framework and are essential for developing a climate-aware rating model and conservative planning.

The first type of risk, referred to as the *lower capacity threshold*, allows for the reduction of the impact of extreme or adverse weather in relation to a defined baseline horizon. Such weather may include conditions like low wind speeds, low moisture, or elevated ambient temperatures, which can significantly reduce the thermal capacity of transmission components. In the qDTR methodology, this risk is addressed by selecting the parameter x_R in Eq. 2.19, which denotes the fixed-probability threshold selected by planners (e.g., 0.1% or 1%) to select the conservative fixed threshold of the rating distribution. Through this approach, the conventional methodology used to determine STR is expanded, explicitly allowing for the specification of a fixed-probability threshold, thereby incorporating climate adverse variability and extremes into long-term planning assessments.

For example, if an operator determines the rating of a OHL under conservative conditions based on a traditional estimation of STR, it could be exceeded if the actual wind speeds fall below the selected threshold, resulting in conductor temperatures exceeding the nominal safe operating value (also described in Fig. 1.2), which would reflect a simple and direct correlation between wind and conductor temperature. However, as detailed in previous chapters, the rating is influenced by the interaction of multiple meteorological variables, illustrated in Fig. 3.3 and subject to the temporality of the meteorological event for a OHL. Therefore, an operator must analyze the distribution of key meteorological parameters shown in Subfigure (a), highlighting the lowest quantile values in red. On the other hand, Subfigures (b) and (c) present a scatter plot that emphasizes how low wind speeds, coinciding with high solar radiation, tend to produce critical reductions in thermal capacity. Finally, Subfigure (d) displays the probability density function of the rating, with an emphasis on the bottom 10%; the dashed red lines indicate the 2nd and 0.1 percentiles, which define the *Lower Capacity Threshold*, thus delineating the selected risk.

When component loading falls within this risk region, as defined in subfigure (d), there is a high probability of thermal stress or overheating in the system component. This phenomenon, also referred to as *temperature Risk* in [144], is particularly critical in long-term planning scenarios, where conservative assumptions must consider the possibility of unfavorable, non-sequential weather conditions. By formally integrating this lower capacity threshold into the qDTR structure to limit overload exposure, the methodology facilitates more robust and climate resilient operational planning and decision-making. It is important to note that, within this definition, the flow is not treated as a variable but as a fixed condition consistent with the defined thermal rating. This assumption isolates the thermal performance from operational variability, ensuring that the analysis focuses solely on the influence of meteorological conditions on rating determi-

nation.

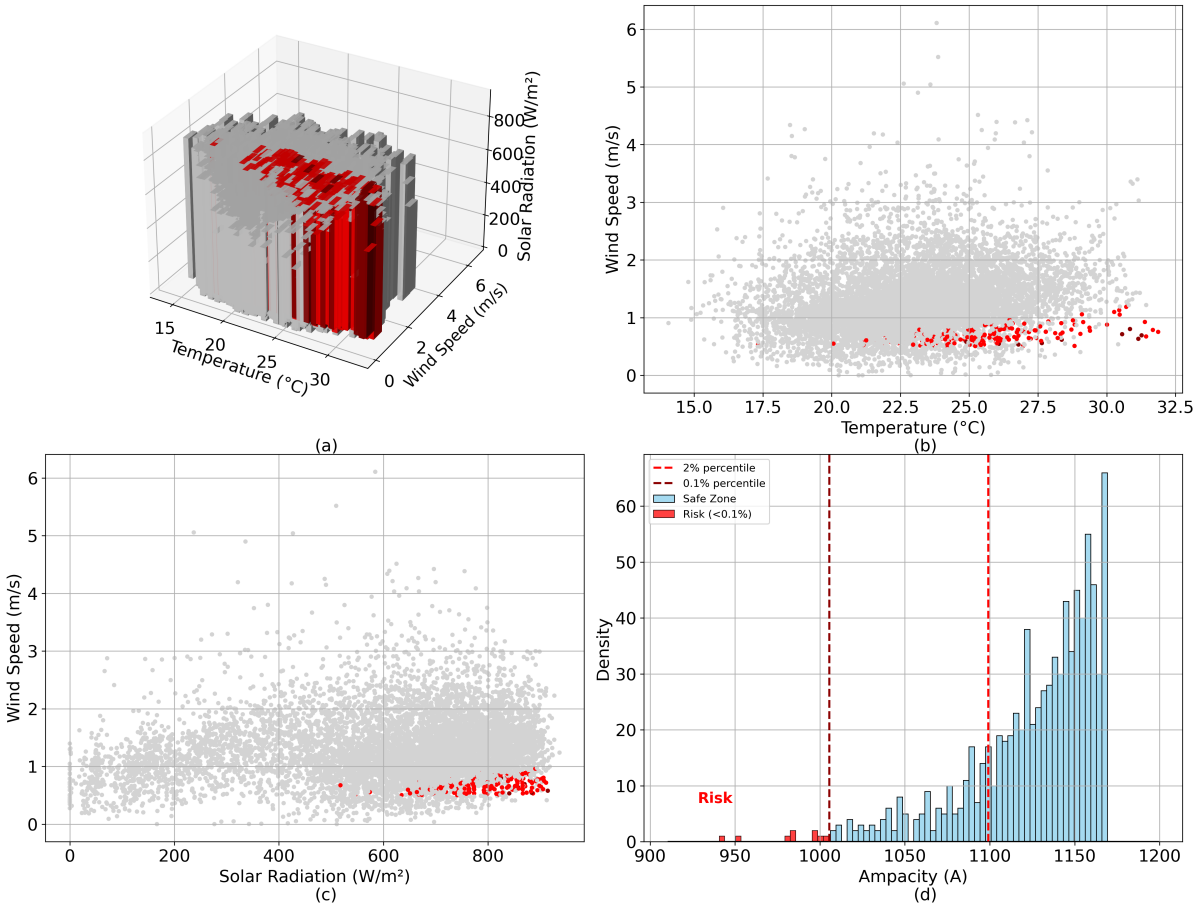

Figure 3.3: Illustration of temperature risk assessment for an OHL conductor. Subfigure (a) shows meteorological parameter distributions with lower quantiles in red; (b)–(c) show scatter plots highlighting the combined effect of wind and solar radiation; (d) presents the rating probability density with the lower capacity threshold (red dashed lines).

Furthermore, it is important to note that this temperature risk depends not only on severity but also on frequency. A short-term overheating event (e.g., lasting only minutes) may be tolerable. However, a persistent exceedance lasting several hours, particularly during seasonal peak load periods, can pose significant reliability and safety concerns. This introduces a second dimension of risk, referred to as *temporal risk* in [144], which quantifies the system's vulnerability to prolonged periods of elevated conductor temperature. As illustrated in Fig. 3.4, the potential risk area is delineated by the region in which the component current exceeds the steady-state thermal rating, increasing the probability of overheating, performance degradation, or even failure. Therefore, this new risk management not considers not only the statistical extremes of weather data but also the temporal recurrence of these conditions, allowing for a more resilient and realistic characterization of system boundaries.

Furthermore, the second risk considered in this work is the frequency with which thermal ratings are exceeded over the planning horizon. This risk is particularly relevant for operational and investment decisions, as frequent violations, even if minor, can accumulate and lead to

significant system stress, equipment aging, or failure. By statistically analyzing the CDF of the ratings, separated into different intraday time frames (e.g., day/night, month/hour), the model allows planners to identify periods of increased vulnerability and adapt their operational strategies accordingly.

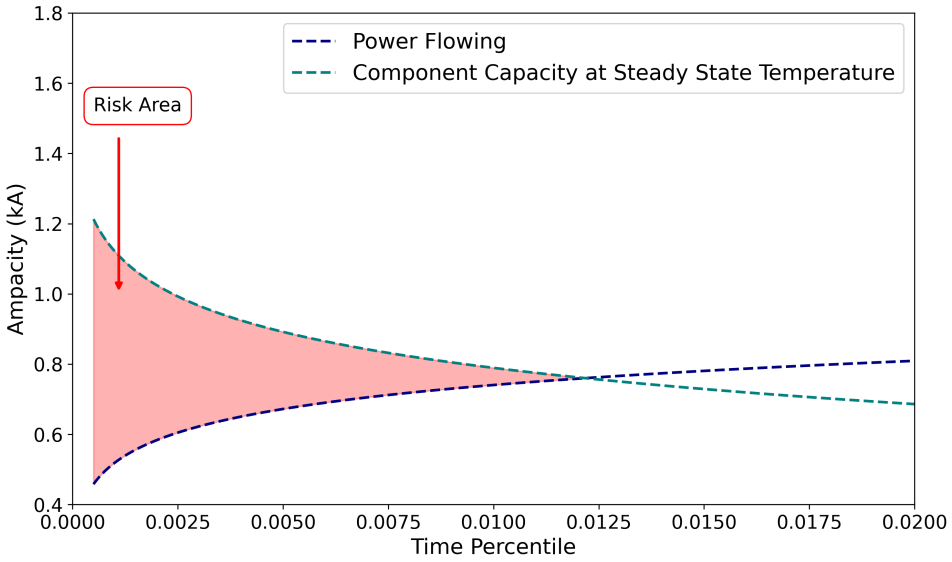

Figure 3.4: Temporal Risk Assessment Analysis for a component, showing the risk area caused when the power flow exceeds the component capacity

This dual-risk perspective aligns with emerging industry practices, which emphasize the need to plan for worst-case conditions: scenarios that, while rare, materialize and can severely compromise system integrity [10] and the frequency of component overload. In this context, the proposed methodology facilitates the assessment of both high and low load operating profiles and remains consistent with the widely accepted (N–1) reliability criterion, ensuring that the system maintains operational stability in the event of a non-simultaneous outage of any component. By explicitly incorporating both lower capacity threshold and temporal frequency risks, into the qDTR methodology, eliminates the gap inherent in the fixed-probability threshold approach, where flow is not treated as a variable but rather as a fixed condition consistent with the defined thermal rating. Additionally, the methodology remains consistent with the N–1 security criterion by ensuring that, even under rare but severe conditions, flows respect probabilistic thermal limits. With this, the method proposed provides a comprehensive framework for long-term transmission planning in a context of increasing climate uncertainty.

3.4.1 qDTR Risk Management Under Climatic Scenarios

Therefore, the proposed methodology aims to assess the rating in individual transmission components by evaluating both the flow and temperature intensity and frequency of a potential overload within a defined planning interval, that is, it performs this process for each hour, year, or frequency required in the TEP. This approach also makes it possible to identify the transmission components where capacity can be increased under contingency conditions with-

out compromising system reliability over the long term, through the qDTR methodology. As illustrated in Fig. 3.5, the qDTR method is applied to Line 27 of the test network [145] to estimate steady-state and contingency ratings (see Fig. 1.5 - concept of ratings in steady state and contingency) under historical weather conditions. The red shaded region in the figure represents the rating improvement potential while maintaining a temperature and flow risk below 0.017%, equivalent to approximately 600 hours over a 40-year horizon. This new probabilistic threshold reflects a conservative bound that ensures thermal safety, allowing system planners to exploit additional capacity during infrequent, but permissible, operating conditions.

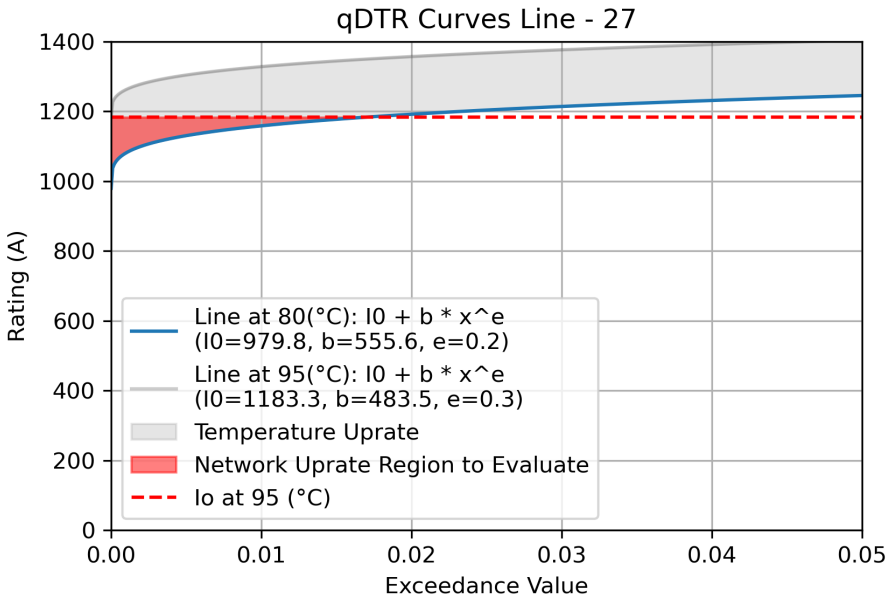

Figure 3.5: Temporal Risk (red zone) Assessment Analysis for the Line 27 of of the test network [145], where is represented the steady-state (80 C°) and contingency ratings (95)C°

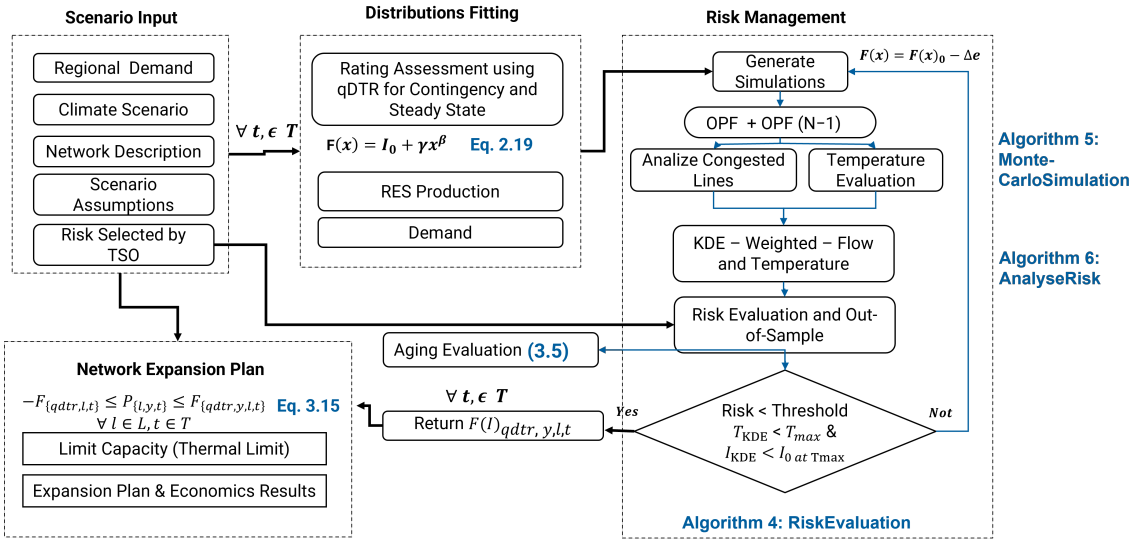

Figure 3.6: Overview Thermal Risk Management into long-term transmission expansion planning

In order to asses the ratings under risk management to be updated into the Eq. 3.15, it is introduced a probabilistic approach, influenced by weather ($\mathcal{W}$) and power flows (P_L) over the network, to determine the thermal ratings limits required for TEP, graphically described in Fig. 3.6. The main objective of this method is to identify the risk area (red-shaded region in Fig. 3.7), representing the potential for rating improvement while keeping temperature and flow risks below a conservative threshold (equivalent to approximately hours over the asset's lifetime). This approach ensures thermal safety while allowing system planners to utilize additional capacity during non frequent, yet permissible, operating conditions.

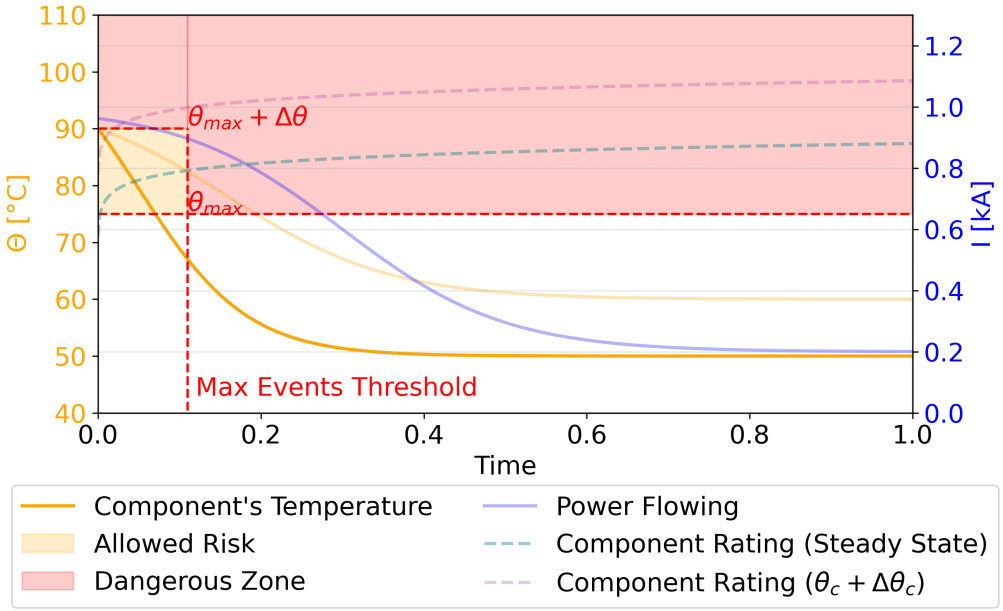

Figure 3.7: Temporal Risk Assessment Analysis for a component, showing the risk area caused when the power flow exceeds the component capacity, mainly limited by the maximum temperature and the low probability rating selected by the operator.

First, the initial conservative with fixed probability threshold in steady state and contingency thermal rating (at $Tmax$) of each transmission line l at period y and time t is calculated using a quasi dynamic method described in 2.2.2, where the function fitted, using thermal models with the influence of climate data (e.g., wind speed, ambient temperature) and physical parameters is:

$$F_{l,y,t}^{qDTR} = A_l \, X_{l,y,t}^{b_l} + F_{l,t}^{0} \tag{3.27}$$

However, while fixed-threshold rating (i.e $X_{l,y,t} = 0.1\%$) assessments provide an initial reference point for both continuous and contingency ratings, they fail to capture the variability and uncertainty inherent in long-term system planning. To address this limitation, a dynamic Monte Carlo Simulations (MCS) approach, as described in Alg. 4, is implemented at each time step ($t \in y, \mathcal{T}$) of the TEP optimization.

Ratings are obtained via MCS by first evaluating the network at each time step using $F_{l,y,t}^{qDTR}$, together with the CDF of demand and RES production. A DCOPF is then performed to determine line flows under both steady-state and contingency conditions. Based on the resulting power flows, conductor temperatures are computed using the thermal models in [29] for OHL and [51] for UGL, with meteorological data sampled for each component. The resulting temperature and flow samples for each line are then characterized using fast kernel density estimation [146] to obtain their corresponding Probability Density Functions (PDFs).

To derive a single PDF per line representing its behaviour under the evaluated scenario and time step, a weighted composite kernel method $\mathcal{F}_{KDE,P_L}$ and $\mathcal{F}_{KDE,\theta_o}$ [146] is applied, where w_p

denotes the probability weight associated with each contingency. An illustrative example of this procedure is shown in Fig. 3.24, which details the weighted density and associated contingencies for each power flows/temperature combination during the evaluation of the fourth epoch (year 2045).

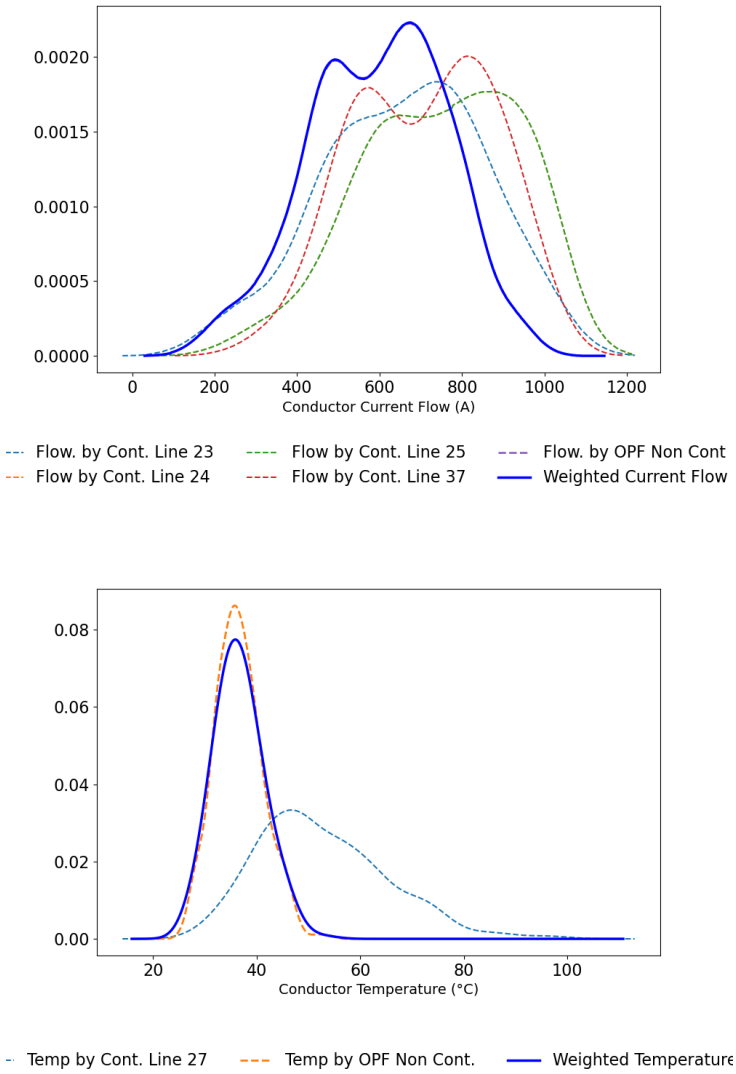

Figure 3.8: KDE estimation for a line. Power flow and conductor temperature, incorporating congestion probabilities

Using the resulting CDF for each line, the risk is assessed according to the operator-defined quantile q. If the risk thresholds are not satisfied, the method reduces the capacity of the critical transmission lines by Δe_ℓ, updating the effective thermal limits:

$$\text{CDF}_{qDTR}(\ell).e \leftarrow \text{CDF}_{qDTR}(\ell).e - \Delta e_\ell \tag{3.28}$$

This reduction is determined based on the line overload frequencies, and the updated capac-

ities are then used in the subsequent MCS iteration. Furthermore, the convergence of the MCS is assessed using the **Expected Energy Not Delivered (EENS)** as the primary stopping criterion, as described in Eq. 3.29.

$$\text{EENS} = \mathbb{E}_u \left[\sum_{d \in D} P^{Ls}(u) \right] \tag{3.29}$$

The simulation progresses until the relative standard error (or, equivalently, the coefficient of variation) of the estimated EENS falls below a predefined threshold. This approach is established in reliability studies, where a 5% of coefficient of variation is commonly adopted to balance computational efficiency with accuracy [147]. However, in this approach to ensure convergence, the algorithm evaluates the relative standard error (RSE):

$$\text{RSE}_u = \frac{\sigma(\text{EENS})}{\sqrt{u} \cdot |\mu(\text{EENS})|}, \tag{3.30}$$

Finally, once the risk-managed rating is obtained, the method validates the result using an out-of-sample procedure to confirm the robustness of the risk-aware rating selection [148]. If both the in-sample and out-of-sample probability estimates fall within the allowable limits, the loop terminates and the component is deemed to lie within the safe risk zone. Otherwise, additional iterations with an increased number of MCS samples are performed until both criteria converge within the acceptable thresholds.

Algorithm 4: RISK$_{\text{MANAGEMENT}}$ $(net_t, CDF_{qDTR,t}, \mathcal{W})$

while *true* **do**
  $net \leftarrow net_t(F_{l,t}^{qDTR_{(Tmax)}})$;
  if $\mathcal{U} >$ `Min`$_{\texttt{MC}}$ **then**
    foreach *(ℓ, Δe_ℓ) in* `Risk`$_{out}$ **do**
      $CDF_{qDTR}(\ell) \leftarrow CDF_{qDTR}(\ell) - \Delta e_\ell$;
  while *Risk* **do**
    foreach *line ℓ with Δe_ℓ in Risk* **do**
      $CDF_{qDTR}(\ell).e \leftarrow CDF_{qDTR}(\ell).e - \Delta e_\ell$;
    while $\frac{\sigma(EENS)}{\sqrt{k}\,|\mu(EENS)|} > \gamma$ **do**
      $net \leftarrow CDF_g(u),\ CDF_d(u)$;
      $\text{cont}_u \leftarrow$ `RunDCOPF(N-1)` (net);
      $\text{PF}_u \leftarrow$ `RunDCOPF` (net);
      $\mathcal{F} \leftarrow \mathcal{F} \cup \{cont_u\} \cup \text{PF}_u$;
      if $|\mathcal{F}| \geq 2$ **then**
        $\text{EENS} = \mathbb{E}_{\mathcal{F}}\left[\sum_{d\in D} P_d^{Ls}(\mathcal{F})\right]$;
        $\text{RSE}_{\mathcal{F}} = \frac{\sigma(\text{EENS})}{\sqrt{|\mathcal{F}|}\,|\mu(\text{EENS})|}$;
        if $\text{RSE}_{\mathcal{F}} \leq \epsilon$ **then**
          break;
        else
          $u \leftarrow u + 1$;
    $\mathcal{L} \leftarrow \{\ell : \text{Line}[\ell] \in \{UGL, OHL\}\}$;
    $\mathcal{C}, \mathcal{O} \leftarrow \emptyset$;
    foreach $\ell \in \mathcal{L}$ **do**
      if $\max(line\_data[\ell]) > I_0(\ell)$ **then**
        update $\mathcal{C}, \mathcal{O}$;
    if $\mathcal{O} = \emptyset$ **then**
      return 0
    foreach $(f, \ell) \in \mathcal{C}$ **do**
      foreach *sample* I_{flow} **do**
        $\theta_{o,c}[f, \ell] \leftarrow$ `TModel`$(I_{flow}, \mathcal{W})$;
        $P_L[f, \ell] \leftarrow I_{flow}$;
    foreach $o \in \mathcal{O}$ **do**
      $\mathcal{F}_{KDE,\theta_o}(\theta_o, \hat{f}_{\theta,o}) \leftarrow$ `KDE`$(\theta_{o,c}, w_p)$;
      $\mathcal{F}_{KDE,P_L}(I_o, \hat{f}_{I,o}) \leftarrow$ `KDE`(P_L, w_p);
    $\text{CDF}_{\theta,o}(q) \leftarrow$ `KDE_CDF`$(\hat{f}_{\theta,o}, \theta_o, q)$;
    $\text{CDF}_{I,o}(q) \leftarrow$ `KDE_CDF`$(\hat{f}_{I,o}, I_o, q)$;
    foreach $o \in \mathcal{O}$ **do**
      if $\text{CDF}_{I,o}(q) \leq I_{\max}$ ***or*** $\text{CDF}_{\theta,o}(q) \leq \theta_{\max}$ **then**
        Find $q^\star$ in $\text{CDF}_{I,o}$;
        $\text{Risk}[o] \leftarrow q^\star$;
    if *Risk is empty* **then**
      break
  $Risk_{out} \leftarrow$ `OutSample`$(CDF_{qDTR}, \epsilon, \mathcal{W})$;
  if *Risk* = `False` ***and*** $Risk_{out}$ = `False` **then**
    $F_{l,t}^{DTR_R} = CDF_{qDTR}$;
    break;
  else
    $\mathcal{U} \leftarrow \mathcal{U} + \text{Min}_{\text{MC}}$;
$net_t \leftarrow$ update with final $F_{l,t}^{\text{DTR}_R}$;
return net_t

3.5 Aging Evaluation

As previously mentioned, the thermal limits and aging of transmission components are intrinsically linked through their temperature, joule losses, and surrounding environmental conditions. To support network planning, this work review generalized aging models that can be integrated into OPF formulations, considered not as dynamic constraints but as dynamic outcomes influenced by system operation and environmental variability.

The methodological approach is developed in two main stages. First, the thermal aging behavior of individual components is characterized, and an expression is derived to represent aging as a function of temperature over time. Second, a thermally informed rating model is established to relate component temperature to electrical power flows and worst-case ambient meteorological conditions (used in the algorithm $\texttt{Risk}_{Management}$ 4). This combination enables the dynamic estimation of component capacity evolution and provides a basis for assessing asset degradation and thermal risk in a climate-sensitive, system-wide context.

3.5.1 Aging Modelling

As indicated in Section 1.3.4, it is demonstrated that aging depends on the operating temperature of the component, which is in turn influenced by Joule losses and environmental conditions.

Aging is often modeled using Arrhenius' law [149], considering it a chemical reaction that alters the properties of the object, with a reaction rate that accelerates with increasing temperature. This is particularly relevant for electrical cables and PT, where aging corresponds to the degradation of dielectric insulation (or oil in the case of transformers), which loses its dielectric properties. Also, in the case of OHLs this model has been proposed to describe the impact of temperature on the annealing.

This relationship can be generally expressed as Eq. 3.31 [150], which represents Arrhenius; where $L(\theta_c)$ is a measurable indicator of life, θ_c is the absolute temperature in centigrade, and A and B are empirical constants; however, it must be related to the key parameter concerning aging/temperature.

$$L(\theta_c) = A \exp\left(\frac{B}{\theta_c + 273}\right), \tag{3.31}$$

For example, in PT, as previously described, the critical temperature variable is HotST, as it represents the location most susceptible to thermal aging. Consequently, the variable θ_c can be determined using Equation 3.32, which follows the same form as Equation 2.16. Refer to List of Symbol section at page xi for a complete list of variable definitions.

$$\theta_{\mathrm{c}} = \theta_{\mathrm{HST}} = \theta_o = \left[\frac{1 + K^2 R_{ll}}{1 + R_{ll}}\right]^{x_r} (\Delta\theta_{or}) + \theta \tag{3.32}$$

Together, these formulas allow us to link the operational load and environmental conditions with the winding temperature, and from there, estimate the degradation of the PT's lifespan using the Arrhenius model.

In the case of OHL, the calculation guide [29], presented in Section 2.2.1.1, is implemented within the thermal model of the conductor. This approach determines the steady-state conductor temperature (θ_c) by formulating a root-finding problem, where the target condition is that the calculated ampacity equals the imposed loading. The procedure relies on the heat balance equation introduced in Eq. 2.1. The formulation iteratively adjusts θ_c, using a bisection method to ensure convergence.

Similarly, this same concept applies to the UGL, where the thermal behavior of insulated electrical cables is described in [32], and the temperature of the conductor is given as Eq. 3.33 derived from Eq. 2.4.

$$\begin{aligned}\theta_c = \theta &+ W_d \left(\tfrac{1}{2}T_1 + n(T_2 + T_3 + T_4)\right) \\ &+ I^2 R_{UGL} \left[T_1 + n(1+\lambda_1)T_2 + n(1+\lambda_1+\lambda_2)(T_2+T_4)\right]\end{aligned} \tag{3.33}$$

3.6 Databases and Data Overview

Variable	Units	Section	Source
Weather Databases (Historical)			
Ambient Temperature	°C	3.7.2,3.7.4	Europe [6]
Wind Speed	m/s	3.7.2,3.7.4	Europe [6]
Soil Temperature	°C	3.7.2,3.7.4	Europe [6]
Solar Radiation	W/m^2	3.7.2,3.7.4	Europe [6]
Network Characteristics			
Regional Transmission Description	kV	3.7.1.1	PyPSA Network Data [151]
Transmission Description	kV	3.7.4, 3.7.3	IEEE Test Network Data [145]
OHL Conductor Type	Unit	3.7.1.1	490-AL1/64-ST1A
Transformer	Unit	3.7.2	PyPSA Network Data [151]
Socio-Economic Parameters			
GDP per Capita	EUR	3.7.2	Eurostat / Regional [152, 153]
Population	Person	3.7.2	Eurostat / Regional [152, 153]
CO_2 Emissions Constraint	tCO_2/MWh	3.7.1.1, 3.7.2, 3.7.4	Scenario Data [154–159]
Generation and Demand Profiles			
Load	MWh	3.7.2 3.7.4	$Regional_{\text{historical}}$ [160, 161]
Wind	MW	3.7.2	Wind Dataset [162]
Solar / Wind Density	$\frac{MW}{Km^2}$	3.7.2	Euro [163, 164]
TEP & Planning Parameters			
Load Shedding Max (λ)	pu	3.7.4	[165]
Curtailment Cost	\$/MWh	3.7.4	[165]
CO_2 Cost	€/MWh	3.7.4	[166]
Photovoltaic Plant (PV)/Wind Capex	€/kW	3.7.4	Advance Scenario [167, 168]
Line/Cable CAPEX	€/MW/m	3.7.4	Lower Scenario [169]

Table 3.1: Input Data Overview for Long-term Transmission Expansion Planning

3.7 Results

As shown in previous chapters, due to variable meteorological conditions, transmission system components are increasingly vulnerable. This has increased the importance of climate influence and adaptive planning methodologies that go beyond traditional static assumptions. This chapter explores the results of integrating qDTRs with risk-based planning approaches, presenting both conservative with fixed probability threshold and stochastic methods (from the rating selection perspective) to optimize long-term electric system capacity and resilience, across different time scales.

As previously described, the qDTRs represent an evolution beyond the gap between DTRs and STRs, incorporating weather data. By using probability distributions fitted to the capacity-tail for the long-term climate simulations, qDTRs allow planners to capture the variability in environmental conditions while maintaining a predefined level of tolerance to the risk of thermal overload.

The following sections will focus on 1) Conservative with fixed probability threshold approaches for estimating component ratings, integrated into different network expansion models using climate historical data. This enables a fixed assessment of transmission capacity, helping to optimize infrastructure sizing and investment decisions under specific projected scenarios. 2) The stochastic approach from a risk selection perspective, which introduces climate impacts across transmission power components. This allows operators to assess risk-adjusted trade-offs in investment and operating strategies under weather influence.

To demonstrate this integration, this chapter leverages standard methodologies and case studies applied at the European level. These studies use machine learning, thermal modeling, and long-term G&TEP simulations to compare traditional fixed STR or $qDTR_{year}$, and $qDTR_{month/hour}$ on power system components. Given the absence of a model that simultaneously integrates all the variables that influence component temperature, the following subsections present demand and generation models applied specifically to support this research. Although they are not the main focus of this thesis, these models were generated to facilitate a broader understanding of the operational implications and potential benefits of implementing qDTR. They provide the necessary context to evaluate how variations in load and generation profiles interact with dynamic thermal rating methodologies under different temporal and climatic conditions.

By introducing conservative, fixed-probability threshold and stochastic rating strategies, this chapter demonstrates how qDTR bridges the gap between operational flexibility and long-term strategic planning, establishing it as a key framework for assessing the capacity impacts of transmission components under changing climatic conditions

To strengthen the benchmark, the proposed applications extend the scope of qDTR by systemic uncertainties to evaluate and select the level of risk for each transmission system component (see Section 3.3.1). These uncertainties encompass projected demand growth, which reflects both socio-economic trends and sectoral electrification; the spatial and temporal availability of generation resources, particularly variable RES; and weather parameters, such as ambient temperature, wind speed, soil temperature, and moisture, all of which directly affect the thermal

capacity of transmission assets. Furthermore, the methodology considers outages of system components, which influence operational reliability, as well as evolving investment trajectories in new RES, which shape future network topology and new component stress. These are implemented either within established tools or through proprietary optimization models. By integrating these factors, the qDTR methodology positions itself not only as a method for rating optimization, but also as a conservative and forward-looking method for resilient and cost-effective energy system planning under climatic scenarios.

The first part of this integration challenge involves modeling expansion plans using established energy systems tools that combine conventional generation with RES, which have been widely studied in recent literature. In particular, [170] provides a comprehensive review of methods and tools for simulating hybrid energy systems, highlighting the growing relevance of open-source frameworks for system-level planning and analysis.

In the context of this thesis, the modeling scope is specifically limited to: (i) power transmission and transmission networks implemented; (ii) time horizons ranging from hourly to multi-decadal projections; (iii) spatial resolutions ranging from individual network elements to national-level aggregation; and (iv) techno-economic assessments based on quasi-static power flow analyses. To identify suitable tools that meet the defined modeling requirements, a targeted literature review of existing simulation platforms was conducted. The primary objective of this evaluation is not to provide a comprehensive benchmark or performance comparison of the tools themselves, but rather to determine their ability to accommodate the proposed methodology, particularly the integration of terminal capacity limits, such as those introduced by qDTR. Therefore, the evaluation presented here is intended to support methodological alignment. A more comprehensive comparative evaluation of software capabilities, modeling accuracy, and computational efficiency remains an important avenue for future research. Finally, the findings, summarized in Table 3.2, highlight the characteristics of selected open-source, Python-based modeling tools with respect to OPF, long-range planning capabilities, integration of environmental factors, support for dynamic thermal ratings, and regional-level system representation.

Description	OPF	Planning (Long-Term)	Environmental	Ratings	Regional
PyPSA / PyPSA-Eur (A)	√	√	√	DTR OHL	√
PandaPower	√	√ (SimBench)	–	Thermal model OHL	–
OpenDSS	√	–	–	–	–
Antares (R-based)	√	√	√	–	–
Gurobipy	√	–	–	–	–

Table 3.2: Capabilities of Selected Open-Source Power System Modeling Tools (Python-Based)

With this assessment, the following section focuses on the practical application of qDTR in a network planning context, using some of these open source tools. Specifically, procedures are developed and applied in papers **A**, **B**, **F**, and **D**, primarily to present and evaluate how fixed-probability threshold derived from qDTR influence transmission system expansion and associated investment costs across Europe or in regions within Europe.

3.7.1 Network Planning under qDTR with Fixed-Probability Constraints

3.7.1.1 European Power System Expansion: Climate-Aware Transmission approach

Firstly, a procedure was developed to quantify the impact of the qDTR method on power network transmission capacity and network costs expected in Europe in paper **B**. This method is described in Fig. 3.9 and can be divided into four steps:

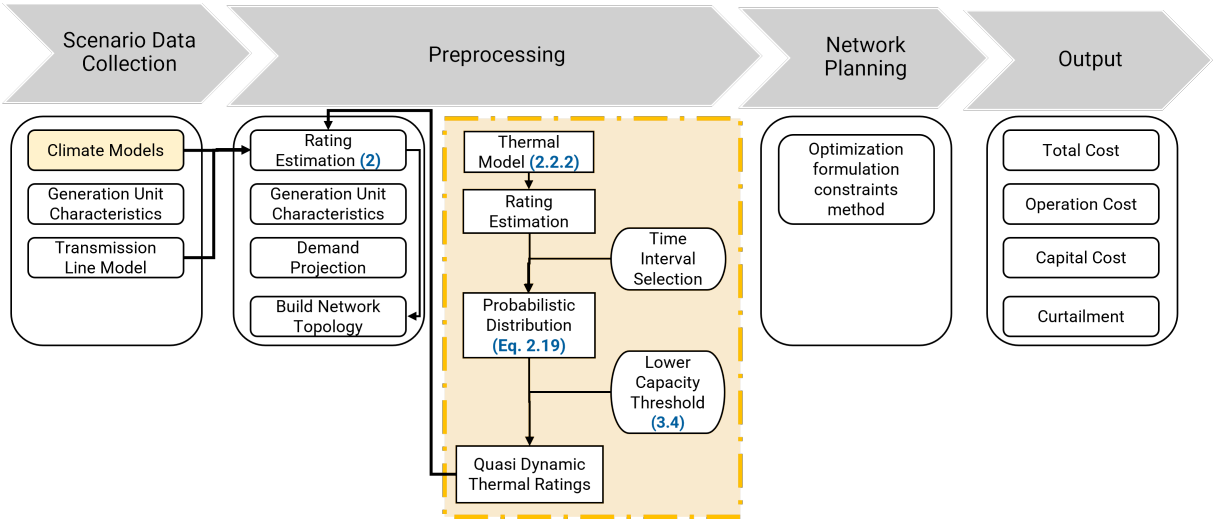

Figure 3.9: Visual representation of the procedure, the integration of the qDTR methodology is highlighted in yellow

The main objective of this case study is to integrate a regional network expansion model with the long-term climate influence component rating methodology, incorporating modules for RES and other energy sources, into a detailed transmission network model and optimization framework. This is done to assess the impact of modifying the component's thermal capacity limits, as is detailed in the previous chapter. Specifically, we incorporate the qDTR at month/hour and year temporal resolutions into the transmission model to more accurately reflect the rating under variable weather conditions. This approach allows for an evaluation with transmission impacted by the weather, enabling all the benefits of the thermal component rating model and the reliability of the system, especially in scenarios with a high proportion of RES, within the PyPSA-Eur modeling framework [28]. This process is initiated through he data collection step, and it is divided into two broad categories: climate models and network characteristics. The climate models used to assess component capacity are extracted from the European historical meteorological database for the period 1970–2020, obtained from the historical reanalysis [6]. It should be noted that Pypsa-Eur also allows the extraction of climate information; however, it is not temporally extensive, evaluated historically, and is primarily used to support the demand and generation modules. Within the network characteristics, this application extracts the list of transmission lines as input data.

Second, ratings estimation begins with the use of component thermal models based on the steady state models described in section 2.2.1. This methodology allows for measuring changes in transmission capacity caused by surrounding weather. It should be noted that transmission

capacity is also affected by factors such as voltage dips and stability. However, these aspects are beyond the scope of this research. The methodology presented here focuses on the analysis of thermal limits and serves as a guide for long-term planning.

Third, a G&TEP for Europe is calculated with a 2050 time horizon using PyPSA-Eur, integrating historical weather projections to estimate the updated thermal capacity of transmission lines based on the STR and qDTR methodologies. This allows quantifying the impact of climate on network costs from the perspective of transmission constraints. At the end, the economic results of each of the rating methodologies are collected to understand the benefits of each method. However, it is important to note that while PyPSA-Eur already has an option to natively accept a DTR version within optimization [171], it has been manually parameterized to accept qDTR values.

To understand the scope of the analysis, a geo-representation of the lines is shown in Fig. 3.10 taken from [172], to exemplify a visual representation of the impacts of the first and second steps. To do that, for each of them, at each coordinate and for each hourly time step available in the climatic dataset, the five-step procedure described in section 2.2.2 is performed to calculate the $qDTR_{month/hour}$ (288 combinations for representing annual variance) and annual fix $qDTR_{year}$ value to represent the new version of the traditional STR. As a result, a probability distribution of the form of Eq. 2.19 is generated for each component and is evaluated with a fixed conservatism of fixed-probability threshold (x_R) of 0.1% and $c = 0$. Now these new calculated ratings are introduced into the thermal capacity restriction in the Pypsa-Eur model and thus are able to perform the analysis.

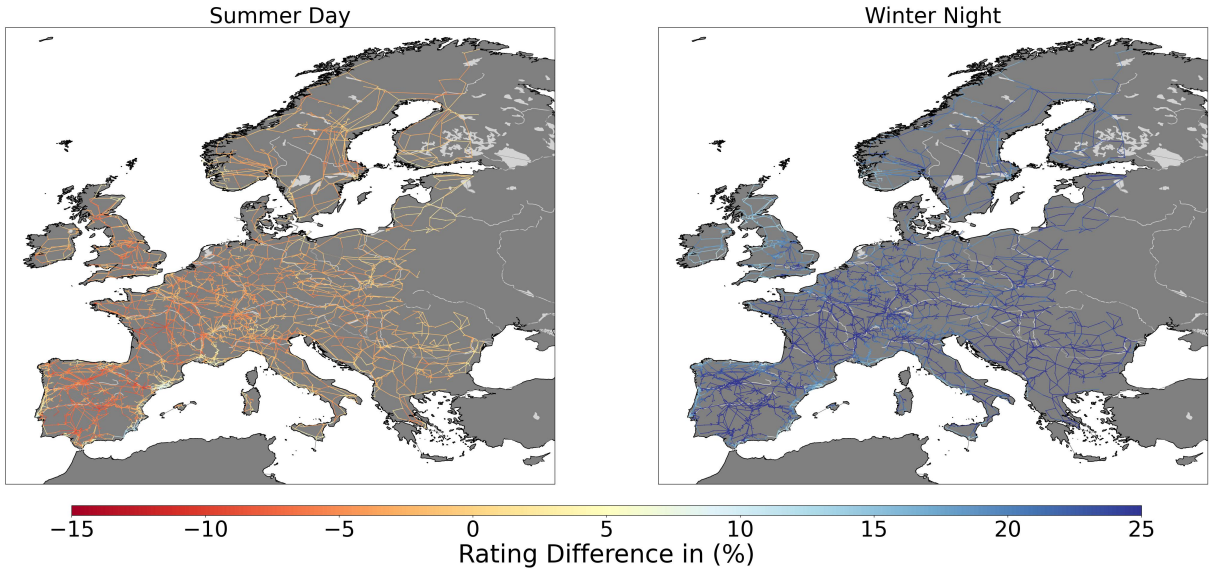

Figure 3.10: Rating Difference on transmission capacity in European Transmission, the difference in capacity for qDTR (Percentage Change $\Delta_{\%} \frac{qDTR_{Month/Hour}}{qDTR_{year}}$) in June at 14 h for Summer and October at 22 h for Winter

The analysis in the figure shows trends suggesting that incorporating regional climate effects using historical weather data significantly improves the performance of qDTR compared to

the traditional year fix value, especially during winter periods. This improvement is evident in several countries, including southern Spain and transmission components, where weather impact analysis allows for more efficient use of thermal ratings. However, during summer periods, a relative decrease in qDTR values reflects an improvement in the conservatism of overload risk management. This result indicates that the proposed rating methodology not only enables planners to exploit asset capacity more effectively under favorable conditions (winter nights) but also reduces the probability of thermal overheating during warmer seasons. As a result, qDTR offers a more adaptive, risk-based strategy for long-term transmission planning, balancing capacity maximization with operational safety under variable climate regimes.

For the third step, the financial impacts resulting from these new ratings are assessed through the G&TEP using $STR_{Historical}$ and $qDTR_{Historical}$ with month/hour temporal resolution, to estimate changes in Capital expenditure (CAPEX), Operational expenditure (OPEX), and RES curtailment. The comparison shows the benefits of using qDTR with a better temporal resolution to recover the lost transmission capacity.

This solution allows us to rely on a model to test the hypotheses' impact and obtain solid results. However, it has some limitations, particularly the fact that the network used in PyPSA-Eur is made of zones and interconnections, generated by the clustering algorithm used to aggregate zones and interconnecting lines. At the same time, a real network has a much higher number of nodes and, more importantly, lines. Knowing these limitations, this case study uses the already parameterized optimization model of Pypsa-Eur, where, for a more complete explanation, the reader can refer to [28]. However, in order to facilitate the main key parameters, the aspects that the authors have identified of the model implemented from [28] are summarised below.

- 37 nodes are parameterized for the analysis, similar to the countries described in the configuration.
- Planned horizon to 2050.
- CO2 levels have been updated according to the IPCC [156–159].
- Overnight Scenario, characterized by calculating an expansion of the energy system to meet demand, with sector option activates as Electrification of Transport, Industry, and Agricultural sector described in [173].
- Extendable Carriers: Solar, onshore wind, offshore wind, hydro, nuclear, oil, open/combined cycle gas turbine, coal, lignite, geothermal, biomass.
- The time resolution is set to 1 hour
- Assumptions for each type of generation technologies (cost, efficiencies, annualized interest rate for investment (4%), and emissions) are extracted from the PyPSA v0.28.0.
- Global correction factor of 1.9 for the load for all analyzed projections.

- Information about the optimization model can be found at [151], which has been updated in compliance with $f_{l_{qDTR}}$ limiting the capacity over the lines by applying the methodology proposed for the long-term evaluations.

- For the purpose of replicability, a configuration file is attached to know the full extent of parameter settings in the supplementary material of the paper **B** and available at HAL open archive.

The results are summarized in Table 3.3, which displays: The outcomes of a baseline simulation with qDTR evaluated annually or reference case, and the improvements achieved by using $\text{qDTR}_{\text{month/hour}}$ instead of $\text{qDTR}_{\text{year}}$, providing information on the economic results. It also reports the expected amount of reduction and the total cost of the system. However, these values are only relative to new investments and do not take into account the existing infrastructure. The aim is to determine the different generation capacity portfolios necessary to meet specific emission reduction targets.

The table details are: *(i)* The variation in system costs using the same historical weather data, but now changing the carbon emission constraints CO_2 maximum future scenario in Europe. *(ii)* $qDTR_{year}$ refers to annual static values, $\text{qDTR}_{\text{Hourly}}$ to month/hour temporal resolutions with the use of historical weather data, for the selected 2018 year. *(iii)* Values are in % and calculated as 1-y/x, meaning that positive values represent cost reductions and negative values represent cost increases. *(iv)* The results are reported in terms of CAPEX and OPEX in billion euros (B€) and RES curtailment in gigawatt-hours (GWh).

- Traditional Static $\text{qDTR}_{\text{year}}$ (Reference Case): In this case analysis study, the G&TEP model was employed to evaluate the optimal planning and operation of the power system under the carbon emission constraints imposed by the RCPs. However, despite the CO_2 limits, the scenarios exhibited slight but noteworthy divergences in CAPEX of 355.5B€ and OPEX of 18.9B€/y and RES curtailment levels. These differences imply that, while the economic optimization metrics remained stable, the system's ability to fully integrate and utilize RES was further limited by the assumptions and constraints of each RCP scenario. Now, based on this use case, the qDTR is integrated with month/hour resolution, allowing us to observe the benefits or impacts that can be obtained with this change in resolution.

Case 1 - $qDTR_{month/hour}$ **:** In this extended analysis, the G&TEP is executed under an alternative configuration of transmission capacity with hourly constraints. The primary objective is to assess the value added by $qDTR_{month/hour}$, especially their capacity to exploit enhanced transmission availability during nighttime and colder seasonal conditions.

As shown in Table 3.3, incorporating qDTR results in a modest but consistent reduction in both CAPEX and OPEX across all three scenarios. These findings highlight the cost mitigation potential offered by dynamic ratings, especially in the context of infrastructure constraints influenced by the climate, even when using a predefined expansion model.

Beyond the limitations of the model, the analysis reveals a steady decline in RES curtailment, likely driven by increased transmission asset utilization during cooler ambient temperatures. This behavior supports the methodology's objective of providing temporal flexibility, enabling

REFERENCE CASE									
Section A	$qDTR_{year}$								
$CO_2 Scenario$	RCP 26			RCP 45			RCP 85		
Metric	CAPEX	OPEX	Curtailment	CAPEX	OPEX	Curtailment	CAPEX	OPEX	Curtailment
Fossil	1.02E+11	4.58E+09	0.00E+00	1.18E+11	8.74E+09	0.00E+00	1.18E+11	8.74E+09	0.00E+00
Renewable	1.34E+11	5.84E+09	7.32E+06	1.18E+11	1.68E+09	7.30E+06	1.18E+11	1.68E+09	7.32E+06
Nuclear	8.61E+10	8.50E+09	0.00E+00	8.61E+10	8.50E+09	0.00E+00	8.61E+10	8.50E+09	0.00E+00
Line	5.71E+09	0.00E+00	0.00E+00	5.71E+09	0.00E+00	0.00E+00	5.71E+09	0.00E+00	0.00E+00
Storage	2.78E+10	4.44E+06	0.00E+00	2.78E+10	4.45E+06	0.00E+00	2.78E+10	4.43E+06	0.00E+00
Load	0.00E+00	0.00E+00	0.00E+00	0.00E+00	0.00E+00	0.00E+00	0.00E+00	0.00E+00	0.00E+00
Total	**3.55E+11**	**1.89E+10**	**7.32E+06**	**3.55E+11**	**1.89E+10**	**7.3015E+06**	**3.55E+11**	**1.89E+10**	**7.32E+06**
CASE 1									
Section B	$1 - qDTR_{\text{month/hour}}$ / $qDTR_{\text{year}}$								
$CO_2 Scenario$	RCP 26			RCP 45			RCP 85		
Metric	CAPEX	OPEX	Curtailment	CAPEX	OPEX	Curtailment	CAPEX	OPEX	Curtailment
Fossil	-1.59E-01	-9.02E-01	0.00E+00	5.65E-04	3.56E-03	0.00E+00	6.56E-04	3.66E-03	0.00E+00
Renewable	1.21E-01	7.12E-01	6.49E-03	-1.81E-04	1.48E-03	8.45E-05	-3.88E-06	-1.09E-03	4.26E-03
Nuclear	1.16E-05	-5.99E-04	0.00E+00	-2.23E-05	-9.25E-04	0.00E+00	9.43E-06	-6.09E-04	0.00E+00
Line	1.31E-03	0.00E+00	0.00E+00	1.26E-03	0.00E+00	0.00E+00	1.38E-03	0.00E+00	0.00E+00
Storage	0.00E+00	2.62E-03	0.00E+00	0.00E+00	-9.14E-04	0.00E+00	0.00E+00	-1.81E-04	0.00E+00
Load	0.00E+00	0.00E+00	0.00E+00	0.00E+00	0.00E+00	0.00E+00	0.00E+00	0.00E+00	0.00E+00
Total	**2.32E-04**	**1.44E-03**	**6.49E-03**	**1.42E-04**	**1.36E-03**	**8.45E-05**	**2.41E-04**	**1.32E-03**	**4.26E-03**

Table 3.3: Variation (in %) for G&TEP Cases

more efficient planning of power flows during periods of lower thermal demand.

Despite these benefits, the scale of improvement remains relatively limited. The overall impact (less than 0.1%) suggests that, while qDTR improves system performance, its effect on macroeconomic indicators is marginal, offset by the system's inherent adaptability. Therefore, it is necessary to seek better alternatives to this tool that allow for evolving flexibility in the constraints.

3.7.2 Regional Power System Expansion Under Climate Influence: Integrating Generation, Demand, and Transmission Capacity

To address this gap and presented at **D**, this case study seeks to improve the flexibility and applicability of the PyPSA framework [151] in the context of this research. This approach analyzes a regional network by focusing on long-term generation and demand dynamics, while leveraging open-source datasets. Specifically, the method facilitates the estimation of national or regional data into spatially disaggregated profiles suitable for smaller planning units; in this case, the Nomenclature of Territorial Units for Statistics (NUTS)-2 regional level. This spatial disaggregation enables a more precise assessment of transmission infrastructure needs. The overall structure of the methodology is illustrated in Fig. 3.11, where the dotted lines represent newly introduced modules integrated into the existing modeling workflow. The following procedure describes the main steps of this approach:

- A regression machine learning model is trained with historical, techno-economic, regional, and meteorological data to project demand by region, limited to France and Italy.
- Data describing the electrical network configuration is collected to group and construct the network, since in previous methodologies, this process was native to PyPSA-Eur.
- Transmission information, including location details and meteorological time series, is used in thermal models of the components to estimate capacity. These ratings are then incorporated into a G&TEP model, allowing for the calculation of optimal investments and operating costs.

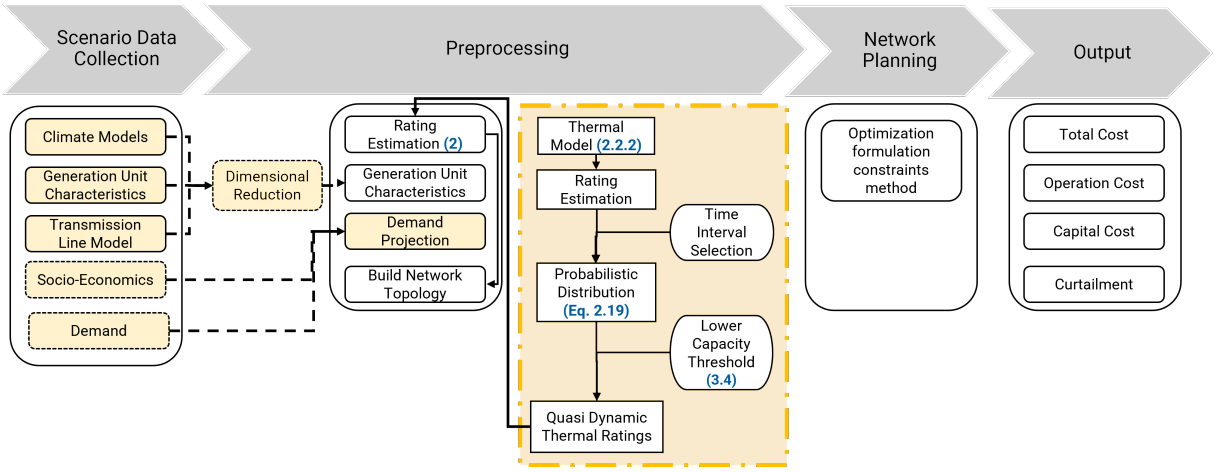

Figure 3.11: Visual representation of the procedure, the integration of the Generation, Demand, and Ratings Approach influenced by the climate, is highlighted in yellow.

Demand Model

As described above, the conductor's temperature is directly impacted by the current flow through it, which, combined with unfavorable environmental conditions, can jeopardize the component's overload risk. Therefore, this process provides the methodology with a demand projection model that allows for flexible parameterization of different regional scenarios, while aligning with climate projections for long-term planning.

The long-term regional energy demand projection assesses the factors that determine future electricity consumption patterns, such as the region's economic parameters, seasonal variations in demand, and population distribution. Based on that, the pre-selection of features that the model acquired as input variables was carried out through a combination of time-series meteorological data, demographic factors, and demand observations ([160, 161]), based primarily on bibliographical analyses, which can be detailed in [152, 153].

This selection process aligns with the nonlinear relationship described in Eq. 3.34, where i represents the year and a, b, and c are parameters extracted from historical observations. Because our extension is at the European level, we relied on the open sources described in the Section 3.6.

$$D_i = a(\text{per capita income}) \cdot b_i(\text{population}) \cdot c_i \tag{3.34}$$

The profile and shape of the hourly demand result depend primarily on the economic influences and temperature conditions of the region. Demand curves are calculated for the subregion by compiling the demand profile of the aforementioned region (country or region) from [153], Gross Domestic Product (GDP), population, and hourly temperatures described in Eq. 3.35. In order to synchronize the result with the other modules of the methodology, this model is parameterized at an hourly resolution (t in the equation) to determine the demand profile of each subregion to be examined in MWh.

$$\mathbf{x}_t = [\text{GDP}_t, \sin_d(t), \cos_d(t), \text{Pop}_t, \theta_t] \tag{3.35}$$

As shown in Fig. 3.12a, spatial regions across France and Italy were selected to segment energy consumption data for the model. The lower time series shows electrical load patterns from 2015 to 2023, highlighting seasonal fluctuations and regional profiles. These patterns serve as foundational input for training predictive algorithms in energy demand forecasting.

As is detailed, due to the nature of the input data described in Eq. 3.35, it was necessary to implement preprocessing methods to improve the fidelity of the result, the following preprocesses were implemented:

a) Minimum and maximum scaling

b) Cyclical day-of-the-year encoding

c) Hourly interpolation at the required resolution

d) Target transformation

Similar to the machine learning process performed for the UGL, as a first phase, various regression machine learning techniques were evaluated to determine the most appropriate approach for our method. This evaluation focused on key error metrics, such as Root Mean Squared Error (RMSE) and Mean Absolute Error (MAE). It is important to note that, in order to obtain geographically targeted results, the dataset is divided by geographic regions for training and testing the models.

The training set is initially randomly divided into 70%, with an additional 10% reserved for tuning the model's hyperparameters, using the techniques described in [122]. The remaining 30% is designated as the validation set for model testing. N-fold cross-validation is used to mitigate overfitting and divides the test dataset into five folds. This ensures that all region sizes are represented in each fold, thus maintaining a homogeneous selection.

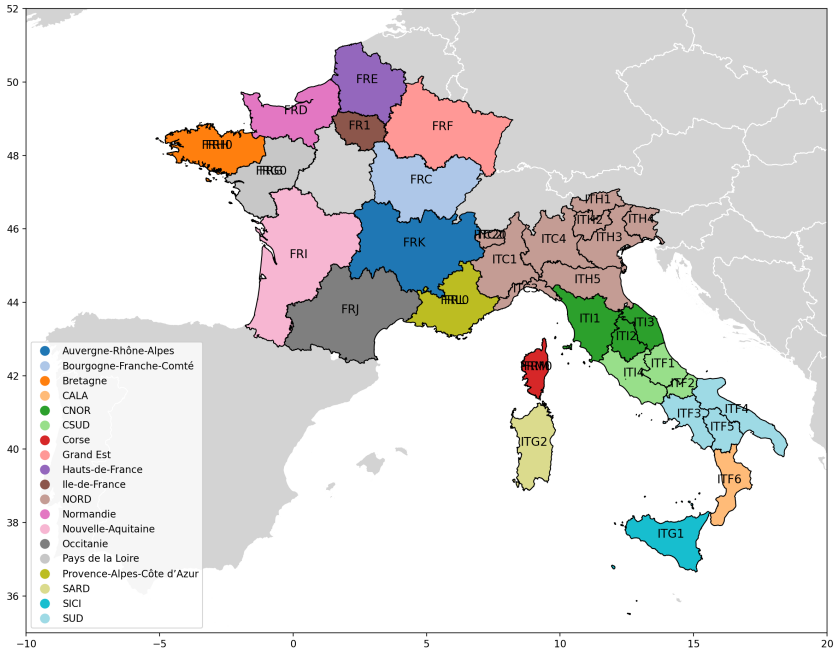

(a) Spatial Coverage of Selected Zones with Detailed Identification of NUTS Regions

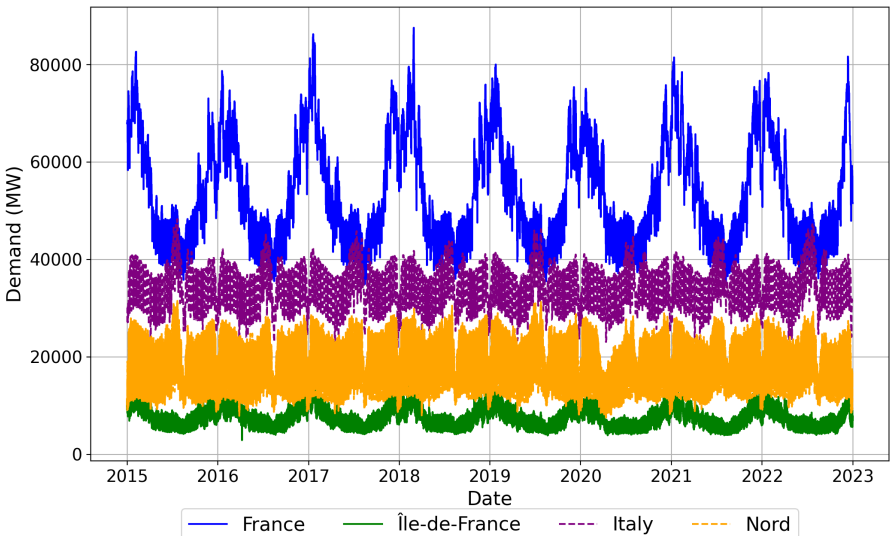

(b) Illustrative Load Profiles Across National and Regional Levels

Figure 3.12: Overview of Spatial and Temporal Demand: Regional Mapping and Demand Profiles

$$\mathrm{RMSE}_q = \sqrt{\frac{1}{H}\sum_{i=1}^{H}(y_{q,i} - \hat{y}_{q,i})^2} \tag{3.36a}$$

$$\mathrm{MAE}_q = \frac{1}{H}\sum_{i=1}^{H}|y_{q,i} - \hat{y}_{q,i}| \tag{3.36b}$$

In the equations, $y_{q,i}$ represents the observed load demand, while $\hat{y}_{q,i}$ represents the predicted value. The subscript H denotes the forecast horizon. Metrics are evaluated by region, denoted as q, to ensure spatial granularity in the model assessment.

Dimensional Reduction

The process begins with the categorized regions to be analyzed at level zero of the NUTS or countries and extends to the administrative department level (NUTS level 3). This analysis incorporates geographic information on electricity generation and transmission networks, combined with open-source technical and economic data.

This regional approach to the electricity system follows the same methodology, using the geographic boundaries of [174], with special constraints that were determined deterministically to obtain a more realistic perspective. That is, for example, taking into account the nature of RES, each region is analyzed using wind energy production density, with the information already processed in [163, 164]. For each region, the most appropriate coordinate is selected for analysis and production calculations, based on the following criteria:

- Reflecting an average velocity greater than 4.5 m/s during the analyzed period
- Ensuring that it is not located more than 1,000 m above sea level
- Not within a protected natural area [175].
- As the data provided in the database for the wind records estimates at a height of 100 meters, it was necessary to make an adjustment to the height of the turbine as follows.

$$u_{h_w}(t) = u_{100}(t) \cdot \frac{\ln(h_w/z_0(t))}{\ln(h_{\mathrm{ref}}/z_0(t))} \tag{3.37}$$

- Using the information on location and turbine feature selection from [176], the output power $P_{\mathrm{curve}}(\hat{u}_h(t))$ estimation is performed according to the output from turbine power curve at speed $\hat{u}_{50}(t)$.

$$\theta_r(t) = \frac{\cos(\theta)}{\cos(\alpha_S(t) - 180°)} \tag{3.38}$$

$$I_{\text{eff}}(t) = I_{\text{GHI}}(t) \cdot \theta_r(t) \tag{3.39}$$

$$\eta(t) = 0.14 \cdot [1 - 0.004 \cdot (T(t) - 25 + 0.028 \cdot I_{\text{eff}}(t))] \tag{3.40}$$

$$P_{\text{solar}}(t) = I_{\text{eff}}(t) \cdot \eta(t) \tag{3.41}$$

For the network topology, based on the geographic locations of the transmission lines and the electrical parameters from [172], their locations are analyzed to generate a synthetic network. To achieve this, a geographic mask is generated for each line based on its departure and arrival points, using its regional codes from NUTS level 2 and 3. Lines are classified by voltage and linearly aggregated in their bundles to maintain transmission capacity. Additionally, a single transformer is configured between the high voltage and the low voltage at each regional location.

Selection of Representative Days

Because analyzing each hour over the entire period can be computationally demanding, a representative set of days is selected, applying a regional clustering algorithm described in **D**. This set incorporates diverse input time series and is evaluated over the scenario horizon. A scaling method is selected to normalize all data points, and one representative day and one extreme day are selected per month, region, and country. This ensures the inclusion of critical points from each subregion and maintains the representation of typical days for the entire system.

Generation, Transmission, and Expansion Planning

The economic implications of capacity reduction due to climatic conditions are assessed using G&TEP from Pypsa [151], and the transmission capacity estimation is carried out with historical data, similar to the previous case study.

The main aspects of this case are as follows: The G&TEP is configured to use both $qDTR_{year}$ and $qDTR_{month/hour}$, enabling a comparison that highlights the advantages of different time resolution qDTRs for recovering lost transmission capacity. On the generation side, conventional power plants (CCGT, OCGT, oil, and hydroelectric) are subject to technical constraints, including capacity limits ($p_{nom_{max}}$), CO_2 emissions, and technological efficiency. The simulations were conducted with hourly resolution, based on a set of representative days across the planning horizon. The analysis encompasses 69 deterministically selected regions, as illustrated in Fig. 3.12a, under the assumption of a linear increase in demand until 2050.

The operating limits and simulation assumptions are described in Table 3.4. It should be noted that to create the demand profile for each region, the model described in section 3.7.2 was developed using hourly resolution with machine learning techniques, which were then subjected to training, validation, and selection phases. The results are shown visually in Fig. 3.13, where the evaluation confirmed the effectiveness of the linear regression and XGBoost approaches, with average prediction errors approaching 12% in relation to actual measurements.

Category	Parameter	Value / Reference	Units
Socio-Economics	Technology Financial	[155, 163, 177]	MEUR/MW$_e$
	CO_2 Emissions	[154]	tCO_2/MWh
	Spatial Resolution	25	km^2
Electrical	Low Thermal Risk	0.1%	–
	PV Density	2.60 [163]	MW/km^2
	Wind Density	6.64 [164]	MW/km^2
	Hydro p_{max}	9%	–
	OHL Conductor	490-AL1/64-ST1A	Unit
	Bus Voltage	220 / 380	kV
Scenarios Description	Weather Timeframe	1973–2024	-
	Resolution	24	hours
	Days Selection	(2) Representative (1) Extreme per Region	days
	Expansion Limit	1.5 to 4.5 (220 kV – 380 kV)	times
	Modeling Tools	PypSA [151]	–

Table 3.4: Case Specifications Parameters

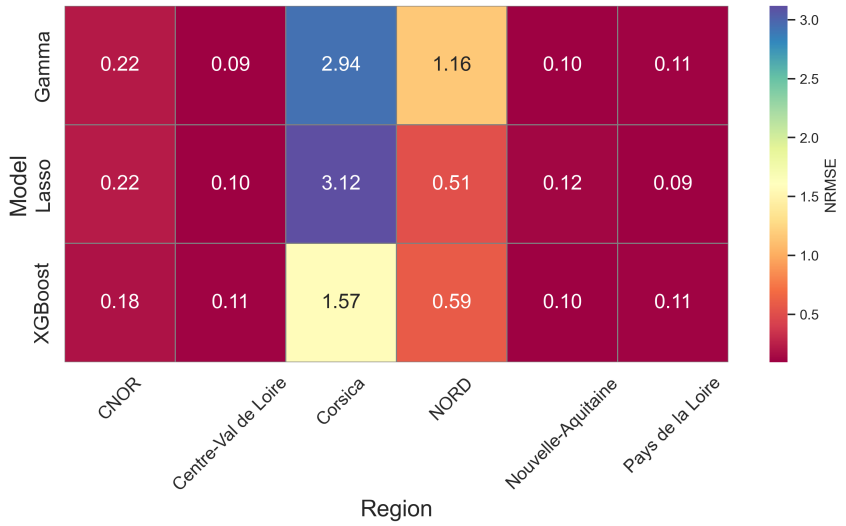

(a) Models Performance

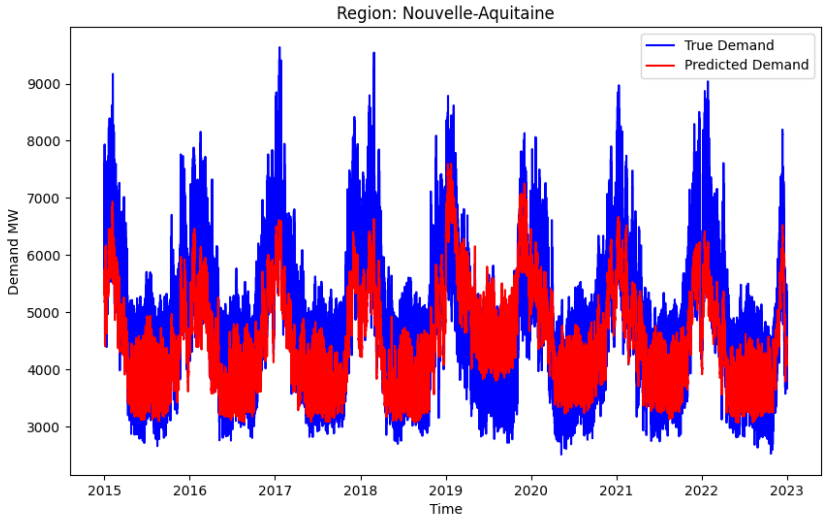

(b) XGBoost Performance

Figure 3.13: Demand Projection performance

In this case, the rating qDTR is only used to evaluate the OHL, with the reference described in the Table 3.4, following the thermal model described in the section 2.2.1.1 and using a fixed-probability threshold (X_R) of 0.1%. As shown in Table 3.5, using qDTR with month/hour temporal resolution increases the capacity of the component and alleviates pressure on the network compared to the fixed annual $qDTR_{year}$, and therefore reduces load shedding events by 100% and decreases expansion on transmission by 30% and on fossil-based generation by 13%. These same results are presented geographically in Fig. 3.14, where the colour red denotes a reduction in the element analysed.

Technologie	**Reduction**
Biomass	13%
Coal	13%
Gas	71%
Hydro	90%
Load shedding	100%
Nuclear	95%
Oil	11%
Solar	13%
Wind	10%
Transmission	30%

Table 3.5: Reduction percentages $\frac{qDTR_{year}-qDTR_{hour}}{qDTR_{year}} \times 100$ by Generation Technology

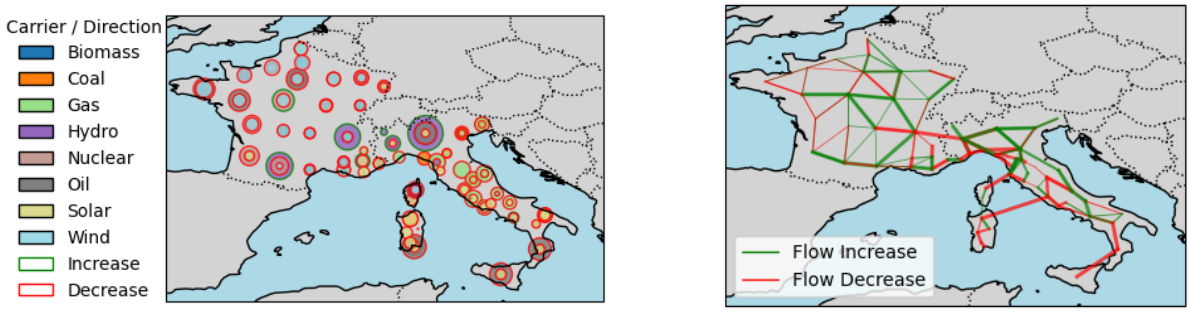

(a) Generation Expansion Difference 1: $\Delta qDTR_{\text{month/hour}}$ / $qDTR_{\text{year}}$

(b) Transmission Flow Difference: $\Delta qDTR_{\text{month/hour}}$ / $qDTR_{\text{year}}$

Figure 3.14: Temporal Resolution Analysis of qDTR: month/hour vs year $\frac{qDTR_{year}-qDTR_{hour}}{qDTR_{year}}$ Impacts on Generation Expansion and Transmission

One limitation of this study lies in the optimisation, which is conditioned by the structure and predefined assumptions within the PyPSA environment. Although open-source data is used to improve transparency and reproducibility, the underlying network topology remains synthetic and does not fully reflect the configurations of the systems that would allow for comparison. To preserve the academic rigour of the analysis and ensure meaningful interpretation, future studies should reposition the examined cases within research frameworks on recognised use cases and reference scenarios. This approach allows for comparative evaluation with other models and supports the validation of results within an established methodological context.

3.7.3 IEEE 24-bus reliability test system Transmission Expansion Plan

Since the methodologies described above allow for a evaluation of qDTR with a fixed-probability threshold selection, they are limited by the structural constraints of the selected modelling tools, which do not fully support a more flexible evaluation of the implementation or comparison of qDTR within a standardised network framework. These tools are often based on predefined topologies and parameter settings, limiting scalability and replicability in various planning contexts. To address this shortcoming, a TEP analysis is performed to assess the financial implications of infrastructure development in paper **A**, following the methodological framework described in Section 3.3.1-Section 3.3.2 and illustrated in Fig. 3.15.

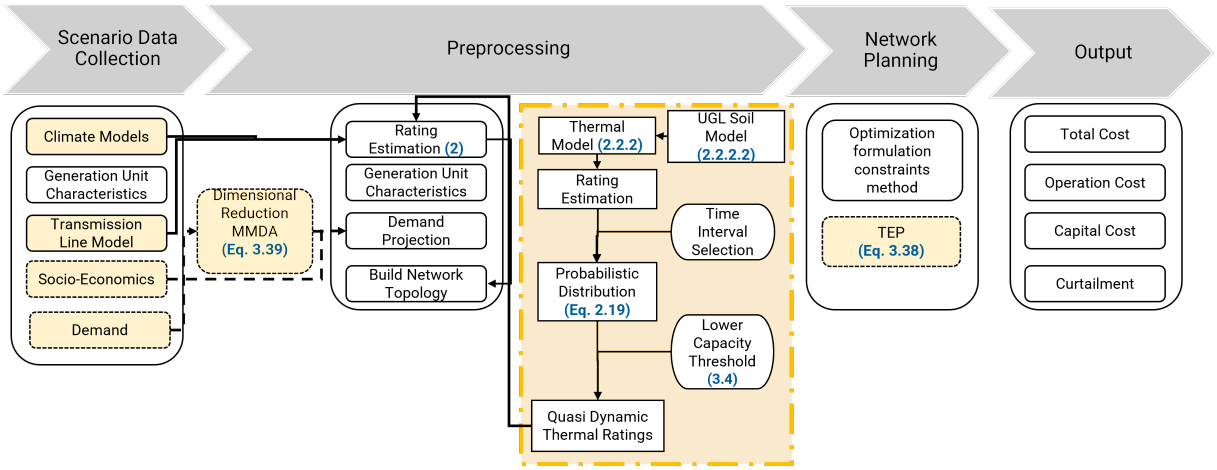

Figure 3.15: Visual representation of the transmission expansion procedure.

This analysis is based on predefined parameters, including the application of a standardised test network [145], but adapted with geographical coordinates corresponding to a region in southern France. The network configuration includes fixed distances between nodes and deterministic electrical parameters for nodes, lines, and demand. This approach allows the impact of qDTR to be isolated and evaluated under transparent and reproducible conditions. It should be noted that this extrapolation methodology is conceptually consistent with the method proposed in [178].

Using this topology, a deterministic formulation of the TEP is proposed to identify the optimal investments in transmission lines that minimise the total system costs, as presented in Eq. (3.42). Parameters marked with an asterisk denote the influence of the integration of qDTR. The objective function (3.42a) minimises costs by jointly optimising generation dispatch and transmission investment decisions, encapsulated in the binary vector z_{nm}. The coefficients P_L, P_g, and P_d correspond to nodal active power flows, generation output, and load demands, respectively.

$$\min \quad \sum_{\mathcal{N}} I_{n,m} z_{n,m} + \sum_{g} c_g P_g \tag{3.42a}$$

$$\text{st:} \quad \sum_{l \in \mathcal{L}_n} P^0_{L_{n,m}} + \sum_{l \in \mathcal{L}_n} P^1_{L_{n,m}} + P_{gn} = P_{dn}, \quad n \in \mathcal{N} \tag{3.42b}$$

$$P^0_{L_{n,m}} - (\theta_n - \theta_m)/x^0_{n,m} = 0, \quad n, m \in \mathcal{L} \tag{3.42c}$$

$$|P^k_{L_{n,m}} - (\theta_n - \theta_m)/x^k_{n,m}| \leq \mathcal{M}(1 - z^k_{n,m}), \quad n, m \in \mathcal{N} \tag{3.42d}$$

$$|P^0_{L_{n,m}}| \leq F^0_{L_{n,m_{\text{qDTR}}}*}, \quad n, m \in \mathcal{N} \tag{3.42e}$$

$$|P^k_{L_{n,m}}| \leq F^k_{n,m_{qDTR}*}, \quad n, m \in \mathcal{N} \tag{3.42f}$$

$$P_{ming} \leq P_g \leq P_{maxg} \tag{3.42g}$$

$$z^{k+1}_{n,m} \leq \bar{z^k}_{n,m} \quad \forall (n, m) \in \mathcal{N} \tag{3.42h}$$

$$z_{n,m} \in \{0, 1\}, \quad n, m \in \mathcal{N} \tag{3.42i}$$

The set of constraints begins with the power balance condition at each bus in Eq. 3.42b. Flow relationships in the existing lines are expressed in (3.42c), while Eq. 3.42d incorporates a big-M formulation using a sufficiently large constant $\mathcal{M}$ to model the activation of candidate lines. Capacity constraints for both current and proposed lines are defined in Eq. 3.42e and Eq. 3.42f, reflecting thermal ratings derived from the qDTR assumptions. The binary variable z governs the decision to build or not to build, with a cap on the number of improvements allowed per line. Generator output limits are specified in Eq. 3.42g, while expansion logic constraints, such as sequential construction limits, are encoded in Eq. 3.42h. Binary integrality conditions are imposed in Eq. 3.42i.

While this approach can be extended to optimise conductor selection or integrate new installation cost constraints, the present formulation focuses exclusively on thermal rating constraints.The first key aspect of the analysis involves the application of qDTRs in UGL replacing the existing 132 kV lines with their (12 in total), with a three times expansion potential for all lines, either by direct burial installation or by the use of backfill. These ratings are then substituted into the deterministic parameters of equations (3.42e) and (3.42f). In parallel, annual load and generation profiles are adjusted to reflect the characteristics of the analyzed scenario.

To reduce computational effort, the study employs a representative one-year load demand profile sourced from [145], in conjunction with the Modified Maximum Dissimilarity Algorithm (MMDA) algorithm outlined in [141]. For greater clarity in formulating the method, a mathematical explanation is provided below. Specifically, for a series of annual demand data, we define:

$$P_D = \{P_{d_1}, P_{d_2}, \ldots, P_{d_n}\} \quad \text{Set of all days} \tag{3.43a}$$

$$L_{p_i} = (l_{p_{i1}}, l_{p_{i2}}, \ldots, l_{p_{i24}}) \quad \text{Load profile vector for day } P_{d_i} \tag{3.43b}$$

$$T_{pd_i} = \sum_{h=1}^{24} l_{p_{ih}} \quad \text{Total daily demand for day } P_{d_i} \tag{3.43c}$$

Let $\Omega_J \subseteq P_D$ be the candidate set and $k_R \in \mathbb{N}$ the number of representatives to select.

However, our approach must reflect a combination of typical demand Eq. 3.44b, with an additional selection towards the extremes of load (where transmission networks suffer from greater thermal stress), represented in Eq. 3.44c. The percentage reflects the average amount to be selected from each group.

$$\text{Low Demand} = \{P_{d_i} \mid T_{pd_i} \text{ in lowest } q_L\%\} \tag{3.44a}$$

$$\text{Typical Days} = \{P_{d_i} \mid P_{d_i} \notin \text{Low Demand} \cup \text{Extremes}\} \tag{3.44b}$$

$$\text{Extremes} = \{P_{d_i} \mid T_{pd_i} \text{ in highest } q_H\%\} \tag{3.44c}$$

The first step involves selecting the minimum-maximum representative days and then iteratively selecting.

$$s^* = \arg\max_{c \in C} \min_{s \in \Omega_K^{(t-1)}} d(c, s) \tag{3.45a}$$

where function d(c, s):

$$d(c, s) = \|\mathbf{l}_c - \mathbf{l}_s\|_2 \tag{3.46a}$$

$$= \sqrt{\sum_{h=1}^{24} \left(l_c^{(h)} - l_s^{(h)}\right)^2} \tag{3.46b}$$

For the typical, the first selected day s_0 must be closest to the median total demand.

$$s_0 = \arg\min_{c \in C} |T_c - \text{median}(\{T_{pd_i}\})| \tag{3.47a}$$

And similar to the previous, iterative selection of the days.

$$s^* = \arg\min_{c \in C} \max_{s \in \Omega_K^{(t-1)}} d(c, s) \tag{3.48a}$$

Where C is the current candidate set and the final set of representatives is represented by:

$$\Omega_K = \Omega_{K_H} \cup \Omega_{K_{mean}} \cup \Omega_{K_L} \tag{3.49}$$

Using this method, 36 days are selected, including typical and extreme high scenarios (80%), non-low demand days. This can be visually represented in Fig. 3.16. The process for assigning weights to representative profiles is finally defined by comparing each representative day with the demand series using Euclidean distance through 24-hour characteristics

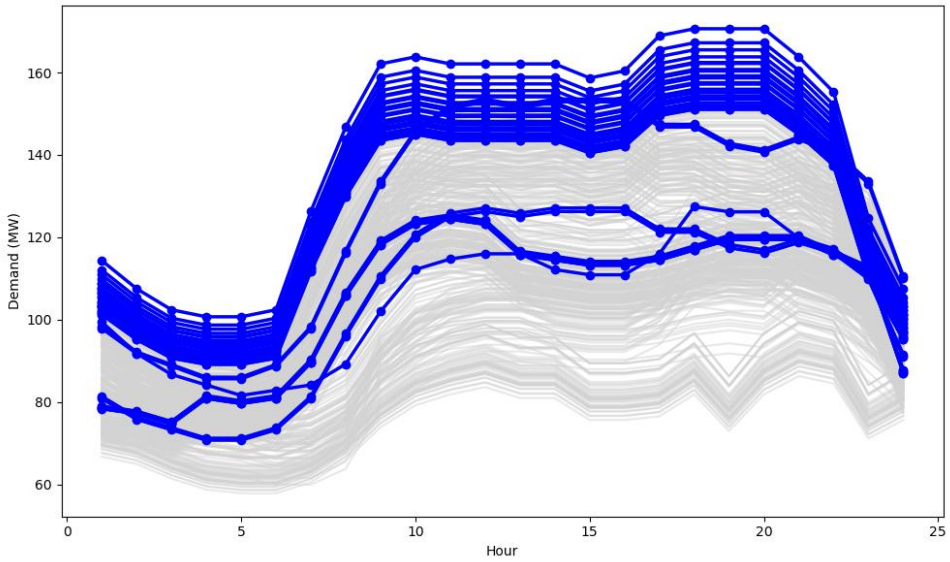

Figure 3.16: MMDA Selection Days Results Example

Finally, four cases are analyzed, each one with static $qDTR_{year}$ and $qDTR_{month/hour}$: 1) Base case load and generation increased by 60% a) with backfilled and b) direct buried installation. 2) PV Generators added at nodes 3, 5, 16, 21) with backfilled and d) direct buried installation. Table. 3.6 and Fig. 3.18 summarise the comparative analysis of capital expenditure and operating expenditure in two scenarios, each evaluated in four data configurations: month/hour and annual ratings, with and without backfill (direct buried). The results reveal that OPEX is highly sensitive to temporal resolution, while CAPEX is influenced by two key factors.

Scenario / Variation	**Case 1**		**Case 2**	
	CAPEX	**OPEX**	**CAPEX**	**OPEX**
Hour Backfilled	0.00	600.81	23.00	435.18
Hour Direct Buried	0.00	600.70	23.00	434.58
Year Backfilled	18.00	594.56	13.00	470.97
Year Direct Buried	18.00	594.97	14.50	472.63

Note: All values are expressed in millions of currency units.

Table 3.6: Results for the two scenarios concerning investment and costs, the scenarios covering historical and projected static $qDTR_{year}$, and $\mathrm{qDTR}_{\mathrm{Hour}}$

First, in Case 1, higher load levels cause an increase in power flowing throughout the year. Under these conditions,$qDTR_{month/hour}$, particularly during peak periods in winter, provides greater operational flexibility, allowing for higher power transfers and reducing the need for additional investments, however, with a minimal difference regarding the production of the generators, as shown in Fig. 3.17a.

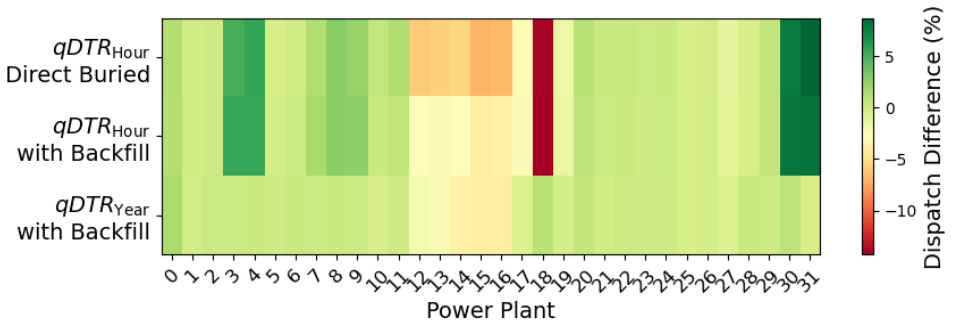

(a) Case 1: Percentage Difference in Total Generation production Compared to $qDTR_{year,backfill}$

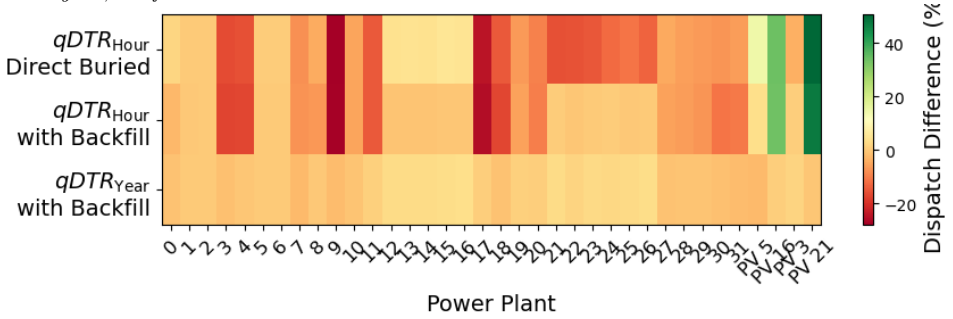

(b) Case 2: Percentagh Difference in Total Generation production Compared $qDTR_{year,backfill}$

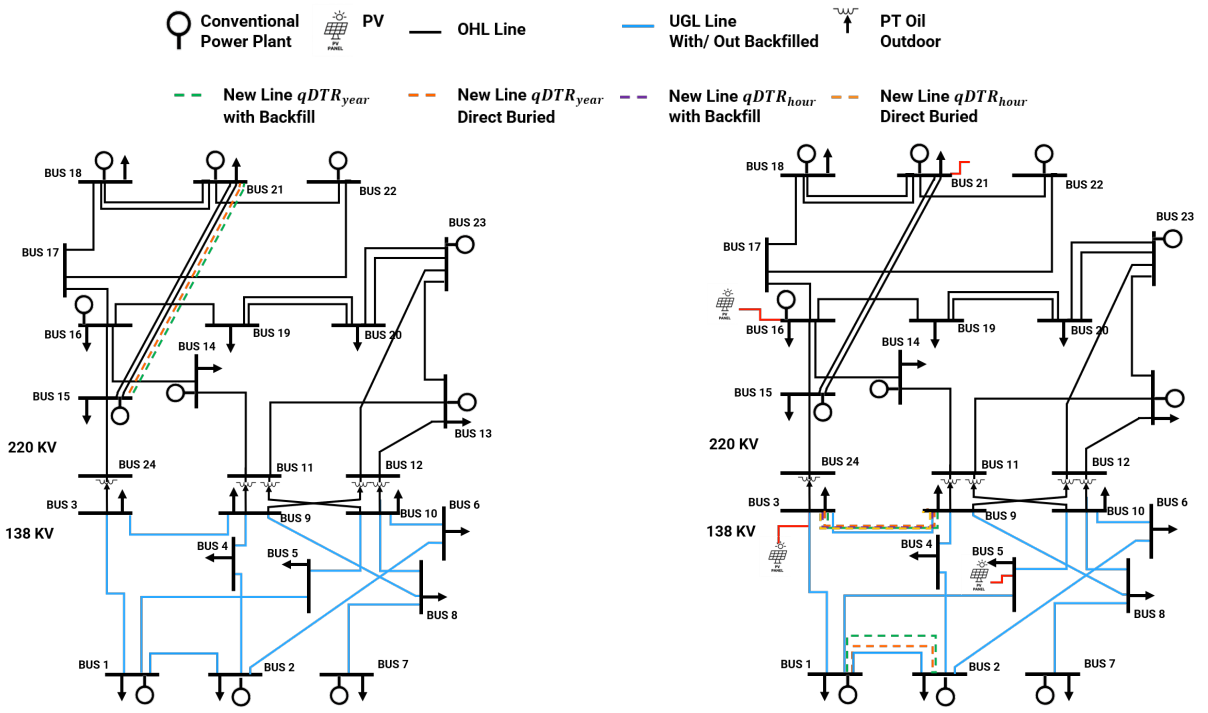

(a) Single Line Network results for Case 1, where new investments in the annual case are required in Line 20

(b) Single Line Network results for Case 2, where new investments in all cases are required in Line 1 and Line 6

Figure 3.18: Comparison of generation production and network investment requirements under two planning scenarios.

This effect is illustrated in Fig. 3.18a, where only the $qDTR_{year}$ requires an investment in line 20, whether with backfill or without it. Second, when RES are integrated into the system in Case 2, particularly PV generation, the characteristics of capacity limitation during periods of high temperature conditions of the qDTR become critical. During solar production peaks, which often coincide with high ambient temperatures and high solar irradiation, $qDTR_{month/hour}$ captures the risk of thermal overload, but it is countered by its better capacity, which requires line reinforcement in the year case, such as the addition of an extra conductor bundle, as shown in the Fig. 3.18b, unlike dynamic $qDTR_{year}$. A significant observation is the improvement in PV generation when qDTR is computed month/hour as detailed in Fig. 3.17b. For example, the PV system at node 21 shows an increase of more than 30%, which can be attributed to the transmission efficiency effect described previously.

In conclusion, this temporal resolution analysis provides valuable information on the cost implications of temporary rating strategies, enabling more informed decisions to be made in terms of infrastructure planning, investment optimisation, and resource allocation. However, the parameter X_R of the cumulative distribution function within the qDTR methodology remains deterministic and is applied uniformly to all elements of the network. This uniformity overlooks the different risk profiles associated with different components, in particular, the relationship between risk exposure, component load, and the resulting temperature dynamics. The following section addresses this limitation by exploring methodologies that explicitly take these

interdependencies into account, to improve the integration of qDTR into NEP.

3.7.4 Network Planning with Stochastic Risk-Aware

Considering the limitations in selecting the X_R parameter for thermal rating estimation, previous results show that the maximum steady-state operating condition of a component is often constrained to ensure network reliability and safety. The proposed practice of applying a conservative fixed-probability threshold (e.g., 0.1%) to estimate the qDTR is not always warranted for all network elements [179]. Many components may operate well below their thermal limits, leading to underutilization of transmission assets.

To address this, an extended TEP framework is proposed in Section 3.3.3, which incorporates risk management directly into the asset rating evaluation process (detailed in Section 3.4) and embeds it into the broader decision-making workflow, as illustrated in Fig. 3.19. The enhanced methodology leverages probabilistic models and scenario based simulations to capture uncertainties arising from demand variability, RES intermittency, contingency events, and extreme weather conditions.

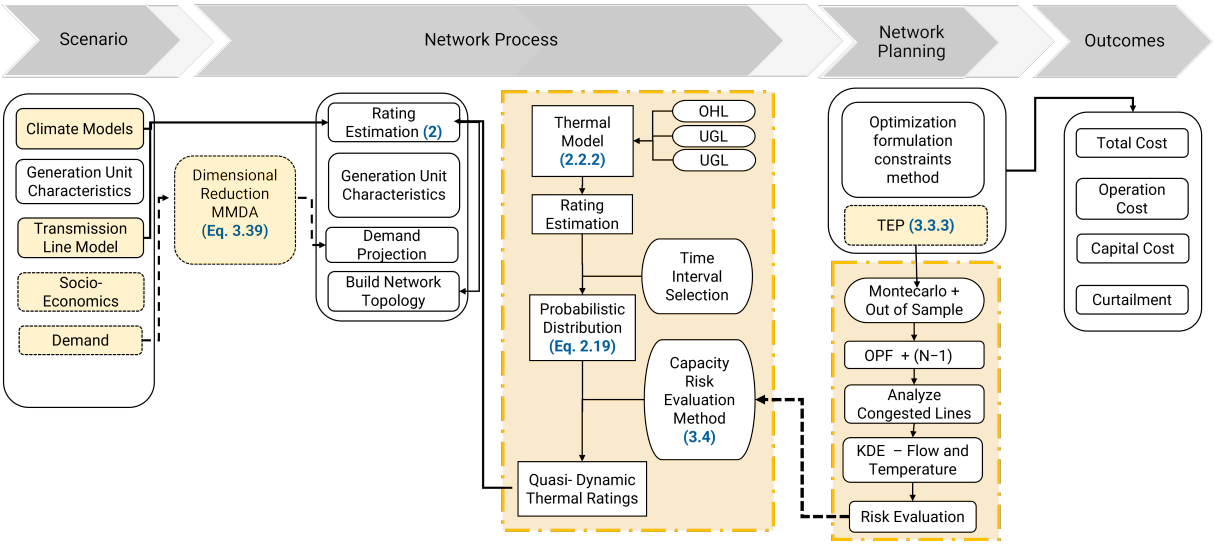

Figure 3.19: Visual representation of the procedure for risk-aware transmission planning.

This study fills a critical gap by formulating a long-term, overload-risk-aware transmission expansion model that explicitly quantifies the probability and impact of network overloads. A comparative analysis is conducted between risk with fixed-Probability Threshold and risk-aware planning settings to evaluate differences in the scale and timing of transmission reinforcements, overall transmission efficiency, and the penalties associated with both energy not supplied and RES curtailment.

This optimization problem is solved using a formulation described in the section 3.3.3, but extended to the risk selection level, allowing for qDTR calculations in a representation of the IEEE 24-bus test network [145]. Although the formulation has limitations such as the use of a DCOPF, it demonstrates that incorporating the thermal risk in transmission can materially alter both the scale and spatial layout of future investments and the production of RES. In summary, this study advances the planning and assessment of transmission network ratings by introducing an enhanced methodology that extends the probabilistic approach (conservative X_R)

into a risk management method. This framework incorporates historical load profiles, weather variability, expected energy not supplied, and contingency events, thereby enabling more robust and clear prioritisation of transmission components for qDTR. The subsequent sections present the methodological framework, as outlined in Fig. 3.19.

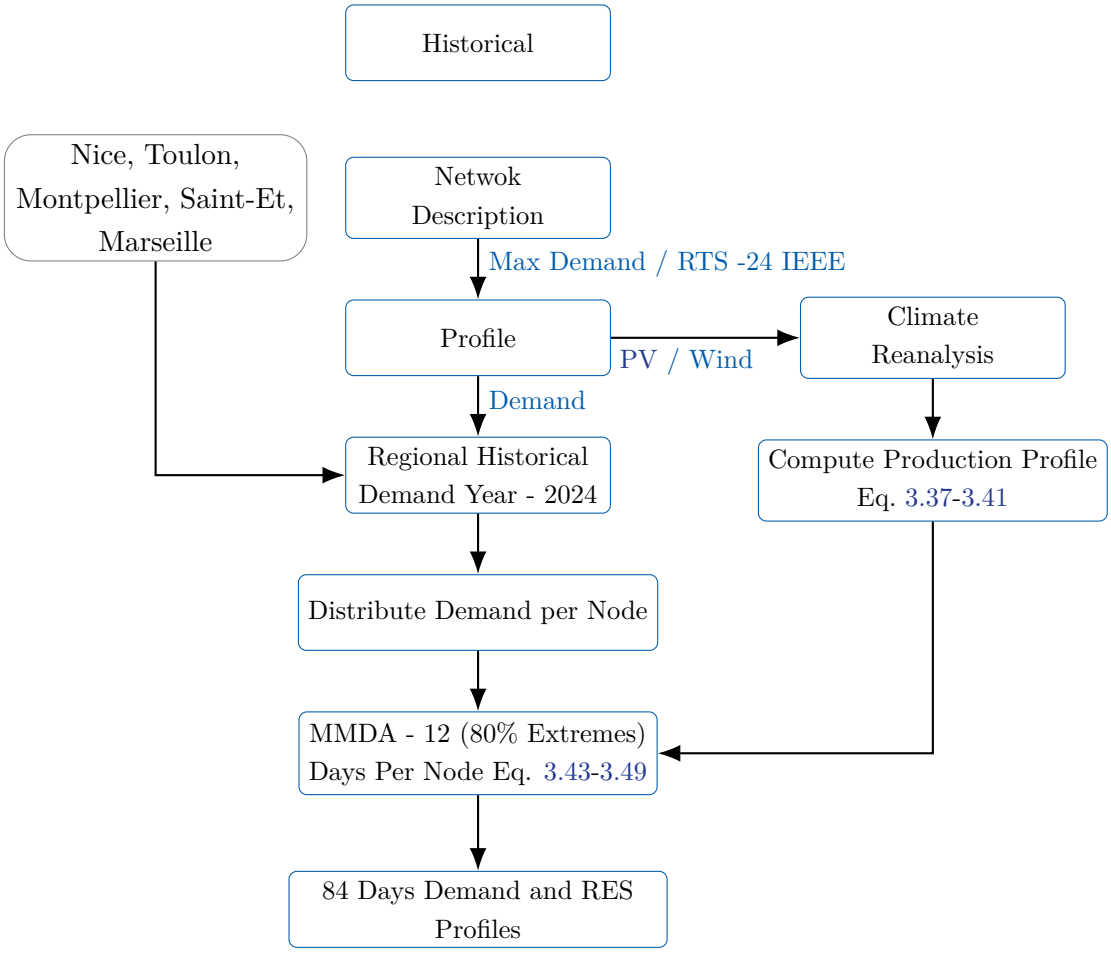

Figure 3.20: Scenario input flowchart showing historical demand and RES profiles

3.7.4.1 Scenario

In this module (see Fig. 3.20), historical demand and RES production profiles are processed. Due to data availability from [160], the year 2024 is selected, and the network is configured accordingly. Regional demand profiles from Nice, Toulon, Montpellier, Saint-Étienne, and Marseille are extracted, distributed among network nodes, and representative days are selected using the MMDA method (80% of extreme cases, see equations 3.43–3.49). Climate historical data are used in parallel to calculate wind and PV production profiles according to equations 3.37 - 3.41. Integration of demand and RES profiles results in a consolidated dataset of 84 representative days, capturing temporal and spatial variability in operational scenarios.

Additionally, Table. 3.7 presents the input parameters used in the case study for transmission

expansion planning under climatic influence. The parameters and data are economic factors such as restriction costs and CO_2 costs, specific scenario climate data, and technical configurations related to demand growth, generation capacity, and infrastructure reinforcement.

Table 3.7: Input Parameters

Parameter	**Value**	**Description / Notes**
Load Shedding Max (λ)	0.01	Maximum load shedding factor
Curtailment Cost	2000	\$/MWh — From [165]
Climatic Scenario	Hist	Climate scenario From [6]
Resolution	0.25	Spatial resolution of climate scenario
Analisis resolution	Hour & Year	Temporal resolution of analysis
Backfill	0	No Backfilled
Typical day per Zone	5	Number days for MMDA
Load Factor	1.2	Initial load increase factor to base case
Years	5	Planning horizon per Epoch
Epochs	5	Number of epochs
$Wind_{ini}$	0.13	Initial wind penetration per Node
PV_{ini}	0.07	Initial solar PV penetration per Node
Int_{rate}	0.08	Interest rate
Nodes Up	[1, 20, 2, 13, 4, 15]	Nodes selected for RES
CO_2 Prices	AM5S2 scenario	From [166]
PV Increase	2050 M2 Trajectoire de référence	From [180] detailed in Annex B
Wind Increase	2050 M2 Trajectoire de référence	From [180] detailed in Annex B
PV Capex	Advance Scenario	€/KW From [167]
Wind Capex	Advance Scenario	€/KW From [168]
Line and Cable Costs	Lower Scenario	€/MW/m From [169]

3.7.4.2 Network modeling and Component rating integration

The network topology and extrapolation maintain the same configuration of the geographically adapted test network from the case study 3.7.3, and are detailed in Fig. 3.21 and with a geographical description in Table. 3.8 , in order to ensure continuity with the standardized framework.

However, the qDTR estimation of the component is calculated at the maximum temperature under steady-state conditions and in contingency. For the STR calculation, the following assumptions and parameters were adopted based on guidance from Cigré Technical Brochure and

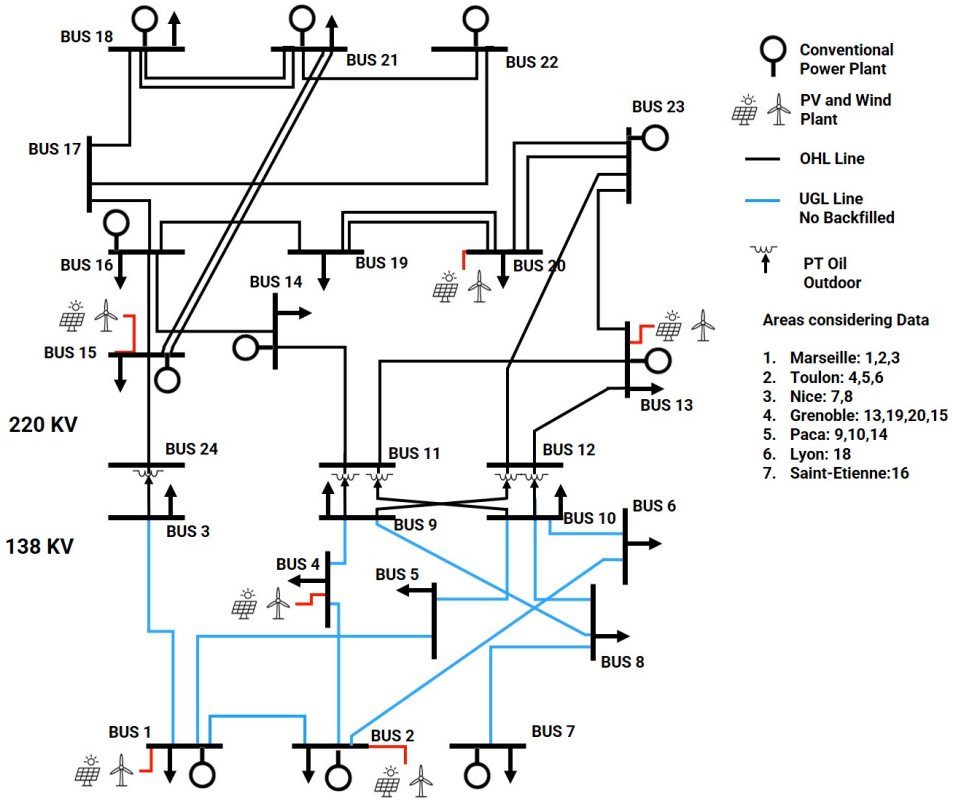

Figure 3.21: IEEE RTS 24-Bus Test System Overview: 11 existing conventional units, 17 loads, 38 existing lines with 32 candidates and new RES Power Plants

Bus ID	Location	Bus ID	Location	Bus ID	Location	Bus ID	Location
101	(43.291, 5.952)	102	(43.266, 5.921)	103	(44.107, 5.727)	104	(43.457, 6.334)
105	(43.550, 6.122)	106	(43.749, 6.116)	107	(43.719, 7.188)	108	(43.673, 6.947)
109	(43.941, 6.228)	110	(43.924, 6.227)	111	(43.927, 6.216)	112	(43.941, 6.217)
113	(44.094, 6.635)	114	(44.344, 5.882)	115	(44.691, 5.421)	116	(44.749, 5.565)
117	(45.002, 5.352)	118	(45.134, 5.257)	119	(44.880, 5.733)	120	(44.942, 6.118)
121	(45.372, 5.126)	122	(45.302, 4.377)	123	(44.825, 6.325)	124	(44.097, 5.738)

Table 3.8: Geographical coordinates of the 24 buses in southern France

in accordance with IEC 60287 [51]. The ambient temperature was set to 40°C, and the solar irradiation was assumed to be 1000 Wm^{-2}. Soil thermal resistivity is set to be 1 KmW^{-1}, and the soil temperature was set to 20°C. These values reflect typical conservative conditions for thermal analysis and ensure consistency with established international standards. To represent this, Fig. 3.22 illustrates the estimated rating of line 22 as a function of X_R, derived from historical climate datasets with different temporal resolutions. By directly comparing continuous hourly assessments of T_{max} in steady state, contingency, and annual, the figure reveals how the sensitivity of quasi-dynamic ratings depends on the time resolutions of analysis. In particular, it is important to highlight not only the advantage offered by month/hour ratings during the night, but also the improved risk assessment during peak hours.

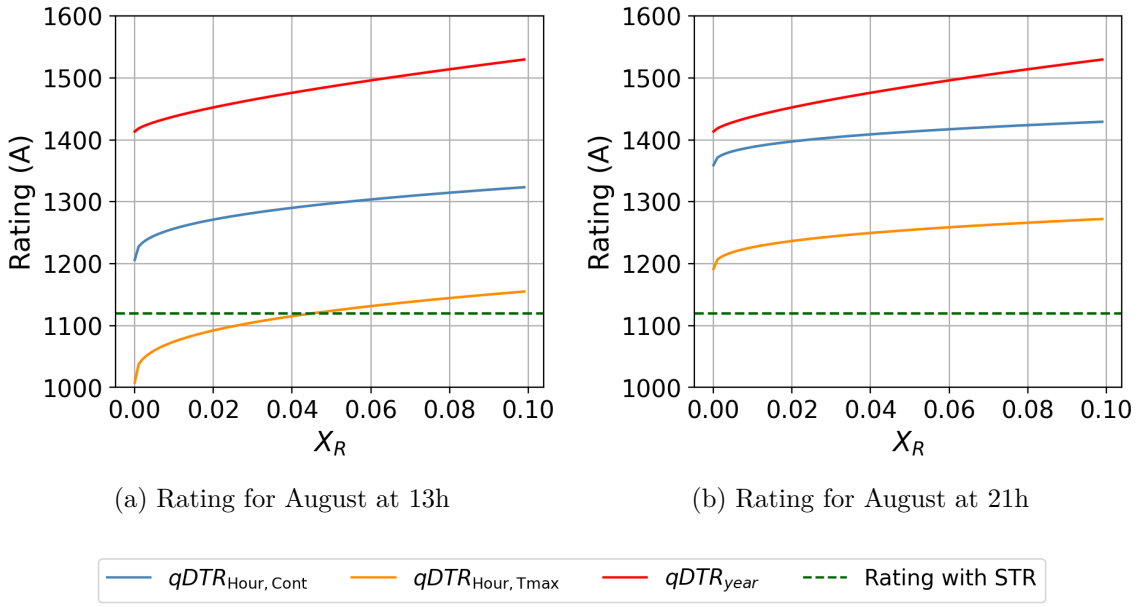

(a) Rating for August at 13h

(b) Rating for August at 21h

Figure 3.22: CDF of Line 22 rating as a function of X_R, evaluated across multiple temporal resolution, using historical climate datasets. The curves illustrate how rating estimates vary with increasing X_R, highlighting the influence of temporal resolution on thermal rating assessments. The dashed green line represents the standard rating with STR for comparison.

3.7.4.3 Overload Risk assessment

The Fig. 3.23 shows a complete stochastic workflow for overload risk assessment, based on the qDTR and MCS, with a more extensive algorithm 4. The diagram integrates probabilistic ratings, generation, and demand to evaluate conductor temperature and component loading by simulating a number of system states and performing both base case and contingency OPF analyses (only for UGL and OHL). In addition, it assesses line congestion and thermal ageing effects. This procedure is executed at each time step of the optimization process; for instance, when one year is represented by 8760 hourly intervals, the corresponding analysis is carried out for each hour.

Next, KDE estimation employing the fast convolution-based kernel method proposed by [146], is applied to derive weighted power flow distributions for each congested line and temperature. An illustrative example of this procedure is shown in Fig. 3.24, which details the weighted density and associated contingencies for each power flows/temperature combination during the evaluation of the fourth epoch (year 2045) and the third iteration. It is important to emphasize that each congestion event is weighted by its probability of occurrence, as reported in [145]. Consequently, the weighed KDE function generated provides a statistical representation of the flows on the congested line, enabling a detailed analysis of both the power flow and the corresponding conductor temperature.

These distributions are then employed to quantify the risk of exceeding a predefined threshold (i.e 0.17% [110]), corresponding to a maximum of operating hours under contingency conditions at maximum temperature and rating over the expected lifetime of the component (i.e 40 years).

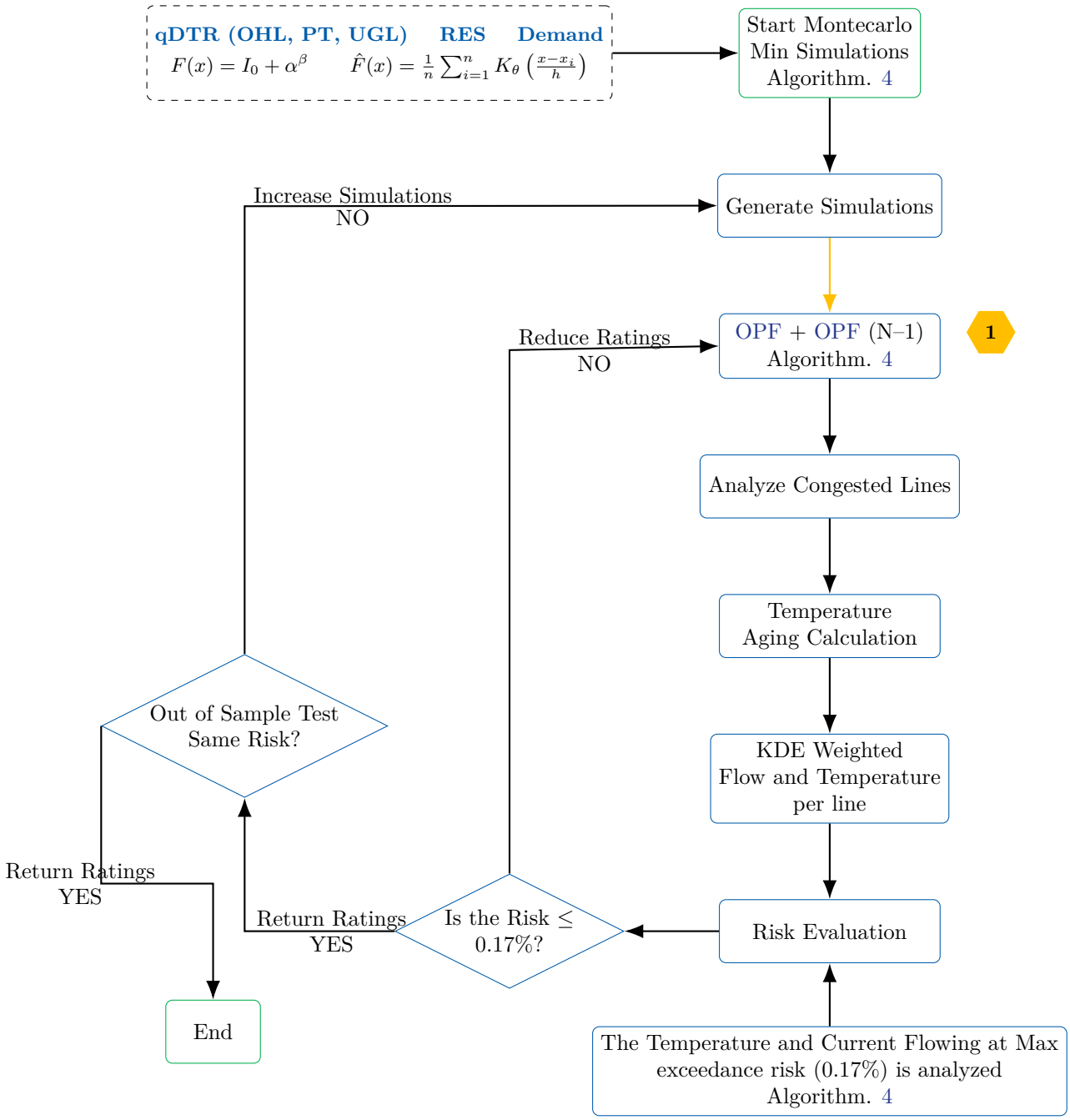

Figure 3.23: Flowchart of overload risk assessment using Monte Carlo with out-of-sample as the outcome evaluation method

An iterative loop, which includes out-of-sample validation from [148], reinforces the result obtained.

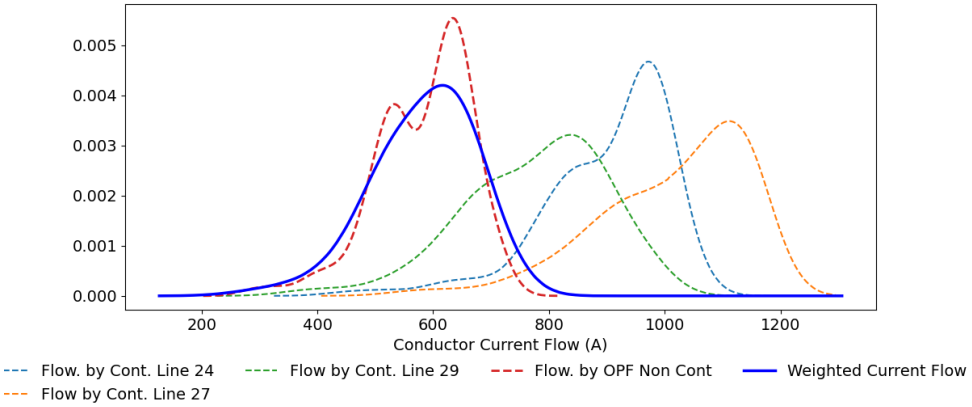

(a) Weighted and contingencies of the current flowing per line congested fitted withing Guassian Kernel densities from [146]

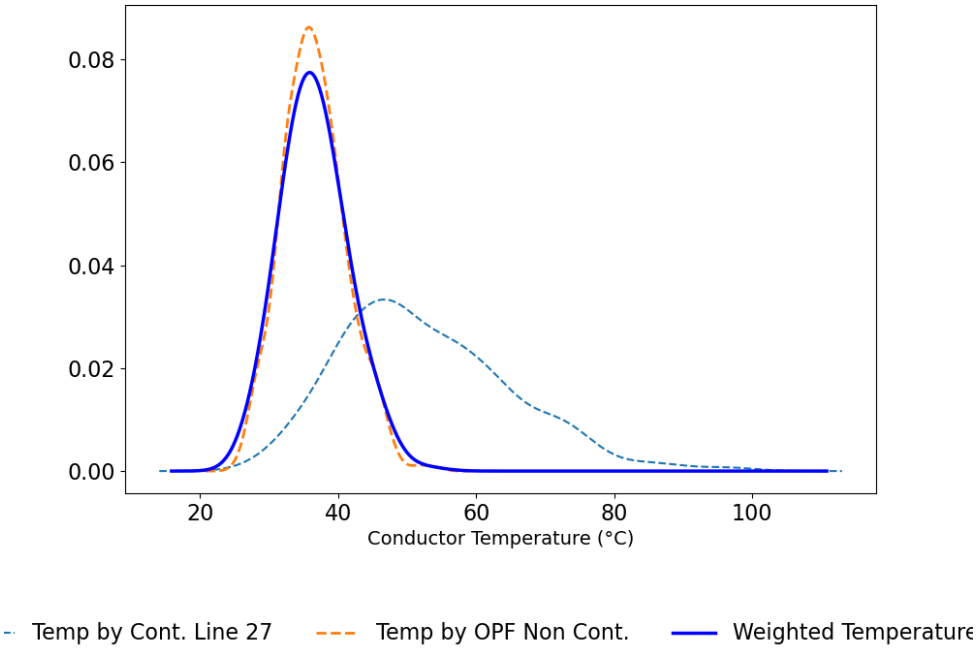

(b) Weighted and contingencies of the conductor temperature per line congested fitted withing Guassian KDE from [146]

Figure 3.24: KDE estimation for the Line 26. Power flow and conductor temperature during the fourth epoch in yearly time resolution, incorporating congestion probabilities

In order to assess the sensitivity of the proposed methodology with respect to the temporal resolution of the qDTR, two rating temporal resolutions are analyzed using historical information: the first considers annual ratings, while the second adopts month/hour ratings. Both cases

are compared against the traditional STR approach.

Case 1: Annual Ratings

The advantage of this analysis is that it establishes a comparative model using a fixed annual rating, similar to the traditional STR, but explicitly influenced by climatic conditions. As a result of the risk estimation, three categories of line evaluations can be identified, as illustrated in Fig. 3.25a-3.26a.

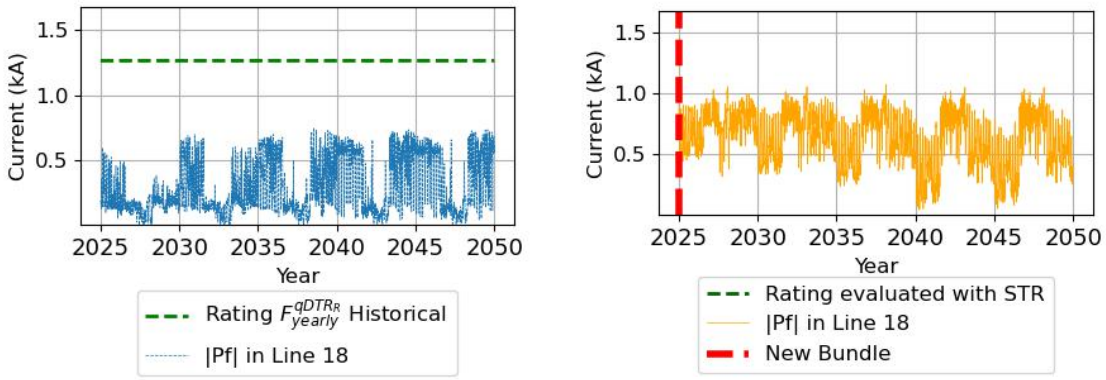

(a) Historical power flow in Line 18: $|P_f|$ and thermal limit with F_{yearly}^{qDTR}. Indicates no additional reinforcement is required

(b) Historical power flow in Line 18: $|P_f|$ and the thermal limit under the steady-state STR. Details the reinforcement in the first period

Figure 3.25: Power flow in Line 18 using Historical information

The first result concerns the performance of line 18 in Fig. 3.25a, which highlights the advantage of applying the fixed annual rate F_{yearly}^{qDTR} instead of the conservative steady-state power rate STR. With this approach, the line can safely support higher power transfers, since the prevailing local conditions allow a higher thermal capacity limit than that defined by STR. Consequently, additional transmission capacity is achieved without new investments, unlike Fig. 3.25b, where the STR approach requires the installation of an additional line in the first planning period.

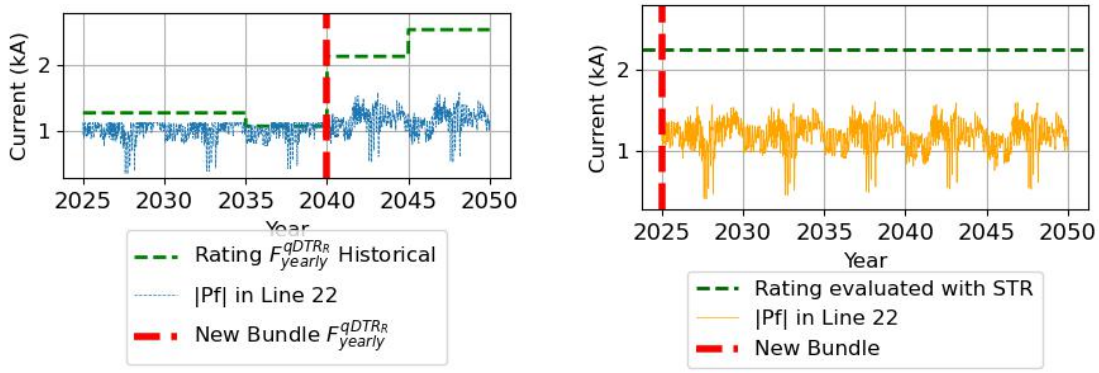

(a) Power flow in Line 22: $|P_f|$ and the thermal limit with F_{yearly}^{qDTR}. Shows rating changes, and also the investment is delayed.

(b) Power flow in Line 22: $|P_f|$ and thermal limit with the steady-state STR. Details the reinforcement in the first period

Figure 3.26: Power flow in Line 22 using Historical information

The second result, presented in Fig. 3.26a, corresponds to line 22, where, according to a multi-horizon analysis, the risk of overload increases due to climate variability, combined with changing demand and generation patterns. This condition drives the need for reinforcement by 2040. However, F_{yearly}^{qDTR} still offers an advantage by deferring investment, in contrast to the STR approach, which requires immediate reinforcement in the first period, as shown in Fig. 3.26b.

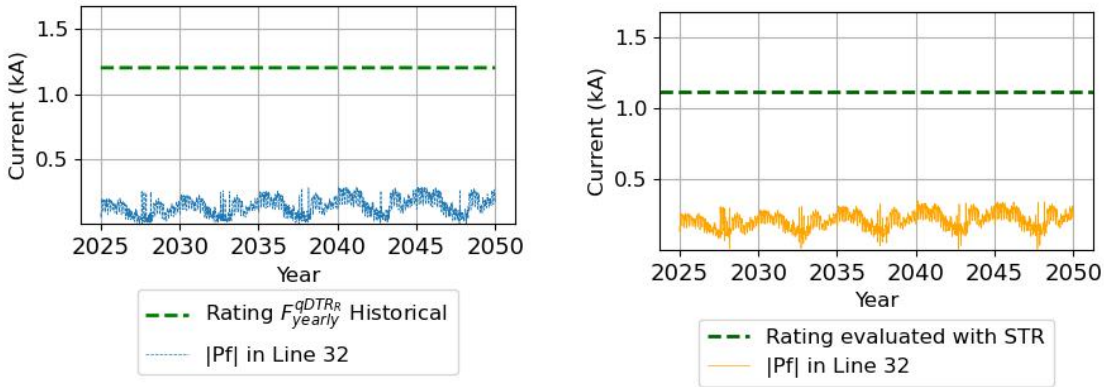

(a) Power flow in Line 32: $|P_f|$ and the thermal limit with F_{yearly}^{qDTR}.

(b) Power flow in Line 32: The $|P_f|$ is constrained by the thermal limit under the steady-state STR.

Figure 3.27: Power flow in Line 32 using Historical information

Finally, the third thermal limit, shown in Fig.s 3.27a and 3.27b, details a line with zero overload risk, which maintains its maximum transfer capacity throughout the optimisation horizon without the need for investment. Therefore, it is concluded that for this line, a conservative risk limit is not required.

These findings highlight two key insights: *(i)* Imposing a uniform fixed risk across all lines is inherently conservative, leading to under-utilization of transmission capacity, and *(ii)* in some

Scenario	ΔOPEX	ΔCAPEX	ΔCO2cost	ΔLosses	ΔCurtCost	ΔShedding
$qDTR_{year}$	0.36	-68.11	0.70	10.46	-2.37	-0.15

Each Δ% value represents the relative change between a scenario-specific outcome and its baseline, calculated as $\frac{F_{yearly}^{qDTR} - STR}{STR} \times 100$. This includes operational expenditure, capital expenditure, CO_2 cost, total power flow, curtailment cost, and load shedding.

Table 3.9: Percentage Change (Δ%) Across Historical Scenario

cases, usually under non favourable conditions, the overload risk may exceed that associated with the traditional STR, underscoring the importance of incorporating risk-based dynamic rating into planning and operation. Since the method explicitly calculates and evaluates conductor temperature during the overload risk assessment, it ensures that the resulting values remain within the prescribed limits shown in Fig. 3.23. Therefore, long-term deterioration associated with elevated temperatures is not modeled as an optimization variable, since safe operation is already ensured by the established thermal capacity limits.

As a result of the overload risk assessment, the TEP results are directly impacted. To quantify the effect of historical scenarios on the system, Table 3.9 indicates the percentage change (Δ%) between the $qDTR_{year}$ scenario and the reference configuration STR. The assessment considers six outcomes: OPEX, CAPEX, CO_2 cost, RES production curtailed, and load shedding penalties. Each entry represents the relative deviation with respect to the STR case, which overlies a reduction trend when applying the F_{yearly}^{qDTR} on CAPEX, curtailment, and load shedding, however, with a neutral result in system costs (OPEX) and CO_2. This result highlights that even with a conservative overload risk (maximum 600 hours every 40 years), the operator can achieve positive economic results. Conversely, line losses increase by 10.5%. This is due to the fact that the proposed formulation only estimates them but does not consider them within the economic minimization variables.

3.8 Conclusion

This chapter presents a methodology for evaluating and integrating the qDTR into power system expansion planning. It demonstrates potential of the proposed rating methodology through different case studies, enabling broader analyses and inclusion of historical climate data. The methodology first applies the qDTR using a fixed-probability threshold selection for planning purposes, allowing consistent climate-based assessments across diverse geographical contexts. Building upon the probabilistic nature of the qDTR, a new approach to risk management is then introduced, transitioning from fixed probabilistic threshold selection to stochastic assessment, considering component temperature and overload.

A key contribution of this chapter is the transition from annual static ratings to month/hour ratings, reflecting the climate dependent nature of thermal ratings. This shift allows transmission planners to reconfigure long-term investment strategies efficiently, particularly in systems with increasing RES penetration and variable demand conditions.

Results from continental and regional case studies show that integrating qDTR to network planning with lower investment and better adaptation to the local climate. The European analysis demonstrates that even marginal reductions in total system expenditures (less than 0.1%) can provide substantial local benefits in areas with frequent thermal constraints. This highlights the strategic value of targeting qDTR applications on the most congested lines, and defer or eliminate investments while maintaining safety margins.

The regional analysis allows to migrate toward a climate influenced planning methodology that integrates dynamic demand models, generation profiles, and the integration of the qDTR into long-term transmission planning. The results indicate that incorporating month/hour qDTR into regional system expansion planning allows for significant reductions in infrastructure investment and operational costs. Specifically, transmission expansion needs decreased by 30%, while investments in fossil fuel generation were reduced by up to 13%. Furthermore, this analysis reinforces the notion that thermal capacity planning must respond to the geographic and temporal heterogeneity of climate exposure.

At the regional scale, the IEEE 24-bus reliability test system was employed and modified to isolate and evaluate the impacts of qDTR under different configurations, UGL installation configuration, and generation-load scenarios. This analysis was performed using an improved optimization model, adapted from [140], which facilitated appropriate modeling for transmission expansion planning with qDTR. Application of month/hour qDTR resulted in consistent reductions in operating expenditures, confirming that higher temporal resolution allows for more efficient use of the thermal margin. In contrast, capital investment was shown to be more sensitive to the type of cable installation particularly if backfill was used and to the thermal conservatism inherent in annual ratings. These results validate the cost-saving potential offered by more dynamic ratings, especially under peak load conditions and high RES. Furthermore, the use of representative days selected using a modified maximum dissimilarity algorithm illustrates a practical approach for selecting extreme events and typical demand profiles. However, the exclusion of rare events and limited intraday variability suggest opportunities for future

refinement, especially in high-risk or thermally constrained regions.

Finally, the methodology moves toward integrating qDTR into a probabilistic scenarios to control the overload risk for transmission expansion planning, providing a balance between reliability, safety, and economic efficiency where usually uniformly conservative STR are used, leading to significant under-utilization of network capacity. When the transmission component overload risk assessment is incorporated, based on historical demand, RES production influenced by weather conditions, allows system operators to quantify and manage the probability of thermal limit violations instead of relying on fix constraints. The results confirm that incorporating overload risk assessment into planning modifies both total costs and the timing of investments, while simultaneously reducing expenditures related to curtailment and load shedding and enabling the postponement of network reinforcements.

Overall, this chapter presents a methodological contribution that integrates qDTR and risk management into long-term transmission planning, enhancing transmission power component utilization, reducing system costs, and facilitating RES integration, while maintaining safe and stable grid operation. *This work bridges the gap between deterministic ratings and climate resilient planning, offering operators a practical path toward thermal risk-aware NEP strategies.*

It directly addresses the RQ3, achieved through a methodological framework that evolves from static thermal ratings to climate influenced and risk-aware assessments. This integration is supported by the following key developments: **(i)** A shift in the thermal rating methodology, where conservative annual ratings (STR) are replaced by probabilistic qDTR models at multiple temporal resolutions annual, monthly, weekly, and month/hour, reflecting a more dynamic influence of the surrounding weather conditions. Allowing to consider the variability of the temperature of the components, the intermittency of RES and the risk of stochastic overload by using MCS and estimation of probability densities in high thermal stress scenarios such as contingencies (N-1). **(ii)** the integration to different TEP methods through case studies. For instance, the European system study (using PyPSA[28]) showed small system cost savings but significant local benefits where thermal constraints were binding. The regional 24-bus IEEE study confirmed that month/hour qDTR reduced transmission reinforcements and fossil fuel investments while improving asset utilization. This enables planners with different expansion planning model approaches to extend their methodology by benchmarking reinforcement needs and operating costs against quantified thermal risks, thereby ensuring reliability thresholds are met.

This demonstrates that qDTR can be integrated as a capacity limit across power components (OHL, PT, UGL), scalable over time, and adaptable to climate conditions in different TEP. Transitioning from static annual ratings to month/hourly rating, and from probabilistic with fixed-probability threshold risk to stochastic risk management, the probabilistic qDTR allows for a more responsive and localized analysis.

As a result of the integration of qDTR into expansion planning, it is possible to quantify benefits at both investment and operational levels in RQ4. Regional studies, which applied a fixed-probability threshold of 0.1%, show reductions up to 30% in transmission expansion needs and 13% in fossil fuel generation investment. Operational efficiency improves through

better utilization of thermal margins under favorable temperature conditions, making investment strategies related to the weather. However, incorporating stochastic thermal risk reveals two key effects compared to STR: (a) Investment decisions can be delayed by more than a decade. (b) Reinforcements are reduced on lines where favorable climatic conditions increase effective capacity and alleviate congestion. Overall, this approach allows operators to prioritize thermal behavior analysis on critical components, improving investment scheduling and the assessment of congested lines while integrating accurate climate models.

3.9 Limitations

Despite its contributions and results, the method faces several limitations:

- The simulation software used in Section 3.7.1.1 (PyPSA-Eur [28]) reduces the network into clustered areas by performing regional studies, significantly reducing the number of lines and nodes compared to current transmission networks. This abstraction limits the ability to capture localized constraints and generate more accurate analyses.
- In all the scenarios evaluated, although historical meteorological data are incorporated, future climate variability, including potential extreme events, is not explicitly simulated. This underestimates the potential impacts of the networks analyzed in the future scenarios.
- While simulations software supports DTR to a limited extent, manual integration of qDTR required a custom implementation (Sections 3.7.1.1 and 3.7.2), which can limit reproducibility and scalability. It is critical to continue developing natively supported rating modules as qDTR in open-source planning tools.
- While the rating methodology uses hourly and annual resolution, the expansion plan focuses on a representative historical year (e.g., 2018 in 3.7.1.1 and 2020 in 3.7.2). Multi-year or scenario-based assessments are required to generalize the results under different climate patterns and system configurations.
- Due the fact, that proposed models in 3.7.2 and 3.7.3 were based on open libraries and nor realistic networks, the lack of benchmarking against observed operational data or industry-standard tools limits the direct applicability of model results.
- The qDTR implementation applies a fixed-probabilistic threshold X_R value to all assets in the analyzed networks with a conservative value, which may under-rate components or represent an additional restriction to the network.
- The analysis proposed in Section 3.7.2 and 3.7.3 does not incorporate forecast uncertainty, demand variability, or probabilistic profiles of RES, which are essential for long-term robustness.
- Although MMDA improves efficiency, the 36n day demand-based representation per year may exclude high-impact events where compound weather phenomena exist. An expanded set of scenarios or probability sampling may better capture these events in future analyses.
- The current formulation considers hourly qDTR as non-sequential and does not model thermal inertia or the cumulative effects of heating over consecutive hours. While non-sequential variation can provide flexibility, it can also lead to an overestimation of system capacity. This same effect in the formulation of the transmission and expansion model results in the failure to include generation inertia, during the MCS and optimization ramp up/down.

- The stochastic MCS approach, while capturing temporal variability and climate uncertainty, significantly increases computational complexity, especially when integrated into large-scale expansion models with thousands of candidate assets. This limits the temporal resolution and the number of scenarios that can be realistically evaluated.

Chapter 4

Impact of climate change on transmission systems

Résumé en Français

Ce chapitre analyse les implications du changement climatique sur la capacité thermique des réseaux de transport d'électricité, ainsi que les défis qui en découlent pour la planification à long terme. L'analyse montre que l'augmentation de la variabilité des conditions climatiques et la fréquence accrue des événements météorologiques extrêmes constituent des facteurs de stress critiques, non pris en compte dans les pratiques traditionnelles d'évaluation thermique statique.

En étendant la méthodologie de capacité thermique quasi-dynamique pour intégrer les projections climatiques ($qDTR_{RCP}$), le chapitre propose une approche permettant de quantifier les impacts électriques et économiques du changement climatique sur les réseaux électriques.

4.1 Introduction

The previous chapters highlighted the benefits of applying qDTR, particularly: (1) long-term operational flexibility through spatio-temporal analysis and (2) improved risk integration and management that yields economic and operational gains under historical weather conditions, this retrospective insight overlooks the increasing impact of climate change. An example of this is that the rising local and regional weather variability alters the environmental conditions that directly affect the heat dissipation capacity of transmission components and their long-term limits, thereby challenging the reliability of the static or quasi-static thermal capacity assessment assumptions employed with historical data. As environmental conditions become increasingly dynamic and less predictable, it is imperative to reconsider and adapt the method to ensure resilience, safety, and efficiency of the network under changing climate realities.

This leaves open the question of how future environmental variability, driven by climate change, can be systematically integrated into long-term transmission system planning. To address this challenge, this chapter is dedicated to answering the following research questions:

RQ5: What is the impact of climate change on the thermal ratings of individual power system components, considering both temporal variations and regional climatic differences?

RQ6: What is the impact of climate change on network expansion planning, considering its influence on the thermal capacity of electrical system components?

To investigate these questions, climate projection models are considered in this chapter as frameworks that provide a consistent way to assess the impact of long-term environmental variability on transmission capacity. As presented in Section 1.3.5, scenario analyses using RCPs allow for the assessment of electricity system performance under a wide range of possible future climates. These models provide insight into how different emissions trajectories and socioeconomic developments, visually compared in Fig. 4.1, are based on the extent of effort made to reduce greenhouse gas emissions. It illustrates the consequences of each pathway in terms of temperature rise, extreme weather, and adaptation costs between 2081 and 2100, in comparison to the period from 1986 to 2005. These consequences could affect variables crucial to assessing the qDTR, such as ambient temperature, wind, and solar radiation, among others, over the long term, geographically broad, and with clear results.

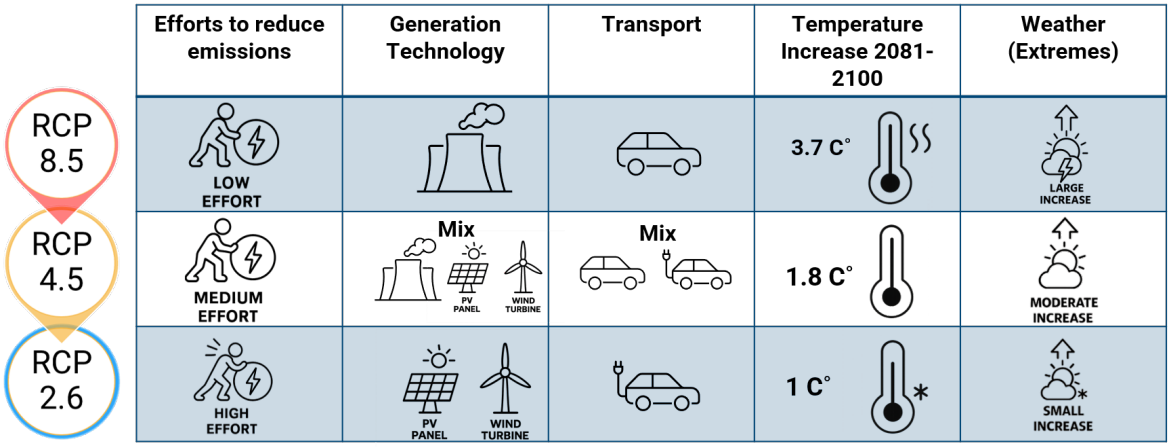

Figure 4.1: Climate Change: RCP Scenarios Consequences. Updated from [181]

In this context, dynamic thermal ratings using qDTR_{RCP} with plausible trajectories of climate conditions from climate models emerge as a natural extension of the $\text{qDTR}_{\text{Historical}}$ methodology (with historical information), allowing for the integration of projected climate data. Thus, qDTR_{RCP} provides a framework for assessing the future performance of the network under different climate scenarios, facilitating more adaptive long-term planning decisions. The following sections present the methodology, datasets, and results of applying this extension to transmission expansion planning.

4.2 Methodology

This section presents the methodology developed to incorporate the previous qDTR framework into long-term planning under climate change conditions. The objective is to extend both fixed-threshold probabilistic and stochastic planning models by explicitly accounting for future variability in meteorological conditions, as derived from climate projection data (Section 1.3.5).

The methodology is designed to answer research questions **RQ5** and **RQ6** by linking probabilistic thermal ratings to climate influenced network planning, as illustrated in Fig. 4.8. The approach integrates climate projections into system operation and expansion planning, through the following proposed structure:

1. Component ratings are no longer considered static-historical but adapt to projected environmental conditions, capturing the effects of temperature, wind, and solar radiation on thermal limits.

2. Plausible future climate trajectories are integrated into planning scenarios, allowing the evaluation of both typical and extreme conditions over long-term horizons.

3. By combining stochastic models with climate projections, the methodology evaluates operational risks and investment requirements under uncertainty, and long-term demand and generation changes.

By incorporating thermal variability influenced by climate change into long-term planning, the methodology provides a flexible and scalable framework applicable to different networks and climatic conditions. Through detailed case studies, scenario analyses, and operational assessments presented in later sections.

4.3 Impact of climate change on transmission systems

Climate change affects all segments of the electrical network, from generation to consumption, mainly through its influence on extreme weather events and the increasing variability of key meteorological parameters that impact the transmission power system components. This includes changes in the frequency, intensity, duration, spatial extent, and timing of extreme temperatures. Fig. 4.2 illustrates these changes through the density curves of air and soil temperatures (estimated at 1.8 meters), over the last fifty years, which highlights a clear trend toward a warmer climate. Moreover, it demonstrates that for decades, both average temperatures and the occurrence of extreme heat events have been on the rise, surpassing critical thresholds. However, generating scenarios for the next three decades, applying or utilizing these historical thresholds as has been done in the previous chapters, has direct implications for network reliability, demand, transmission capacity performance, and long-term planning.

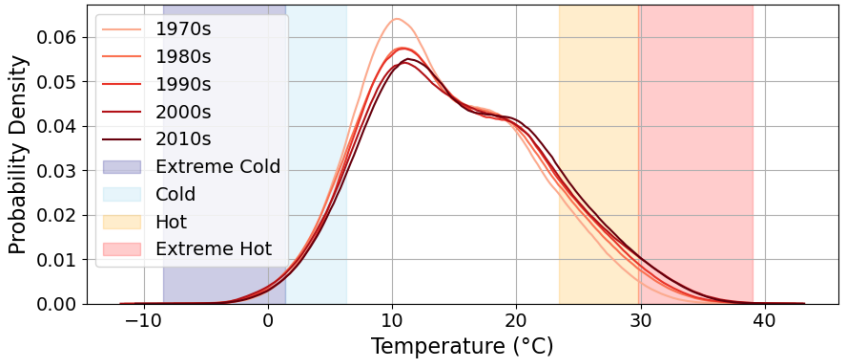

(a) Air Temperature

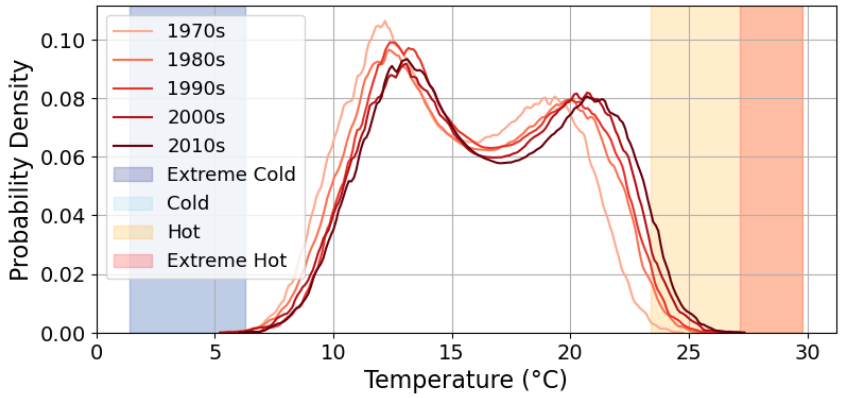

(b) Soil Temperature

Figure 4.2: Changes in the distribution of daily mean air and soil (1.8 mts) temperature in Sardinia over the decades (from 1970 to 2010), based on the reanalysis. The curves illustrate a progressive shift towards higher mean temperatures over time. The shaded color areas represent thresholds for cold, warm, and extreme events, defined using the percentile limits from [2] and calculated on the last period 2010-2020 as a reference.

4.3.1 Integrating qDTR and Climate Models in Transmission Planning

To overcome this limitation, emission scenarios represented by the RCPs (see Table 1.2) are employed. These projections are not designed to capture short-term fluctuations typically relevant for operational or medium-term planning, but rather to describe long-term trends influenced by socioeconomic development, energy consumption, and production policies. Incorporating these scenarios enables the assessment of how climate change, driven by varying greenhouse gas concentration pathways, may affect regional environmental conditions and, consequently, the transmission components' thermal limits [111].

In addition, complementary scenarios that influence transmission expansion are integrated, such as those describing future energy demand and generation patterns, which in turn determine emissions trajectories. When combined with environmental scenarios, these data provide a more comprehensive perspective, allowing for the assessment of not only the direct effects of climate change on transmission thermal stress but also broader systemic impacts on NEP. These scenarios are essential for evaluating adaptation, resilience, and mitigation strategies.

This new framework, illustrated in Fig. 4.3, primarily links climate scenarios to the temporal resolution used in the probabilistic estimation of transmission component ratings. It is designed to ensure flexibility for incorporating different climate model databases and projections, enabling comparative or multi-scenario assessments. In some cases, specific scenario-based projections for generation and demand are also incorporated, enabling a comprehensive assessment of how climatic variations influence the probabilistic thermal performance of transmission infrastructure and the energy system under diverse future conditions.

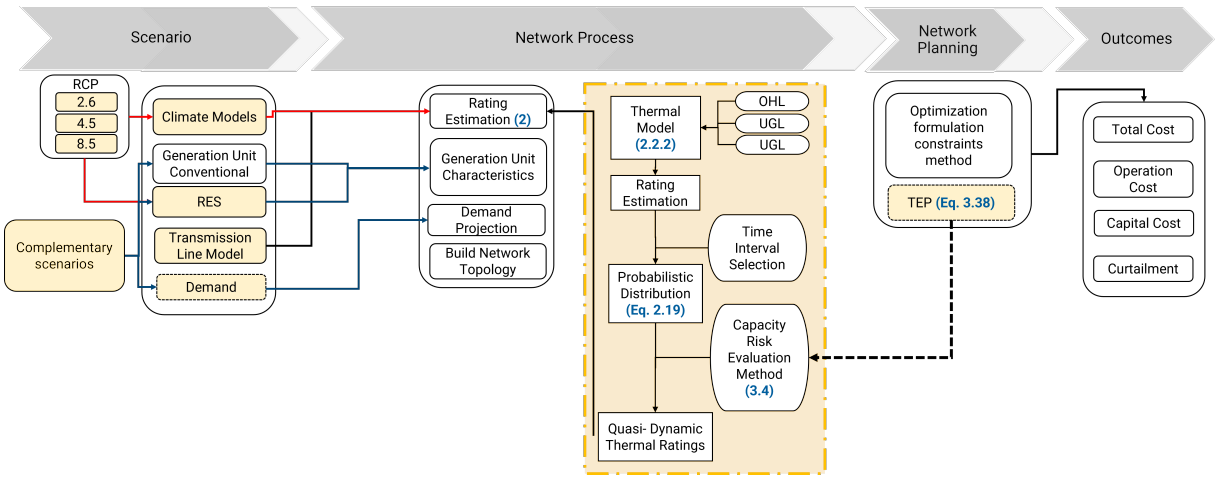

Figure 4.3: Conceptual Framework Linking qDTR and Climate Modeling for Enhanced Transmission Planning

To facilitate the estimation of $qDTR_{RCP}$, the following methodology describes a process to acquire the necessary climatic and environmental variables. This process is aligned with the operational scenario and the type of transmission components involved. It begins with the selection of appropriate environmental datasets and thermal models according to the specific characteristics of each transmission component. For instance, OHL ratings are estimated using

a thermal balance model governed by convective cooling due to wind and radiative heat exchange influenced by ambient temperature. In contrast, UGL ratings are assessed through a thermal model that integrates soil temperature, soil moisture, and precipitation, variables to which these systems are particularly impacted.

In the subsequent stage, it is processed five principal inputs: the selected climate scenario (historical or future RCP trajectory), temporal horizon, geographic location, technical parameters of the component, and spatial resolution. The coordinates of the study site are rounded to the nearest grid cell corresponding to the chosen spatial resolution, ensuring spatial consistency with the climatic dataset. Only land-based coordinates are retained to extract relevant climatic information within the specified temporal horizon, for example, from 2024 to 2070. However a fundamental problem was encountered when applying a climate-driven thermal model for the future: the climate projections used did not contain information about deep soil moisture, but only in the top 10 cm below the surface. Therefore, it is necessary to apply the methodology described in section 2.2.1.2, for UGL to calculate the the $qDTR_{RCP}$.

4.4 Databases and Data Overview

Variable	Units	Section	Source
Climate and Weather Inputs			
Climate Scenarios	RCP 2.6, 4.5, 8.5	4.5.1	[182]
Baseline Climate	Historical 1970–2022	4.5.1	[6]
Component and Cable Data			
Overhead Lines, Transformers, Cables	–	4.5.1	Tables B.1, B.2, B.3
Cable 1	245 kV, XLPE 22 mm	4.5.1/B	B.4
Cable 2	500 kV, XLPE 31 mm	4.5.1/B	B.5
Generation and Demand			
RES Growth	2050 (M2, N2, N03)	4.5.2/C	[180]
PV/Wind CAPEX	€/kW	4.5.2/C	[167, 168]
Line/Cable CAPEX	€/MW/m	4.5.2/C	[169]

Table 4.1: Input Data Overview for Long-Term Thermal Ratings and Transmission Expansion Planning under Climate Change

4.5 Results

This section presents the results of the assessment of potential impacts of climate change on long-term transmission, both in terms of transmission capacity limits and the economic implications. These assessments were based on established methodologies in Section. 2.2.2 and 3.3 and expanded with the process described in the previous section. This approach ensures methodological continuity, allowing the analysis to remain consistent with historical results while incorporating updated climate-change scenarios and data, and the use of new profiles for generation and demand.

The analysis not only provides comparability over time but also allows for the integration of new parameters, evolving demand patterns, and generational shifts driven by decarbonization strategies. The improved method allows for a more detailed examination of when, where, and how transmission systems may become constrained or require reinforcement under different climate trajectories. This includes assessing regional differences, the robustness of current transmission assets to climate stress, and the economic trade-offs involved in adapting or expanding transmission capacity.

4.5.1 Impact of climate change on network transmission capacity

A. Impact of climate: Analyzed at the Regional and Component Level

The results presented in paper **Paper B** investigate the influence of weather and future climatic scenarios on electric transmission network capacity, analyzing impacts both at the individual component level and on broader regional systems. The assessment is based on the methodology described in Section 2.3.2 and 3.7.1.1 and is structured in two progressive stages. First, it examines how the qDTR modifies allowable transmission capacity under varying climate scenarios at the component scale and extended analysis to the regional level, where qDTR is applied to larger network segments to assess the aggregate impacts of climate variability on overall transmission capacity. Second, the study broadens its scope to examine the long-term implications of these climate-driven changes for transmission system planning, including the need for adaptation measures and infrastructure investments, presented in Section. 4.5.2.

Here, the qDTR are calculated based on the RCP projections for the upcoming decades (2023-2070) instead of historical weather data (1970-2022). This assessment covers Europe, maintaining a spatial resolution of 0.25^o. To this end, and for the sake of representation only, this study averaged the values of qDTR by the coordinates of its hourly representation and, therefore, assesses the annualized impacts of climate change in Europe by comparing future and historical scenarios. In Fig. 4.4, the results of carrying out this process for three different components with characteristics are outlined in Tables B.1,B.2, B.3. Each of the rows shows the spatial percentage variation of qDTR in Europe under different climate scenarios, which are primarily negative, with significant decreases in central Spain, the Arctic, and mountainous regions. However, for UGL, smaller variations are observed due to the high thermal inertia of the soil. To better present this graphic representation, the Table. 4.2 presents the average and extreme differences in transmission capacity based on historical weather data and future

projections, and essentially shows the negative impact across all scenarios. PT are the component with the greatest variation (from -0.9% to -2.1%), followed by OHL (from -0.4% to -1.53%) and UGL (from -0.1% to -0.2%). This is explained by the fact that the thermal model of OHL is primarily influenced by air temperature and wind speed, while PT depends solely on air temperature. Since in some cases the hottest periods are accompanied by non-zero wind speeds, the cooling effect of the airflow partially offsets the negative impact of high temperatures on OHL, while in this case the PT experiences full thermal stress. For UGL, the narrower temperature range of the soil prevents significant reduction effects. The most severe RCP scenario indicates maximum reductions in ratings of -3.9%, -4.4%, and -1% for OHL, PT, and UGL, respectively.

Component	**OHL**	**PT**	**UGL**
Rating Difference Scenario RCP 2.6 $\Delta_{\%}(\mathbf{qDTR_{RCP2.6}}, \mathbf{qDTR_{Historical}})$[1]			
Mean	-0.4	-0.9	-0.1
Max	-1.4	-2.12	-0.5
Min	0.75	0.5	0.8
Rating Difference Scenario RCP 4.5 $\Delta_{\%}(\mathbf{qDTR_{RCP4.5}}, \mathbf{qDTR_{Historical}})$[1]			
Mean	-0.7	-1.5	-0.2
Max	-1.7	-2.8	-0.6
Min	0.9	-0.4	0.5
Rating Difference Scenario RCP 8.5 $\Delta_{\%}(\mathbf{qDTR_{RCP8.5}}, \mathbf{qDTR_{Historical}})$[1]			
Mean	-1.53	-2.1	-0.2
Max	-3.9	-4.4	-1
Min	0.32	-0.7	1.0

[1] The variation of transmission capacity calculated with the specific climatic scenario versus historical weather. Before evaluating the statistical results, an average of the hourly values of each coordinate is calculated.

Table 4.2: Variation for the three scenarios concerning historical values for qDTR for the European region.

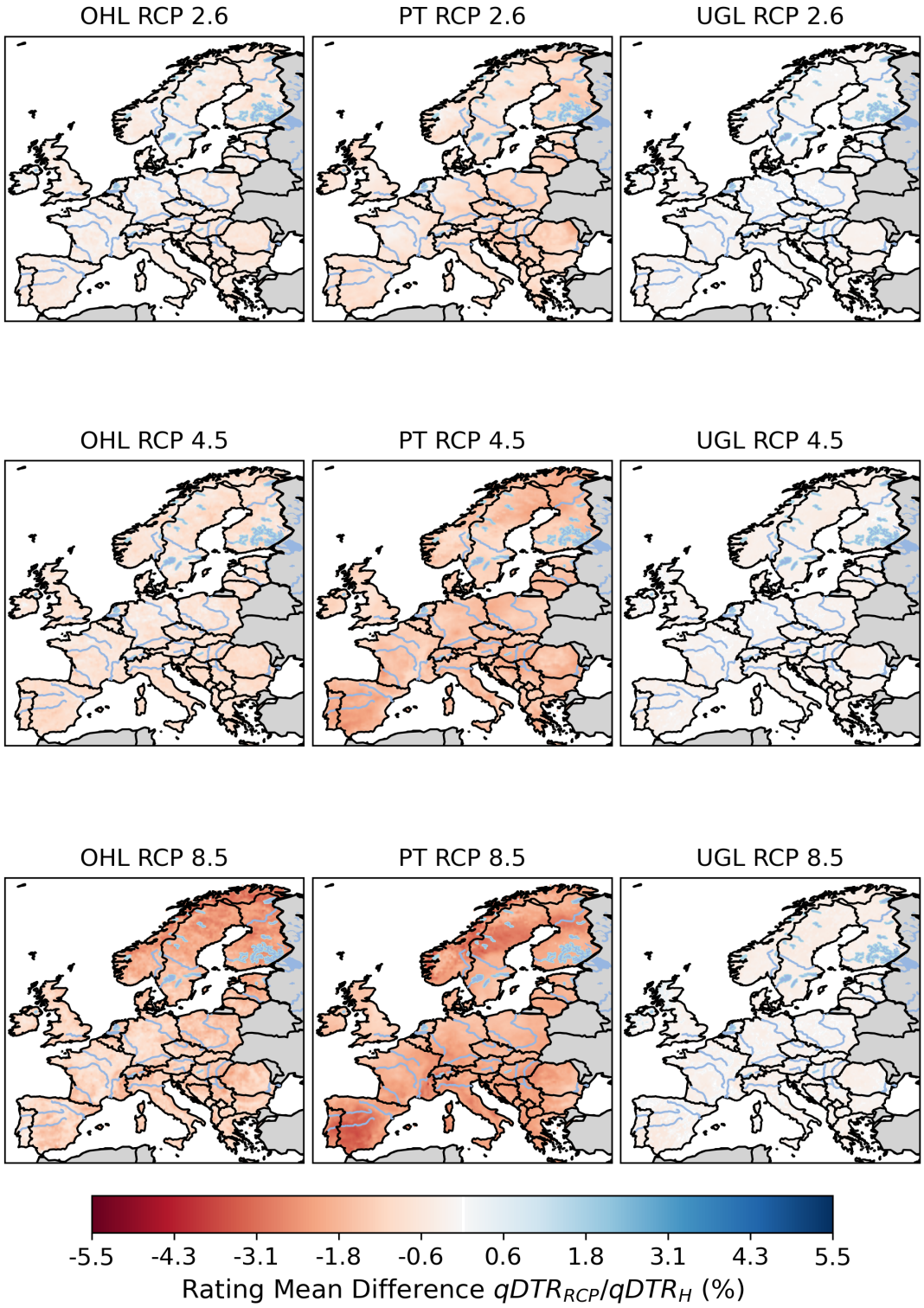

Figure 4.4: Geographical distribution of the mean qDTR difference at the country level over fifty years for the RCPs and the historical. This is performed for the main power components (OHL - PT and UGC), described in Tables B.1,B.2, B.3. The first row reflects the difference in the variation of the historical average for the region, and the subsequent rows illustrate the variation in the average for each RCP.

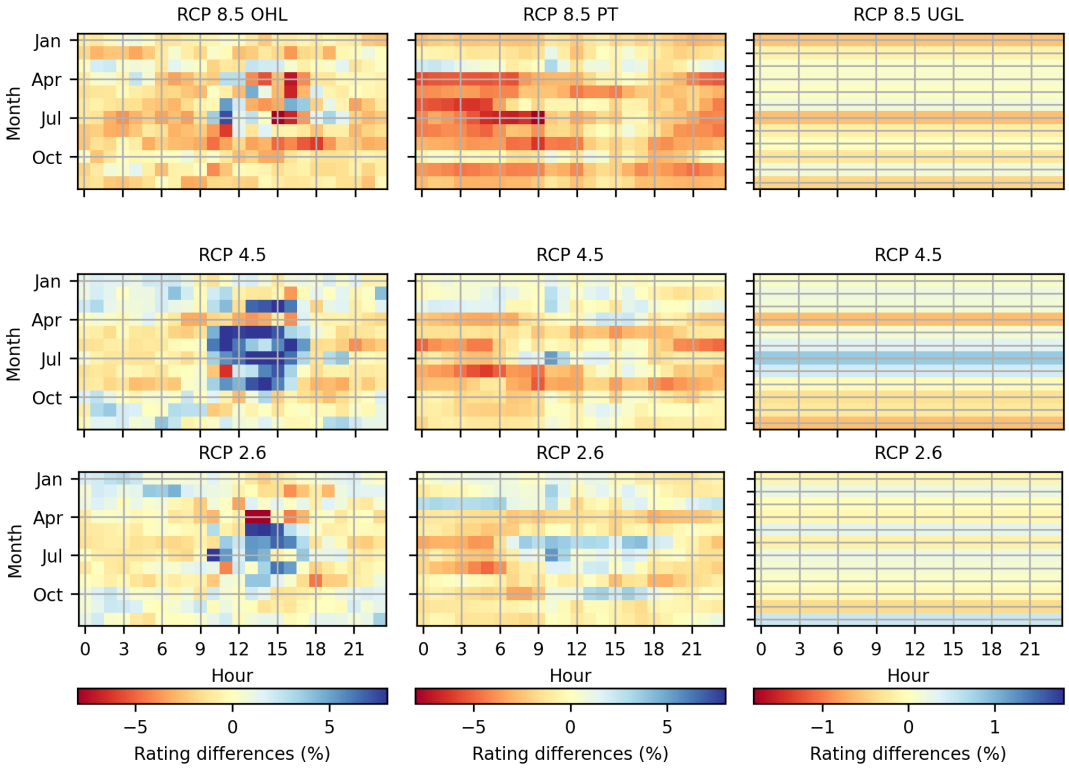

Figure 4.5: Difference in the calculated $qDTR_{month/hour}$ between historical values and RCP projections 2.6, 4.5, 8.5. Performed for (OHL - PT, and UGL) in a node located in Tavel, southeast France.

Finally, to further explore the seasonality of the impact, the heat map in Fig. 4.5 shows the monthly and hourly variation of qDTR_{RCP} at the same analyzed node in southeast France (Tavel) of Fig. 2.14. This heat map reveals the effects of increasing component temperature in the three RCP scenarios. The observed variations, which are moderately significant, translate, for example, into an average rating reduction of -2.3% in July for $\text{qDTR}_{\text{RCP8.5}}$ and -0.7% for $\text{qDTR}_{\text{RCP4.5}}$ in PT. This could be translated into a variation in the level of risk to the network operator in terms of equipment lifetime. On the other hand, the opposite effect can also be observed in certain months and hours, such as -0.9% on February mornings for $\text{qDTR}_{\text{RCP8.5}}$, +0.7% for $\text{qDTR}_{\text{RCP4.5}}$, and +0.02% for $\text{qDTR}_{\text{RCP2.6}}$.

B. Evaluating Climate Change's Impact on Underground Cables

As observed, the effects of climate change on UGL are comparatively moderate due to the thermal inertia of the soil, which dampens short-term (day-to-day) temperature fluctuations and mitigates the direct impact of environmental climate variations. To assess these effects on a broader scale, a regional analysis is performed using weekly and annual values of $qDTR_{RCP}$ with a fixed-threshold set at 0.1%. The analysis retains the same temporal horizons used in previous assessments at the component level, allowing for a consistent comparison and integration of results. It is applied to the range of underground cable configurations described in Tables B.4, and B.5. Finally, it is carried out across the entire geographical extent of France at a spatial resolution of 0.25°.

When calculating the $qDTR_{RCP}$ instead of historical meteorological data, a moderate but significant impact of the increase in component temperatures is observed, as illustrated in Fig. 4.6, that is, it is evident that these climatic changes result in worse weather conditions that influence the capacity, increasing component temperature, and negatively impacting the rating. Table 4.3 presents the mean values of temporal differences in rating, highlighting seasonal dynamics: i.e, colder ambient temperatures, higher precipitation, and lower irradiance levels tend to improve cable rating during winter months.

Type	**Install**	**Impact of qDTR**				**Impact of Climate Change**			
		Fall	**Sprg**	**Sum**	**Wint**	**Fall**	**Sprg**	**Sum**	**Wint**
$RCP_{8.5}$		**($qDTR_{8.5}$, $STR_{8.5}$)$_{\Delta_{\%}}$**				**($qDTR_{8.5}$, $qDTR_{Hst}$)$_{\Delta_{\%}}$**			
Cable 1	Buried	7.11	6.22	1.09	16.5	-5	-4.9	-6	-4
	Backfill	4.72	3.44	0.91	8.4	-0.5	-0.4	-0.4	-0.1
Cable 2	Buried	7.02	19.05	4.44	18.4	-0.2	0.3	-0.5	0.1
	Backfill	7.06	6.25	-2.29	10.7	-0.5	0.1	-0.4	-0.1
$RCP_{4.5}$		**($qDTR_{4.5}$, $STR_{4.5}$)$_{\Delta_{\%}}$**				**($qDTR_{4.5}$, $qDTR_{Hst}$)$_{\Delta_{\%}}$**			
Cable 1	Buried	8.6	6.8	-2.3	13	-4.8	-5.1	-5.8	-3.9
	Backfill	7.5	19.2	5.6	19.6	-0.37	-0.36	-0.3	-0.12
Cable 2	Buried	1.72	3.8	1.3	11.3	0.65	0.36	-0.5	1.6
	Backfill	7	18.2	4.6	18	-0.35	-0.35	-0.31	-0.12
$RCP_{2.6}$		**($qDTR_{2.6}$, $STR_{2.6}$)$_{\Delta_{\%}}$**				**($qDTR_{2.6}$, $qDTR_{Hst}$)$_{\Delta_{\%}}$**			
Cable 1	Buried	9.04	19.4	4.94	20.9	-4.4	-4.9	-5.8	-3.8
	Backfill	7.9	19.3	5.6	19.5	-0	-0.2	-0.3	-0.1
Cable 2	Buried	12	9.2	0	7.9	1.1	0.6	-0.5	1.7
	Backfill	7.4	18.3	4.6	17.9	-0	-0.2	-0.1	-0.1

[1] Cable 1 - A2X(F)K2Y-800RM: Circular stranded aluminium conductor with a nominal voltage of 245 kV. The XLPE insulation has a nominal thickness of 22 mm, see Table B.4.
[2] Cable 2 N2XS(FL)2Y 1x1200: Circular stranded aluminium conductor with a nominal voltage of 500 kV. The XLPE insulation has a nominal thickness of 31 mm Table B.5.
[3] Here, the STR is evaluated using the $qDTR_{year}$ method.

Table 4.3: Percentage Change $\Delta_{\%}$) in Seasonal Mean qDTR Capacity Over Fifty Years Under $RCP_{2.6,\ 4.5,\ 8.5}$ Scenarios (month/hour Resolution)

Among the results summarized in Table 4.3, the following key observations can be made:

- **Impact of climate change:** In the last three columns, the rating decreases when the $qDTR$ values are calculated using RCP climate scenarios instead of historical data. The reduction ranges from 3.8% to 6% for the smaller Cable 1, while the effect is negligible for the larger Cable 2.
- **Impact of using qDTR instead of STR:** In the first three columns, ratings based on qDTR result in increases for Cable 1 ranging from -2.3% to 20.9% and for Cable 2 from 0% to 19%, highlighting the performance improvements.
- **Impact of backfill material:** The presence of backfill significantly reduces the sensitivity of cables to the effects of climate change, particularly for smaller conductors like Cable 1, by improving the thermal conductivity of the soil.
- **Importance of voltage level:** Higher voltage conductors, which are typically designed

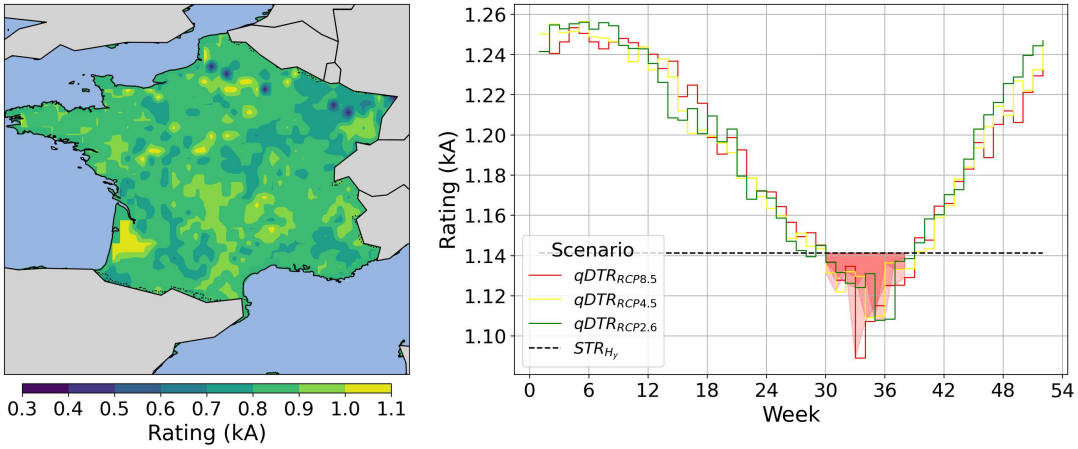

Figure 4.6: Geographical distribution of annual $qDTR_{8.5}$ across France for Cable 2. The second panel shows the yearly evolution of $qDTR_{week}$ for historical $qDTR_{H}$ and projected $qDTR_{RCP}$ in the Île-de-France region. The red zone indicates overload risk if $qDTR_{RCP\text{-}year}$ is applied. This figure is reproduced from **Paper A**.

with greater insulation and cross-sectional area, are less affected by external variations in the soil's thermal resistivity, providing greater resilience to climate change.

Fig. 4.6 illustrates the spatial distribution of thermal ratings across France's regions, highlighting regional disparities in the effects of climate change on underground cable capacity. The visualization captures the spatial variability of $qDTR_{RCP}$ across the country, revealing fluctuations of up to 2%. This predominant variability is influenced by the diversity of soil types present in each region, which significantly affects thermal resistance and moisture retention characteristics, crucial to the performance of underground cables.

Unlike STR methods, the use of qDTR preserves the inherent thermal inertia of deep soils. As shown in Figure 4.6, this inertia manifests as a time lag in the thermal response, with a notable four-week delay in the annual thermal cycle and a corresponding decrease in transmission capacity around September. However, it is important to note that the actual heterogeneity of soil composition is often much more complex than can be captured at the 0.25° grid resolution used in the analysis. Therefore, in the absence of engineered fill, detailed site-specific soil characterization is essential.

4.5.2 Impact of climate change on network costs

This section examines the investment decisions of transmission planning, incorporating various future climate scenarios, different planning methodologies, and the qDTR methodology for the power system components. These results have already been published in papers **Paper B** and **Paper F**.

A. European Power System Expansion: Climate Change Transmission Impacts

The procedure described in Section 3.7.1.1 is employed, applying $\text{qDTR}_{\text{year,Historical}}$ and $\text{qDTR}_{\text{Hour,RCP}}$ calculated from historical or climate projections, and for the OHL lines from [172]. To illustrate this and highlight the influence of future scenarios, Fig. 4.7 shows the impact of climate change on the transport capacity in the European transmission network. For this example, the summer month (June) has been selected, as it is a month typically influenced by high temperature conditions. This influence translates into reductions that, in certain regions such as the south of the Iberian Peninsula, can exceed -5% under high greenhouse gas emission scenarios (RCP 8.5).

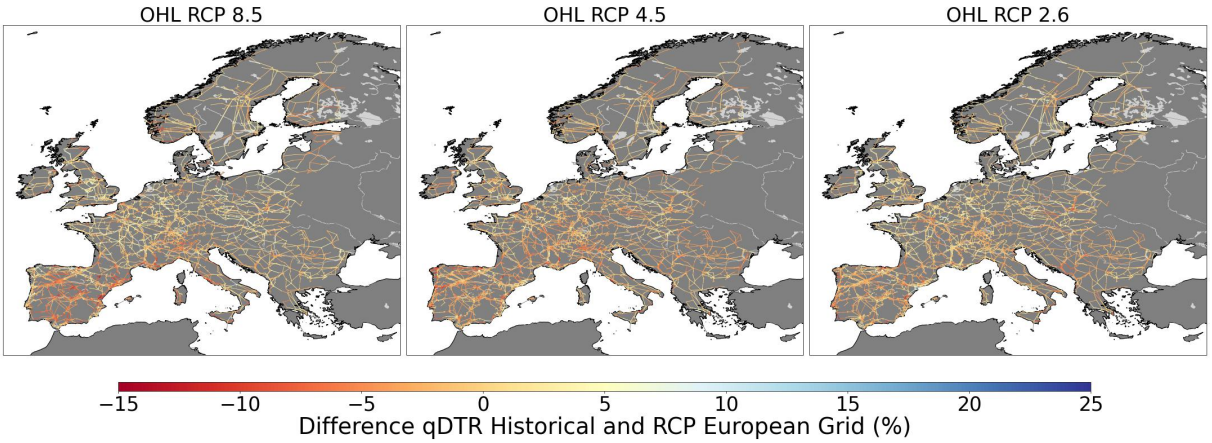

Figure 4.7: Climate impacts on transmission capacity, the difference in capacity for qDTR (Percentage Change $\Delta_{\%} \frac{qDTR_{RCP}}{qDTR_H}$) for summer day (June) at 14 h RCP 2,6, 4.5 and 8.5 scenarios for OHL. This figure is reproduced from **Paper B**.

Using a procedure similar to the case in Section 3.7.1.1, the network model is subsequently applied to conduct a G&TEP analysis. The results of this analysis are presented in Table 4.4, which includes: *(i)* The outcomes of the base scenario utilizing $\text{qDTR}_{\text{year,Historical}}$, *(ii)* the differences that arise when substituting climate projections with historical weather data within the framework of qDTR_{RCP}, and *(iii)* the performance gains achieved by replacing $\text{qDTR}_{\text{year,Historical}}$ with $\text{qDTR}_{\text{month/hour,RCP}}$. It is important to emphasize that in all cases, the qDTR was evaluated with a lower threshold capacity (X_R) than 0.1%. The table also reports on the anticipated level of RES reduction and the total system cost. It is important to note that these figures refer solely to the newly planned infrastructure and do not reflect the cost or performance of existing assets.

Case 1. In this scenario, the G&TEP model was executed using qDTRs derived from the corresponding RCP climate projection. As shown in Table 4.4, cost dynamics vary notably across the scenarios. In particular, under the $RCP_{8.5}$ pathway, reduced effective transmission capacity results in the underestimation of both CAPEX and renewable curtailment. This leads to a projected mismatch of approximately 42.7 M€ in capital expenditure.

Case 2, shown in the final row of Table 4.4, compares the costs associated with using a static transmission rating based on historical against those obtained with climate influenced

	CASE : Variation Evaluated	$RCP_{2.6}$	$RCP_{4.5}$	$RCP_{8.5}$
INDICATORS	**REFERENCE : (STR_H)**			
	CAPEX (B€)	3.55E+2	3.55E+2	3.55E+2
	OPEX (B€)	1.89E+1	1.89E+1	1.89E+1
	System Cost (B€)	4.00E+2	4.00E+2	4.00E+2
	Curtailment (GWh)	7.32E+0	7.30E+0	7.32E+0
	CASE 1 (Δ($qDTR_{month/hour,\ RCP}$/$qDTR_{month/hour,H}$))			
	CAPEX (%)	-6.26E-3	4.59E+0	-1.20E-2
	OPEX (%)	4.88E-3	2.20E+1	1.68E-2
	System Cost (%)	-5.02E-3	6.52E+0	-8.81E-3
	Curtailment (%)	4.57E-2	4.20E-1	-6.10E-2
	CASE 2 (Δ($qDTR_{month/hour,RCP}$, STR_H))			
	CAPEX (%)	1.70E-2	4.61E+0	1.21E-2
	OPEX (%)	1.49E-1	2.21E+1	1.49E-1
	System Cost (%)	3.16E-2	6.55E+0	2.72E-2
	Curtailment (%)	6.94E-1	4.28E-1	3.65E-1

[1] Here, the reference STR is evaluated, using the $qDTR_{year}$ frequency method.

Table 4.4: Variation in system costs for the three scenarios (RCP 2.6, 4.5, 8.5) in Europe. STR refers to annual static values, qDTR to month/hour. Subscripts $_H$ and $_{RCP}$ indicate historical vs. projected weather data. Values are in % and calculated as $1 - y/x$.

qDTRs, with month/hour temporal resolution. The results consistently indicate cost savings across all RCP scenarios, even when accounting for increased ambient temperatures and reduced transmission capacities. For the low-emissions scenario, these savings are estimated at around 126 M€.

B. Integration of Climate Impacts into Network Planning Using Fixed-Probability qDTR Ratings: IEEE 24-Bus and Regional Expansion Case Studies

Based on the qDTR framework described in Sections 3.7.2 and 3.7.3, the method is extended by incorporating RCP climate projections, maintaining the same fixed-probability threshold for overload ($X_R = 0.1\%$).

First, the deterministic TNEP problem is addressed using the IEEE 24-bus reliability test system [145], with annual load and generation uniformly scaled by a factor of 1.5 and a detailed case/scenario description in 3.7.3. For each RCP scenario, the projected demand for the period 2023-2050 is incorporated following the projections reported in [182]. The results in Table 4.5 highlight three main findings. First, climate change introduces a moderate increase in network and operating costs in both extreme ($RCP_{8.5}$) and moderate ($RCP_{2.6}$) scenarios, reflecting the conservative risk tolerance inherent in the qDTR approach. Second, replacing STR with qDTR under high-emissions conditions ($RCP_{8.5}$) reveals a higher overload risk due to lower heat dissipation, requiring additional line investment in Scenario 2 / Case 1. Finally, despite these localized reinforcements, the qDTR method consistently yields higher average ratings over most of the year, translating into lower operating costs (up to -8.36%) and, in some cases, fewer network

expansions (e.g., Scenario 1 / Case 2). These findings underscore the robustness of extending qDTR to climate change influenced by projections, while maintaining long-term planning based on a fixed-probability threshold.

Scenario 1 - base case load and generation increased by 50%			
Case 1	**Impact of qDTR ($\mathbf{qDTR_{RCP}}$,$\mathbf{STR_{RCP}}$)**		
	$\mathbf{RCP_{8.5}}$	$\mathbf{RCP_{4.5}}$	$RCP_{2.6}$
$CAPEX_{\Delta_\%}$	-29.8	-	-100
$OPEX_{\Delta_\%}$	-33×10^{-2}	-40×10^{-2}	-3×10^{-3}
ΔLines $_{build}$	$Branch_5 : -1$	0	$Branch_5 : -1$
Case 2	**Impact of Climate change ($\mathbf{qDTR_{RCP}}$,$\mathbf{qDTR_H}$)**		
	$\mathbf{RCP_{8.5}}$	$\mathbf{RCP_{4.5}}$	$RCP_{2.6}$
$CAPEX_{\Delta_\%}$	–	-	–
$OPEX_{\Delta_\%}$	50×10^{-3}	10×10^{-3}	30×10^{-3}
ΔLines $_{build}$	-	-	-
Scenario 2: generators added at nodes 3, 5, 16, 21			
Case 1	**Impact of qDTR ($\mathbf{qDTR_{RCP}}$,$\mathbf{STR_{RCP}}$)**		
	$\mathbf{RCP_{8.5}}$	$\mathbf{RCP_{4.5}}$	$RCP_{2.6}$
$CAPEX_{\Delta_\%}$	76.9	-	-
$OPEX_{\Delta_\%}$	-8.36	-1.3	-42×10^{-2}
ΔLines $_{build}$	$Branch_1 : -1$, $Branch_8 : +1$	-	-
Case 2	**Impact of Climate change ($\mathbf{qDTR_{RCP}}$,$\mathbf{qDTR_H}$)**		
	$\mathbf{RCP_{8.5}}$	$\mathbf{RCP_{4.5}}$	$RCP_{2.6}$
$CAPEX_{\Delta_\%}$	–	-	–
$OPEX_{\Delta_\%}$	30×10^{-2}	70×10^{-3}	4×10^{-3}
$\Delta Lines_{build}$	-	-	-

Table 4.5: $\Delta_\%$ Variation for the three scenarios concerning investment and costs, the scenarios covering historical and projected static (STR), historical ($qDTR_H$), and projected ($qDTR_{RCP}$). From **Paper A**.

Second, based on the methodological framework established in Section 3.7.2, this section extends the application of the qDTR approach by incorporating climate projections into the long-term G&TEP. While the earlier analysis focused on historical data to assess transmission component ratings, the results in Table 4.6, introduce the influence of RCP to explicitly capture the impacts of future climatic variability on network investment decisions. In this context, both STR_{RCP} and $qDTR_{RCP}$ are evaluated, enabling a comparative assessment of annual versus temporal finer resolution in rating methodologies under projected climate conditions. The resulting G&TEP outcomes reflect adjustments in CAPEX, OPEX, and RES curtailment, thereby linking operational efficiencies with investment strategies. As summarized in Table 4.6, the findings confirm three central insights: first, on the operational side (OPEX), consistent reductions are observed across all $qDTR_{RCP}$ scenarios, with total costs falling by 33% under $RCP_{8.5}$, 26% under $RCP_{4.5}$, and 27% under $RCP_{2.6}$. Second, CAPEX shows moderate variation, with RES largely stable, fossil generation increasing under $RCP_{8.5}$ (+13%) but falling under $RCP_{2.6}$ (–10%), and nuclear capacity decreasing, contributing to total reductions of up to 11%. Third, all this is translated into substantial reductions in overall system costs, with savings of 27%, 21%, and 24% across the three RCP pathways, confirming the economic value of integrating finer resolution thermal ratings into climate influenced expansion planning.

	$\mathbf{RCP_{8.5}}$,STR_{RCP}	$\mathbf{RCP_{4.5}}$,STR_{RCP}	$\mathbf{RCP_{2.6}}$,STR_{RCP}
CAPEX			
Renewable	< 1	-7	-7
Fossil	13	9	-10
Nuclear	-9	-100	-100
Total	1	-9	-11
OPEX			
Renewable	-12	-9	-1
Fossil	-2	-2	-6
Nuclear	< 1	-4	-6
Total	-33	-26	-27
Curtailment	-2.6	-13	-14
System Cost	-27	-21	-24

Table 4.6: Variation (in %) for the three scenarios concerning yearly fixed rating and costs. In this table the STR is calculated using the $qDTR_{year}$ and RCP with $qDTR_{month/hour}$

C. Climate influence in Network Planning: Incorporating Stochastic Thermal Risk management in a Changing Environment

According to the results presented in section 3.7.4, the conservative practice of applying a fixed lower threshold limit (e.g., $X_R = 0.1\%$) to estimate qDTR fails to adequately capture the flexibility or conservatism experienced by the network when historical weather scenarios are considered. Moreover, evaluating transmission capacity solely on the basis of historical information can lead to similar limitations as assuming a deterministic capacity. To address this issue, this chapter updates the methodology introduced in section 3.4 by incorporating the climate information presented in section 4.3.1. As illustrated in the framework of Fig. 4.8, climate scenarios are explicitly integrated to influence demand, renewable generation, and transmission capacity, accounting for their geographical variability.

Based on the case study that utilizes historical datasets (as presented in Table 3.7 and Fig. 3.21) for the IEEE RTS 24-Bus Test System [145], is extended to incorporate future climate scenarios. This enhancement enables the model to account for both adverse and typical conditions projected under various RCP scenarios, as detailed in Table 4.7. By doing so, the qDTR methodology can integrate expected changes in climate factors affecting the transmission system components, while also adapting to evolving demand profiles, and the production of RES.

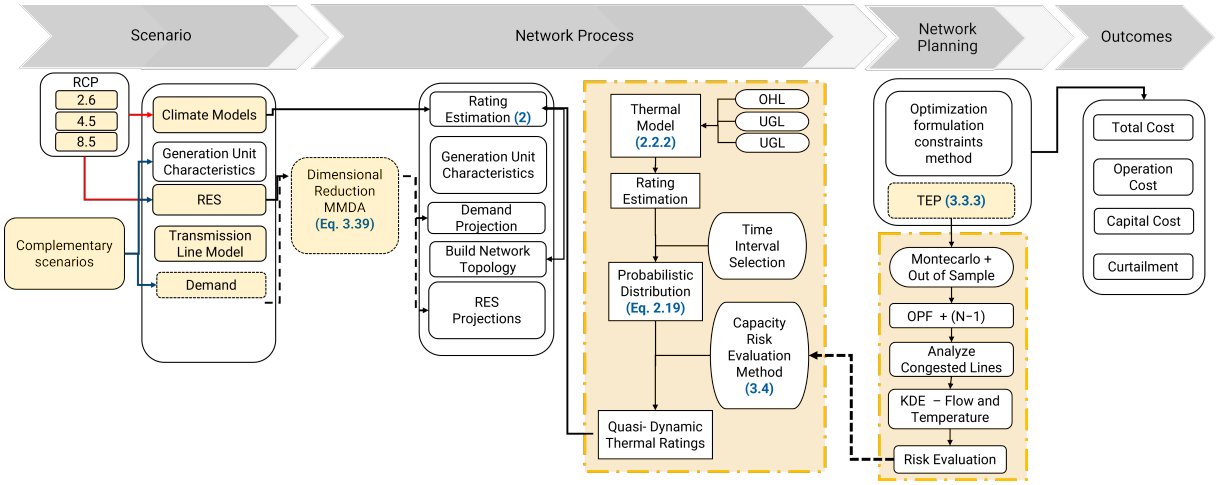

Figure 4.8: Visual representation of the procedure, mainly showing the inclusion of different climate scenarios and risk assessment.

Table 4.7: Input Parameters

Parameter	**Value**	**Description / Notes**
Load Shedding Max (λ)	0.01	Maximum load shedding factor
Curtailment Cost	2000	\$/MWh — From [165]
CO2 Cost	99	€/MWh
Climatic Scenario	RCP 2.6,4.5,8.5	Climate scenario From [182]
Resolution	0.25	Spatial resolution of climate scenario
Analisis resolution	Hour & Year	Temporal resolution of analysis
Backfill	0	No Backfilled
Typical day per Zone (each 5 years)	5	Number of days per zone to apply in MMDA
Load Factor	1.2	Initial load increase factor to base case
Years	5	Planning horizon per Epoch
Epochs	5	Number of epochs
$Wind_{ini}$	0.13	Initial wind penetration per Node
PV_{ini}	0.07	Initial solar PV penetration per Node
Int_{rate}	0.08	Interest rate
Nodes Up	[1, 20, 2, 13, 4, 15]	Nodes selected for RES
CO_2 Prices	AM5S2, AM5S3 and AM5S4 scenario	From [166]
PV Increase	2050 M2, N2 and N03	From [180], detailed in Annex B
Demand Increase	2050 M2, N2 and N03	From [180], detailed in Annex B

Wind Increase	2050 M2, N2 and N03	From [180] , detailed in Annex B
PV CAPEX	Advance, Moderate and Conservative Scenario	€/KW From [167]
Wind CAPEX	Advance, Moderate and Conservative	€/KW From [168]
Line and Cable CAPEX	Lower and Higher Scenario	From €/MW/m[169]

These projections are integrated into the scenario input module, as detailed in Fig. 4.9, where the proposed framework evaluates how different trajectories of extreme weather events and gradual climate changes may affect transmission capacity, thermal overload risk, and ultimately impact investment needs. This allows for a new planning perspective, where expansion strategies are guaranteed while remaining robust not only to operational variability but also to structural climate changes over long horizons.

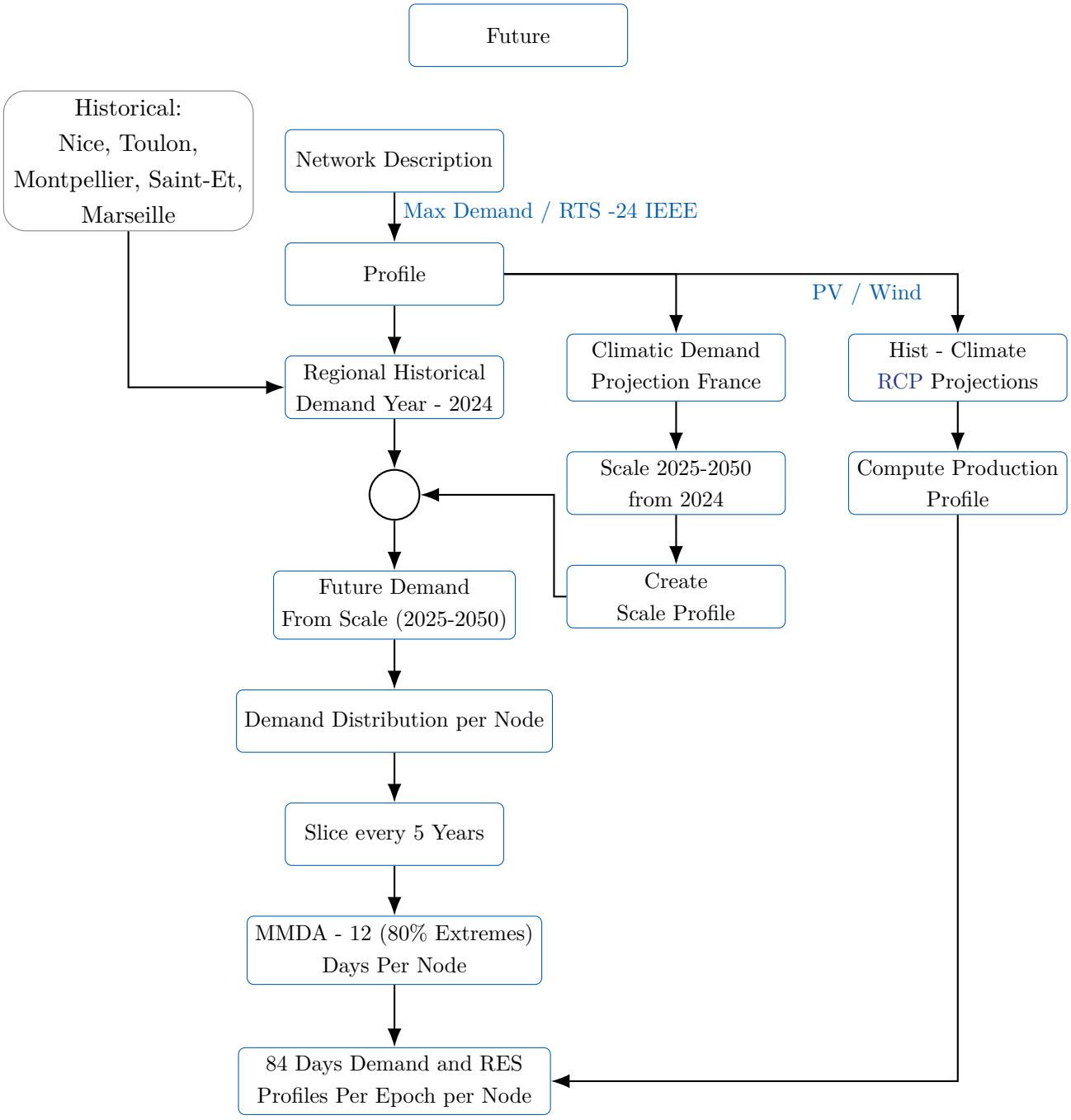

Figure 4.9: Scenario input flow diagram for network planning: Integrating RCP-based demand projections, renewable energy generation, and transmission capacity

To evaluate the flexibility and applicability of the proposed qDTR methodology, three cases were analyzed:

1. **Historical Baseline:** This case, already introduced in Section 3.7, employs historical meteorological datasets (1970-2024) to calculate year and month/hour qDTR values. It

establishes a reference point for comparison with future climate projections.

2. **Future Climate Projections (Annual *qDTR*):** Annual $qDTR_{year}$ values were derived using representative concentration pathways (RCP 2.6, 4.5, and 8.5) for the period 2024–2070. These values are computed based on year frequency distributions to evaluate how long-term average climate changes affect thermal capacity thresholds. While the approach is conceptually similar to the application of STR, the key distinction lies in the nature influence of the climate of the qDTR methodology, which explicitly incorporates projected environmental conditions into the assessment.

3. **Future climate projections (Month/Hour qDTR):** Beyond fixed annual ratings, higher temporal resolution qDTR values were estimated at month/hour for the same RCP scenarios. This more finest temporal scale allows for a sensitivity analysis of intra-hourly and seasonal climate variability, which influences thermal capacity thresholds. Also, according to previous results, it improves the system's ability to capture both risks and opportunities in long-term planning, especially in systems with high renewable energy penetration and dynamic demand profiles.

Fig. 4.10–4.12 illustrate the power flows of selected transmission lines under the different RCP scenarios. The dashed lines indicate the thermal rating limits used in the TEP model as branch capacity constraints derived from the annual risk-aware method to derive the qDTR ratings for RCP 2.6, 4.5, and 8.5. Meanwhile, the heatmaps show the hourly utilization of each line over the horizon 2025-2050, highlighting how future climate variations affect transmission performance relative to their thermal limits. In the Line 12 (Fig. 4.10), the results highlight how all climate projections reduce transmission capacity, leading to higher utilization levels and narrower operating margins. Seasonal patterns are also evident, where summer months approach critical limits more frequently than winter periods.

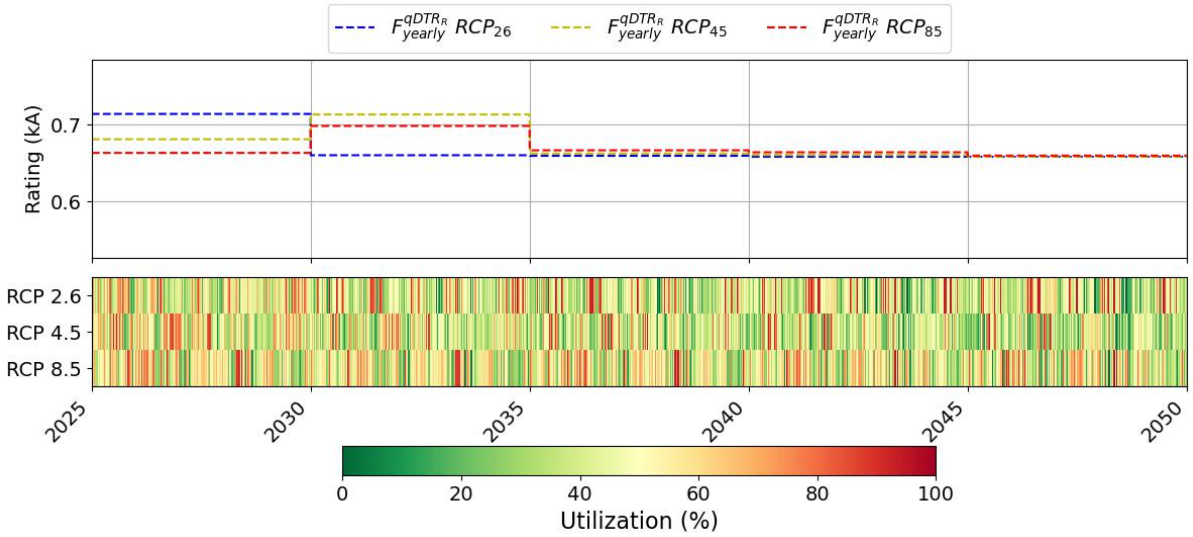

Figure 4.10: Power flow in Line 12: Heatmap of $|P_f|$ normalized by the thermal limit with $qDTR_{year,RCP}$. The results indicates.

In the Line 22 (Fig. 4.11), a similar effect is observed but at higher power flows. The comparison suggests that future trends of RES penetration under $RCP_{2.6}$ impose binding constraints, especially after 2040, where a gradual decrease in thermal rating results in recurrent operation close to capacity, and consequently imposes an expansion of a new line. Conversely, in Line 32 (Fig. 4.12), the correlation of the flow over the line and the future ambient conditions does not impose thermal restrictions during the future horizon, indicating that for this type of corridor, a assessment with DTR technologies will not be necessary in the future.

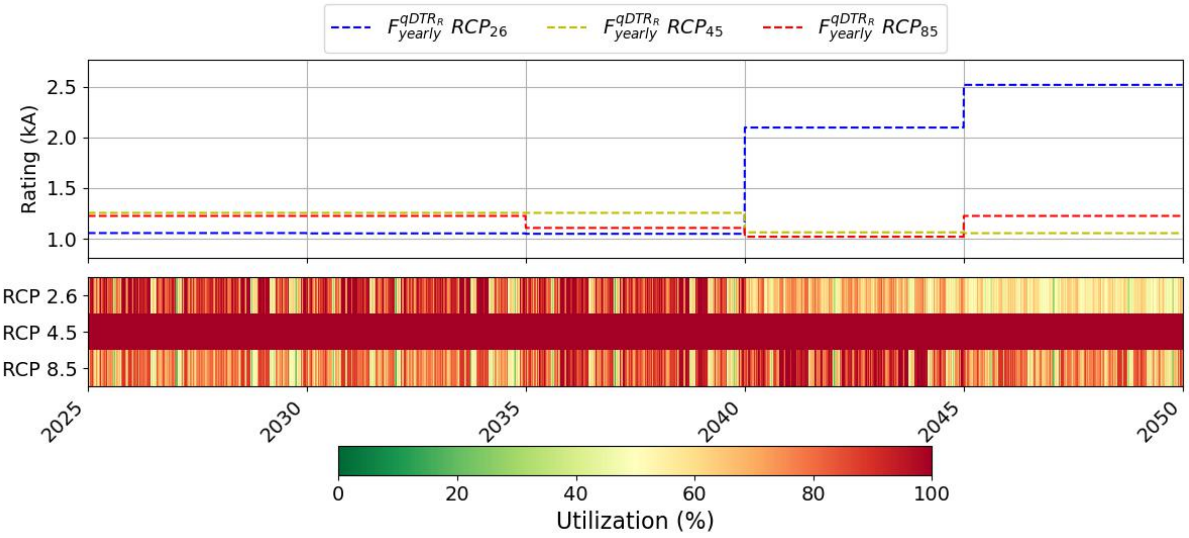

Figure 4.11: Power flow in Line 22: Heatmap of $|P_f|$ normalized by the thermal limit with $qDTR_{year,RCP}$. The plot a

Those figures evidence demonstrates how the $qDTR_{year}$ limits provide a broader perspective on line congestion according to its future scenario, which is influenced either by the most critical conditions in terms of environmental factors or by stress conditions due to overload caused by the expansion of both generation and demand, identifying periods of underutilization (green) and critical load (red). Comparing these annual scenarios allows the operator to develop more adaptive planning strategies that harness favorable conditions and mitigate the risks of overheating.

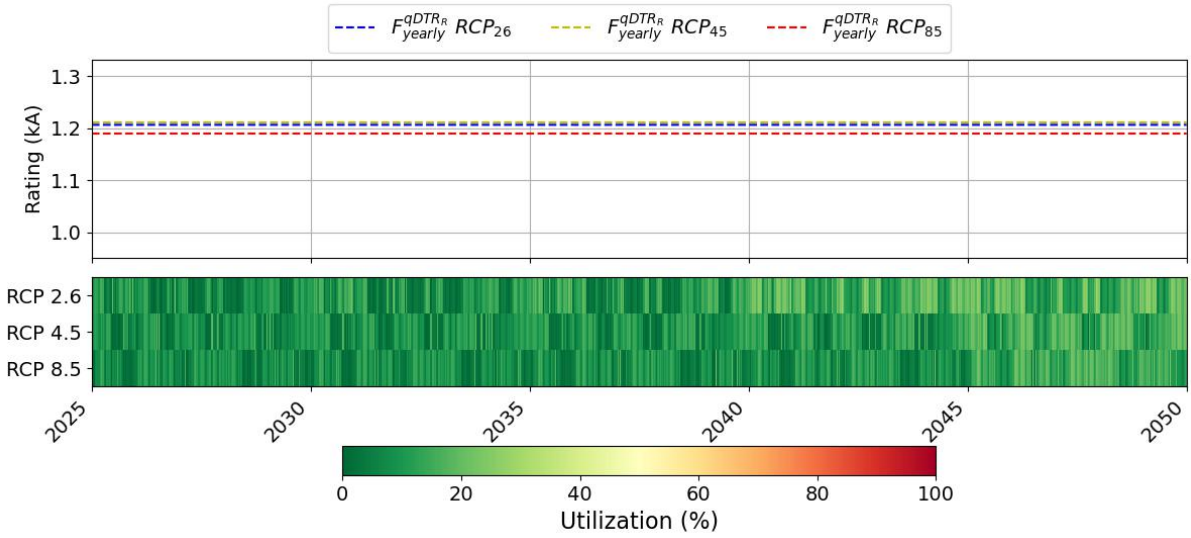

Figure 4.12: Power flow in Line 32: Heatmap of $|P_f|$ normalized by the thermal limit with $qDTR_{year,RCP}$. The figure shows no restriction caused by the thermal limit.

Finally, Table 4.8 summarizes the operational, capital, and economic impacts of the evaluated scenarios. Compared to static STR, annual qDTR provides moderate improvements in system performance, as it allows for the use of less conservative conditions to which the component is subjected during climate projection. For example, using annual qDTR results in a slight increase in OPEX of 0.36%, a reduction in CAPEX of 68.1%, small reductions in load shedding (-0.15%), and a moderate increase in losses (10.46%). These benefits reflect the fact that annual ratings using qDTR improve line efficiency over the period, providing a better overall estimate of thermal limits, but omit more accurate temporal variability.

Table 4.8: Comparative Analysis of Climate Scenarios: Operational, Capital, and Economic Impacts. The percentage change is calculated using the formula: $(Scenario_A - Scenario_B)/Scenario_B \times 100$.

Scenario	ΔOPEX	ΔCAPEX	ΔCO_2 Cost	ΔShedding	ΔLosses
Results 1: STR vs Annual/(month/hour) qDTR					
$qDTR_{year}$	0.36	-68.11	0.70	-0.15	10.46
$qDTR_{hour}$	-0.24	-100.00	0.14	-0.60	-20.14
Results 2: Annual qDTR - Historical vs qDTR - Future Climate Projections (RCP 2.6, 4.5, 8.5)					
$qDTR_{year,26}$	-57.74	-64.94	-65.62	57.35	-30.23
$qDTR_{year,45}$	-48.75	+100	-78.46	+99.4	-39.4
$qDTR_{year,85}$	-54	+100	-84.37	+100	-31.17
Results 3: Annual vs (month/hour) qDTR - Future Climate Projections (RCP 2.6, 4.5, 8.5)					
$qDTR_{hour,45}$	-0.66	-100	-1.32	-0.63	-34.05
$qDTR_{hour,85}$	-0.34	-100	-0.40	-1.54	-31.48

Scenario	ΔOPEX	ΔCAPEX	ΔCO_2 Cost	ΔShedding	ΔLosses

Note:

1. $qDTR_{year}$, $qDTR_{hour}$ — Thermal Rating scenarios compared to static STR.
2. 26 / 45 / 85 — Climate-based scenarios using RCP 2.6, 4.5, and 8.5 projections.
3. Annual vs Hour — Indicates whether the scenario uses annual or month/hour resolution to calculate the qDTR.

In contrast, the monthly/hourly qDTR captures night-time and daytime weather conditions in line ratings, resulting in significantly higher benefits. Specifically, operating expenses decrease moderately by 0.24%, capital expenses are avoided entirely (100%), and losses are reduced by 20.14% likely associated with a better alignment between generation and demand patterns, which may enhance the overall efficiency of transmission utilisation. Finer temporal resolutions, such as month/hour allow the system to take advantage of thermal capacity during colder periods or less thermally stressed hours, which cannot be captured in annual ratings, resulting in more efficient utilisation of existing infrastructure, avoiding unnecessary investments and improving reliability.

Under the high-emission RCP 8.5 scenario, annual qDTR shows the greatest decrease in operational efficiency, with a 54% reduction in OPEX, a 100% increase in CAPEX, and an important 100% increase in outages compared to historical conditions. This increase arises because the annual ratings now take into account a more stressed network than the historical baseline, shaped by weather and RES scenario parametrization. As a result, extreme conditions caused by climate change, such as heat waves or high load peaks, cause significant stress on the system. In contrast, the low-emission RCP 2.6 scenario shows a smaller decrease in efficiency (OPEX and CAPEX reduction of 57.63% and increase 64.9%), due to less warming and greater integration of RES, which provides less flexibility than high-emission scenarios.

The monthly/hourly qDTR, by capturing seasonal and intraday variations, mitigates some of the adverse impacts even under the RCP 8.5 scenario. It reduces losses by 31.48% , maintaining OPEX reductions (-0.34%), and not imposing any line expansion, although overall margins continue to decline under severe warming conditions. This demonstrates that finer temporal resolution thermal ratings can partially offset the negative effects of climate change by leveraging transient transmission capacity. To expand this result, Figures 4.13 and 4.14 compare the behavior of qDTR in two scenarios, detailing the evolution of transmission line ratings over time, while illustrating the corresponding utilization levels normalized by the thermal limits. This highlights: *(i)* Lower annual ratings compared to historical baselines, reflecting the impact of unfavorable conditions growing from 2025, *(ii)* conversely, reaffirming that the application of month/hour qDTR overcome this, providing greater temporal flexibility, capturing favorable meteorological conditions most of the time horizon, however reducing the risk during non favourable conditions illustrated with a yellow triangle, *(iii)* Heat maps confirm, that while annual ratings result in higher congestion levels (redder utilization patterns), finer temporal

resolutions distribute load more dynamically over time, reducing persistent overloads. Furthermore, the differences between $RCP_{4.5}$ and $RCP_{8.5}$ indicate that more severe warming scenarios exacerbate thermal constraints, reinforcing the importance of adopting a probabilistic approach with finer resolution.

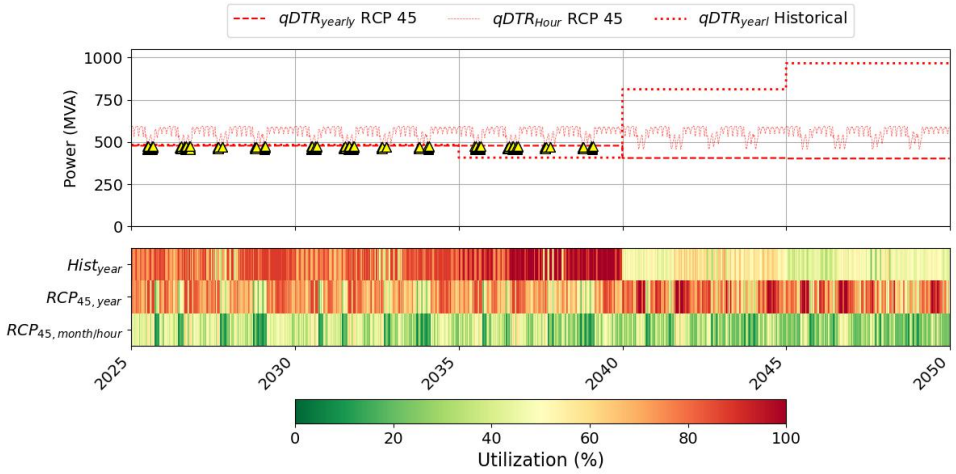

Figure 4.13: Thermal ratings and utilization under historical and RCP 4.5 climate scenario in Line 22. The yellow triangle highlights ratings that fall below historical benchmark areas, indicating that the monthly/hourly performance does not underestimate the associated risk.

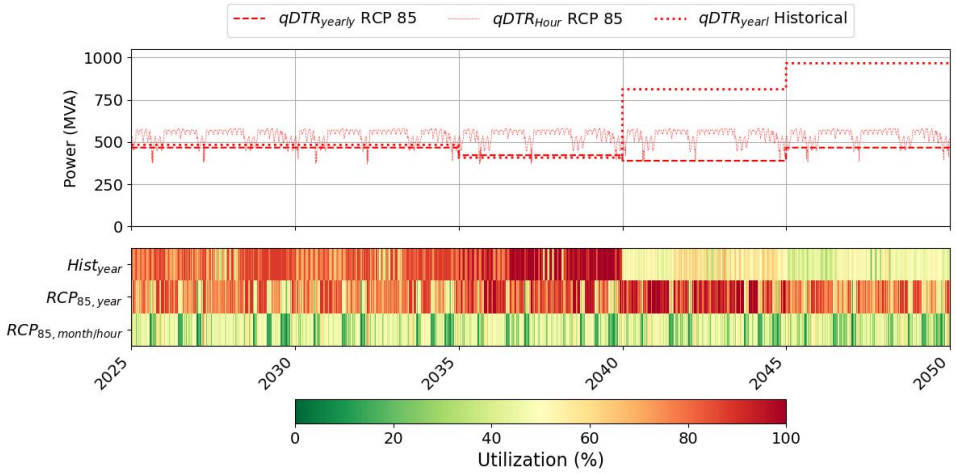

Figure 4.14: Thermal ratings and utilization under historical and RCP 8.5 climate scenario in Line 22.

Overall, qDTR improves transmission utilisation and reduces investment costs, but climate change introduces countervailing trends. Annual ratings provide moderate improvements in reliability but may underestimate the risk of peak load events, while monthly/hourly ratings maximise utilisation and minimise both operating and capital costs. *The dual effect where finer temporal resolution ratings improve efficiency, but climate stress reduces capacity over time, underscores the importance of integrating probabilistic, finer temporal resolution thermal ratings into long-term network planning.* This ensures optimisation of infrastructure investments,

maintains operational reliability, and increases resilience to extreme weather events.

4.6 Conclusion

This chapter analyzes the implications of climate change for the thermal capacity of transmission systems and the resulting challenges for long-term planning. The analysis demonstrates that increasing variability in climatic conditions and adverse weather events represent critical stress factors that are not quantified in traditional static thermal rating practices. By extending the quasi-dynamic thermal rating methodology to integrate climate projections ($qDTR_{RCP}$), the chapter provided a method capable of quantifying both the electrical and economic impacts of climate change on power networks.

The comprehensive analysis of climate projections for Europe, complemented by a detailed case study of France under the high-emission scenario $RCP_{8.5}$ for 2070, revealed average reductions in transmission capacity of 1.53% for OHL, 2.1% for PT, and 0.2% for UGL, when is compared to the historical reference period. These averages hide substantial spatial and temporal variability, as evidenced in Fig. 4.4. Regional soil properties and environmental conditions, particularly with low moisture, were found to significantly influence UGL performance, while OHL and PT were more sensitive to frequent heatwaves, with localized capacity drops of up to 40%. Such findings highlight the importance of region specific assessments and component adaptation measures.

Moreover, the comparative evaluation of annual, monthly, and month/hour qDTR temporal resolutions revealed that more temporal dynamic ratings deliver substantial operational and economic benefits. While annual qDTR offered only moderate improvements relative to STR, month/hour qDTR enabled more time sensitive utilisation of transmission assets. These new temporal resolutions, for instance under the mid-emission scenario (see Section 4.5.2), reduced capital expenditures by up to 100% and losses by more than 34%, while maintaining neutral operational costs. This demonstrates their role in balancing investment efficiency with system reliability across both historical and projected climate conditions. However, even finer temporal resolutions of qDTR could not fully offset the reduction in operational margins under severe climate warming, underscoring the need for integrated new strategies in planning.

Although the methodology was applied the climate of France, it is readily transferable to other regions using available climate, meteorological, and demand projection datasets. The method can be adapted to both transmission and distribution levels and enhanced with further refinements such as modelling thermal ageing, conductor degradation under recurrent high currents, and N-1 contingency analysis.

All these findings provide the necessary support to capture the final contribution of the methodology, called $qDTR_{RCP}$, which establishes data-driven approach to assessing the capacity of transmission networks in plausible future climates. It allows for the explicit quantification of temporal variability (daily, month/hour, seasonal, and annual) at both the local and regional levels, thus providing a framework that takes climate into account for both component-level analysis and system planning. In this way, it addresses both the effects of climate change on the capacity of transmission components (RQ5) and the implications for planning and investment under conditions of uncertainty (RQ6), as follows.

The impact of climate change on transmission components (RQ5) was assessed by combining historical trend analysis and prospective projections in climatic scenarios RCP, yielding results that capture not only the alteration of capacity under optimal conditions but also under extreme unfavourable conditions. The results for Europe show the negative impact across all RCP scenarios. PT are the component with the greatest variation (from -0.9% to -2.1%), followed by OHL (from -0.4% to -1.53%) and UGL (from -0.1% to -0.2%). However, in buried UGL, the thermal inertia of soils can mitigate losses, while OHL and PT show a pronounced vulnerability to prolonged heat waves. The backfill in the UGL installation plays a crucial role in mitigating the impact of climate change, ensuring that the deviation from historical scenarios remains below 1%.

The incorporation of stochastic for risk management analyses further advanced this research question by quantifying the probability distributions of thermal ratings rather than relying solely on fix lower threshold values. The results shown in Tab. 4.8 how the risks increase in high-emission scenarios. This revealed that relying on static thresholds underestimates the probability of extreme overloads, which can compromise reliability. Thus, these findings show that climate change not only reduces rated capacities but also increases overload risks among components, highlighting the need for dynamic, probabilistic, and climate-based rating strategies.

The integration of $qDTR_{RCP}$ into planning frameworks (RQ6) demonstrates how climate change adjusted ratings influence long-term analysis, investment, and operational strategies. While the fixed-probability threshold selection of qDTR ($X_R = 0.1\%$) constrains overload exposure, the incorporation of climate RCP projections significantly shapes long-term expansion outcomes. In the European case (Fig. 4.7 and Table 4.4), the rising temperatures under $RCP_{8.5}$ lead to increased projected capital requirements and operating costs when static ratings are retained. Conversely, in the IEEE 24-bus test system (Table 4.5), climate influenced qDTR with finer temporal resolution (*month*/*hour*) enables both localized reinforcement reductions and potential savings up to 8.36% in OPEX and 29.8% in CAPEX under $RCP_{8.5}$. These results highlight how high-emission scenarios exacerbate overload risks, yet demonstrate that finer-resolution qDTR can effectively mitigate such impacts.

Stochastic method to risk assessment provided a new dimension by integrating the uncertainty of climate change thermal stress directly into expansion planning. Scenario analyses, illustrated in simulations in Section 4.5.2/C, demonstrated the trade-offs between investment deferral and projected cost-effectiveness. Planning exercises based on historical data revealed that annual qDTR moderated investment requirements, achieving up to 68.1% savings in CAPEX, but failed to adequately capture intra-annual variability, thereby exposing the system to higher operational risks. By contrast, month/hour qDTR provided a finer resolution of system behaviour, enabling more efficient asset utilisation, achieving up to 100% CAPEX savings, and delivering modest yet measurable reductions in operational costs. Figures 4.10-4.12 illustrate that, under the applied climate projections, ratings are reduced, increasing utilization and narrowing operating margins, with seasonal peaks in summer months. This effect is evident in specific cases; for example, the results for Line 22 indicate reinforcement requirements, while other lines, such as Line 32, remain largely unaffected. Overall, table 4.8 highlights that annual

qDTR in a general improves efficiency over historical static ratings, but month/hour qDTR slightly reduces operating cost, however, capital is eliminated by capturing temporal variability. As an exemplification of the impact of the resolution in the projections, in high-emission scenarios (RCP 8.5), annual ratings underestimate stress, whereas finer temporal resolutions partially mitigate climate impacts (Figs. 4.13-4.14). This demonstrated that adaptive strategies in which planners consider both expected capacity reductions and the probability of extreme events are more resilient and cost-effective than traditional deterministic planning.

In conclusion, this chapter provides evidence that incorporating climate change into thermal rating estimations is indispensable for the reliable and efficient planning of transmission networks. By bridging climate projections with power system analysis methods, the $qDTR_{RCP}$ framework equips planners with the methods to anticipate and adapt to future variability. While the results emphasise the significant benefits of finer temporal resolutions, they also highlight the persistent challenges posed by extreme events under severe climate trajectories. Future research should therefore focus on combining climate adaptive rating strategies with broader resilience measures, including robust optimisation, probabilistic investment frameworks, and the explicit integration of climate change projections into regulatory and policy processes.

4.7 Limitations

- The uncertainty in climate scenarios is inherent to techno-economic conditions, the political environment, and the differences in the representations of processes and relationships in the evaluation models of different laboratories. Therefore, a comprehensive study of a network must adapt these assumptions to the region being analyzed.
- Since the analysis is based on a single climate model, the results should be interpreted as scenario- and model-dependent and do not capture the full range of uncertainty, particularly with respect to climate extremes, which are known to exhibit substantial inter-model variability.
- Similar to historical databases, it is important to note that the actual heterogeneity of soil composition is often much more complex than can be captured at the 0.25° grid resolution used in the analysis. Therefore, in the absence of backfill, detailed site-specific soil characterization is essential.
- The weather variables obtained from existing climatic databases often suffer from limited spatial and temporal resolution, which can reduce the accuracy of site-specific predictions. Current datasets may not fully capture local variations in wind speed, temperature, or solar irradiation. To address this limitation, future research should explore advanced improve approaches, such as the underground variables used during this approach, combined with machine learning techniques, to generate higher-resolution and more accurate environmental data for these parameters.

Chapter 5

Findings, Discussion and Perspectives

5.1 Conclusions

This final chapter summarizes the main contributions, findings, and implications of the research on the impacts of climate change on power transmission components, emphasizing the role of the qDTR methodology as the core methodology, enabling the assessment of these impacts through probabilistic thermal rating analysis.

It consolidates the results of the methodological contributions on the interaction between climate change, thermal ratings, and network planning, using case studies and responses to the guiding research questions. Also, provides a perspective on both the potential and the limitations of adopting probabilistic thermal ratings in network planning. Furthermore, the analysis emphasizes the role of qDTR in bridging the gap between short-term operational models and long-term expansion strategies, thereby promoting more resilient, cost-effective, and climate influenced network planning.

This chapter is structured in three complementary subsections. The first provides an overview of the methodological contributions, highlighting the key points within each chapter. The second directly addresses the research questions, providing detailed results and outlining the relationships between the proposed approaches. Finally, the chapter describes the underlying limitations and open questions for future research.

5.2 Methodological Contributions

A framework that incorporates long-term thermal ratings into transmission expansion planning through the use of qDTR is introduced. The method was developed to evolve from probabilistic with a fixed threshold ratings toward stochastic, risk-aware models that account for the climatic and temporal variability of component capacities. The main contributions of this research can be summarized as follows:

5.2.0.1 Integrating Thermal Models into qDTR

The implementation of thermal models was an important step toward integrating qDTR into transmission expansion planning. The models implemented in this thesis were extended (in the case of PT) or evaluated using different environmental options (in the case of UGL) to reflect temporal and climatic variability, capturing the hourly and seasonal dynamics that directly affect the performance of transmission components.

The results presented in Section 2.3 demonstrate how these models, when combined with the qDTR methodology, provide a flexible, time-varying representation of component capacities under varying climatic conditions. By analyzing OHL, PT, and UGL at both the component and regional scales, it confirms the technical feasibility and planning value of integrating probabilistic thermal models into long-term expansion frameworks.

Overhead Lines

The assessment of the 225 kV line (from [115] and detailed in Fig. 2.2) highlighted the ability of thermal ratings to capture temporal variability. Annual thresholds based on $qDTR_{year}$ provided a conservative baseline; however, the day/night and *month/hour* methods revealed more dynamic behavior, allowing for a 5.21% and 6.77% increase in average capacity, respectively. Notably, the *month/hour* strategy reduced overload excesses to only 36 events, compared to 185 for the day/night approach, demonstrating that finer temporal resolution reduces instances of underutilization and operational risk. *This confirms that qDTR enables a more efficient balance between line thermal performance and reliability.*

Power Transformers

The thermal model emphasized the dominant role of ambient temperature and the secondary impact of solar radiation. When $qDTR_{yearly}$ was applied as a replacement for traditional STR, overload risks reached almost 10% during extreme summer conditions. By applying $qDTR_{hour}$, these risks were mitigated, while higher capacities were achieved during colder periods. *This validates qDTR's ability to enhance seasonally available capacity*, improving both operational safety and investment planning.

Underground Cables

Soil temperature and moisture were modeled using machine learning techniques, allowing for better estimation and the possibility of future projections, highlighting the importance of this contribution. Integrating these factors into qDTR generated monthly and seasonal ratings that minimized overload risks, taking advantage of favorable soil conditions. However, the soil's inherent thermal inertia limited variability, resulting in smaller relative gains (around 6%) compared to previous transmission system components. This highlights that while qDTR improves UGL utilization, the potential benefits are more modest due to soil physical limitations.

Regional Assessment

At the continental scale detailed in Fig. 2.15, the spatial variability analysis showed that qDTR captures geographic and climatic differences with high resolution: 20% variability for OHL, 31% for PT, and up to 87% for UGL due to soil diversity (Europe average $qDTR_H/qDTR_{H_{\text{Europe}}}$ (%)). Notably, in countries like Greece, average improvements reached 22% for PT and 24% for OHL, while UGL remained below 10%. In contrast, in warmer regions like Spain, summer overload risks worsened, with qDTR below static references by up to 12%. These findings demonstrate the dual role of qDTR as a approach to analyze different regional locations and temporalities with positive results within the component performance, and keeps the risk controlled caused by climate stress.

Overall, the integration of thermal models into qDTR provides a consistent, probabilistic method. The methodology links short-term climatic variability with long-term analysis, quantifying both the opportunities and risks of climate driven capacity changes. Component and regional level results confirm that qDTR improves asset utilization and improves the technical conservatism of traditional ratings. However, the results also highlight limitations that must be acknowledged, such as the steady-state assumption that doesn't include short-term transient dynamics, soil properties homogenized, and the exclusion of climatic loads such as wind and ice, which omit relevant stress factors under extreme conditions.

5.2.1 Integrating qDTR into Network Planning

The implementation of the rating methodology or qDTR for NEP was investigated, comparing different temporal resolutions and incorporating stochastic risk assessment to optimize long-term decision-making. This is evidenced by three principal findings:

Temporal Resolution Selection Analysis

The analysis of *month/hour* versus annual qDTRs revealed that finer ratings provide greater operational flexibility during peak demand periods, especially in winter, enabling larger energy transfers without additional infrastructure investment. Annual ratings offer a conservative but simplified approach, which can delay or avoid investments, but also underutilize transmission capacity. The integration of RES highlights the importance of temporal resolution: hourly qDTR captures the risks of thermal overload during periods of high temperature and high generation, while improving the integration of RES. Particularly in the second case of analysis in the IEEE 24-bus reliability test system in section 3.7.3, where PV production increased by more than 30% at certain nodes due to improved transmission efficiency. This allows operators or planners to strike a practical balance between operational flexibility and planning simplicity by selecting annual or finer resolution ratings.

Network Planning with Risk Assessment

The extended TEP model incorporates probabilistic risk assessment, MCS, and probabilistic densities functions to assess the probability of line overloads. This approach allows planners

to quantify the probability of exceeding thermal limits and prioritize reinforcements based on operational and economic considerations. Applying the traditional STR methodology to all lines results in underutilization, while the risk-aware qDTR model differentiates between lines with zero, moderate, or high risk, allowing for more targeted investment and the deferral of unnecessary reinforcements. Incorporating overload risk allows for specific thermal ratings limits per component, time step, and horizon, reflecting variability in demand, weather, and generation.

Economic and Operational Impacts

The qDTR applied with finer resolution reduces capital expenditures, curtailments, and load shedding penalties, while keeping OPEX and CO_2 costs in minimal increase. The methodology demonstrates that dynamic, risk thermal ratings can improve asset utilization, optimize investment scheduling, and optimize RES integration without compromising grid reliability.

Overall, it is established that quasi-dynamic ratings and risk thermal control are crucial for modern transmission planning. They improve operational flexibility, enable greater RES penetration, defer unnecessary investments, and reduce overall costs, while maintaining safety and reliability under realistic environmental and operating conditions. This approach builds a methodological framework for transmission planning with climate scenarios and approaches to integration with RES, taking the first steps toward building more robust and variable regional socioeconomic scenarios in the future.

5.3 Summary of Research Contributions Across Chapters and Case Studies

5.3.1 Long-Term Thermal Rating Method

5.3.1.1 RQ1: How can thermal ratings of power system components be defined in a manner that effectively incorporates both temporal and spatial variability?

Explored and addressed in **Section 2.3.1** (*Component-Level Analysis*) and **Section 2.3.2** (*Regional-Level Analysis*), where the results highlight both the temporal and spatial patterns of qDTR as follows: 1) At the temporal scale, hourly, daily, monthly, and yearly qDTR estimates provide a systematic characterization of time/weather influence. 2) At the spatial scale, the integration of soil and climate datasets allows the identification of regional heterogeneity (from regions to countries). When extended to the continental level, the analysis reveals significant variability across components: OHL exhibits deviations of around 20%, PT around 31%, and UGL reaching up to 87%. Finally, the results illustrated in Fig. 2.15 and Fig. 2.14, demonstrate the distinct behavioural differences that emerge from applying the qDTR methodology to the three network components, thereby underscoring its capacity to quantify localized and large-scale variability.

5.3.1.2 RQ2: *How can thermal ratings be defined to simultaneously maximize transmission capacity and limit operational risk?*

The probabilistic qDTR methodology extends the deterministic formulation by explicitly incorporating overload threshold into the methodology (see Sections 2.3 and 3.4). Within this framework, acceptable risk levels are defined at 0.17% (equivalent to a maximum of 600 hours over a 40-year horizon) used in the method described in section 3.4 or fix probability thresholds 0.1% for a more conservative reliability margin, applied in method illustrated in section 2.2.2. For instance, in the Danish case study, this capacity assessment enabled substantial capacity gains while remaining within the prescribed risk limits: +17% for OHL, +22% for PT, and +6.8% for UGL, when evaluated against the conservative 0.1% threshold. Seasonal patterns, as shown in Fig. 3.10, demonstrate that integrating regional climate effects through historical weather series markedly enhances qDTR relative to the conventional static yearly rating, with particularly pronounced improvements during winter periods.

Moreover, the extension of the probabilistic framework into stochastic risk assessment further validates these findings. Case studies (Figs. 3.26a and 3.26b) confirm that the probabilistic qDTR not only increases available transfer capacity but also reduces the possibility of thermal overload, impacting the utilization of the line. This outcome reflects the efficiency gains achieved compared with STR, thereby demonstrating the robustness of the probabilistic approach under variable operating and climatic conditions. Finally, the integration of climate projections and line loading effects alters both the overload risk and impacts the transmission capacity across annual and *month/hour* timescales. This dynamic is illustrated in Figures 4.14 and 4.13, where the *month/hour* qDTR, by accounting for seasonal and short-term variability, demonstrates a capacity to mitigate adverse impacts even under the high-emission $RCP_{8.5}$ and $RCP_{4.5}$ scenario.

5.3.2 Integration of Thermal Ratings into Network Planning:

5.3.2.1 RQ3: *How can probabilistic Thermal Ratings be integrated into long-term transmission expansion planning methodology?*

The qDTR can be integrated into long-term transmission expansion planning by: **(a)** Using steady-state thermal models for each transmission power component type (OHL, PT, UGL) to include environmental factors (ambient temperature, wind, solar radiation, soil temperature/humidity) into hourly maximum component thermal limit. See Section 2.2.2 and the thermal model descriptions in Section 2.2.1 (OHL in Section 2.2.1.1, PT in Section 2.2.1.3, UGL ML soil model in Subsection 2.2.1.2). **(b)** Follow by fitting the function 2.19, described in the method in 2.2.2 of allowable ratings from long-term meteorological data (historical and future projection) and select temporal resolution (hourly, monthly, or annual) thermal ratings limits or $qDTR_{frequency}$. **(c)** Finally, by choosing component-specific a fixed-probability thresholds derived from operator conservative selection or deriving one by incorporating a risk stochastic assessed by using MCS risk management (Chapter 3.4) and integrating those bounds into a G&TEP-TEP optimization using scenario-based. Implemented in Sections 2.3, 3.7.1.1, 3.7.2, 3.7.4 and 4.5.2 and showing concrete numerical results in Table 3.3, Table 3.5 and Table 3.9.

5.3.2.2 RQ4: *What are the operational and investment implications of incorporating thermal risk considerations into transmission planning?*

This addresses the operational and investment implications of qDTR integration, drawing on evidence from multiple case studies and modeling results in: **(a)** Operationally, hourly/monthly qDTRs increase available capacity during favorable conditions (night, cold seasons) detailed in (Results in section 3.7.2, Fig. 3.14a–3.14b), reduce renewable curtailment (Tables 3.3, 4.4, 4.6) and load shedding (Tables 3.5, 4.8), and allow more flexible dispatch. **(b)** Deferred or reduced transmission reinforcement (CAPEX savings), qDTRs often reduce the need for near-term transmission reinforcements (deferred CAPEX), shift the spatial layout of investments, and influence the optimal generation mix (reducing some fossil generation build-out) reported up to ∼13% reduction in fossil-based generation investment (Section 3.7.2, Table 3.5). In IEEE-24 TEP results show reduction and deferral of investment in Table 3.6 and Fig. 3.25-3.26, in the regional example, transmission expansion needs decreased by ≈30% (Section 3.7.2, Table 3.5, Section 4.5.2/C , Table 4.8). However, these benefits can be modest at the continental scale but substantial locally, (system cost changes <0.1% in the PyPSA-Eur; see Table 3.3 and discussion in Section 3.7.1.1), but local impacts are meaningfully reduced local CAPEX, curtailment, and load-shedding.

5.3.3 Impact of Climate Change on Transmission Capacity and Economics:

5.3.3.1 RQ5: *What is the impact of climate change on the thermal ratings of individual power system components, considering both temporal variations and regional climatic differences?*

The third contribution of this thesis lies in extending the qDTR methodology into a climate-influenced and risk-management, denoted as $qDTR_{RCP}$. By integrating historical analyses with future climatic projections under multiple RCP scenarios, the results show that climate change systematically alters the thermal ratings of power system components, with both average capacity reductions and greater spatio-temporal variability.

At the system level but in regional analysis, the results (see Section 4.5.1, Table 4.2) show that by 2070 under the high-emission $RCP_{8.5}$ scenario, Europe experiences mean reductions of 1.53% for OHL, 2.1% for PT, and 0.2% for UGL. These averages detailed in Fig. 4.4, however, do not reflect the change between coordinates and temporal extremes; they are only a continental and regional measure of ratings trends. For example, OHL and PT demonstrate significant vulnerability to prolonged heatwaves, with localized rating reductions reaching up to 2.3% in July (Fig. 4.5). In contrast, UGL benefit from the higher thermal inertia of surrounding soils and the use of backfill materials, which effectively dampen short-term (day-to-day) temperature fluctuations. This thermal damping contributes to its relatively stable performance, with projected rating reductions limited to approximately 0.37% in the same high-emission scenario. However, when UGL are directly buried, thermal effects over the summer season can still lead to rating reductions of up to 6% (Table 4.3).

The impact of temporal with different qDTR resolutions is captured in Section 4.5.2 Ta-

ble 4.8. While annual $qDTR_{year}$ ratings reveal moderate improvements compared to static, they underestimate critical short-term stress events. By contrast, *month/hour* $qDTR$ values capture intra-day and seasonal variability, reducing load shedding, while avoiding 100% of planned reinforcements. This underscores that climate change not only shifts mean capacities downward, but also reshapes the distribution of risks in time. Similarly, Figs. 4.13 and 4.14 illustrate how annual ratings understate risk compared to *month/hour* ratings, which capture favourable meteorological windows while safeguarding against overload during critical periods.

5.3.3.2 RQ6: *What is the impact of climate change on network expansion planning, considering its influence on the thermal capacity of electrical system components?*

A second part of the third contribution extends the qDTR methodology into long-term expansion planning by integrating climate change effects on component ratings. Results highlight that climate induced shifts in thermal capacity significantly alter both the scale and timing of investment decisions, highlighting the necessity of climate-influenced planning models. This integration is conducted using two complementary approaches to evaluate the risk of overload. The first applies a predefined fixed-probability threshold ($X_R = 0.1\%$), selected by the planing operator, uniformly across all qDTR values in the network. The second employs a stochastic risk assessment method, in which the lower risk bound is derived probabilistically and analyzed over the planning horizon.

While qDTR ratings are selected based on a fixed-probability threshold to limit overload exposure, climate RCP projections have a marked impact on long-term expansion decisions. In the European case (Fig. 4.7 and Table 4.4), the rising temperatures under $RCP_{8.5}$ lead to increased projected capital requirements and operating costs when static ratings are retained. Conversely, in the IEEE 24-bus test system (Table 4.5), climate influenced qDTR with finer temporal resolution (*month/hour*) enables both localized reinforcement reductions and potential savings up to 8.36% in OPEX and 29.8% in CAPEX under $RCP_{8.5}$.

On the other hand, for the risk management approach through MCS, as reported in Section 4.5.1, Table 4.8, the selection of $qDTR_{year}$ ratings using historical datasets compared to static STR reduces the need for network reinforcements by 68.11% (CAPEX savings), while marginally increasing operating costs (OPEX +0.36%) and system losses (+10.46%). However, climate projections further reshape these outcomes. Under $RCP_{8.5}$, the $qDTR_{year}$ ratings show important increase in planning indicators (CAPEX +100% smf shedding +98.03%), as thermal limits are reached more frequently during extreme conditions. In contrast, the *month/hour* $qDTR$ still maintains robust performance, mitigating load shedding (–31.4%) and avoiding reinforcements, even under high-emission pathways when it is used instead $qDTR_{year}$. This resilience is due to its ability to exploit intraday and seasonal thermal flexibility, thereby offsetting part of the capacity reduction caused by warming.

The spatial (Climate and demand/generation location) heterogeneity of impacts is highlighted in Figs. 4.10–4.12, where Line 22 exhibits constraints under RCP 2.6 and for the yearly case, requiring expansion after 2040, whereas Line 32 shows no congestion throughout the hori-

zon.

In summary, RQ6 is resolved by showing that climate change affects expansion planning in two main ways: (*i*) it reduces the thermal capacity of assets, leading to higher congestion and investment needs in vulnerable corridors, and (*ii*) highlight the role of probabilistic and finer temporal resolution qDTR approaches, which defer costly reinforcements and enhance system resilience. Thus, future network planning requires integrating climate-influenced dynamic thermal ratings into both operational and investment decision-making.

5.4 Broader Implications and Future Directions

The findings of this research highlight the contributions made in specific case studies and could have broader implications for both academia and industry. In particular, the framework developed here can be extended to address additional challenges, such as heterogeneous soil conditions, other power system component as thermal generation, and asset degradation, while broadening the scope of optimization from transmission expansion alone to integrated generation and transmission planning. To this end, the following points are proposed:

- Regulatory frameworks should be adapted to the analyzed network to support probabilistic planning approaches. This includes defining acceptable overload probabilities, penalties, the integration of new generation technologies, and explicitly recognizing asset degradation metrics into the optimization formulation as variable.
- Future applications of qDTR should incorporate updated climate projections for the years 2025–2026, revising the factors that influence current climate models. This includes future scenarios derived from selected CMIP6 global climate models [183]. In addition: *(i)* more detailed soil surveys should be integrated to capture heterogeneity in thermal resistivity and local humidity, thereby enhancing UGL modeling and supporting more accurate long-term planning; *(ii)* the probabilistic method could be extended to assess the influence strength of loads such as wind and ice on OHL assets.
- While representative day approaches mitigate computational costs, future work should explore advanced techniques (e.g., machine learning-based scenario reduction) to further improve scalability. This is especially relevant when jointly optimizing transmission and generation expansion, considering both thermal ratings and dynamic loss calculations within the optimization.
- Another important limitation concerns the fact that the model described in Section 3.3.3 does not include losses as part of the objective function and is based on a simplified DC-OPF formulation. This could influence the results towards underestimated efficiency gains. Incorporating an AC-OPF formulation in future work could allow for a more realistic treatment of losses, reactive power, and voltage constraints, which is particularly valuable when extending the framework to distribution networks.
- Linking short-term operational planning (DTR) with long-term planning (qDTR) offers opportunities for unified frameworks that optimize both real-time operations and future investments. qDTR can serve as a gauge for potential bottlenecks and limit the expansion of DTR technology over those critical lines, thus focusing investments and further expanding the advantages of dynamic ratings technologies.
- Extending the methodology to regions with limited meteorological, soil, and network data requires the development of robust models and validation techniques. Machine learning and related approaches, similar to the soil moisture and temperature explored in this thesis,

could help improve the accuracy of environmental variables such as wind, temperature, and enhance the spatio-temporal resolution.

- Beyond the MCS, future research should test constraint-based stochastic methods, such as chance-constrained formulations, robust optimization, among others. These approaches may reduce computational burden while maintaining a rigorous treatment of uncertainty in thermal ratings, climate inputs, and system operations.

Appendix A

Annex A : Mathematical Formulation of Thermal Models

A.1 Overhead Lines

The numerical model used to calculate the thermal rating for a given maximum conductor temperature under steady-state conditions, as described in [29], is adopted in this thesis to determine the component ampacity.The following is a general overview of the thermal models used, however a more detailed explanation of its implementation can be found in [29].

A.1.1 Parameters

- w_s = Wind speed (m/s)
- θ_a = Ambient air temperature (°C)
- $T_a = \theta_a + 273.15$ = Ambient air temperature (K)
- θ_c = Conductor surface temperature (°C)
- $T_c = \theta_c + 273.15$ = Conductor surface temperature (K)
- H_r = Global solar radiation (W/m^2)
- h_{alt} = Altitude above sea level (m)
- g = Gravitational acceleration (9.807 m/s^2)
- α_s = Solar absorptance of conductor (-)
- ε = Emissivity of conductor (-)
- D_c = Overall conductor diameter (m)
- R_{ref} = DC resistance at reference temperature θ_{ref} (Ω/m)

- α = Temperature coefficient of resistance (1/°C)
- λ_f = Thermal conductivity of air (W/m · K)
- μ_f = Dynamic viscosity of air (Pa · s)
- ρ_f = Density of air (kg/m^3)
- c_p = Specific heat capacity of air (J/kg · K)

A.1.2 Heat Solar Power Gain

$$Q_s = \alpha_s \, H_r \, D_c \tag{A.1}$$

A.1.3 Radiative Power Loss

$$Q_r = \pi \, D_c \, \varepsilon \, \sigma_B \left(T_c^4 - T_a^4 \right) \tag{A.2}$$

where $\sigma_B = 5.670374419 \times 10^{-8}$ W · m^{-2} · K^{-4} is the Stefan–Boltzmann constant.

A.1.4 Convective Power Loss

Convective cooling power Q_c is determined using the Nusselt number (Nu), Reynolds number (Re), Grashof number (Gr), Prandtl number (Pr), and thermal conductivity of air λ_f:

$$Q_c = f(T_c, T_a, g, D_c, H, d, W_s) \tag{A.3}$$

A.1.4.1 Reynolds Number

$$Re = \frac{w_s \cdot D_c}{V_f} \tag{A.4}$$

A.1.4.2 Grashof Number

$$Gr = \frac{(0.001 \cdot D_c)^3 (\theta_s - \Theta_a) g}{(\theta_f + 273.15) V_f^2} \tag{A.5}$$

A.1.4.3 Prandtl Number

$$Pr = \frac{c_p \mu_f}{\lambda_f} \tag{A.6}$$

where:

$$\theta_f = \frac{\theta_c + T_a}{2} \tag{A.7}$$

$$\lambda_f = 2.368 \times 10^{-2} + 7.23 \times 10^{-5}\theta_f - 2.763 \times 10^{-8}\theta_f^2 \tag{A.8}$$

$$\mu_f = \left(17.239 + 4.635 \times 10^{-2}\theta_f - 2.03 \times 10^{-5}\theta_f^2\right) \times 10^{-6} \tag{A.9}$$

$$\rho_f = \frac{1.293 - 1.525 \times 10^{-4} h_{\text{alt}} + 6.379 \times 10^{-9} h_{\text{alt}}^2}{1 + 0.00367\theta_f} \tag{A.10}$$

$$\nu_f = \frac{\mu_f}{\rho_f} \tag{A.11}$$

A.1.4.4 Convective Cooling Calculation

$$Q_c = \pi \lambda_f Nu(\theta_c - T_a) \tag{A.12}$$

where Nu_h is obtained based on empirical formulas.

A.1.5 DC Current Calculation

$$I_{\text{dc}} = \sqrt{\frac{Q_c + Q_r - Q_s}{R_{\text{ref}}\left[1 + \alpha(\theta_c - \theta_{\text{ref}})\right]}} \tag{A.13}$$

A.2 Power Transformers

The thermal rating under steady-state conditions is determined using a numerical model adapted from the methodology presented in [128]. In this thesis, the model has been modified to better reflect transformer-specific thermal environmental influence. These adjustments are explicitly detailed in the corresponding mathematical formulations.

A.2.1 Parameters

- θ = Ambient temperature (°C)
- H_r = Solar radiation (W/m²)
- $\Delta\theta_{or}$ = Top-oil temperature rise at rated load (°C)
- $\Delta\theta_{hr}$ = Hot-spot temperature rise over top-oil (°C)
- x, y = Empirical exponents
- H_s = Hot spot temperature rise (C°)
- P_{base} = Base power rating (MVA)
- Vol_L, Vol_h = Transformer voltage levels (kV)

- R_{ll} = Winding loss ratio
- P_{ll} = Load losses (MW)
- P_{nl} = No-load losses (MW)
- A, c = Transformer Area (m^2) and Temperature correction factor
- $install$ = Installation type (Indoor/Outdoor), this to include or not include solar irradiation

A.2.2 Power Loss Calculations

If P_{ll} and P_{nl} are not provided, they are estimated using empirical formulas, from [127]:

$$P_W = 20.454P_{base}^2 - 1682.2P_{base} + 227954 \tag{A.14}$$

$$P_E = 33454\ln(P_{base}) - 120431 \tag{A.15}$$

$$P_{ll} = \frac{P_W + P_E}{10^3} \tag{A.16}$$

$$P_{nl} = \frac{1.1896P_{base}^2 + 541.22P_{base} - 3019.4}{10^3} \tag{A.17}$$

A.2.3 Temperature Correction Factors [127]

Reference temperature:

$$\theta_{ref} = 75°\text{C} \tag{A.18}$$

Load and no-load loss correction factors:

$$f_{wp} = \frac{234.5 + \theta}{234.5 + \theta_{ref}} \tag{A.19}$$

$$f_{ps} = \frac{234.5 + \theta_{ref}}{234.5 + \theta} \tag{A.20}$$

Adjusted power losses:

$$P_{LL} = P_{ll} f_{wp} \tag{A.21}$$

$$P_{NL} = P_{nl} f_{ps} \tag{A.22}$$

A.2.4 Newton's Method for Transformer Loading Factor

The method verify that the Newton residual $f(K)$ correctly enforces the hot-spot temperature limit. Starting from the thermal model

$$\left(\frac{1 + K^y R_{ll}}{1 + R_{ll}} + \frac{H_r \text{Ac}}{P_{LL} + P_{NL}}\right)^y \cdot \Delta\theta_{\text{or}} = \Delta\theta_h \quad \text{where } \theta_h = \theta + \Delta\theta_{or} + \Delta\theta_{hr} \tag{A.23}$$

the rating problem becomes solving

$$f(K) = \theta_a + K^y \Delta\theta_{or} + \Delta\theta_{hr}(K) - \theta_{h,\max}$$

$$K_{n+1} = K_n - \frac{f(K_n)}{\frac{df}{dK}(K_n)} \quad with \quad f\left(K_n\right) = \theta_h\left(K_n\right) - \theta_{h,lim} \tag{A.24}$$

- If $|f(K)| \leq 10^{-3}$, return $P_T = P_{\text{base}} \cdot K$ W.

A.2.5 Transformer Rated Power and Current

$$P_T = P_{base} \cdot K \tag{A.25}$$

$$I_{rated} = \frac{P_T}{\sqrt{3} \cdot Vol_h} \tag{A.26}$$

A.3 Underground Lines

The thermal rating of components under steady-state conditions is assessed in this thesis using a numerical approach aligned with the IEC methodology for UGL systems. This model estimates ampacity based on the maximum allowable conductor temperature, following the formulations outlined in [51] and [27]. Further details regarding its available in [51].

A.3.1 Parameters

- θ_s = Soil Ambient temperature (°C).
- $Backfill$ = Type of backfill material.
- A_s = Sheath area (m^2).
- K_s, K_p = Skin and proximity effect factor constants.
- α_{20} = Temperature coefficient.
- θ_x = Maximum allowable temperature.
- T_1, T_2, T_3, T_4 = Thermal resistances
- ρ_s = Soil thermal resistivity ($K \cdot m/W$).
- S_g = Cable spacing factor.
- C_u = Capacitance for a circular conductor (F/m) .
- U_0 = Voltage to earth (V).
- tan_d = loss tangent.

- R_{ugl} = AC resistance of conductor. (Ω/m)
- R_{20} = DC resistance at 20°C (Ω/m).
- W_d = Dielectric losses (W/m).
- I_{ac} = AC current (A).
- L_d = Cable Installation Depth (m).
- S_1 = Distance between Axes (m).

A.3.2 Thermal Resistance Calculation

This model estimates λ_s by limiting it between the dry and saturated thermal conductivities (λ_{dry}, λ_{sat}) and using the Kersten number K_e, which captures the nonlinear effects of soil moisture:

$$\lambda_s = (\lambda_{sat} - \lambda_{dry})K_e + \lambda_{dry}, \quad \forall i \tag{A.27}$$

$$K_e = \exp\left(\alpha_s - \psi_i^{-\beta_s}\right) \tag{A.28}$$

In the above equations:

- ψ_i: Volumetric water content
- λ_{sat}, λ_{dry}: Saturated and dry thermal conductivity, respectively
- K_e: Kersten coefficient capturing moisture influence on thermal transfer

The shape parameters α_s and β_s govern the sensitivity of K_e to moisture content and are computed from the soil's particle size distribution and organic content:

$$\alpha_s = a_1 S_{\text{Sand}_\%} + a_2 S_{\text{Silt}_\%} + a_3 S_{\text{Org}_\%} + a_4 \tag{A.29}$$

$$\beta_s = b_1 S_{\text{Clay}_\%} + b_2 S_{\text{Org}_\%} + b_3 \tag{A.30}$$

The coefficients for these empirical relationships are listed in Table A.1:

a_1	a_2	a_3	a_4	b_1	b_2	b_3
0.493	0.860	0.014	0.778	0.736	0.006	0.222

Table A.1: Empirical coefficients for estimating thermal conductivity of soil

$$\rho_s = \frac{1}{\lambda_s} \tag{A.31}$$

A.3.3 Thermal Model Equations

$$u_3 = \frac{L_d^2}{S_g} \tag{A.32}$$

$$T_4 = \frac{\rho_s}{2\pi}\left[\ln\left(u_{t3} + \sqrt{u_{t3}^2 - 1}\right) + \ln\left(1 + \left(\frac{2L_d}{S_1/10^3}\right)^2\right)\right] \tag{A.33}$$

For backfill conditions:

$$G_b = \ln\left(u_b + \sqrt{u_b^2 - 1}\right) \tag{A.34}$$

Thermal resistance including backfill:

$$T_{4bf} = N_b \frac{(\rho_s - \rho_b)}{2\pi} G_b \tag{A.35}$$

where N_b is the number of cables in backfill.

A.3.4 Electrical Resistance Calculation

$$R_{ugl} = R_{20}\left[1 + \alpha_{20}(\theta_c - 20)\right](1 + y_s + y_p) \tag{A.36}$$

A.3.5 Dielectric Losses

$$W_d = w\ C_u\, U_0^2\ \tan\delta \tag{A.37}$$

A.3.6 Current Calculation Using IEC 60287

$$I_{ac} = \sqrt{\frac{(\theta_x - \theta_s - W_d(0.5T_1 + n(T_2 + T_3 + v_p T_4)) + (v_p - 1)\Delta\theta_x)}{(R_{ugl}T_1 + nR_{ugl}(1 + \lambda_1)T_2 + nR_{ugl}(1 + \lambda_1 + \lambda_2)(T_3 + v_p T_4))}} \tag{A.38}$$

where λ_1, λ_2 are sheath loss factors.

Appendix B

Annex B : Power System Components Description

B.1 Power System Components Parameters

The physical and electrical parameters of the power system components used in this are presented below. These descriptions are made according to the journal used and section. It should be noted that the additional components not explicitly described in this document are mainly adopted from the reference state used within the standard.

B.1.1 Paper B

These parameters were employed during the analyses carried out in the sections.

Designation	Former Code	Cross Section (mm^2)	Number of Strands	Diameter (mm)	DC Resistance (Ω/km)	Current Rating (A)
243-AL1/39-ST1A	240/40	282.5	26	21.8	0.1188	645

Table B.1: Overhead Line Characteristic Data

Note: To model the system used in Section 3.7.1.1, the distribution of wires according to the voltage is followed in accordance with [28].

Cross section (mm^2)	Current Rating (A)	Physical Properties					
	90°C	Diameter of conductor (mm)	Nominal insulation thickness (mm)	Diameter over insulation (mm)	Metallic screen cross-section (mm^2)	Diameter over screen (mm)	Outer diameter (mm)
800RM	870	33.0	10.0	54.8	370	61.3	69.0

Table B.2: Underground Cable Characteristic Data [184]

Rated power [MVA]	Cooling Type	Voltage ratio [kV]	Total losses (No Load) [kW]	Total losses (Load) [kW]	Color
180	ONAN	500/115	123	211	White

Table B.3: Power Transformer Characteristic Data [185]

B.1.2 Paper A

Cross section (mm^2)		Physical Parameters - 245kV					
	Current Rating (A) 90°C	Diameter of conductor (mm)	Nominal insulation thickness (mm)	Diameter over insulation (mm)	Metallic screen cross-section (mm^2)	Diameter over screen (mm)	Outer diameter (mm)
800RM	855	33.0	22.0	79.6	530	86.9	96

Table B.4: Underground Cable Characteristic Data Cable 1 [184]

Cross section (mm^2)		Physical Parameters - 550 kV					
	Current Rating (A) 90°C	Diameter of conductor (mm)	Nominal insulation thickness (mm)	Thickness of Insulation Screen (mm)	Cross-Sectional Area (mm^2)	Thickness of Outer Sheath (mm)	Outer diameter (mm)
N2XS(FL)1200	870	43.5	31	1.2	3.2	4.9	140

Table B.5: Underground Cable Characteristic Data Cable 2 [186]

B.2 Demand Projections by Trajectory [180]

Trajectory	**2019**	**2025**	**2030**	**2035**	**2040**	**2045**	**2050**
N2	475.2	472.4	508.3	535.2	567.2	608.8	645.0
M2	454.9	487.1	537.6	580.2	631.4	631.4	751.7
N3	475.2	458.2	479.3	491.6	508.7	535.3	554.0

Table B.6: Electricity demand projections by trajectory (in TWh), used in the case studies of sections 3.7.4 and 4.5.2.

B.3 Installed capacity projections by Trajectory [180]

Trajectory	**2019**	**2030**	**2040**	**2050**	**2060**	**Filière**	**Unité**
M2	17	33	49	59	71	Éolien terrestre	GW
	9	35	127	214	262	Photovoltaïque	GW
N2	17	33	41	52	53	Éolien terrestre	GW
	9.4	35	61	90	93	Photovoltaïque	GW
N3	17	33	39	43	43	Éolien terrestre	GW
	9	35	53	70	70	Photovoltaïque	GW

Table B.7: Installed capacity projections by trajectory and technology (in GW), used in the case studies of sections 3.7.4 and 4.5.2

B.4 Published Papers: Paper A

Long Term Climate-Driven Underground Cable Thermal Ratings for Network Planning

Sergio Daniel Montana Salas, Andrea Michiorri

Long Term Climate-Driven Underground Cable Thermal Ratings for Network Planning

Montana-Salas Sergio[a], Michiorri Andrea[a]

[a]*PERSEE - Mines Paris - PSL, Centre for processes, Sophia Antipolis, 06160, Alpes-Maritimes, France*

Abstract

The capacity of underground cables is influenced by their thermal balance with the environment, with a strong dependence on soil temperature and thermal resistivity. This study estimates the long-term effect of climate conditions and soil dynamics on underground cable capacity, thanks to the use of: climate models, machine learning, and soil and cable dynamic models. In particular, two models are trained to estimate soil temperature and moisture at a depth between 0.8 and 2 meters, completing the information present in existing datasets. The approach is applied to different Reference Pathways Scenarios for the region of France, and results show an improvement in ratings in the region of 9.3% compared with static seasonal ratings, with a further exploitable variation in the order of 10% between the winter and summer seasons.

Keywords:

Underground Power Transmission Lines, Climate Change, Dynamic Thermal Rating, Soil, Thermal Factors.

1. Introduction

The sustained growth of renewable generation plants (RES) and the rising electricity demand, pose a challenge for transmission network expansion. For this, congestion events in the network are expected to become more severe, requiring enhanced transmission capacity. Furthermore, climate change can severely affect the transmission capacity of Underground Cables (UGC), as it relies on soil's ability to dissipate joule losses. For instance, in [1], estimates potential reductions up to 50%. Nonetheless, this reduction is not accurately reflected in traditional UGC static or seasonal capacity estimations used by energy utilities.

In this context, a method for estimating long-term thermal capacity limits, influenced by soil temperature variations, plays a crucial role. To address the effects of rising temperatures and optimize the current-carrying capacity of cables, the Dynamic Thermal Rating (DTR) methodology is actively proposed as a solution. Due to its advantages, the DTR has been studied for integration in power system applications for networks configured with UGC, such as the day-ahead [2, 3], RES integration [4] in the distribution network, real-time operation [5], long-term techno-economic assessments [6] and medium-term distribution network expansion planning [7]. However, despite the development of real-time and medium-term models combining data with observations in the last decade, there is a notable gap in long-term analysis using climate projections and for burial depths of 1 to 2 meters.

As temperature is the primary variable in DTR, weather and mechanical characteristics can be determined using two methods: i) Real-time measurement equipment, known as direct measurement. Nowadays, this is usually performed for brand new circuits with an embedded optical fiber as described in [8], offering excellent accuracy and precision, but with barriers such as capital costs and non-applicability to already installed networks. ii) A thermal mathematical model based on information on meteorological conditions, combined with a non-steady-state thermal model using historical data or numerical weather predictions [9]. This method increases capacity compared to static thermal power but reduces the risk of overloading.

Estimating the DTR ratio [10] is fundamental to transmission capacity calculations, driven by energy conservation and heat transfer mechanisms [11]. Poor heat dissipation in directly buried UGC presents challenges for assessing thermal performance and efficiency. A crucial parameter influencing the rating within the soil's thermal properties is the soil thermal resistivity, which is highly correlated with the moisture content [12, 13]. This effect becomes particularly significant when its impact is translated into temperature. In [1], a 50% reduction in the rating is observed when the soil thermal resistivity is three times greater and the ambient temperature increases by 5 ^{o}C. This reinforces its high dependence and the correlation between the temperature and moisture of the surrounding soil, among other factors, such as laying depth and physical properties [14].

The utilization of in-situ sensors for measuring soil moisture and temperature at various spatial scales, as discussed in [15], presents an opportunity to comprehend the interrelationship and devise a solution to estimate the intricate interaction in exchange processes between land-atmosphere interactions and soil. Consequently, considerable research efforts have been directed towards this objective over the past few decades. Noteworthy contributions include satellite observations [16], microwave remote sensing, and physically-based models [17], providing spatiotemporal estimations. However, these methods may experience deviations in performance due to complex topography and transient climate conditions [18, 16]. On the other hand, Machine-Learning models (ML) employing remote sensing data have been applied in various research studies [18, 19, 20] with a broad spectrum of data integration. These models, primarily influenced by climatic conditions and soil taxonomy, including texture and soil type, present a novel alternative that challenges conventional processes. By "learning" the intricate interdependencies between meteorological variables and soil dynamics, they redefine the approach to understanding and modelling these intricate connections.

A limited number of strategies have been developed, incorporating ML in DTR for UGC [3, 21]. As outlined in [22], an approach that involves the development of a day-ahead DTR forecast relies on a Support Vector Regression (SVR) method for soil temperature. However, the physical-statistical model for predicting thermal conductivity, applying a regression model for soil-specific heat, exhibits reduced simulation accuracy across diverse soil types, limiting its general applicability. To analyze the thermal conductivity and cover a wide range of soil textures, bulk densities, temperatures, and moisture levels, several estimation models have been proposed in the last decades [23, 24]. In [25], a new empirical model for estimating soil thermal conductivity was developed. This involved comprehensively evaluating several approaches, influenced by many factors such as organic matter, soil texture, and particle composition. Resulting in a performance of R^2 of 0.98, the method successfully increased simulation accuracy for ten soil types.

As temperature and soil moisture conditions are becoming increasingly common variables in planning and managing the capacity of UGC [10], establishing projec-

tions related to the energy transition is a critical step to quantify and understand the impacts associated with climate change. A fundamental problem was encountered when applying a weather-driven thermal model in the future: the climatic projections used did not contain information about deep soil moisture but only at the first 10cm layer below the surface. Furthermore, deep soil temperature appeared too smooth relative to observations, preventing the capture of the extreme conditions that drive static ratings. To tackle the issues outlined above, the contributions of this paper are:

a) Apply a probabilistic quasi-dynamic Thermal Rating method aiming to exploit transmission capacity efficiently and minimize the risk of overloading as part of long-term power system planning.

b) Develop machine learning models for better estimation of soil thermal properties at cable burial depths, applicable also with future climatic scenarios.

c) Assess trends and possible impacts of climate change on UGC in the long-term horizon, both in terms of pure transmission capacity and costs in transmission expansion planning.

The paper is organized as follows: Section 2 illustrates the machine learning process, thermal model, and methodology. The results are described in Section 3, and conclusions are drawn in Section 5.

2. Methodology

2.1. Overview

We develop a model to quantify the long-term effect of climate conditions on UGC capacity, summarized in the block diagram in Fig. 1. First, supervised ML models are trained using historical in-situ measurements [26, 27] and meteorological information [28] in module **2.2**. Secondly, historical meteorological time series data [28] are collected in the module **2.3**, as projections [29] and resulting from machine learning. These data are fed to components' thermal models to calculate the time series for the transmission capacity in modules **2.5**,**2.4**. Subsequently, a **2.6**, a

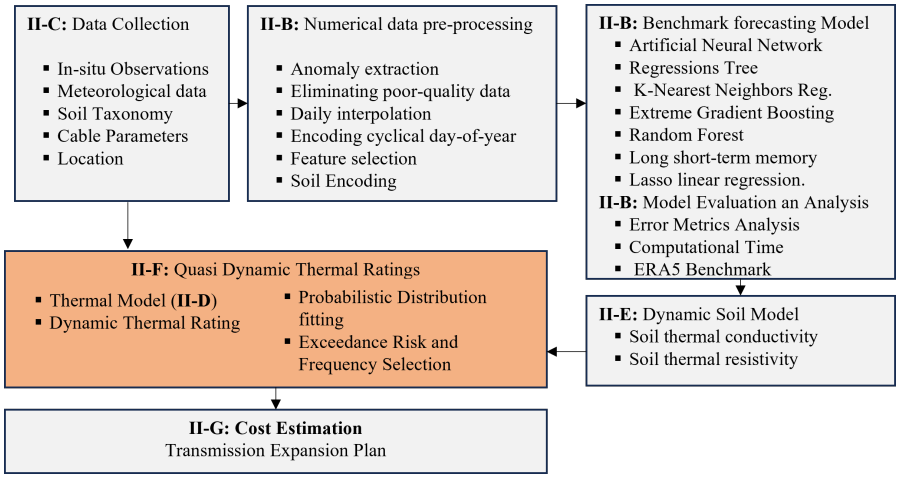

Figure 1: Block scheme of the approach proposed for calculating quasi Dynamic Thermal Ratings in UGC.

probabilistic approach integrated into DTR is proposed [30] by fitting a probability distribution to the lower tail of the simulations for each month/hour combination and selecting an accepted level of risk tolerance to thermal overload (0.1% in this case). The final module describes the transmission network expansion planning model applied as a method of analysis and application of the proposed approach **2.7**.

2.2. Machine Learning Model

This module aims to model soil moisture $(\hat{\psi})$ and temperature $(\hat{\Theta})$ data at 0.25°, with a daily resolution in a depth range between 0.8 and 2 meters based on hourly-recorded input data. The pre-selection of the features was performed under a combination of time series of meteorological data, soil properties, and observations, mainly based on bibliographic analysis [18, 19, 20]. For this task, We rely on the dataset described in section 2.3 relative to the whole European area.

Due to the problem's complexity, we implemented the following preprocessing and numerical transforms: a) Anomaly extraction. b) Elimination of poor-quality data [31] c) Exclusion of stations with less than three months of annual information d) Daily interpolation e) Encoding of cyclical Day of the Year (t_c). f) Minimum and maximum scaling. g) Feature selection conducted to achieve the highest prediction

accuracy. h) Finally, to ensure broad operability, each analyzed soil was encoded (S_{code}) by a soil texture classification according to [32] and a texture represented in Table 1.

Table 1: Revised USDA Soil Texture Classification, indicating soil codes used in this study

Texture Class	Sand %	Silt %	Clay %	Code
Sand (S)	> 85	0-15	0-15	5
Loamy Sand (LS)	70-85	0-20	0-15	5
Sandy Loam (SL)	43-70	7-20	0-27	4
Loam (L)	20-40	40-60	7-27	4
Silt Loam (SiL)	0-20	≥ 70	0-27	4
Silt (Si)	0-10	80-90	0-10	4
Sandy Clay Loam (SCL)	20-35	28-50	27-40	3
Clay Loam (CL)	20-35	28-50	27-40	3
Silty Clay Loam (SCLa)	0-20	50-70	27-40	3
Sandy Clay (SC)	0-20	0-28	40-60	2
Silty Clay (SCla)	0-10	50-70	40-60	2
Clay (C)	0-20	0-20	≥ 60	1

In the initial phase, an evaluation of various machine-learning techniques was carried out in order to select the most appropriate for our method. This assessment focused on key error measurement indicators such as Root Mean Squared Error (RMSE) and Mean Absolute Error (MAE), with particular emphasis on the computation time of the predictions. As described in the previous section, a reduction in the UGC rating is associated with lower moisture and higher temperature. Thus, our analysis focuses on the heightened risk of overloading so that the metrics described in the equations are evaluated in the lower 20th quantile for moisture and the 80th quantile for temperature.

The importance of the calculation time is due to the expected regional application of the continental-scale model, highlighting the need for accuracy and efficiency. The techniques evaluated include Artificial Neural Network (ANN), Regressions Tree (RT), K-Nearest Neighbors (k-NN), Extreme Gradient Boosting (XgBoost) [33], Random Forest (RF), Long short-term memory (LSTM), and Lasso linear regression [34].

Considering the soil-inertia [18], this model is trained with a five-day rolling window for lagged observations. This lag was determined through time series analysis

using a partial auto-correlation function (PACF). The dataset is divided by station and soil types to train and test the models. The training set is equivalent to 70% of the ful dataset, with 10% reserved for tuning the model hyper-parameters using techniques from [35]. The remaining 30% serves as a validation set to test the model. To avoid overfitting, N-fold cross-validation is performed by applying the metrics described. Thus, our analysis focuses on the heightened risk of overloading so that the metrics described in the equations are evaluated in the lower 20th quantile for moisture and the 80th quantile for temperature and denoted as dividing the test dataset into five folds, ensuring all soil types are present in each fold, thus guaranteeing homogeneity of selection.

2.3. Datasets

The impact on UGC capacity is quantified by processing data from soil properties and meteorological variables for the region of interest, as outlined in Table 2.

Table 2: Datasets and Parameters

Variable	Units	Process	Source	
Meteorological				
Temp. Air at 2 m (Θ_a)	K	2.2	a,b	Dynamic
Total precipitation (P_t)	mm	2.2	a,b	Dynamic
Net surface solar radiation (S_r)	Jm^{-2}	2.2	a,b	Dynamic
u - v - wind at 10 m	ms^{-1}	2.2	a,b	Dynamic
Soil Proprieties				
Silt ($S_{silt_{\%}}$)	%	2.5,2.2	c	Static
Sand ($S_{sand_{\%}}$)	%	2.5,2.2	c	Static
Clay ($S_{clay_{\%}}$)	%	2.5,2.2	c	Static
Organic ($S_{org_{\%}}$)	%	2.5	c	Static
Texture Composition (S_{text})	-	2.2	c	Static
Bulk (S_{bulk})	kgm^{-3}	2.5,2.2	c	Static
Soil Measurements				
Temperature (Θ)	K	2.2,2.6	d	Dynamic
Moisture (ψ)	%	2.2,2.5	d	Dynamic

Considering 100year horizons, ECMWF ERA5 and Copernicus climate change service (C3S) datasets provide the historical reanalysis[(a)] [28] and climate projections with a Representative Concentration Pathway (RCP) of 2.6, 4.5, and 8.5[(b)] [29]. The high-grid resolution of 0.25° datasets provides a time series from Jan-

uary 01, 1970, to December 31, 2072. However, climatic projections are linearly interpolated with a time resolution of one day to match the frequency of the in-situ data.

Observing temporal variations in the soil is crucial for estimating soil moisture and temperature behaviour and assessing sensitivity to climate change and soil taxonomic properties. This mandates the availability of soil moisture datasets that exhibit superior quality, extended duration, continuity, and consistency. In this study, in situ soil moisture[(d)], taxonomy[(c,d)], and temperature measurements[(d)] sourced from the International Soil Moisture Network [26] and [27] are employed. The dataset involves data from 52 networks, spanning 2006 to 2022, covering depths from 0.05 to 120 m.

2.4. Steady-state Thermal model with Moisture Migration

After gathering the information necessary to understand the ability of the surrounding soil to dissipate heat, this paper estimates the current-carrying capability of an operational buried UGC with the use of the thermal model for steady-state ratings outlined in IEC standard 60287 [12]. This thermal capacity is influenced by the interaction between the medium in which the cables are installed and several parameters, as outlined in (1). Readers can refer to [12, 1] for a more comprehensive explanation. However, to facilitate the reading of this document, the key aspects of the models employed are summarized below.

$$I_{DTR_i} = I(\Theta_i, \psi_i, \text{cable construction, installation}) \tag{1}$$

According to [12], the current-carrying capability of a cable, with the influence of a dry area formation, is calculated per day (i) as follows:

$$\begin{aligned} I_i &= \sqrt{\frac{\Delta\Theta_i - B + (v-1)\Delta\Theta_x}{R_{\mathrm{i}}T1 + nR_i(1+\lambda_1)T_2 + C}} \quad \forall i = 1..H \\ B &= W_d \left[\tfrac{1}{2}T_1 + n\left(T_2 + T_{3\mathrm{i}} + v_i T_{4_\mathrm{i}}\right)\right] \\ C &= nR_i\left(1 + \lambda_1 + \lambda_2\right)\left(T_2 + v_i T_{4_i}\right) \end{aligned} \tag{2}$$

The above equation focuses on the critical temperature of the boundary between the wet and dry zones $\Delta\Theta_x$ and the ratio between the thermal resistivity of the dry and wet zones of the backfill soil v_i. With high dependence on variable factors such as ambient temperature, moisture, and precipitation, the other parameters such as λ_{1-2}, C, R, T_{1-3}, W_d obey the cable construction. These parameters can be determined and calculated according to [12, 1], guides and suggestions. Where the thermal resistance T_4 of the surrounding medium for a single core cable, lay horizontally, is defined as :

$$T_{4_i} = \frac{\rho_{s_i}}{2\pi}\left\{\ln\left(u+\sqrt{u^2-1}\right)+\ln\left(1+\left(\frac{2L}{S_1}\right)^2\right)\right\} \tag{3}$$

Where ρ_{s_i} is the thermal resistivity of soil, S_1 is the distance between cables axes, u is the ratio of the burial depth L, and the external diameter of the cable D_e. Notably, equation (3) can be adapted for three-core cables and installations involving backfill, as discussed [12]. Therefore, it is crucial to calculate ρ_{s_i}, and the analysis must also incorporate considerations based on the cable environment. This relationship holds true for uniform soils, where thermal properties remain constant at each coordinate.

2.5. Dynamic Soil Model

Modelling soil moisture and temperature dynamics is an area that has been developed over the last century. Differential equations considering various factors have been presented, as described in the previous section. A one-dimensional representation of heat flow in a vertical direction (x) is outlined in (4), in which the thermal diffusivity α_s is characterized as a direct relationship between the thermal conductivity (λ_s) and the inverse of the soil density and specific heat capacity.

Our approach implements the dynamics model addressing the physical properties and processes within soils using machine learning, as described in Section 2. However, a mathematical model correlating the soil's hydraulic-physical properties with thermal conductivity (λ_s) needs to be established to determine the thermal resistivity of each soil analyzed.

$$\frac{\partial \Theta}{\partial t} = \alpha_s \frac{\partial^2 \Theta}{\partial x^2} \tag{4}$$

To address this, the estimation of soil thermal conductivity, which is the inverse of ρ_s, is conducted following the interrelation proposed in [36, 25]. This involves unsaturated soils and incorporates parameters such as λ_{dry}, λ_{sat}, and the Kersten coefficient K_e.

$$\lambda_{s_i} = (\lambda_{sat_i} - \lambda_{dry_i}) K_{e_i} + \lambda_{dry_i} \quad \forall i = 1..H \tag{5}$$

$$K_{e_i} = \exp\left(\alpha - \psi_i^{-\beta}\right) \tag{6}$$

$$\alpha = a_1 S_{\text{Sand}_\%} + a_2 S_{\text{Silt}_\%} + a_3 S_{\text{org}_\%} + a_4 \tag{7}$$

$$\beta = b_1 S_{\text{Clay}_\%} + b_2 S_{\text{org}_\%} + b_3 \tag{8}$$

Here, α and β represent the shape factors of the volumetric water content (ψ) and thermal conductivity curve, respectively. These factors exhibit linear relationships with particle size distribution ($S_\%$) and organic matter content ($S_{org_\%}$), as defined below. Where the weighting factors of the physical parameters of the model are as follows

Table 3: Weighting factors for the empirical model of soil thermal conductivity

a_1	a_2	a_3	a_4	b_1	b_2	b_3
0.493	0.86	0.014	0.778	0.736	0.006	0.222

At this point, each soil's thermal conductivity is calculated using the features described in Table 2. This, in turn, allows us to estimate the v ratio and the thermal resistivity of the soil ρ_s per day.

2.6. Quasi Dynamic Thermal Ratings

A key challenge for system operators in implementing DTR systems is the variability of thermal ratings. To address this, the quasi-dynamic Thermal Ratings (qDTR) are applied to calculate the ratings for a long-term horizon, as proposed in [30]. After collecting the time series and parameters described in Sections 2.3 and 2.5, the DTR is calculated using (2). These time series are fitted with a probability

distribution described in [37], in the lower tail of the simulations for each month/day combination. An accepted tolerance level to the risk of thermal overload (0.1% in this case) is then selected.

This method is described in [30] and reported here and in Fig. 2 to facilitate the reader of this paper. First, the thermal model calculates the real time DTR over a one-year period. The Static Thermal Rating (STR) (black dashed line), applies a fixed value throughout the year. In the same way, seasonal ratings (long-short dashed lines) can be calculated for winter, summer or autumn/spring. For them a fixed probability of overload is used, in this work set as 0.1%. With the same approach the qDTR (solid blue line) is calculated considering the same risk of overload across a 50-year time horizon for each month/year combination. Historical data (RCP_H) are evaluated from 1970 to 2022 and future meteorological projections (RCP_x) are evaluated from 2023 to 2070.

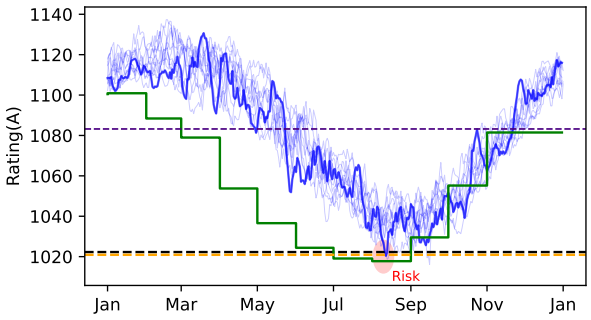

Figure 2: The conceptual illustrations of this proposed method display the DTR calculated throughout one year (2000-2022) for a specific coordinate, represented in blue. The STR_H is depicted in black, the monthly $qDTR_H$ in green, and the $qDTR_{H_s}$ for the winter and summer seasons in indigo and orange, respectively.

2.7. Transmission Expansion Plan

A transmission expansion planning study is being carried out to quantify the financial implications in planning. It is based on assumptions such the use of an established test system network with assigned geographic locations relative to the south of France, consistent distances, and a deterministic transmission expansion model.

The compact equations for the deterministic TEP that focus on selecting transmission lines to minimize total costs are represented in (9), where * remarks indicate the impact of the qDTR. The objective function (9a) is represented by the minimization of costs and investments, which defines the operating power production from each generating unit decision variables and the transmission investment decisions gathered in vector $z_{i,j}$. The coefficient vectors f,g and d represent for each node-branch, the active-power flows, the generated active power and demand, respectively. Constraints (9b), (9c) and (9d) guarantee power balance at each bus. Additionally, a big-M transformation technique is implemented, using a large positive constant $\mathcal{M}$ in (9d).

$$\min \quad \sum_{i,j} I_{ij} z_{ij} + \sum_{g} c_g g_g \tag{9a}$$

$$\text{st:} \quad \sum_{l \in \mathcal{L}_i} f_{ij}^0 + \sum_{l \in \mathcal{L}_i} f_{ij}^1 + g_i = d_i, \quad i \in \mathcal{N} \tag{9b}$$

$$f_{ij}^0 - (\theta_k - \theta_l)/x_{ij}^0 = 0, \quad ij \in \mathcal{L} \tag{9c}$$

$$|f_{ij}^k - (\theta_i - \theta_j)/x_{ij}^k| \leq \mathcal{M}(1 - z_{ij}^k), \quad ij \in \mathcal{N}_{\mathcal{L}} \tag{9d}$$

$$|f_{ij}^0| \leq \bar{f}_{ij_{\text{qDTR}}{}^*}^0, \quad ij \in \mathcal{L} \tag{9e}$$

$$|f_{ij}^k| \leq \bar{f}_{ij_{qDTR_{\text{N}}}{}^*}^k, \quad ij \in \mathcal{N}_{\mathcal{L}} \tag{9f}$$

$$0 \leq g \leq \bar{g} \tag{9g}$$

$$z_{ij}^{k+1} \leq \bar{z^k}_{ij} \quad \forall (i,j) \in \mathcal{N}_{\mathcal{L}} \tag{9h}$$

$$z_{ij} \in \{0,1\}, \quad ij \in \mathcal{N}_{\mathcal{L}} \tag{9i}$$

Operational limits described in (9e) and (9f), with $\bar{f}_{i,j_{qDTR}}$ implement limits on existing and proposed lines. Finally, binary variable z represents the decision-making process of the build/not-build, bounded by the limit of the max expansion per line k. It is important to note that this proposed methodology can be extended to select the optimal dimensions of the corrective backfill and best thermal performance, considering economic constraints [38, 39]. However, the methodology presented here focuses on analyzing thermal limits and serves as a long-term planning guide.

It acts as a link between the time-varying ampacity DTR, mainly used in operations, and the fixed STR, which is unaffected by climate change along transmission line corridors.

3. Results

In this section, a series of studies are conducted to demonstrate the use of qDTRs in UGC for long-term power system planning, either by direct burial installation or by the use of backfill [40]. The goal is to assess the method's effectiveness in quantifying qDTRs, accounting for the heat transfer mechanisms of various terrains and the complexities introduced by climate-induced changes.

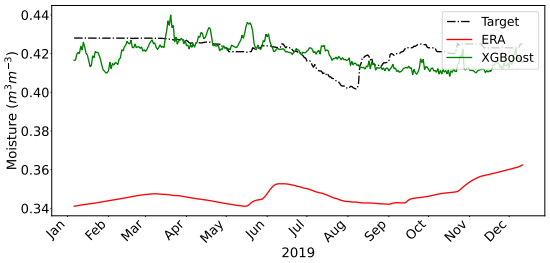

(a) Moisture

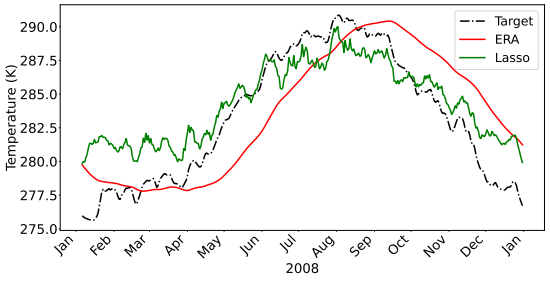

(b) Temperature

Figure 3: Daily time series of estimated soil moisture with (a) XGBoost at Soil 5 and (b) LASSO (green) at Soil 2 compared to ERA5 data (red) and test values (black dashed).

Firstly, to apply qDTR, the data described in 2.3 had to be retrieved. To project moisture and temperature based on each representative concentration pathway, a machine learning model with a daily step was trained, validated, and selected as outlined in 2.2. The performance of each model was compared with the ERA5 data, which were used as a benchmark. Results not shown in this paper indicate

that techniques such as k-NN and LSTM, with deviations of $+0.05m^3m^{-3}$ over the observations, increase the computational cost. On the other hand, XGBoost [33] exhibited the most favourable performance for moisture and temperature in the technique evaluation process. This was evidenced by achieving the lowest error values among all models, outlined in Table 4.

Table 4: Machine Learning Performance - Moisture and Temperature

Moisture at 20th Percentile								**Temperature at 80th Percentile**							
	CV	Model					ERA_5		CV	Model					ERA_5
		0	1	2	3	4				0	1	2	3	4	
$RMSE_{20}$	0	0.29	0.07	0.13	0.08	0.14	0.22	$RMSE_{80}$	0	2.23	2.03	2.29	2.15	2.39	2.72
	1	0.05	0.21	0.08	0.09	0.08	0.15		1	2.69	2.43	2.73	2.63	2.83	3.64
	2	0.05	0.03	0.10	0.04	0.04	0.09		2	2.92	4.81	3.19	3.16	3.37	2.76
	3	0.05	0.06	0.06	0.16	0.05	0.07		3	2.02	1.85	2.25	1.90	2.14	2.90
	4	0.13	0.08	0.11	0.05	0.19	0.24		4	2.89	3.48	2.60	3.11	2.70	3.56
	Avg.	**0.11**	**0.09**	**0.10**	**0.08**	**0.10**	**0.16**		Avg.	**2.71**	**3.16**	**2.83**	**2.74**	**2.95**	**3.10**
MAE_{20}	0	0.29	0.06	0.11	0.07	0.13	0.22	MAE_{80}	0	2.23	2.03	2.29	2.15	2.39	2.72
	1	0.04	0.21	0.08	0.08	0.07	0.14		1	2.56	4.61	2.85	2.84	3.06	2.18
	2	0.04	0.03	0.11	0.03	0.04	0.08		2	1.71	1.55	1.95	1.61	1.87	2.32
	3	0.04	0.05	0.05	0.17	0.04	0.06		3	2.55	3.14	2.26	2.77	2.38	2.58
	4	0.12	0.07	0.10	0.04	0.19	0.24		4	2.64	2.96	3.03	2.56	3.41	2.21
	Avg.	**0.11**	**0.08**	**0.09**	**0.08**	**0.09**	**0.15**		Avg.	**2.34**	**2.86**	**2.48**	**2.39**	**2.62**	**2.40**

The results are derived from diverse stations selected through cross-validation on the various soil codes used. For a graphical representation of the performance across different soil codes, refer to Fig. 3. At first glance, the XGBoost moisture model demonstrates lower average error values than the ERA5 model. With marginally superior performance, the Lasso temperature models denote the robustness of ERA5, establishing them as a dependable choice for historical references.

3.1. Evaluating Climate Change's Impact on Transmission Capacity

As outlined in 2.6, qDTR is employed to estimate the effects of climate change on UGC transmission capacity by calculating week/year qDTRs with a 0.1% exceedance probability. This analysis is applied to the cable configurations described in Table 5 and all geographical coordinates across France.

When the qDTR is calculated using the three RCP scenarios for the coming decades instead of historical meteorological data, rising temperatures' moderate but significant impact is observed, as illustrated in Fig. 4. In turn, Table 5 presents the

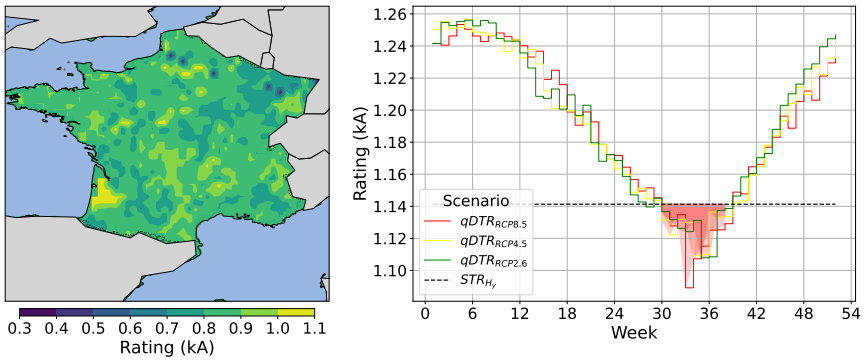

Figure 4: Geographical distribution of yearly $qDTR_{8.5}$ across France for Cable 2 Over Fifty Years. Followed by the annual representation of $qDTR_{week}$ for historical $qDTR_{H}$ and projections $qDTR_{RCP}$ for the region Île-de-France. The red zone represents the overload risk if the STR is applied

mean values of this temporal difference in carrying capacity, where results suggest that colder temperatures, increased precipitation, and reduced irradiance levels contribute to increased capacity during winter. Among the results in Table 5, notable observations include:

- Impact of Climate Change: In the lower three sections, ratings decrease when qDTRs are calculated with RCPs instead of historical data. The reduction ranges from 3.8% to 6% for the smaller Cable 1, while it remains negligible for the larger Cable 2.
- The impact of using qDTRs instead of STR: In the top three sections, qDTRs increase the ratings of Cable 1 by -2.3 to 20.9%, and for Cable 2 by 0 to 19%.
- The impact of using backfill: Backfill considerably reduces the effect of climate change, even for smaller cables such as Cable 1.
- The importance of the voltage level: Higher voltage conductors with larger electrical insulation are less affected by external changes in soil thermal resistivity.

Fig. 4 illustrates the spatial distribution of thermal ratings across NUTS-2 regions in France (Nomenclature of Territorial Units for Statistics [41]), highlighting regional differences in the effects of climate change on underground cable capacity.

The visualization showcases the spatial variability of $qDTR_{RCP}$ in France, with fluctuations of up to 2%. This variability, which is almost unanimously negative, is influenced by diverse soil types across regions and significantly impacts thermal diffusivity and moisture retention. In contrast, using qDTR allows the thermal memory inherent in buried cabling to be maintained. Fig. 4 shows the inertia with a 4-week shift of the annual temperature cycle, with lower capacity around September. It is important to note that the actual soil composition on the ground can be much more variable than what the 0.25^o x 0.25^o grid map can depict. Therefore, when backfill is not used, a thorough soil analysis must be conducted, or conservative assumptions must be made.

Table 5: $\Delta_{\%}$ Seasonal qDTR mean capacity differences over fifty years with $RCP_{2.6,\ 4.5,\ 8.5}$

Type	**Install**	**Impact of qDTR**				**Impact of Climate Change**			
		Fall	**Sprg**	**Sum**	**Wint**	**Fall**	**Sprg**	**Sum**	**Wint**
$RCP_{8.5}$		**$(qDTR_{8.5}, STR_{8.5})_{\Delta_{\%}}$**				**$(qDTR_{8.5}, qDTR_{Hst})_{\Delta_{\%}}$**			
Cable 1	Buried	7.11	6.22	1.09	16.5	-5	-4.9	-6	-4
	Backfill	4.72	3.44	0.91	8.4	-0.5	-0.4	-0.4	-0.1
Cable 2	Buried	7.02	19.05	4.44	18.4	-0.2	0.3	-0.5	0.1
	Backfill	7.06	6.25	-2.29	10.7	-0.5	0.1	-0.4	-0.1
$RCP_{4.5}$		**$(qDTR_{4.5}, STR_{4.5})_{\Delta_{\%}}$**				**$(qDTR_{4.5}, qDTR_{Hst})_{\Delta_{\%}}$**			
Cable 1	Buried	8.6	6.8	-2.3	13	-4.8	-5.1	-5.8	-3.9
	Backfill	7.5	19.2	5.6	19.6	-0.37	-0.36	-0.3	-0.12
Cable 2	Buried	1.72	3.8	1.3	11.3	0.65	0.36	-0.5	1.6
	Backfill	7	18.2	4.6	18	-0.35	-0.35	-0.31	-0.12
$RCP_{2.6}$		**$(qDTR_{2.6}, STR_{2.6})_{\Delta_{\%}}$**				**$(qDTR_{2.6}, qDTR_{Hst})_{\Delta_{\%}}$**			
Cable 1	Buried	9.04	19.4	4.94	20.9	-4.4	-4.9	-5.8	-3.8
	Backfill	7.9	19.3	5.6	19.5	-0	-0.2	-0.3	-0.1
Cable 2	Buried	12	9.2	0	7.9	1.1	0.6	-0.5	1.7
	Backfill	7.4	18.3	4.6	17.9	-0	-0.2	-0.1	-0.1

[1] Cable 1 - A2X(F)K2Y-800RM: Circular stranded aluminium conductor with a nominal voltage of 245 kV. The XLPE insulation has a nominal thickness of 22 mm [42].
[2] Cable 2 N2XS(FL)2Y 1x1200: Circular stranded aluminium conductor with a nominal voltage of 500 kV. The XLPE insulation has a nominal thickness of 31 mm [43].

3.2. Impact of climate change on network costs

To evaluate the performance of long-term ratings (qDTR), we address the deterministic TNEP problem using an IEEE 24-bus reliability test system [44] deployed in southern France. The problem is solved using an expanded version of [45]. This study involves replacing the existing 132 kV lines with their UGC counterparts,

with a three times expansion potential for all lines. We model operational variability using the one-year load demand profile from [44] and the modified maximum dissimilarity algorithm outlined in [46].

The TEP applies qDTR to estimate UGC's maximum allowable line capacity. Instead of relying on STR, qDTRs are derived from historical and projected weather reanalysis data to assess transmission capacity. These dynamic estimates replace the deterministic values in equations (9e) and (9f). Annual load and generation values are also adjusted to 1.5 times the base case data, and for each RCP scenario, the demand projection 2023-2050 is subtracted from [47].

Table 6: $\Delta_{\%}$ Variation for the three scenarios concerning investment and costs, the scenarios covering historical and projected static (STR), historical (qDTR_{H}) and projected (qDTR_{RCP}).

Scenario 1 - base case load and generation increased by 50%			
Case 1	**Impact of qDTR ($\mathbf{qDTR_{RCP}}$,$\mathbf{STR_{RCP}}$)**		
	$\mathbf{RCP_{8.5}}$	$\mathbf{RCP_{4.5}}$	$\text{RCP}_{2.6}$
$\text{CAPEX}_{\Delta_{\%}}$	-29.8	-	-100
$\text{OPEX}_{\Delta_{\%}}$	-33×10^{-2}	-40×10^{-2}	-3×10^{-3}
$\Delta\text{Lines}_{\text{build}}$	$\text{Branch}_5 : -1$	0	$\text{Branch}_5 : -1$
Case 2	**Impact of Climate change ($\mathbf{qDTR_{RCP}}$,$\mathbf{qDTR_{H}}$)**		
	$\mathbf{RCP_{8.5}}$	$\mathbf{RCP_{4.5}}$	$\text{RCP}_{2.6}$
$\text{CAPEX}_{\Delta_{\%}}$	–	-	–
$\text{OPEX}_{\Delta_{\%}}$	50×10^{-3}	10×10^{-3}	30×10^{-3}
$\Delta\text{Lines}_{\text{build}}$	-	-	-
Scenario 2: generators added at nodes 3, 5, 16, 21			
Case 1	**Impact of qDTR ($\mathbf{qDTR_{RCP}}$,$\mathbf{STR_{RCP}}$)**		
	$\mathbf{RCP_{8.5}}$	$\mathbf{RCP_{4.5}}$	$\text{RCP}_{2.6}$
$\text{CAPEX}_{\Delta_{\%}}$	76.9	-	-
$\text{OPEX}_{\Delta_{\%}}$	-8.36	-1.3	-42×10^{-2}
$\Delta\text{Lines}_{\text{build}}$	$\text{Branch}_1 : -1$, $\text{Branch}_8 : +1$	-	-
Case 2	**Impact of Climate change ($\mathbf{qDTR_{RCP}}$,$\mathbf{qDTR_{H}}$)**		
	$\mathbf{RCP_{8.5}}$	$\mathbf{RCP_{4.5}}$	$\text{RCP}_{2.6}$
$\text{CAPEX}_{\Delta_{\%}}$	–	-	–
$\text{OPEX}_{\Delta_{\%}}$	30×10^{-2}	70×10^{-3}	4×10^{-3}
$\Delta\text{Lines}_{\text{build}}$	-	-	-

The operational and planning results are summarized in Table 6, reflecting two possible scenarios: the first involves increasing demand, and the second involves installing new generators in specific nodes to reduce congestion, in contrast to network reinforcements. For each scenario, two cases are analyzed to assess the impact

of climate: (1) To illustrate the impact of the qDTR approach, the results were obtained by using $qDTR_{RCP}$ instead of STR_{RCP}, and (2) the difference incurred by using historical weather instead of climate projections in the qDTR estimation to reveal the climate impact on the network. Overall, Table 6 reveals:

- Impact of Climate Change: A slight increase in operating and total network costs due to the impact of climate change for both extreme $RCP_{8.5}$ and $RCP_{2.6}$ scenarios. This is believed to be because of a conservative risk selection in qDTR.

- The impact of using qDTRs instead of STR becomes evident in the $RCP_{8.5}$ scenario, where the risk of overloading increases due to reduced dissipation of the Joule heat effect. This situation eventually necessitates an additional investment in one transmission line for Case 1 in Scenario 2. Interestingly, the qDTR methodology demonstrates its ability to yield higher average ratings throughout most of the year across all case/scenario combinations, with a maximum impact of -8.36% in operating costs. This is also reflected in the investment costs, where a reduction in line construction is observed during Scenario 1 / Case 2.

4. Discussion

The methodology used to calculate qDTR is designed to capture the range of weather phenomena and the effects of heat waves or changing precipitation patterns on component ratings by focusing on the lower tail of the probability distribution while maintaining both seasonal and long-term consistency. This method is established to increase the effective performance of the UGLs while ensuring adequate safety margins for their operation. This study demonstrates that the STR approach fails to fully utilize the available transmission capacity, significantly raising the risk of thermal overload during high-temperature seasons. It is important to acknowledge that transmission capacity is also impacted by electrical factors such as voltage drops, stability, and environmental conditions like drought, aridity, and land use,

particularly in the context of direct-buried cables. However, these aspects are beyond the scope of this research. The methodology outlined here focuses on analyzing UGL thermal limits, providing a framework for long-term planning.

5. Conclusions

Through an assessment conducted employing a grid resolution of 0.25^o x 0.25^o, this analysis investigates the impact of climate change on transmission network capacity using established thermal models. Employing the quasi-dynamic Thermal Rating method to estimate maximum capacity with a low-risk exceedance probability, our findings highlight non-moderate reductions in the $RCP_{8.5}$ scenario for UGC, showing sensitivity to potential climate changes, with a mean reduction from 6% to 4%. This value is reduced for deep-buried and backfill cables.

When this capacity reduction is integrated into a TEP study, it leads to different outcomes in terms of CAPEX and OPEX, resulting in overall system cost increases for all greenhouse gas concentration scenarios considered $\Delta_{\%}\mathbf{(qDTR_{RCP},STR_{RCP})}$, smaller than 1%.

In addition, this paper estimated soil moisture and soil temperature at a depth of 2 meters. The results, obtained through 5-Fold validation, demonstrate mean absolute errors of 0.08 ($\pm$ 0.02) m^3m^{-3} for soil moisture and 2.51 ($\pm$ 0.17) (^oK) for soil temperature. This demonstrates better accuracy than the benchmark model and gives more strength to the present study. Among future improvements to this module, we suggest integrating additional soil layers, potentially up to 5, and extending the extrapolation to depths of 5 meters. Furthermore, expanding the scope of station inclusion to a global scale is recommended to ensure comprehensive coverage of all soil types.

Another factor to consider is that soil characteristics may vary more frequently. However, the database used considers soils with a spatial resolution of 1 km. Therefore, practical applications of this methodology may require the following actions: 1) selecting the worst-case scenario, 2) conducting a detailed soil survey, or 3) using trench backfill. For the latter, calculations for the use of controlled backfill have been incorporated into the thermal model.

The primary advantage of the qDTR methodology is its ability to yield higher average ratings throughout most of the year compared to the annual static rating, resulting in an average increase of 9.3%. Moreover, it has the potential to further widen the disparity between winter and summer seasons, with an increase of up to 10% in winter. This ultimately translates into a reduction in system costs in all three future scenarios, reaching a maximum of 8.36%. In general, qDTR tends to increase the average rating, with this advantage being more pronounced in certain regions or soil types compared to others. In general, it can be said that ratings are expected to fall in regions experiencing longer heat waves and low precipitation. An example can be seen in the map for the region of Charente-Maritime department, where the conductor's rating could be reduced by up to 40%. However, climate change impacts are not limited only to rising temperatures but also include heat waves or changing precipitation patterns. As long as these factors are properly incorporated into the climate models used as input, they are integrated into both the machine learning model used to better estimate soil properties and the qDTR calculation methodology.

The study has focused exclusively on France due to limitations related to the data set's size and the test case's deployment. It is believed that, with the exception of extreme conditions such as an artic or desertic climate, the climates observed in France can be representative of most of the climates found in Europe and sufficient to show the results of the methodology in practical conditions. However, the methodology can be easily replicated in other regions, when the proper datasets for weather, climatic projections and soil are replaced. The use of open access data from [26, 27, 28, 29] makes this task trivial. Regarding the machine learning model, it already improves the estimation of soil variable parameters across diverse soil types and is adaptable for application in other regions worldwide. This capability is made possible by utilizing a consistent and sufficiently large dataset encompassing various areas and soil types. However, its performance could be further refined by integrating additional data sources, particularly those providing soil moisture and temperature measurements specific to each soil type.

Finally, given the challenges inherent in grid development planning, a more ad-

vanced methodology needs to be developed for future applications. This methodology should consider not only the thermal limit of the conductors but also the frequency of high currents, also related to n-1 events, on the lines and the use of thermal aging to estimate the loss of useful life more accurately.

.

References

[1] H. Brakelmann, G. Anders, *Ampacity Reduction Factors for Cables Crossing Thermally Unfavorable Regions*, IEEE Power Engineering. 16(4) (2001) 444-448. https://doi.org/10.1109/MPER.2001.4311470

[2] Wang, P. and et al., *Dynamic thermal analysis for underground cables under continuously fluctuant load considering time-varying van wormer coefficient*, Electric Power Systems Research. 199 (2021), 107395. https://doi.org/10.1016/j.epsr.2021.107395.

[3] R. Huang, J.A. Pilgrim, P.L. Lewin, D. Scott, D. Morrice, *Use of day-ahead load forecasting for predicted cable rating*, IEEE PES Innovative Smart Grid Technologies. (2014) 1–6. https://doi.org/10.1109/ISGTEurope.2014.7028813.

[4] Y. Li, Y. Wang, C. Kang, J. Song, G. He, Q. Chen, *Improving distributed PV integration with dynamic thermal rating of power distribution equipment*, IScience. 25(8) (2022), 104808. https://doi.org/10.1016/j.isci.2022.104808.

[5] D.A. Douglass, A.-A. Edris, *Real-time monitoring and dynamic thermal rating of power transmission circuits*, IEEE Transactions on Power Delivery. 11(3) (1996) 1407-1418. https://doi.org/1407âĂŞ1418.10.1109/61.517499

[6] S. Liu, K. Kopsidas, *Risk-Based Underground Cable Circuit Ratings for Flexible Wind Power Integration*, IEEE Transactions on Power Delivery. 36(1) (2021) 145-155. https://doi.org/10.1109/TPWRD.2020.2980437

[7] Y. Li, Q. Chen, G. Strbac, K. Hur, C. Kang, *Active Distribution Network Expansion Planning With Dynamic Thermal Rating of Underground Cables and Transformers*, IEEE Transactions on Smart Grid. 15(1) (2024) 218-232. https://doi.org/218âĂŞ232.10.1109/TSG.2023.3266782.

[8] S. Cherukupalli, G.J. Anders, *Types of Power Cables and Cable with Integrated Fibers*, Distributed Fiber Optic Sensing and Dynamic Rating of Power Cables, IEEE. (2019) 77-93. https://doi.org/10.1002/9781119487739.ch5.

[9] D. Douglass, *Increased Power Flow through Transmission Circuits: Overhead Line Case Studies and Quasi-Dynamic Rating*

[10] R.S. Olsen, G.J. Anders, J. Holboell, U.S. Gudmundsdottir, *Modelling of Dynamic Transmission Cable Temperature Considering Soil-Specific Heat, Thermal Resistivity, and Precipitation*, IEEE Transactions on Power Delivery. 28(3) (2013) 1909-1917. https://doi.org/1909âĂŞ1917.10.1109/TPWRD.2013.2263300

[11] C. Kittel, H. Kroemer, H.L. Scott, *Thermal Physics*, 2 (1998).

[12] I.E. Commission, Electric cables – *Calculation of the current rating – Part 1-1: Current rating equations (100 % load factor) and calculation of losses*, General, IEC. https://doi.org/2015.10.1109/IEEESTD.2018.8353815

[13] Dorison, Eric, et al. *Ampacity Calculations for Deeply Installed Cables*, IEEE Transactions on Power Delivery. 25(2) (2010) 524–33. https://doi.org/10.1109/TPWRD.2009.2033961.

[14] B.J. Cosby, G.M. Hornberger, R.B. Clapp, T.R. Ginn, *A Statistical Exploration of the Relationships of Soil Moisture Characteristics to the Physical Properties of Soils*, Water Resources Research. 20(6) 682–690 (1984) https://doi.org/10.1029/WR020i006p00682

[15] A. Tavakol, K.R. McDonough, V. Rahmani, S.L. Hutchinson, J.M.S. Hutchinson, *The soil moisture data bank: The ground-based, model-based, and satellite-based soil moisture data*, Remote Sensing Applications: Society and Environment. 24 (2021) 100649. https://doi.org/10.1016/j.rsase.2021.100649.

[16] ESA CCI *Soil Moisture for improved Earth system understanding: State-of-the art and future directions*, Remote Sensing of Environment, 203 (2017) 185-215. https://doi.org/10.1016/j.rse.2017.07.001.

[17] G. Balsamo, P. Viterbo, A. Beljaars, B.J.J. van den Hurk, M. Hirschi, A. Betts, K. Scipal, *A revised hydrology for the ECMWF model: Verification from field*

site to terrestrial water storage and impact in the Integrated Forecast System, 10(3) (2009) 623-643. https://doi.org/10.21957/yzyeh0vlw.

[18] O. Sungmin, R. Orth, *Global soil moisture data derived through machine learning trained with in-situ measurements*, Scientific Data. 8 (2021) 170. https://doi.org/10.1038/s41597-021-00964-1.

[19] M. Taheri, H.K. Schreiner, A. Mohammadian, H. Shirkhani, P. Payeur, H. Imanian, J.H. Cobo, *A Review of Machine Learning Approaches to Soil Temperature Estimation, Sustainability.* 15 (2023). https://doi.org/10.3390/su15097677.

[20] A. Rani, N. Kumar, J. Kumar, J. Kumar, N.K. Sinha, *Chapter 6 - Machine learning for soil moisture assessment*, in: R.C. Poonia, V. Singh, S.R. Nayak (Eds.), Deep Learning for Sustainable Agriculture, Academic Press. (2022) 143–168. https://doi.org/10.1016/B978-0-323-85214-2.00001-X.

[21] R. Huang, J.A. Pilgrim, P.L. Lewin, D. Payne, *Dynamic cable ratings for smarter grids*, IEEE PES ISGT Europe 2013 (2013) 1–5. https://doi.org/10.1109/ISGTEurope.2013.6695230.

[22] A. Bracale, P. Caramia, P. De Falco, A. Michiorri, A. Russo, *Day-Ahead and Intraday Forecasts of the Dynamic Line Rating for Buried Cables*, IEEE Access. 7 (2019) 4709–4725. https://doi.org/10.1109/ACCESS.2018.2888505.

[23] He, H. and Zhao, Y. and Dyck, M. F. and et al., *A modified normalized model for predicting effective soil thermal conductivity*, Acta Geotechnica. 12 (2017) 1281–1300. https://doi.org/10.1007/s11440-017-0563-z

[24] Xiong, K. and Feng, Y. and Jin, H. and et al.,*A new model to predict soil thermal conductivity*, Scientific Reports. 13 (2023) 10684. https://doi.org/10.1038/s41598-023-37413-5.

[25] Ren, J. and Men, L. and Zhang, W. and et al., *A new empirical model for the estimation of soil thermal conductivity*, Environmental Earth Sciences. 78 (2019). https://doi.org/36110.1007/s12665-019-8360-7.

[26] W. Dorigo, I. Himmelbauer, D. Aberer, L. Schremmer, I. Petrakovic, L. Zappa, W. Preimesberger, A. Xaver, F. Annor, J. Ardö, others, *The International Soil*

Moisture Network: serving Earth system science for over a decade, Hydrology and Earth System Sciences[dataset]. 25 (2021) 5749–5804.

[27] R. Hiederer, *Mapping Soil Properties for Europe - Spatial Representation of Soil Database Attributes*,[dataset], Publications Office of the European Union. https://doi.org/2013.10.24381/cds.e2161bac

[28] J. Muñoz Sabater, *ERA5-Land hourly data from 1950 to present*,[dataset],Copernicus Climate Change Service (C3S) Climate Data Store (CDS), (2019).

[29] Copernicus Climate Change Service, *Climate and energy indicators for Europe from 2005 to 2100 derived from climate projections*, [dataset], Copernicus Climate Change Service (C3S) Climate Data Store (CDS), 2021. https://doi.org/36110.1007/10.24381/cds.f6951a62.

[30] S. Hadiwidjaja, S.D. Montana Salas, A. Michiorri, *Quasi-dynamic line rating spatial and temporal analysis for network planning*, in: 27th International Conference on Electricity Distribution (CIRED 2023), 2023: pp. 276–280.https://doi.org/10.1049/icp.2023.0291

[31] W. Dorigo, A. Xaver, M. Vreugdenhil, A. Gruber, A. Dostálová, A.D. Sanchis-Dufau, D. Zamojski, C. Cordes, W. Wagner, M. Drusch, *Global Automated Quality Control of In Situ Soil Moisture Data from the International Soil Moisture Network*, Vadose Zone Journal. 12 (2013), vzj2012.0097. https://doi.org/10.2136/vzj2012.0097

[32] *Soil Taxonomy: A Basic System of Soil Classification for Making and Interpreting Soil Surveys*, 2nd ed., U.S. Department of Agriculture Handbook 436, (1999).

[33] T. Chen, C. Guestrin, *XGBoost: A Scalable Tree Boosting System*, in: Proceedings of the 22nd ACM SIGKDD International Conference on Knowledge Discovery and Data Mining, ACM. (2016) 785–794. http://doi.acm.org/10.1145/2939672.2939785.

[34] R. Tibshirani, *Regression Shrinkage and Selection Via the Lasso*, Journal of the Royal Statistical Society: Series B (Methodological). 58 (2018) 267–288. https://doi.org/10.1111/j.2517-6161.1996.tb02080.x.

[35] T. Akiba, S. Sano, T. Yanase, T. Ohta, M. Koyama, *Optuna: A Next-generation Hyperparameter Optimization Framework*, Proceedings of the 25th ACM SIGKDD International Conference on Knowledge Discovery and Data Mining, (2019).

[36] Johansen, Oistein, *Thermal Conductivity of Soils*, 322 (1977).

[37] A. Clauset, C.R. Shalizi, M.E.J. Newman, *Power-Law Distributions in Empirical Data*, SIAM Review. 51 (2009) 661–703,http://doi.org/10.1137/070710111.

[38] Ocłoń, P.,The effect of soil thermal conductivity and cable ampacity on the thermal performance and material costs of underground transmission line, Energy. 231 (2021), 120803. https://doi.org/10.1016/j.energy.2021.120803

[39] A. Cichy, B. Sakowicz and M. Kaminski, Economic Optimization of an Underground Power Cable Installation, IEEE Transactions on Power Delivery. 33(3) (2018) 1124-1133. https://doi.org/10.1109/TPWRD.2017.2728702.

[40] B.K. Shivakumar, S.K. Rout, *Special thermal back fill material surround for better performance of EHV cables*.

[41] Eurostat, *Statistical regions in the European Union and partner countries — NUTS and statistical regions 2021*, European Union, (2022). http://doi.org/10.2785/850262.

[42] T.-F.K. S.A., *High and extra high voltage cables*, Edition, www.tfkable.com, (2019).

[43] D. Cable, *66 - 500 kV XLPE Cable: High and Extra High Voltage Cable System*, Demirer Cable, Head Office: Barbaros Bulvarı 59,

[44] C. Grigg, P. Wong, P. Albrecht, R. Allan, M. Bhavaraju, R. Billinton, Q. Chen, C. Fong, S. Haddad, S. Kuruganty, W. Li, R. Mukerji, D. Patton, N. Rau, D. Reppen, A. Schneider, M. Shahidehpour, C. Singh, *The IEEE Reliability Test System-1996. A report prepared by the Reliability Test System Task Force of the Application of Probability Methods Subcommittee*, IEEE Transactions on Power Systems. 14 (1999). http://doi.org/1010âĂŞ1020.10.1109/59.780914.

[45] Gurobi Optimization, LLC. *Gurobi Optimods* [Software]. Retrieved from https://www.gurobi.com/resource/gurobi-optimods/

[46] Á. García-Cerezo, R. García-Bertrand, L. Baringo, *Computational Performance Enhancement Strategies for Risk-Averse Two-Stage Stochastic Generation and Transmission Network Expansion Planning*, IEEE Transactions on Power Systems. 39 (2024). http://doi.org/273âĂŞ286.10.1109/TPWRS.2023.3236397.

[47] Réseau de Transport d'Électricité, *Futurs énergétiques 2050. Rapport complet*, RTE (Réseau de Transport d'Électricité), (2022).

B.5 Published Papers: Paper B

Assessment of the Influence of Climate Change on Power Grid Transmission Capacity

Montaña-Salas Sergio, Michiorri Andrea

Mines Paris – PSL, PERSEE, Sophia Antipolis, France

Abstract

In order to propose effective solutions to mitigate the effects of climate change on the electrical power system, it is essential to have a comprehensive understanding and quantification of the relevant issues. This article explores the impact of climate on transmission network capacity, employing established thermal models and a regional expansion plan, fed by historical and climatic projections on a 0.25° grid resolution over the European continent. The results indicate that, under the high greenhouse gas emissions scenario (RCP 8.5), the area studied will experience average reductions of 1.53%, 2.1%, and 0.2% capacity by 2070, for overhead lines, power transformers, and underground cables, respectively. We propose a quasi-dynamic thermal rating method to estimate maximum capacity. This results in a capacity improvement of up to 22% for power transformers in winter and up to 17% for overhead lines during nighttime hours. This solution represents a viable alternative for electricity operators seeking to solve the dilemma of temperature-driven capacity reduction in the context of challenging network reinforcements.

Keywords:
Climate Change, Dynamic Thermal Rating, Power Systems Planning, Power transmission.

1. Nomenclature

I	Component Thermal Rating (A)
R_T	Electrical resistance of the component at temperature T
RCP	Representative Concentration Pathways (2.6, 4.5 and 8.5)
$qDTR$	quasi Dynamic Thermal Rating (A)
STR	Static Thermal Rating (A)
Meteorological	
θ_a	Ambient temperature (°C)
θ_s	Soil temperature (°C)
P_t	Total precipitation
W_s	Wind velocity (m/s)
S_r	Net surface solar radiation (W/m^2)
ψ	Soil Moisture
$Winter$	December, January, February
$Summer$	June, July, August
Ratings	
$qDTR_H$	quasi Dynamic Thermal rating calculated from historical data (1970-2022) (A)
STR_H	Static thermal Rating calculated from historical data (1970-2022) (A)
$qDTR_{RCP_x}$	quasi Dynamic Thermal rating calculated from RCP projection, where x represents the RCPs scenario (2023 to 2070) (A)
STR_{RCP_x}	Static Thermal Rating calculated from RCP projection, where x represents the RCPs scenario (2023 to 2070) (A)
Power Transformer (PT)	
θ_h	Hot-spot Temperature (°C)
$\Delta\theta_h$	Hot-spot gradient rise (°C)
P_{NL}	No-load losses (kW)
P_{LL}	Load losses (kW)
R_{ll}	Ratio of Load Losses to No-Load Losses
Underground Cables (UGC)	
R_{UGC}	Cable electrical resistance ($\Omega \cdot m^{-1}$).
$T_{1,2,3,4}$	Cable layer thermal resistance ($K \cdot m/W$).
$\Delta\theta$	Conductor temperature rise
v	Ratio between the thermal resistivity of the dry and wet zones
W_d	Dielectric losses per unit length per phase (W/m)
λ_{1-2}	Sheath and armor loss factor
$\hat{\psi}$	Projected moisture (1m)
$\hat{\theta}_s$	Projected soil temperature (1m)
Overhead Lines (OHL)	
R_{OHL}	Resistance of conductors ($\Omega \cdot m^{-1}$).
θ_c	Conductor Temperature
Q_c	Convective Heat Loss
Q_r	Radiative Heat Loss
Q_s	Solar Heat Gain

2. Introduction

Climate change projections estimate an average increase in atmospheric temperature of 2-4^{o}C by the end of the century [1, 2]. This is expected to have a direct and negative impact on the electricity system in terms of transmission capacity, generation, demand, and congestion.

In terms of transmission, which is the focus of this study, the current carrying capacity of overhead lines (OHL), power transformers (PT), and underground cables (UGC) is determined, among other things, by their ability to dissipate joule losses to the external environment. This in turn, depends on the ambient temperature: the lower the external temperature, the higher the transmission capacity, and vice versa. In the United States, for example, the effects of global warming are expected to reduce OHL capacity by an average of 1.9% to 5.8% between 2040 and 2050, compared to the 1990–2010 period [3].

In terms of power generation, higher temperatures lead to a reduction in production capacity: on the one hand, a higher ambient temperature increases the sink temperature in thermodynamic cycles, reducing the overall conversion efficiency. On the other hand, it reduces air density, which in turn reduces the mass flow intake of fossil fuel generators [4]. In addition, factors such as water discharge temperatures and declining water flows are expected to affect over 80% of the world's thermal power plants due to drought and shifting seasonal patterns, as detailed in [5].

Electricity demand it tends to increase with higher ambient temperatures due to the thermal sensitivity of air-conditioning-driven loads. This, in turn, is exacerbated by the increasing penetration of air-cooling in power systems, including in developing countries. In the analysis conducted in [6] on 36 global cities by 2050, the predicted average annual change in per-capita demand under different scenarios ranges from -2.7% to 5.7% for tropical cities, with peak per-capita demand increases of up to 9.5% for mid-latitude temperate climates. These increases could be further exacerbated during heat waves, with electricity demand in regions such as California projected to increase by as much as 21% on hot days for 2100 [7].

The combination of lower transmission capacity, lower distributed generation production, and higher loads can increase the likelihood of congestion in transmission and distribution infrastructure. This leads to inefficiencies and spikes in local electricity prices, exacerbating current trends. The US Department of Energy (DOE) reported [8] that real-time congestion costs (developed by individual market operators using common metrics described in [9]) amounted to approximately $4.8 billion in 2016, with the potential to increase as temperatures rise.

Among the solutions proposed to alleviate network congestion problems, Dynamic Thermal Rating (DTR) [10–13] is actively proposed for critical lines. This technology aims to identify network components' real-time current carrying capacity, which is generally higher than their Static Thermal Rating (STR). On the one hand, this value is highly dependent on weather conditions; on the other hand, DTR allows the reduction or complete elimination of network congestion and associated curtailments. It can also delay network reinforcements.

Various studies have incorporated DTR into power system expansion plans[14, 15] and highlighted its importance in renewable energy sources integration and penetration [16–21]. These studies employ control and sensing devices [22, 23] or data-driven probabilistic methods to calculate the rating of OHL [11, 24]. All these studies yield generalized findings on the efficacy of DTR, among which the following can be empha-

sized: a) Decreased system congestion costs due to less generator re-dispatching. b) Reduction or postponement of investments is required to reinforce or expand existing assets.

In this study, we analyze historical and projected meteorological data (1970–2070) for various geographic locations across Europe, focusing on the position of power system components, with a spatial resolution of 0.25 degrees (approx. 28 km). Using this data, we calculate the maximum current that the system can carry at any point in time without the temperature of any section exceeding a predefined maximum threshold using the quasi-Dynamic Thermal Rating (qDTR) methodology. In doing so, we emphasise the significant potential of qDTR, previously refined by the authors for various power system components [25, 26], now adapted in this study to enhance the flexibility of the power system. To support this claim, we analyse power system planning within the framework of the Generation and Transmission Expansion Plan (G&TEP) using PyPSA-Eur [27] as a power system modeling tool.

This is made possible by the availability of widely accepted component thermal models [28–30], open energy data models [27] and quantitative climatic projections such as the Representative Concentration Pathways (RCPs) [31] and Shared Socio-economic Pathways (SSPs) [32], which constitute a valuable toolset for assessing regional climate changes and their specific impacts on the energy sector.

In summary, although research on the impacts of climate change on the energy system is becoming more mature, the above literature review identifies several notable **research gaps**, highlighting areas where further research and analysis is needed. These include:

1. Previous research on this topic has primarily focused on the impact of generation production [17, 33–35] and load [6]. When network aspects were considered, only OHL were considered [3].
2. To the authors' knowledge, the long-term impact of climate change on power grid transmission, including dynamic thermal rating in OHL [3, 12], UGC[36, 37], and PT [17, 20, 38], has yet to be thoroughly examined. This is mainly due to the conventional focus of DTR applications on short- and medium-term analysis [37, 39], or the focus on single components. To address this gap, a clear distinction between planning horizons is essential. In this context, short-term planning (under 3 years) involves continuous operational analysis to address urgent energy supply needs, while medium-term planning (10-15 years) evaluates periodic adjustments based on market and economic changes. On the other hand, long-term planning (over 15 years) focuses on the broader future structure of the power system, including generation, transmission, and the integration of new technologies [40].

In light of this, this research aims at providing the following main **contributions** :

1. Highlight the potential of quasi-dynamic thermal ratings (qDTR) versus static thermal ratings (STR) in network operation in Europe.

2. Quantify the impact of climate change on the transmission capacity of the power system for OHL, PT, and UGC, considering both historical and future climate projection datasets. This quantification is done in terms of transmission capacity (in MVA) and costs for G&TEP with a 2050 horizon.

3. Methodology

3.1. Overview

We develop a procedure to quantify the impact of climate change on (a) power network transmission capacity and (b) network costs expected in Europe using three RCP scenarios. This method is described in Fig. 1 and can be divided into two steps:

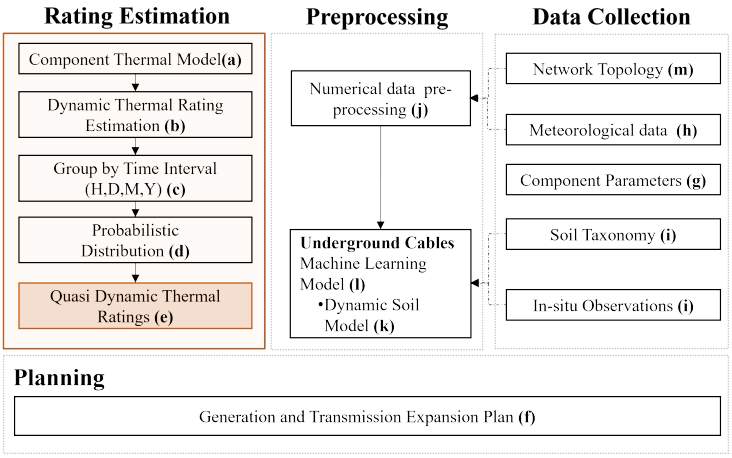

Figure 1: Visual representation of the procedure used in this study.

Firstly, DTR and qDTR are estimated for OHL, PT, and UGC [26] based on thermal models and weather data from historical meteorological and climate projections (from 1970 to 2070). This methodology allows to measure the changes in transmission capacity caused by climate change. It must be remembered that transmission capacity is also impacted by factors such as voltage drops and stability. However, these aspects are beyond the scope of this research. The methodology presented here focuses on analyzing thermal limits and serves as a guide for long-term planning.

Secondly, a G&TEP is computed for Europe with a 2050 horizon using PyPSA-Eur, integrating historical meteorological and RCP projections to estimate the updated thermal capacities of transmission lines based on STR and qDTR methodologies. This allows quantifying the impact of climate change on grid costs from the perspective of transmission constraints.

3.2. Rating estimation

The estimation of ratings starts with the use of (a) component thermal models based on the thermal balance between the heat generated by the Joule effect I^2R and the heat dissipated in the environment by convection or conductivity Q_c, radiation Q_r and the solar heat gain Q_s. This is shown in Eq. 1, where the parameters are influenced by: surface absorbivity for α, surface emissivity, maximum allowable temperature T_c and air temperature T_a for β. The parameter γ, depends on atmospheric values such as wind speed W_s and T_a for OHL, and soil parameters such as soil temperature T_s and soil moisture ψ_s for UGC. This fundamental equation is declined below for each different component.

$$I^2 R_T + \alpha Q_s = \beta Q_r + \gamma Q_c \tag{1}$$

As mentioned above, the OHL thermal limit is calculated using the heat balance equation and applying the model outlined in [30]. The essence of the model can be summarised as follows:

$$I = \left[\frac{(\beta Q_r(\theta_a) + \gamma Q_c(\theta_a, W_s) - \alpha Q_s(S_r)}{R_{OHL}(\theta_c)} \right]^{(0.5)} \tag{2}$$

Where wind speed (W_s) presents the greatest impact [22], coupled with other ambient parameters such as air temperature θ_a and solar radiation S_r. Since the conductor temperature should be calculated as a function of the highest steady-state temperature it can reach under worst-case conditions (observed from the cooling aspect) [4], in our study, we consider the parallel wind direction to estimate the minimum convection area.

With regard to underground cables, in accordance with the standard procedure for quantifying the ampacity of buried UGC, the thermo-electric model described in [29] is used for this component. According to this standard, the capacity, with the influence of the formation of a dry zone, is calculated per day as follows:

$$I = \sqrt{\frac{{}_{\Delta}\theta - W_d \left[0.5T_1 + n\left(T_{2+3} + vT_4\right)\right] + (v-1){}_{\Delta}\theta_x}{R_{UGC}\left[T_1 + n\left(1+\lambda_1\right)T_2 + n\left(1+\lambda_{1+2}\right)\left(T_2 + vT_4\right)\right]}} \tag{3}$$

Here ${}_{\Delta}\theta_x$ is the temperature difference between the conductor and the soil, and T_4 is the thermal resistance of the soil, which is influenced by soil moisture (ψ_s). These two parameters are time-varying. On the other hand, the other parameters such as λ_{1-2}, T_{1-3} are static and depend on the cable construction. For a detailed description of the thermal model, the reader is invited to consult [29, 41].

Finally, several models are available to estimate the thermal state of loaded oil-immersed transformers. Due to its widespread acceptance, this study adopts the IEC 60076-7 [28] loading guide. It is modified to include the temperature correction factor for the losses described in [42] and the solar radiation factor on the component as described in [43], including physical factors such as area and color [44]. PT rating is limited by the hot-spot temperature (HST) θ_h (°C), depending on ambient temperature

θ_a (°C) and the hot-spot gradient rise of temperature within the transformer $\Delta\theta_h$ and it is calculated in Eq. 4. The Top-oil temperature θ_o (°C) with a cold start state assumptions can be calculated in Eq. 5.

$$\Theta_o = \left[\frac{1 + K^2 R_{ll}}{1 + R_{ll}} + \frac{S_r}{P_{LL} + P_{NL}}\right]^{x_r} (\Delta\theta_{or}) + \theta_a \tag{4}$$

$$\Theta_h = \theta_o + \Delta\theta_h \tag{5}$$

Here, $\Delta\theta_{or}$ (°C) denotes the steady-state temperature rise at rated losses; x_r represents the exponent associated with the oil temperature rise due to total losses, while R_{ll} denotes the ratio of load losses at rated current to no-load losses at rated voltage. The HST serves as the central limiting parameter for the design and is instrumental in calculating the load factor K (per unit) per iteration. This load factor is defined as the ratio of the load current to the rated current. Finally, the solar power is normalized into the load P_{LL} and the no-load losses P_{NL} in Eq. 4. Finally, the capacity is calculated using reverse calculation of the steady-state thermal model described in [45].

Subsequently, at each coordinate and for each hourly time step available in the data sets [1], the DTR in (b) is determined by applying the specific thermal model described in Eq. 2-5 to each power system component. At this point, (c) the simulated historical or future DTRs are grouped by time interval (yearly, monthly, monthly/hourly). For each group, a power law function is fitted to the lowest tail of the distribution (d). Finally, an accepted risk for thermal overload is chosen, $x = 0.1\%$ in this work, and the qDTR in terms of current intensity I are calculated (e) as in Eq. 6.

$$I(x) = Ax^{\alpha} \tag{6}$$

To enable generalization and replicability, Algorithm 1 and Fig. 2 conceptually illustrate the thermal estimation method ((a)-(d)), specifically for a PT. The model collects input meteorological data for the analysis period, which in this case is historical (T=1970 to 2022). Specific parameters for the analysis include the time interval (TI = Day/Night) and the exceedance value (x = 0.01). The process begins with the definition of the thermal model to be used, as described in Eq. (4) and Eq. (5) for PT. The next step is to calculate the DTR for each hour within the specified period (T), shown in the figure with a light blue color. In the third step, the calculated DTR values are grouped according to the defined time intervals, which in this case are day/night. Since this model focuses on the lower tail, only data points below the second quantile of each group are taken into account for further analysis. In the fourth step, the power law, described in Eq. (6), is fitted to the selected data sets. Finally, the qDTR is estimated as a function of the exceedance value to provide an annual representation of the input data corresponding to the specified time interval (day/night depicted in blue and green).

A notable result of this methodology is that colder temperatures and lower irradiance levels contribute to increased capacity during the winter season and nighttime hours.

Conversely, days with high temperatures, low wind speeds, and intense solar irradiance pose a risk of conductor overload when employing the STR method, illustrated by a pink color in Fig. 2.

Algorithm 1 PT qDTR Estimation

Input : $(\theta_a, S_r, x, TI) \forall \mathbf{t} \in T$

Output: Thermal Rating $I_{\mathrm{qDTR,TI}}$

1.Define Thermal model for Iteration:

$f(K) = Eq.4 - Eq.5$

2.Calculate DTR :

Solve for $\forall\ t \in \mathrm{T}$

$K' = K - \frac{f'(K)}{f''(K)}$

until $|K' - K| < 1e^{-3}$

$I_{\mathrm{rated\ (K)}} = I_{\mathrm{rated\ (K')}}$

$I_{\mathrm{DTR,t}} = I_{\mathrm{DTR,t}} \cup \{I_{\mathrm{rated\ (K)}}\}$

3.Define Subgroups by $g(TI)$**:**

$I_{DTR,g} = \{i \mid i = g(TI), TI \in I_{DTR,t}(TI)\}$

$I_{\mathrm{DTR,g},<0.02} = \{h \in I_{DTR,g} \mid h < q_{0.02}\}$

Where $q_{0.02} = \{P(I_{\mathrm{DTR,g,}} \leq h) \geq 0.02\}$

4.Compute Power Law Fitting from each $I_{\mathbf{DTR,g,}<0.02}$ **:**

$f(x) = Ax^{\alpha}$

5.Evaluate the qDTR for a thermal exceedance risk x:

$I_{qDTR}(0.1\%)_g \leftarrow \mathbf{A(0.001)}^{\alpha}$

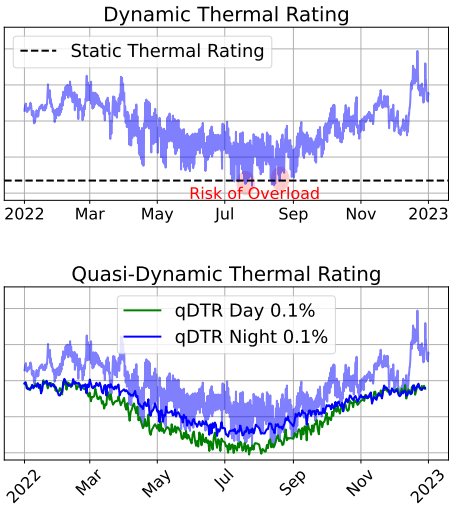

Figure 2: Conceptual illustrations of the qDTR method applied in a PT, using Algorithm 1

3.3. Planning

The financial impacts resulting from the reduction in DTR due to climate change are assessed through a series of G&TEPs (f) using PyPSA-Eur [27], and CO_2 budgets for the RCPs from [46–52]. These studies are based on the use of annual STRs and monthly/hourly qDTRs, corresponding to 288 values calculated for each month/hour combination. However, it is important to note that although PyPSA-Eur which has the option to accept a basic version of DTR capabilities natively [53], it has been parameterized to accept qDTR values. Several comparisons are made:

1. G&TEP are carried out using $\mathrm{STR_H}$ calculated on a historical and $\mathrm{qDTR_{RCP}}$ on the three climate projections. The comparison shows the mismatch that occurs when the impact of climate change on transmission capacity is not taken into account.
2. G&TEP are carried out using $\mathrm{STR_H}$ and monthly/hourly $\mathrm{qDTR_H}$ calculated from historical. The comparison shows the benefits of using frequently changing qDTR to recover the lost transmission capacity.

This solution allows us to rely on a widely used model to test the hypotheses' impact and obtain solid results. However, it has some limitations, particularly the fact that

the network used in PyPSA-Eur is made of zones and their interconnections, generated by the clustering algorithm used to aggregate zones and interconnecting lines. Whereas a real network has a much higher number of nodes and, more importantly, lines. For a more complete explanation, the reader can refer to [27]. However, in order to facilitate the reading of this document, the main aspects that the authors have identified of the model implemented from [27] are summarised below.

- A total of 37 nodes are defined, corresponding to each European country.
- Single planned horizon to 2050.
- CO2 levels have been updated according to the IPCC, with projections extending to 2050. [46–52]
- Overnight Scenario, characterized by calculating an expansion of the energy system to meet demand, with sector option activates as Electrification of Transport, Industry, and Agricultural sector described in [54].
- Extendable Carriers: Solar, onshore wind, offshore wind, hydro, nuclear, oil, OCGT, CCGT, coal, lignite, geothermal, biomass.
- The time resolution is set to 1 hour
- Assumptions for each type of generation technologies (cost, efficiencies, annualized interest rate for investment (4%) and emissions) are extracted from the PyPSA v0.28.0.
- Global correction factor of 1.9 for the load for all analyzed projections.
- Information about the optimization model can be found at [4], which has been updated in compliance with $f_{l_{qDTR}}$ limiting the capacity over the lines by applying the methodology proposed for the long-term evaluations

However, for the purpose of replicability, a configuration file is attached to know the full extent of parameter settings in the supplementary information Section 5.1.

3.4. Data

The data used in this study can be divided into two broad categories: (g) component data (static) and (h) environmental data (static and dynamic). Historical meteorological conditions in Europe for the period 1970-2020 are obtained from the ERA [1], whilst climate projections for the period 2020-2070 are obtained from the Copernicus Climate Change Service (C3S)[1] (EURO-CORDEX driving model id: ICHEC-EC-EARTH). Additional (i) soil properties for underground cable rating calculations are obtained from [55, 56]. A list of the parameters used and their source is reported in Table. 1. Component parameters, relative to the most popular elements, are obtained from the existing literature or data sheets provided by manufacturers or literature, such as [57]

Table 1: Summary of data and sources. A:ERA[1, 2], B:ISMN[55], C:ESDAC [56].

Variable	Units	Source
Meteorological		
Temp. Air at 2 m (θ_a)	K	A
Total precipitation (P_t)	mm	A
Net surface solar radiation (S_r)	Jm^{-2}	A
u - v - wind at 10 m (W_s)	ms^{-1}	A
Soil Proprieties		
Silt ($S_{silt_{\%}}$)	%	C
Sand ($S_{sand_{\%}}$)	%	C
Clay ($S_{clay_{\%}}$)	%	C
Organic ($S_{org_{\%}}$)	%	C
Texture Composition (S_{text})	-	C
Bulk (S_{bulk})	kgm^{-3}	C
Soil Measurements		
Temperature (θ_s)	K	B
Moisture (ψ)	%	B

for OHL, [58] for UGC, and [59] for PT. Described in more detail in the Section 6.1.

The network expansion analysis presented in this Section 3.3 is based on the transmission (m) network topology derived from PyPSA-Eur and [60]. PyPSA-Eur uses the European high voltage grid (220 kV to 750 kV), built from OpenStreetMap data. This grid is geo-referenced and consists of 6,046 nodes and over 6,000 transmission lines, primarily OHL, with a low proportion UGC, accounting for less than 3%, which allows us to integrate local weather conditions and their impact.

3.5. Preprocessing

The raw data described in 3.4 are preprocessed as follows: (j) time series are homogenized to a time step of one hour by cubic interpolation. For instance, projections have a time step of 3 hours whilst historical of 1 hour. Regarding the spatial resolution it is chosen to replicate the 0.25° grid of the projections, because a finer spatial resolution would require, especially for the wind, a much more complex fluid dynamic model than a simple interpolation. If a specific coordinate is required, the weather variables are collected from the nearest coordinate from the given target point. (k) Soil temperature $(\hat{\theta}_s)$ and soil moisture $(\hat{\psi})$ are calculated at a daily resolution in a depth range between 0.8 and 1.2 meters from hourly input data using a dedicated machine learning based model (l) for each coordinate (0.25°) described by the authors in [26]. This is necessary because the values available from [1] are either not available at the typical UGC burial depth (1-2m, in the case of soil temperature) or are absent (in the case of soil moisture).

4. Results

The following section explores how weather conditions affect the capacity of the electricity transmission network. This analysis is conducted both at the component

level and on a regional scale, applying the methodology described in Section 3.2. It proceeds in three steps: (1) assessing how the qDTR influences the allowable transmission capacity at the component scale; (2) evaluating the impact of climatic conditions on grid transmission capacity using qDTR calculations at the regional level; and (3) analyzing the broader implications of climate change for long-term transmission system planning. For clarity, the data presented in the subsequent sections have been selected for their representative value—whether as extreme scenarios, typical cases, or due to their relevance to the study's research objectives.

4.1. Impact of qDTR with respect to STR

As explained above, the qDTR provides a probabilistic representation of the behavior over the period analyzed. By applying the methodology described in Section 3.2, we obtain an annual representation of the analyzed component, consisting of 288 values computed in month/hour combination. To exemplify this representation, we selected a node in southeastern France and applied the qDTR to historical data. This is illustrated in Fig. 3, which depicts the annual and hourly variations ($qDTR_H$) of the three components at this location. It can be highlighted that for OHL and PT, $qDTR_H$ is lower than STR_H during summer daytime hours, mitigating the risk of overload due to high temperatures. On the contrary, in winter and at night, qDTR values increase significantly, resulting in a higher total transmission capacity. In the case of UGC, as expected, its qDTR remains constant throughout the day due to the high thermal inertia of the soil.

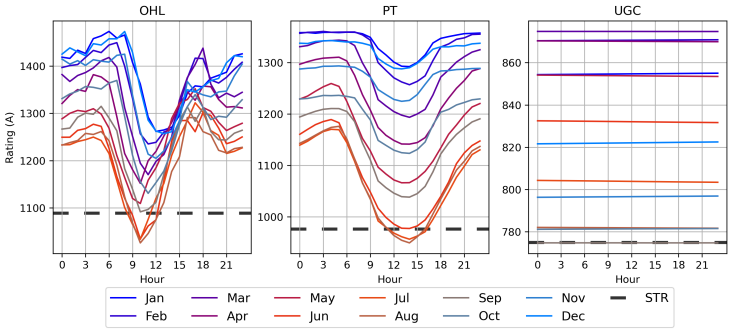

Figure 3: $qDTR_H$ calculated for each month/hour combination for OHL, PT, and UGC calculated in the node of Tavel (southeast France). Colours represent months from the coldest (blue) to the warmest (red). A dashed black line represents STR.

Similarly, but at a broader scale, we extended this analysis to a continental level across Europe, incorporating a comprehensive spatial assessment, using a resolution of 0.25° over the same period. This extended approach allows for a more detailed examination of variations between countries, capturing the distribution of climatic and geographical factors influencing qDTR dynamics.

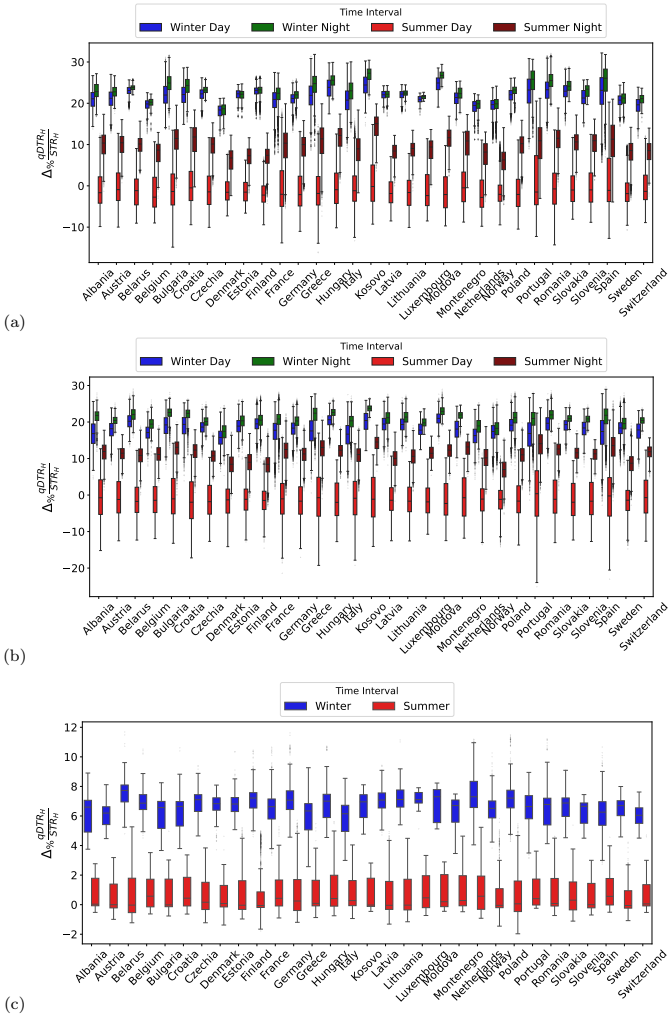

(a)

(b)

(c)

Figure 4: Percentage difference between $qDTR_H$ and STR_H in some Europeans Countries for: (a) PT, (b) OHL, (c) UGC

The results presented in Fig. 4 were obtained by calculating the percentage difference between $qDTR_H$ and STR_H at each coordinate ($\Delta_{\%} \frac{qDTR_H}{STR_H}$), and then analyzed at the country level. To achieve a complete global representation, mean, minimum, and maximum values were calculated by grouping the data into diurnal (6 AM - 6 PM) and nocturnal periods for winter and summer.

The results suggest that incorporating regional climate effects using historical data improves qDTR performance over STR, especially in winter periods, with measurable positive impacts in several countries and components. This trend is particularly evident between PT and OHL, as observed in Greece, where average improvements reach 22% and 24%. On the other hand, the slower response of deep soil temperature exchange in UGC limits its effect to 6%. In the opposite way, but correlated with the risk of warmer days, we can be below the STR with a minimum of 12%, as in areas such as Spain for PT. These differences refer to the deltas of the temperature of the component that can have throughout the year, i.e., an area where its temperature is more stable throughout the year, the delta between qDTR and STR is lower. For a deeper analysis, the reader is invited to check Table 7, Table 8 and Table 9 in the Appendix, covering OHL, PT, and UGC.

4.2. Impact of climate change on network transmission capacity

The qDTRs are calculated on the basis of projections for future decades rather than recent meteorological data. This assessment covers the whole of Europe, while maintaining the spatial resolution of previous analyses. It distinguishes between the historical period (1970-2022) and the projected future (2023-2070).

The study averaged qDTR values per coordinate over 288 month/hour combination to assess annualized climate change impacts in Europe by comparing future and historical scenarios. The first row of Fig. 5 illustrates the spatial variability of $qDTR_H$, measured as the deviation of each coordinate from the European average, with variability reaching approximately 20%, 31%, and 87% for OHL, PT, and UGC, respectively. The lower variability of OHL is attributed to its dual dependence on wind speed and air temperature, while the high variability of UGC results from regional differences in soil properties, which significantly affect thermal diffusivity and moisture retention.

The next three rows show the percentage variation of qDTR across Europe under different climate scenarios, mainly negative, with significant declines in central Spain, the Arctic, and mountainous regions. UGC shows smaller variations due to soil's high thermal inertia. Spatial variations in average carrying capacity for the three components are shown, with key values in Table 2. The table presents average and extreme differences in transmission capacity based on historical and future weather data, and shows declines across all scenarios. Transformers are the component with the highest variation (from -0.9% to -2.1%), followed by OHL (from - 0.4% to -1.53%) and UGC (from -0.1% to -0.2%). This is explained by the fact that OHL is mainly influenced by air temperature and wind speed, whereas PT is only influenced by air temperature. Often the hottest hours are also characterised by non-zero wind speeds, reducing the derating effect of temperature. For UGC, the much narrower temperature range of the ground prevents large derating effects. The worst simulated cases show a maximum reduction of -3.9%, -4.4%, and -1% for the OHL, PT and UGC ratings respectively.

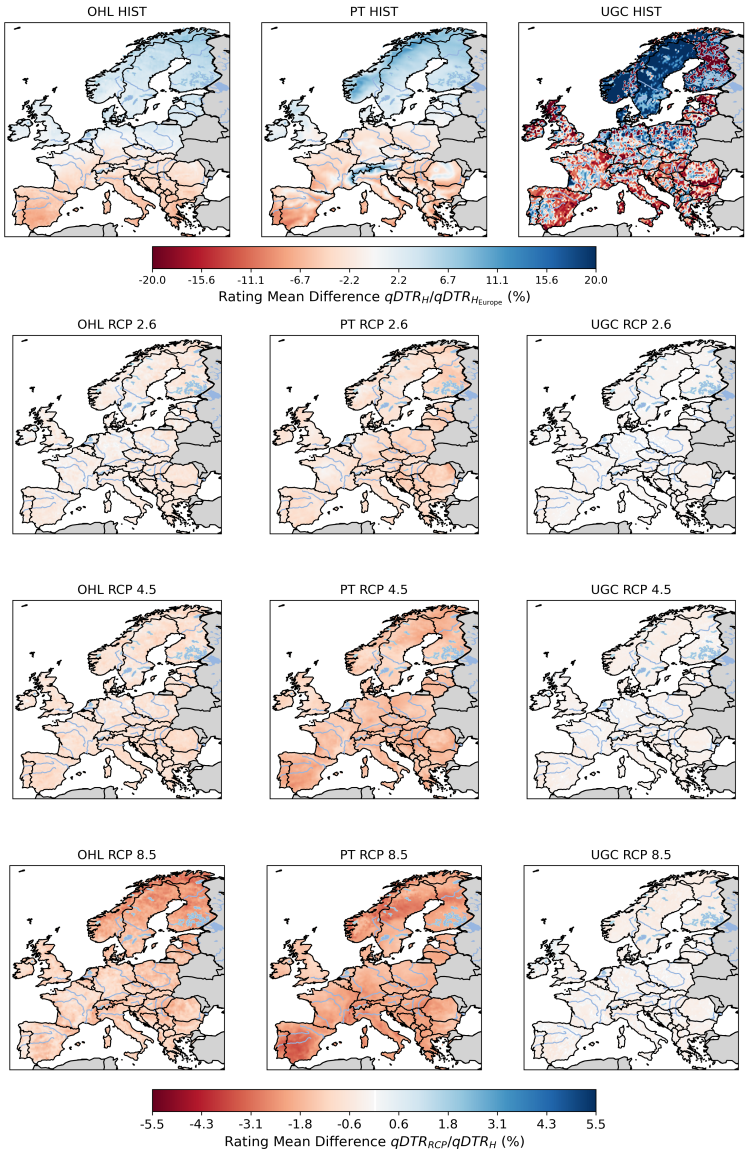

Figure 5: Geographical distribution of the mean qDTR difference at the country level over fifty years for the RCPs and the historical. This is performed for the main power components (OHL - PT and UGC). The first row reflects the difference in the variation of the historical average for the region, and the subsequent rows illustrate the variation in the average for each RCP.

Table 2: Variation for the three scenarios concerning historical values for qDTR for the European region.

	Power System Component		
	OHL	PT	UGC
Rating Difference Scenario RCP 2.6 - $\Delta_{\%}(\mathbf{qDTR_{RCP2.6}, qDTR_H})^1$			
Mean	-0.4	-0.9	-0.1
Max	-1.4	-2.12	-0.5
Min	0.75	0.5	0.8
Rating Difference Scenario RCP 4.5 - $\Delta_{\%}(\mathbf{qDTR_{RCP4.5}, qDTR_H})^1$			
Mean	-0.7	-1.5	-0.2
Max	-1.7	-2.8	-0.6
Min	0.9	-0.4	0.5
Rating Difference Scenario RCP 8.5 - $\Delta_{\%}(\mathbf{qDTR_{RCP8.5}, qDTR_H})^1$			
Mean	-1.53	-2.1	-0.2
Max	-3.9	-4.4	-1
Min	0.32	-0.7	1.0

[1] The variation of transmission capacity calculated with the specific climatic scenario versus historical weather

Finally, to further explore the seasonality of the impact, the heat map in Fig. 6 shows the monthly and hourly variation of qDTR_{RCP} at the same analyzed node of Fig. 3. This heat map reveals the effects of increasing ambient temperature in the three RCP scenarios.

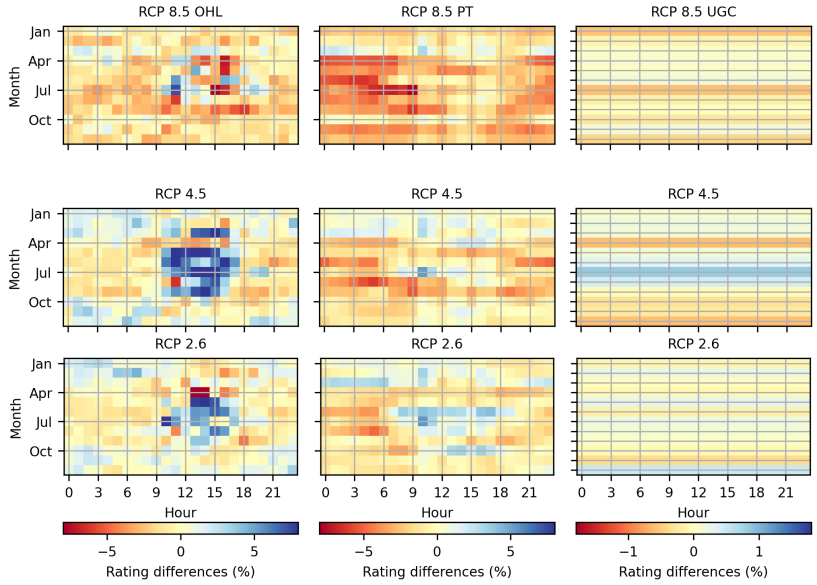

Figure 6: Difference in the calculated qDTR month/hour between historical values and RCP projections 2.6, 4.5, 8.5. This is performed for the three main power components (OHL - PT, and UGC) in a node located in Tavel, southeast France.

The observed variations, which are moderately significant, translate, for example, into an average rating reduction of -2.3% in July for $qDTR_{RCP8.5}$ and -0.7% for $qDTR_{RCP4.5}$ in PT. This could be translated into a variation in the level of risk to the network operator in terms of equipment lifetime. On the other hand, the opposite effect can also be observed in certain months and hours, such as -0.9% on February mornings for $qDTR_{RCP8.5}$, +0.7% for $qDTR_{RCP4.5}$ and +0.02% for $qDTR_{RCP2.6}$.

4.3. Impact of climate change on network costs

This section examines the G&TEP investment decisions, incorporating climate-variant supply and qDTR for power system components. To achieve this, we use the procedure described in Section 3.3, applying STR_H and $qDTR_{RCP}$ calculated from historical or climate projections using weather data, for each OHL described in the model. To illustrate this and to highlight the influence of quasi-dynamic capacities, Fig. 7 shows the impact of climate change on the transport capacity of various OHL. For this example, June has been selected since it is a month typically influenced by high-temperature conditions. This influence results in reductions that, in certain regions such as the southern Iberian Peninsula, can exceed -5% in the high greenhouse gas emissions scenario (RCP 8.5). To support these estimated qDTRs, the complete data for each line in all scenarios are available in the supplementary information chapter.

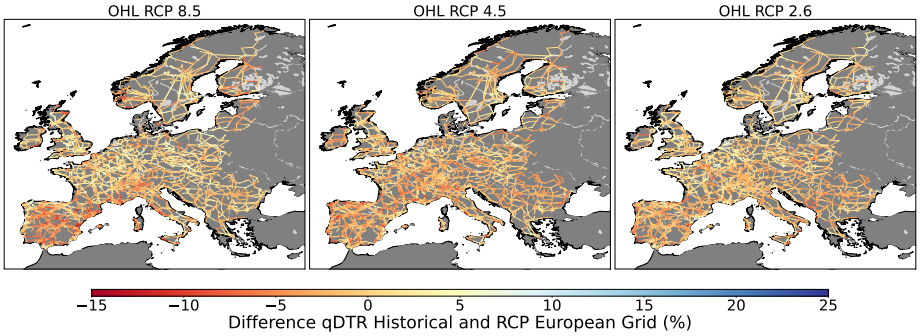

Figure 7: Climate impacts on transmission capacity, the difference in capacity for qDTR ($\Delta_{\%} \frac{qDTR_{RCP}}{qDTR_H}$) in June at 14 h RCP 2,6, 4.5 and 8.5 scenarios for OHL.

The network model is then used to perform a G&TEP to estimate changes in capital expenditure (CAPEX), operational expenditure (OPEX) and renewable curtailment.

The results are summarised in Table 3, which shows:[1] the results of a baseline simulation with STR,[2] the improvements obtained using $qDTR_H$ instead of STR_H, and [3] the mismatch introduced by using historical weather instead of climate projections in the $qDTR_{RCP}$ calculations. The expected amount of curtailment, and total system cost are also reported. However, these values are only relative to new investment and do not take into account existing infrastructure.

Reference case: G&TEP for constrained CO_2 emissions without considering the impact of climate change on network transmission capacity. In this case study, the G&TEP model was used to analyse the optimal planning and operation of the power system under the carbon emission constraints imposed by the RCPs. The model used historical weather data for the STRs. The objective is to determine the different portfolios of generation capacity required to meet specific emission reduction targets. The results of the study are reported in Table 3 and in terms of CAPEX and OPEX in billion euros (B€) and renewable curtailment in gigawatt-hours (GWh). The results show that the three scenarios analysed have virtually the same CAPEX of 355.5B€ and OPEX of 18.9B€/y, with variations confined to the low percentage digits and slightly more visible differences in the curtailment of renewables. However, similar costs hide different allocations in the energy mix, with lower investment in gas plants in $RCP_{2.6}$ offset by higher investment in renewable. For additional information the reader is invited to see the full results in the Appendix.6, Table 10.

4.3.1. Impact of qDTR vs. STR on network transmission capacity and costs

Case 1: The G&TEP is run with a different set of transmission capacity constraints. Instead of using STRs to estimate the available transmission capacity, qDTRs calculated from historical weather are used. The aim is to quantify the benefit of qDTRs, mainly due to the use of higher transmission capacity at night. The results presented in Table 3 show a slight reduction in both capital and operating expenditures in all three scenarios, highlighting how this methodology mitigates costs associated with climate impacts. Moreover, the data indicate a consistent decrease in the curtailment, potentially influenced by factors such as enhanced line capacity during nighttime hours and colder seasons. However, it is crucial to note that while these reductions are more pronounced in investments related to transmission lines and renewable energy generation, their practical impact remains minimal, with less than a 0.1% effect. This can be considered an important finding of the study: the cost increase is of a smaller magnitude than the rating reduction. This is due probably to the ability of the system to reschedule power flows around constraints, or to other characteristics of the methodology used.

4.3.2. Impact of climate change on network transmission capacity and costs

Case 2. In this use case, the G&TEP model was run considering the qDTRs calculated for the respective RCPs. The aim of the study is to highlight the potential mismatch that would occur if the impact of climate change on transmission capacity were not taken into account when using qDTRs. As detailed in Table 3 cost patterns shift across scenarios. Specifically, in $RCP_{8.5}$, the lower effective available transmission capacity leads to an underestimation of CAPEX and renewable curtailment, resulting in a 42.7 M€ mismatch in CAPEX.

Finally, the last row in Table 3 presents **Case 3**, which illustrate the cost difference between maintaining a fixed value based on historical behavior (the conventional approach) and applying climate change influenced qDTRs. Once again, it highlights cost savings across all scenarios, even when accounting for higher temperatures and

Table 3: Variation in system costs for the three scenarios (RCP 2.6, 4.5, 8.5) in Europe. STR refers to annual static values, qDTR to monthly/hourly qDTR. The subscripts $_{H}$ and $_{RCP}$ indicate the use of historical weather data or future projections. Values are in % and calculated as 1-y/x, meaning that positive values represent cost reductions and negative values represent cost increases.

SCENARIO			**RCP**		
			2.6	4.5	8.5
REFERENCE	$\mathbf{STR_H}$	CAPEX (B€)	3.55E+2	3.55E+2	3.55E+2
		OPEX(B€)	1.89E+1	1.89E+1	1.89E+1
		System Cost(B€)	4.00E+2	4.00E+2	4.00E+2
		Curtailment (GWh)	7.32E+0	7.30E+0	7.32E+0
CASE 1	$\mathbf{\Delta(qDTR_H, STR_H)}$	CAPEX (%)	2.32E-2	1.42E-2	2.41E-2
		OPEX(%)	1.44E-1	1.36E-1	1.32E-1
		System Cost (%)	3.66E-2	2.77E-2	3.60E-2
		Curtailment (%)	6.49E-1	8.45E-3	4.26E-1
CASE 2	$\mathbf{\Delta(qDTR_{RCP} / H)}$	CAPEX (%)	-6.26E-3	4.59E+0	-1.20E-2
		OPEX (%)	4.88E-3	2.20E+1	1.68E-2
		System Cost (%)	-5.02E-3	6.52E+0	-8.81E-3
		Curtailment (%)	4.57E-2	4.20E-1	-6.10E-2
CASE 3	$\mathbf{\Delta(qDTR_{RCP}, STR_H)}$	CAPEX (%)	1.70E-2	4.61E+0	1.21E-2
		OPEX (%)	1.49E-1	2.21E+1	1.49E-1
		System Cost (%)	3.16E-2	6.55E+0	2.72E-2
		Curtailment (%)	6.94E-1	4.28E-1	3.65E-1

lower transmission capacities. These savings are quantified at about 126 M€ in the low emissions scenario.

5. Conclusions

The qDTR methodology captures weather variability and heat wave impacts on component ratings by focusing on the lower tail of the probability distribution while ensuring seasonal and long-term consistency. It aims to enhance transmission component performance while maintaining safety margins.

It can be seen as an improved, more granular version of the STR, which consider only a fixed, or seasonal value for the whole rating. However this conservative approach underutilizes available transmission capacity and increases the risk of thermal overload during high temperatures, especially in summer under the business-as-usual $RCP_{8.5}$ scenario.

Thus, qDTR is a probabilistic approach that enables risk tolerance selection in long-term planning. It bridges time-varying ampacity DTR, mainly used in operations, with fixed STR, which remains unaffected by climate change along transmission corridors.

qDTR has also the advantage of being known in advance, and can be used both for planning and for operation.

Overall, this study highlights that:

1. The projected future climate, with higher ambient temperatures on the European continent, leads to average reductions of 1.53%, 2.1% and 0.2% by 2070, for OHL, PT, and UGC, respectively, under the business-as-usual $RCP_{8.5}$ scenario by the year 2070.
2. When this reduction is incorporated into a G&TEP study, it results in a different combination of CAPEX and OPEX, leading to little increase in total system cost for scenarios $RCP_{8.5}$ and $RCP_{4.5}$, but slightly lower costs in $RCP_{2.6}$.
3. The proposed qDTR approach significantly enhances transmission capacities, mitigating the negative effects of climate variability. On average, qDTR improves transmission capacity in the coldest season while reducing overload risk effects in the hottest season. For instance, transmission capacity increases by 17%, 22%, and 6.8% for OHL, PT, and UGC in Denmark, while maintaining a controlled thermal overload probability. This in turn results in lower system costs in the three future scenarios and less curtailment of renewable energy.

Following on from these findings, this work also highlighted the need to develop a complete methodology for integrating the use of qDTR into G&TEP. This step is considered necessary to assess better its impact, not only on the thermal limits but also on the degradation of components due to high currents and the influence of exceedance values in the power law. Furthermore, the G&TEP needs to be replicated in other networks, both at the transmission and distribution level, with more realistic network models and higher UGC penetration. On the other hand, due to the 100-year time span and the temporal resolutions of the databases (1h of historical, 3h of projections),

a steady-state model is accurate, without affecting the nature of the input databases. While RCPs climate model projections provide valuable insights into potential climate futures, their accuracy and consistency are subject to uncertainties that are not accounted for in this study. Future work could incorporate a dynamic intra-hourly model, utilizing higher-resolution databases, to enhance the methodology's precision and address these uncertainties. Finally, the minor differences observed between scenarios may be attributed to the consistent demand scale configuration within PyPSA-Eur, designed to isolate its impact on the networks. Therefore, future G&TEPs could be developed to incorporate diverse socio-economic narratives in alignment with climate policy.

5.1. Supplementary information

Furthermore, data and software developed are available for researchers to facilitate the replication and generalization of this study or its use to build future research. A sample of this is available for the review period before being uploaded to a more suitable platform at the address: https://minesparis-psl.hal.science/hal-04453957v1 The databases of the analysis on the lines are available at https://zenodo.org/records/14039382

References

[1] Climate and energy indicators for Europe from 2005 to 2100 derived from climate projections [dataset]. Copernicus Climate Change Service (C3S) Climate Data Store (CDS) , 2021. Accessed on 14-03-2023.

[2] Bell B. Hersbach, P. Berrisford, G. Biavati, A. Horányi, J. Muñoz Sabater, Nicolas, C. Peubey, R. Radu, I. Rozum, D. Schepers, A. Simmons, C. Soci, D. Dee, and Thépaut. ERA5 hourly data on single levels from 1940 to present [dataset], 2023. Accessed on 14-03-2023.

[3] Matthew Bartos, Mikhail Chester, Nathan Johnson, Brandon Gorman, Daniel Eisenberg, Igor Linkov, and Matthew Bates. Impacts of rising air temperatures on electric transmission ampacity and peak electricity load in the united states. *Environmental Research Letters*.

[4] Konstantin O. Papailiou. *Green Books: Overhead Lines*. CIGRE / Springer, 2017.

[5] Seleshi G Yalew, Michelle TH van Vliet, David EHJ Gernaat, Fulco Ludwig, Ariel Miara, Chan Park, Edward Byers, Enrica De Cian, Franziska Piontek, Gokul Iyer, et al. Impacts of climate change on energy systems in global and regional scenarios. *Nature Energy*, 5(10):794–802, 2020.

[6] Y. Romitti and I. Sue Wing. Heterogeneous climate change impacts on electricity demand in world cities circa mid-century. *Scientific Reports*, 12:4280, 2022.

[7] Michelle Davis and Steve Clemmer. Power failure: How climate change puts our electricity at risk—and what we can do. 2014.

[8] U.S. Department of Energy. Annual u.s. transmission data review. Technical report, 2018.

[9] Federal Energy Regulatory Commission. Common metrics report: Performance metrics for regional transmission organizations, independent system operators, and individual utilities for the 2010-2014 reporting period. Technical report, Federal Energy Regulatory Commission, August 2016. Revised August 2017.

[10] Soheila Karimi, Petr Musilek, and Andrew M. Knight. Dynamic thermal rating of transmission lines: A review. *Renewable and Sustainable Energy Reviews*, 91:600–612, 2018.

[11] Behzad Keyvani, Eoin Whelan, Eadaoin Doddy, and Damian Flynn. Indirect weather-based approaches for increasing power transfer capabilities of electrical transmission networks. *WIREs Energy and Environment*, 12(3):e470, 2023.

[12] Dale A. Douglass, Jake Gentle, Huu-Minh Nguyen, William Chisholm, Charles Xu, Tip Goodwin, Hong Chen, Sarma Nuthalapati, Neil Hurst, Ian Grant, Jose Antonio Jardini, Robert Kluge, Paula Traynor, and Cody Davis. A review of dynamic thermal line rating methods with forecasting. *IEEE Transactions on Power Delivery*, 34(6):2100–2109, 2019.

[13] Soheila Karimi, Petr Musilek, and Andrew M. Knight. Dynamic thermal rating of transmission lines: A review. *Renewable and Sustainable Energy Reviews*, 91:600–612, 2018.

[14] Philipp Glaum and Fabian Hofmann. Enhancing the german transmission grid through dynamic line rating. In *2022 18th International Conference on the European Energy Market (EEM)*, pages 1–7, 2022.

[15] Andrej Trpovski and Thomas Hamacher. A comparative analysis of transmission system planning for overhead and underground power systems using ac and dc power flow. In *2019 IEEE PES Innovative Smart Grid Technologies Europe (ISGT-Europe)*, pages 1–5, 2019.

[16] SeyedeFatemeh Hajeforosh, Amena Khatun, and Math Bollen. Enhancing the hosting capacity of distribution transformers for using dynamic component rating. *International Journal of Electrical Power & Energy Systems*, 142:108130, 2022.

[17] Oscar David Ariza Rocha, Kateryna Morozovska, Tor Laneryd, Ola Ivarsson, Claes Ahlrot, and Patrik Hilber. Dynamic rating assists cost-effective expansion of wind farms by utilizing the hidden capacity of transformers. *International Journal of Electrical Power & Energy Systems*, 123:106188, 2020.

[18] Jiashen Teh and Ching-Ming Lai. Reliability impacts of the dynamic thermal rating and battery energy storage systems on wind-integrated power networks. *Sustainable Energy, Grids and Networks*, 20:100268, 2019.

[19] Ching-Ming Lai and Jiashen Teh. Network topology optimisation based on dynamic thermal rating and battery storage systems for improved wind penetration and reliability. *Applied Energy*, 305:117837, 2022.

[20] Kateryna Morozovska. *Dynamic rating with applications to renewable energy*. PhD thesis, KTH Royal Institute of Technology, 2020.

[21] Yinxiao Li, Yi Wang, Chongqing Kang, Jie Song, Guannan He, and Qixin Chen. Improving distributed pv integration with dynamic thermal rating of power distribution equipment. *iScience*, 25(8):104808, 2022.

[22] Andrea Michiorri, Huu-Minh Nguyen, Stefano Alessandrini, John Bjørnar Bremnes, Silke Dierer, Enrico Ferrero, Bjørn-Egil Nygaard, Pierre Pinson, Nikolaos Thomaidis, and Sanna Uski. Forecasting for dynamic line rating. *Renewable and Sustainable Energy Reviews*, 52:1713–1730, 2015.

[23] Dale Douglass, William Chisholm, Glenn Davidson, Ian Grant, Keith Lindsey, Mark Lancaster, Dan Lawry, Tom McCarthy, Carlos Nascimento, Mohammad Pasha, Jerry Reding, Tapani Seppa, Janos Toth, and Peter Waltz. Real-time overhead transmission-line monitoring for dynamic rating. *IEEE Transactions on Power Delivery*, 31(3):921–927, 2016.

[24] Mohammad Mahmoudian Esfahani and Gholam Reza Yousefi. Real time congestion management in power systems considering quasi-dynamic thermal rating and congestion clearing time. *IEEE Transactions on Industrial Informatics*, 12(2):745–754, 2016.

[25] Sergio-Daniel Montana-Salas and Andrea Michiorri. Weather-based quasi dynamic thermal ratings for power transformers, 2023.

[26] Montana-Salas Sergio and Michiorri Andrea. Long term climate-driven underground cable thermal ratings for network planning. *Electric Power Systems Research*, 241:111401, 2025.

[27] Tom Brown, David Schlachtberger, Alexander Kies, Stefan Schramm, and Martin Greiner. PyPSA-Eur: An open optimisation model of the european electricity system. *Zenodo*, 2020.

[28] International Electrotechnical Commission (IEC). Iec 60076-7:2018, power transformers - part 7: Loading guide for mineral-oil-immersed power transformers. Technical report, International Electrotechnical Commission (IEC), 2018.

[29] International Electrotechnical Commission. Iec 60287-1-1: Electric cables—calculation of the current rating—part 1-1: Current rating equations (100% load factor) and calculation of losses—general. Technical report, International Electrotechnical Commission, Geneva, Switzerland, 2014.

[30] Javier Iglesias, George Watt, Dale Douglass, Vincent Morgan, Rob Stephen, Mark Bertinat, Dzevad Muftic, Ralph Puffer, Daniel Guery, Sidnei Ueda, Kesimir Bakic, Sven Hoffmann, Tapani Seppa, Franc Jakl, Carlos Do Nascimento, Francesco Zanellato, and Huu-Minh Nguyen. *Guide for Thermal Rating Calculations of Overhead Lines*. CIGRE Technical brochure N° 601. CIGRE, December 2014.

[31] Karl Taylor, Ronald Stoufer, and Gerald Meehl. An overview of cmip5 and the experiment design. *Bull. Am. Meteorol. Soc.*, 93:485–498, 2011.

[32] Keywan Riahi, Detlef P. van Vuuren, Elmar Kriegler, Jae Edmonds, Brian C. O'Neill, Shinichiro Fujimori, Nico Bauer, Katherine Calvin, Rob Dellink, Oliver Fricko, Wolfgang Lutz, Alexander Popp, Jesus Crespo Cuaresma, Samir KC, Marian Leimbach, Leiwen Jiang, Tom Kram, Shilpa Rao, Johannes Emmerling, Kristie Ebi, Tomoko Hasegawa, Petr Havlik, Florian Humpenöder, Lara Aleluia Da Silva, Steve Smith, Elke Stehfest, Valentina Bosetti, Jiyong Eom, David Gernaat, Toshihiko Masui, Joeri Rogelj, Jessica Strefler, Laurent Drouet, Volker Krey, Gunnar Luderer, Mathijs Harmsen, Kiyoshi Takahashi, Lavinia Baumstark, Jonathan C. Doelman, Mikiko Kainuma, Zbigniew Klimont, Giacomo Marangoni, Hermann Lotze-Campen, Michael Obersteiner, Andrzej Tabeau, and Massimo Tavoni. The shared socioeconomic pathways and their energy, land use, and greenhouse gas emissions implications: An overview. *Global Environmental Change*, 42:153–168, 2017.

[33] F. Gülşen Erdinç, Ozan Erdinç, Recep Yumurtacı, and João P. S. Catalão. A comprehensive overview of dynamic line rating combined with other flexibility options from an operational point of view. *Energies*, 13(24), 2020.

[34] Carsten Matke, Wided Medjroubi, and David Kleinhans. SciGRID: An Open Source Reference Model for the European Transmission Network (v0.2), July 2016.

[35] Ching-Ming Lai and Jiashen Teh. Comprehensive review of the dynamic thermal rating system for sustainable electrical power systems. *Energy Reports*, 8:3263–3288, 2022.

[36] Rasmus Schmidt Olsen. *Dynamic Loadability of Cable Based Transmission Grids*. PhD thesis, 2013.

[37] Antonio Bracale, Pierluigi Caramia, Pasquale De Falco, Andrea Michiorri, and Angela Russo. Day-ahead and intraday forecasts of the dynamic line rating for buried cables. *IEEE Access*, 7:4709–4725, 2019.

[38] Wílerson Venceslau Calil, Kateryna Morozovska, Tor Laneryd, Eduardo Coelho Marques da Costa, and Maurício Barbosa de Camargo Salles. Determining total cost of ownership and peak efficiency index of dynamically rated transformer at the pv-power plant. *Electric Power Systems Research*, 229:110061, 2024.

[39] Jin Yang, Xuefeng Bai, Dani Strickland, Lee Jenkins, and Andrew M. Cross. Dynamic network rating for low carbon distribution network operation—a u.k. application. *IEEE Transactions on Smart Grid*, 6(2):988–998, 2015.

[40] Friedrich Kiessling, Peter Nefzger, João Felix Nolasco, and Ulf Kaintzyk. *Overhead Power Lines: Planning, Design, Construction*. Power Systems. Springer Berlin, Heidelberg, 1 edition, 2003.

[41] George J Anders. *Rating of electric power cables in unfavorable thermal environment*. 2005.

[42] International Electrotechnical Commission (IEC). Power transformers - Part 2: Temperature rise for liquid-immersed transformers, 2011.

[43] B. Gorgan, P. V. Notingher, J. M. Wetzer, H. F.A. Verhaart, P. A.A.F. Wouters, and A. Van Schijndel. Influence of solar irradiation on power transformer thermal balance. *IEEE Transactions on Dielectrics and Electrical Insulation*, 19(6):1843–1850, 2012.

[44] H. D. Einhorn. Colour and cooling of outdoor transformers. *Transactions of the South African Institute of Electrical Engineers*, 53(9):231–234, 1962.

[45] Irina Lupandina, Wolfgang Gawlik, Michael Schrammel, et al. Evaluation of dynamic loading capability for optimal loading strategies of power transformers. *Elektrotech. Inftech.*, 137:515–522, 2020.

[46] D. van Vuuren, M. den Elzen, P. Lucas, B. Eickhout, B. Strengers, B. van Ruijven, S. Wonink, and R. van Houdt. Stabilizing greenhouse gas concentrations at low levels: an assessment of reduction strategies and costs. *Climatic Change*, 2007.

[47] L. Clarke, J. Edmonds, H. Jacoby, H. Pitcher, J. Reilly, and R. Richels. Scenarios of greenhouse gas emissions and atmospheric concentrations. Sub-report 2.1a of synthesis and assessment product 2.1, U.S. Climate Change Science Program and the Subcommittee on Global Change Research, Department of Energy, Office of Biological & Environmental Research, Washington, DC, USA, 2007.

[48] S.J. Smith and T.M.L. Wigley. Multi-gas forcing stabilization with the minicam. *Energy Journal (Special Issue #3)*, pages 373–391, 2006.

[49] M.A. Wise, K.V. Calvin, A.M. Thomson, L.E. Clarke, B. Bond-Lamberty, R.D. Sands, S.J. Smith, A.C. Janetos, and J.A. Edmonds. Implications of limiting co2 concentrations for land use and energy. *Science*, 324:1183–1186, May 29 2009.

[50] J. Fujino, R. Nair, M. Kainuma, T. Masui, and Y. Matsuoka. Multi-gas mitigation analysis on stabilization scenarios using aim global model. *Multigas Mitigation and Climate Policy. The Energy Journal Special Issue*, 2006.

[51] Y. Hijioka, Y. Matsuoka, H. Nishimoto, M. Masui, and M. Kainuma. Global ghg emissions scenarios under ghg concentration stabilization targets. *Journal of Global Environmental Engineering*, 13:97–108, 2008.

[52] K. Riahi, A. Gruebler, and N. Nakicenovic. Scenarios of long-term socio-economic and environmental development under climate stabilization. *Technological Forecasting and Social Change*, 74(7):887–935, 2007.

[53] Montana-Salas Sergio and Michiorri Andrea. Long term climate-driven underground cable thermal ratings for network planning. *Electric Power Systems Research*, 241:111401, 2025.

[54] Fabian Neumann, Elisabeth Zeyen, Marta Victoria, and Tom Brown. The potential role of a hydrogen network in europe. *Joule*, 7(8):1793–1817, 2023.

[55] W. Dorigo and et al Himmelbauer. The international soil moisture network: serving earth system science for over a decade. *Hydrology and Earth System Sciences*, 25(11):5749–5804, 2021.

[56] Roland Hiederer. *Mapping Soil Properties for Europe - Spatial Representation of Soil Database Attributes*. EUR26082EN Scientific and Technical Research. Publications Office of the European Union, Luxembourg, 2013.

[57] E. Kiessling, P. Nefzger, J.E. Nolasco, and U. Kaintzyk. *Overhead Power Lines Planning, Design, Construction – Hard-drawn AL1 ACSR*. PublisherName, City, edition edition, 2019.

[58] TELE-FONIKA Kable S.A. *High and extra high voltage cables*. www.tfkable.com, City, edition edition, 2019.

[59] 529 Working Group A2.36. Guidelines for conducting design reviews for power transformers. Technical Report Report Number, Publisher Name, April 2013.

[60] B. Xiong, F. Neumann, and T. Brown. Prebuilt electricity network for pypsa-eur based on openstreetmap data (0.3) [database], 2024.

6. Appendix

6.1. Power System Components Parameters

The descriptions of the physical parameters for the power system components utilized in this study are provided below. It is important to note that other components, which are not described here, are primarily sourced from the state used for the technical model.

Table 4: Overhead Line Characteristic Data [57]

Designation	Former Code	Cross Section mm^2	Number of Strands	Conductor Diameter mm	DC Resistance $ohms/km$	Current Rating A
243-AL1/39-ST1A	240/40	282,5	26	21,8	0,1188	645

[1] To model the system used in Section 4.3, the distribution of wires according to the voltage is followed in accordance with [27].

Table 5: Underground Cable Characteristic Data [58]

Cross section (mm^2)	Current Rating (A)	Physical Properties					
	90°C	Diameter of conductor (mm)	Nominal insulation thickness (mm)	Diameter over insulation (mm)	Metallic screen cross-section (mm^2)	Diameter over screen (mm)	Outer diameter (mm)
800RM	870	33.0	10.0	54.8	370	61.3	69.0

Table 6: Power Transformer Characteristic Data [59]

Rated power [MVA]	Cooling Type	Voltage ratio [kV]	Total losses (No Load) [kW]	Total losses (Load) [kW]	Color
180	ONAN	500/115	123	211	White

6.2. Comparative Analysis of the qDTR/STR difference in 32 European Countries

The tables presented below follow the same procedure detailed in Section 4.1, but represent the average value and boundary conditions of the results.

Table 7: Comparison in the percentage of qDTR/STR difference in 32 European countries for Power Transformers

Country	POWER TRANFORMER											
	WINTER						SUMMER					
	Day			Night			Day			Night		
	Mean	Min	Max	Mean	Min	Max	Mean	Min	Max	Mean	Min	Max
Albania	21	14	27	23	16	27	0	-10	13	10	-1	18
Austria	21	12	27	23	18	27	0	-11	13	10	0	16
Belarus	23	18	26	24	22	26	-1	-9	9	10	2	15
Belgium	20	13	23	21	13	23	-1	-13	12	8	-2	13
Bulgaria	22	13	32	25	14	32	-1	-15	13	11	-1	20
Croatia	22	15	28	24	16	28	1	-10	14	11	-1	18
Czechia	22	16	27	23	20	27	0	-10	12	10	-1	16
Denmark	18	11	22	18	12	22	-1	-9	9	6	-3	13
Estonia	22	17	25	22	17	25	-1	-7	6	7	-2	12
Finland	23	16	27	24	16	27	-2	-10	7	7	-6	13
France	21	8	28	22	8	27	0	-14	19	10	-5	21
Germany	22	13	26	23	16	26	-1	-13	14	10	-3	17
Greece	22	8	32	24	9	33	-1	-15	15	11	-5	20
Hungary	24	18	30	26	22	30	0	-10	13	12	0	17
Italy	21	10	30	23	14	30	0	-13	16	9	-5	18
Kosovo	24	15	30	27	22	30	1	-10	15	14	3	19
Latvia	22	17	24	22	17	24	-1	-10	8	8	0	13
Lithuania	22	18	25	23	18	25	-1	-8	9	9	-1	14
Luxembourg	21	18	23	22	21	24	-1	-9	13	9	0	15
Moldova	25	17	29	27	24	30	-1	-9	11	12	0	17
Montenegro	21	14	25	22	18	25	0	-8	13	10	-2	17
Netherlands	20	11	23	20	11	23	-1	-13	12	8	-4	14
Norway	19	10	24	20	10	24	-1	-9	11	6	-5	14
Poland	22	15	26	23	17	26	-1	-12	12	10	-3	16
Portugal	23	10	31	25	12	31	1	-16	20	10	-5	21
Romania	23	13	32	26	19	32	0	-14	13	11	0	19
Slovakia	23	15	29	25	21	29	0	-9	12	11	0	17
Slovenia	22	13	26	23	20	26	0	-9	13	10	1	16
Spain	23	5	32	25	8	32	2	-12	21	11	-5	21
Sweden	21	15	25	21	15	25	-1	-10	10	8	-4	14
Switzerland	20	11	24	21	16	24	0	-10	12	8	-4	14

Table 8: Comparison in the percentage of qDTR/STR difference in 32 European countries for OHL

Country	OVERHEAD LINE											
	WINTER						SUMMER					
	Day			Night			Day			Night		
	Mean	Min	Max	Mean	Min	Max	Mean	Min	Max	Mean	Min	Max
Albania	17	4	26	21	12	28	-1	-15	13	12	1	18
Austria	18	8	24	20	17	25	-1	-13	13	11	5	17
Belarus	20	13	28	22	16	29	-1	-12	13	11	0	19
Belgium	17	8	24	19	11	26	-1	-12	11	11	2	19
Bulgaria	19	7	26	22	13	28	0	-13	14	13	0	20
Croatia	19	4	25	22	11	26	-1	-17	11	12	1	18
Czechia	18	10	25	20	15	25	-1	-13	10	11	4	17
Denmark	16	6	24	17	5	25	-2	-14	11	8	-1	17
Estonia	19	10	26	20	10	26	-1	-13	11	9	-2	17
Finland	19	9	27	20	9	27	-1	-15	10	8	-3	18
France	17	2	26	21	6	28	-1	-21	16	12	0	22
Germany	18	8	25	20	9	26	-1	-17	12	11	1	19
Greece	17	1	27	22	10	28	-1	-19	17	13	-1	21
Hungary	20	13	26	23	18	27	-1	-13	10	12	5	19
Italy	16	2	28	20	9	27	-1	-19	14	11	1	19
Kosovo	20	12	26	24	20	27	-1	-14	11	14	7	19
Latvia	19	10	26	21	8	28	-1	-13	11	10	-2	17
Lithuania	19	12	27	21	12	27	-1	-13	9	10	1	19
Luxembourg	18	12	23	20	17	24	-1	-11	10	11	5	16
Moldova	21	14	28	23	19	29	-1	-12	10	12	4	18
Montenegro	18	8	24	22	16	25	-1	-12	10	13	5	17
Netherlands	16	4	23	19	9	25	-1	-14	11	10	0	19
Norway	17	4	25	18	7	26	-1	-14	11	7	-5	16
Poland	19	8	28	21	7	28	-1	-14	12	11	1	20
Portugal	16	-1	27	20	6	28	1	-25	22	14	1	24
Romania	19	9	28	22	16	29	-1	-13	14	12	1	20
Slovakia	19	11	24	21	17	25	-1	-12	9	11	5	18
Slovenia	18	8	24	21	17	25	-1	-13	10	11	5	15
Spain	17	-3	28	21	7	30	0	-23	21	13	-2	26
Sweden	18	8	27	20	8	28	-1	-15	11	9	-3	20
Switzerland	17	7	23	20	17	24	0	-13	12	12	5	16

Table 9: Comparison in the percentage of qDTR/STR difference in 32 European countries for Underground Cables

Country	UNDERGROUND CABLES					
	WINTER			SUMMER		
	Mean	Min	Max	Mean	Min	Max
Albania	6.2	3.8	8.9	0.7	-0.5	2.8
Austria	6.1	4.5	8.1	0.5	-1	3.2
Belarus	7.5	4.8	11.7	0.5	-1.2	5.3
Belgium	6.9	4.5	10.5	0.8	-0.6	3.5
Bulgaria	6.2	3.7	8.2	0.7	-0.8	5
Croatia	6.3	3.8	10.6	0.8	-0.6	3.4
Czechia	6.9	4.7	9.4	0.5	-1.2	3.8
Denmark	6.7	3.7	8.1	0.5	-1.4	4.6
Estonia	6.8	5.1	10.4	0.8	-1	5.2
Finland	7.1	4.6	10.5	0.6	-1.8	5
France	6.5	3.3	10.7	0.8	-0.9	5.3
Germany	7.1	4.6	11.6	0.7	-1.2	5.7
Greece	6	2.6	9.3	0.7	-0.9	5.5
Hungary	6.8	4.5	10.7	0.9	-0.7	5.6
Italy	5.9	3	8.5	0.8	-0.9	4
Kosovo	6.7	4.8	8.1	0.7	-0.5	2.8
Latvia	7	4.7	9.4	0.6	-1.3	4.9
Lithuania	7.2	5.4	11.1	0.6	-1.2	4.5
Luxembourg	7.1	5.1	7.9	0.8	-0.7	3.3
Moldova	6.9	5.1	8.2	0.7	-0.4	2.9
Montenegro	6.3	3.5	7.5	0.9	-0.5	4.6
Netherlands	7.4	4	11.2	1	-0.9	5.2
Norway	6.5	3.8	10.3	0.4	-1.5	5.8
Poland	7.1	4.3	11.5	0.6	-2	5.5
Portugal	6.5	3.2	8.9	0.9	-0.2	3.6
Romania	6.5	4.1	11.2	0.8	-0.7	4.6
Slovakia	6.7	4.5	9.1	0.7	-1.1	5.4
Slovenia	6.3	4.5	7.4	0.6	-0.7	3
Spain	6.1	2.7	10.7	1	-0.5	4.6
Sweden	6.6	4.6	8	0.3	-1.1	4.2
Switzerland	6	4.5	7.6	0.6	-0.5	4.7

Table 10: Variation (in %) for G&TEP Cases

REFERENCE CASE									
Rating	Historical								
Scenario	RCP 26			RCP 45			RCP 85		
Parameter	CAPEX	OPEX	Curtailment	CAPEX	OPEX	Curtailment	CAPEX	OPEX	Curtailment
Fossil	1.02E+11	4.58E+09	0.00E+00	1.18E+11	8.74E+09	0.00E+00	1.18E+11	8.74E+09	0.00E+00
Renewable	1.34E+11	5.84E+09	7.32E+06	1.18E+11	1.68E+09	7.30E+06	1.18E+11	1.68E+09	7.32E+06
Nuclear	8.61E+10	8.50E+09	0.00E+00	8.61E+10	8.50E+09	0.00E+00	8.61E+10	8.50E+09	0.00E+00
Line	5.71E+09	0.00E+00	0.00E+00	5.71E+09	0.00E+00	0.00E+00	5.71E+09	0.00E+00	0.00E+00
Storage	2.78E+10	4.44E+06	0.00E+00	2.78E+10	4.45E+06	0.00E+00	2.78E+10	4.43E+06	0.00E+00
Load	0.00E+00	0.00E+00	0.00E+00	0.00E+00	0.00E+00	0.00E+00	0.00E+00	0.00E+00	0.00E+00
Total	3.55E+11	1.89E+10	7.32E+06	3.55E+11	1.89E+10	7.3015E+06	3.55E+11	1.89E+10	7.32E+06
CASE 1									
Evaluation Method	$1 - qDTR_{\text{Hist}} STR_{\text{Hist}}$								
Scenario	RCP 26			RCP 45			RCP 85		
Parameter	CAPEX	OPEX	Curtailment	CAPEX	OPEX	Curtailment	CAPEX	OPEX	Curtailment
Fossil	-1.59E-01	-9.02E-01	0.00E+00	5.65E-04	3.56E-03	0.00E+00	6.56E-04	3.66E-03	0.00E+00
Renewable	1.21E-01	7.12E-01	6.49E-03	-1.81E-04	1.48E-03	8.45E-05	-3.88E-06	-1.09E-03	4.26E-03
Nuclear	1.16E-05	-5.99E-04	0.00E+00	-2.23E-05	-9.25E-04	0.00E+00	9.43E-06	-6.09E-04	0.00E+00
Line	1.31E-03	0.00E+00	0.00E+00	1.26E-03	0.00E+00	0.00E+00	1.38E-03	0.00E+00	0.00E+00
Storage	0.00E+00	2.62E-03	0.00E+00	0.00E+00	-9.14E-04	0.00E+00	0.00E+00	-1.81E-04	0.00E+00
Load	0.00E+00	0.00E+00	0.00E+00	0.00E+00	0.00E+00	0.00E+00	0.00E+00	0.00E+00	0.00E+00
Total	2.32E-04	1.44E-03	6.49E-03	1.42E-04	1.36E-03	8.45E-05	2.41E-04	1.32E-03	4.26E-03
CASE 2									
Evaluation Method	$1 - qDTR_{\text{RCP}}/qDTR_{\text{Hist}}$								
Scenario	RCP 26			RCP 45			RCP 85		
Parameter	CAPEX	OPEX	Curtailment	CAPEX	OPEX	Curtailment	CAPEX	OPEX	Curtailment
Fossil	1.38E-01	4.77E-01	0.00E+00	1.38E-01	4.77E-01	0.00E+00	-1.03E-04	2.01E-04	0.00E+00
Renewable	-1.38E-01	-2.47E+00	4.57E-04	3.54E-04	-4.53E-04	4.20E-03	-2.24E-04	2.45E-03	-6.10E-04
Nuclear	-2.47E-05	-1.34E-04	0.00E+00	3.02E-06	6.23E-05	0.00E+00	-3.79E-05	-3.16E-04	0.00E+00
Line	-1.37E-04	0.00E+00	0.00E+00	1.80E-06	0.00E+00	0.00E+00	-1.47E-04	0.00E+00	0.00E+00
Storage	0.00E+00	-2.67E-04	0.00E+00	0.00E+00	1.81E-03	0.00E+00	0.00E+00	-3.62E-03	0.00E+00
Load	0.00E+00	0.00E+00	0.00E+00	0.00E+00	0.00E+00	0.00E+00	0.00E+00	0.00E+00	0.00E+00
Total	-6.26E-05	4.88E-05	4.57E-04	4.59E-02	2.20E-01	4.20E-03	-1.20E-04	1.68E-04	-6.10E-04
CASE 3									
Evaluation Method	$1 - qDTR_{\text{RCP}}/STR_{Hist}$								
Scenario	RCP 26			RCP 45			RCP 85		
Parameter	CAPEX	OPEX	Curtailment	CAPEX	OPEX	Curtailment	CAPEX	OPEX	Curtailment
Fossil	6.89E-04	5.67E-03	0.00E+00	1.39E-01	4.79E-01	0.00E+00	5.53E-04	3.86E-03	0.00E+00
Renewable	-1.14E-04	1.45E-03	6.94E-03	1.73E-04	1.03E-03	4.28E-03	-2.28E-04	1.37E-03	3.65E-03
Nuclear	-1.31E-05	-7.33E-04	0.00E+00	-1.93E-05	-8.63E-04	0.00E+00	-2.85E-05	-9.25E-04	0.00E+00
Line	1.17E-03	0.00E+00	0.00E+00	1.26E-03	0.00E+00	0.00E+00	1.24E-03	0.00E+00	0.00E+00
Storage	0.00E+00	2.35E-03	0.00E+00	0.00E+00	8.94E-04	0.00E+00	0.00E+00	-3.80E-03	0.00E+00
Load	0.00E+00	0.00E+00	0.00E+00	0.00E+00	0.00E+00	0.00E+00	0.00E+00	0.00E+00	0.00E+00
Total	1.70E-04	1.49E-03	6.94E-03	4.61E-02	2.21E-01	4.28E-03	1.21E-04	1.49E-03	3.65E-03

B.6 Submitted Papers: Paper G

Optimizing Distribution Planning with Long-Term Thermal Ratings in the Energy Transition

Montana-Salas Sergio, Ruggeri Simona, Soma Gian Giuseppe, Michiorri Andrea, and Celli Gianni

Abstract— **This paper investigates the significance of incorporating component thermal models in long-term electric distribution network planning. The study focuses on overhead lines, power transformers, and underground cables within medium and low voltage networks, considering stresses from distributed photovoltaic integration and electric vehicle charging stations. Two studies were carried out: a planning study is conducted in the medium voltage network, and a network performance indices calculation for the low voltage system. Both studies employed a probabilistic approach, using convolutional and Monte Carlo methods, respectively. Component thermal behavior was analyzed using quasi-Dynamic Thermal Ratings (qDTR) to maximize current-carrying capacity while controlling overcurrent risks. Weather data relative to the last 50 years in Sardinia were used. The results show that when qDTR is applied to urban distribution networks with a peak demand during evening-night hours, it eliminates the majority of overcurrent violations and reduces investment needs. On the other hand, in rural distribution networks influenced by the expansion of photovoltaic production, lower line and transformer ratings are correlated to peak production during hot sunny summer days, and qDTR correctly identifies this situation highlighting a slight increase in violations and network investments that would have been unchecked with less detailed approaches. Additionally, the long-term ratings calculated are more efficient in alleviating thermal constraints in areas with low exposure to high temperatures and solar radiation. This analysis highlights the trade-offs and benefits of applying qDTR across different network and geographic contexts.**

***Index Terms*—Thermal Ratings, Distribution network, Planning, Risk assessment, Power distribution lines, Power transformers.**

I. INTRODUCTION

The expected increase in renewable electricity generation, coupled with the expansion of charging infrastructure to support an estimated fleet of 191 million electric vehicles (EVs) by 2040 [1], is putting pressure on the distribution network at both medium voltage (MV) and low voltage (LV) levels. As a result, distribution system operators are formulating plans to meet emission reduction targets in the medium (2030) and long term (2050). This increased network exploitation leads to increased energy curtailment [1], transformer overloads [2], cable thermal stress [3], and other technical issues. However, the impact of these violations varies depending on geographical factors (e.g., rural or urban settings), location, and the voltage level at which they occur, necessitating specific considerations.

To overcome this, a paradigm shift in distribution network planning is required, moving beyond traditional solutions such as component upgrades or replacements[4]. This shift involves embracing flexibility and leveraging Distributed Energy Resources (DERs) to address temporal constraints caused by the intermittency of Renewable Energy Sources (RES) or grid reconfigurations following failures, all while maintaining reliability [4],[5]. This requires a detailed analysis of both the temporal and spatial dimensions to identify future grid criticalities and guide investments effectively. For instance, the production of photovoltaic (PV) systems is higher during midday, exerting stress on the grid when its thermal capacity is at its lowest. In contrast, electric vehicle charging is expected to substantially increase demand during the evening, when weather conditions such as wind and low temperatures can enhance heat dissipation in distribution grid power systems.

These findings highlight how DERs and EVs can be limited by the thermal capacity of the weakest upstream distribution feeder. Current practice fixes these limits year-round or seasonally, ignoring shorter or daily variations or extreme weather events like heat waves. To enhance the integration of low-carbon

technologies and mitigate congestion, it's crucial to develop strategies that allow operations at above-rated capacity while keeping component temperatures within safe limits.

Among the available options, Dynamic Thermal Rating (DTR) has emerged as a key solution for power transformers (PT), overhead lines (OHL), and underground cables (UGL), maximizing grid capacity, enhancing efficiency, and postponing the need for costly infrastructure upgrades [6]. Numerous studies have investigated the application and advantages, primarily focusing on operational and short-term planning [7],[8],[9]. In these works, real-time measurements and predictive modeling are used to optimize the performance and reliability of distribution feeders.

Due to its real-time nature, long-term distribution planning with DTR has been less explored. However, studies show that using DTR for cables and transformers, along with distributed generation (DG), energy storage systems [10], and local weather data can reduce system vulnerability and optimize capacity planning [11].

Furthermore, integrating DTR and climate considerations has proven effective in optimizing distributed PV systems [12] and adapting to environmental events through network reconfiguration[13]. The value of flexibility in DERs is also being examined via steady-state applications of DTR for lines and cables in [14]. Finally, as discussed in [15], risk management strategies incorporate failure rates and expected energy not supplied to enhance DTR applications in the transmission system, facilitating EV integration while mitigating outage costs.

To the authors' best knowledge, current studies do not incorporate DTR into risk-oriented capacity planning for MV and LV networks. While some studies focus on individual components, there is a gap in long-term climate impact integration. Comprehensive thermal modeling using long-term data could improve capacity planning, enhance grid resilience, and support the integration of EVs and RES. This would enable more robust, climate-adapted distribution network planning.

This paper extends the capacity planning methodology from [5], which uses risk-oriented probabilistic processes to assess network issues caused by DG and EVs in LV and MV networks. It addresses the challenge

of thermal power variability due to climatic uncertainties by adapting the traditional fixed annual or seasonal capacity method to include a probabilistic solution for risk tolerance in long-term planning, known as quasi-Dynamic Thermal Rating (qDTR) [16].

The main contributions of this work, relative to distribution network planning under different load and distributed generation scenarios, are:

- Evaluate the impact of local climate on components' thermal ratings and the occurrence of capacity violations.
- Evaluate the impact of qDTR on risk-oriented distribution planning for different types of networks.

To illustrate its contributions, this work presents case studies: an LV system evaluates the impact of local environmental conditions on grid issues related to EV and PV integration, while MV networks examine the effect of long-term ratings on risk-oriented distribution network planning.

The paper is organized as follows: Section II describes the components' thermal models, the MV planning approach adopted, and the methodology used to evaluate the LV networks. Section III explains the energy scenarios assumed and gives information on the networks and climate dataset. The results are described in Section IV, and conclusions are drawn in Section V.

II. METHODOLOGY

This methodology, illustrated in Fig 1, integrates weather-dependent local components capacity into grid expansion planning. Components thermal modeling is described in **Section II-A**, whilst their influence on distribution system planning is evaluated in **Section IV,** applying the models described in **Sections II-B** and **II-C**, respectively, for MV and LV networks. Static and dynamic data sources are described in **Sections III** and **IV-A/B**.

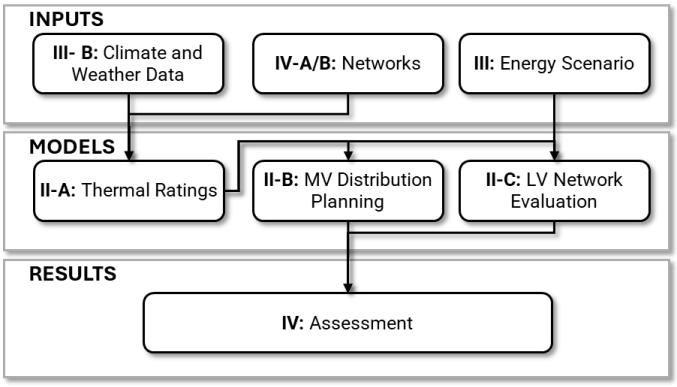

Fig 1 Block scheme of the approach proposed

A. Thermal Ratings

Widely accepted thermal models are used for the calculation of DTR of OHL [17], UGL [18], and PT [19]. These models calculate the steady-state hourly maximum capacity of the selected power system component (I_{OHL}, I_{UGL}, I_{PT}) under environmental conditions at the corresponding local coordinates. The general model is based on the heat balance between the component and the surrounding environment, as described in Eq. (1). Heat is generated from power losses (Q_j), which include Joule heating and core losses, exacerbated by solar radiation or other cables located in the vicinity ($Q_{s/int}$), while environmental factors influence heat exchange through convection (Q_c) from the wind, radiation (Q_r), and conduction (Q_{cd}).

$$\mathrm{Q_j} + \mathrm{Q_{s/int}} = \mathrm{Q_r} + \mathrm{Q_c} + \mathrm{Q_{cd}} \tag{1}$$

In OHL's case, heat is generated by joule losses and gained from solar radiation (ψ_r), while dissipation occurs through convection, influenced by wind speed (w_s) and ambient temperature (θ_a), and radiation, as described in Eq. (2a). The steady state thermal rating is determined in Eq. (2b), where the conductor resistance R_{AC} represents the AC resistance of the conductor at the average temperature of the aluminum strand layers (θ_{avg})

$$\mathrm{Q_j}(I^2R) = \mathrm{Q_c}(\theta_c, \theta_a, w_s, t) + \mathrm{Q_r}(\theta_c, \theta_a, t) - \mathrm{Q_s}(\psi_r, t) \tag{2a}$$

$$I_{OHL} = \sqrt{\frac{Q_r + Q_c - Q_S}{R_{AC}(\theta_{avg})}} \tag{2b}$$

The same formulation can be extended for UGL, as illustrated in Eq. (3a) and (3b), by introducing the conductive heat exchange ($\mathrm{Q_{cd}}$) that depends on the conductor temperature (θ_c) , thermal conductivity (δ_s), and conductor loss factors (λ), while solar heat gain and heat dissipation through radiation and convection are negligible. The current rating is determined from Eq (3b), which is mainly limited by the soil thermal resistivity, represented by the soil thermal resistance (T_4). Additional influencing parameters include the dielectric power loss per unit length (W_d), the number of loaded conductors (n), the maximum allowable conductor temperature rise ($\Delta\theta$), and the series of thermal resistances associated with each part of the cable (T_1, T_2 and T_3) [19].

$$\mathrm{Q_j}(I,\lambda) = \mathrm{Q_{cd}}(\theta_c, \delta_s, \lambda, t) - \mathrm{Q_{int}}(t) \tag{3a}$$

$$I_{UGL} = \left[\frac{\Delta\theta - W_d[0.5T_1 + n(\sum_{b=2}^{4} T_b)]}{RT_1 + nR(1+\lambda_1)T_2 + nR(1+\lambda_1+\lambda_2)(\sum_{b=3}^{4} T_b)}\right]^{(0.5)} \tag{3b}$$

However, insulated conductors (OHL_i) are often found in rural installations, typically in outdoor locations directly exposed to solar radiation. In such cases, external thermal resistance must be adjusted to account for both convective and radiative heat dissipation mechanisms. This additional heat input is quantified by the term $\sigma D^* \psi_r$, where σ denotes the surface absorption coefficient, D^* is the cable's external diameter, and T_4 represents the adjusted thermal resistance of the external environment. The resulting rating expression is adapted as follows:

$$I_{OHL_i} = \left[\frac{\Delta\theta - W_d[0.5T_1 + n(\sum_{b=2}^{4} T_b)] + D^* \psi_r T_4^*}{RT_1 + nR(1+\lambda_1)T_2 + nR(1+\lambda_1+\lambda_2)(\sum_{b=3}^{4} T_b)}\right]^{(0.5)} \tag{3c}$$

For PT, the heat generation includes copper (q_{cu}) and core losses (q_{fe}), while heat is dissipated through convection and radiation, often aided by cooling systems, governed by the oil temperature(θ_o) and the ambient air temperature (θ_a), as shown in Eq. (4a). According to [18], the steady-state top-oil temperature rise above ambient ($\Delta\theta_o$), is related to the load factor K (ratio of actual to rated current) through Eq. (4b). In

this expression, $\Delta\theta_{or}$ is the top-oil temperature rise at rated load, R_{ll} is the ratio of load to no-load losses, P_{LL}/ P_{NL} are load/No-load losses and x is the oil exponent. The corresponding winding hot-spot temperature rise over the top-oil temperature ($\Delta\theta_h$), and the resulting absolute hot-spot temperature (θ_h) is then obtained as Eq. (4b). To ensure that the hot-spot temperature does not exceed the permissible limit ($\theta_{h,lim}$,), K is determined iteratively using Newton's method in Eq. (4c), where $f(K_n)$ represents the nonlinear heat-transfer function. The iteration proceeds until the stopping criterion in Eq. (4d) is met.

$$\mathrm{Q_j}(q_{cu}, q_{fe}) = \mathrm{Q_{c,r}}(\theta_\mathrm{o}, t) + \mathrm{Q_r}(\theta_\mathrm{a}, t) - \mathrm{Q_s}(\psi_\mathrm{r}, t) \tag{4a}$$

$$\left(\frac{1+K^2R_{ll}}{1+R_{ll}} + \frac{\psi_\mathrm{r}}{P_{LL}+P_{NL}}\right)^x \cdot \Delta\theta_{or} = \Delta\theta_\mathrm{h} \text{ where } \theta_h = \theta_a + \Delta\theta_\mathrm{o} + \Delta\theta_\mathrm{h} \tag{4b}$$

$$K_{n+1} = K_n - \frac{f(K_n)}{\frac{df}{dK}(K_n)} \text{ with } f(K_n) = \theta_h(K_n) - \theta_{h,lim} \tag{4c}$$

$$| K_{n+1} - K_n | < \varepsilon \text{ Where } I_{PT} = I_{base} \cdot K_{n+1}\,. \tag{4d}$$

The environmental factors used in each thermal model described in the equations above are obtained from 50-year historical data sets (1973-2023), outlined in Section III-B, to assess the DTR. As expected, the DTR estimation shows significant variability due to complex climatic uncertainties and not a parametric probability distribution, as detailed in [20] for OHL.

To address this variability, this study employs probabilistic thermal ratings or qDTR to calculate the ratings over a long-term horizon, focusing on the lower tail of the probability curve. Readers can refer to [16] for a more comprehensive explanation. However, to facilitate the reading of this document, the procedure followed is briefly summarized here and conceptually illustrated in **Fig *2***:

1. DTRs are calculated hour-by-hour by applying Eq. (2b), (3b), (3c), or (4d) for a period of 50 years, for each geographic location of the component (thin blue lines)
2. The lowest 2% of the results are selected for each month/hour combination of the year.
3. A power law probability distribution is fitted to this set as described in [21] and Eq. (5), where α and β are constants, and x_p is the probability thermal threshold. For instance, the qDTR is represented in red colour for a x_p = 1%.

$$I_{qDTR} = \beta x_p{}^{\alpha} \quad \forall . x \in [0, 2\%] \tag{5}$$

Additionally, **Fig *2***. illustrates how the qDTR framework bridges the gap between the Static and real-time ampacity conditions. The bold blue line traces the hourly ampacity calculated from July to October 2021, revealing temporal variability across the hot season. Red markers indicate specific hours where ampacity fell below the static rating, while the shaded red region highlights periods when qDTR values were lower than the STR. This visualization underscores that even with conservative, fixed annual ratings, a residual risk of line overloading persists, observed in 35 distinct hourly instances. Notably, this risk is almost entirely mitigated when the qDTR method is applied.

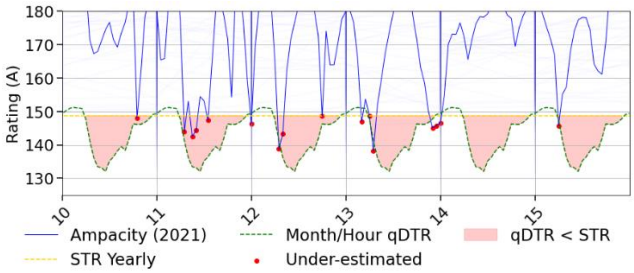

Fig 2 Conceptual illustration of the proposed probabilistic thermal rating. Details hourly ampacity profiles from July to October, with emphasis on August 2021, based on data from 1973 to 2022.

For UGL, monitoring temporal variations in soil conditions is crucial for estimating soil moisture, temperature, and climate change sensitivity. An extended version of the standard methodology [18] is used to capture this variability. Due to the thermal inertia of UGLs, this study estimates conditions monthly [22].

B. MV Distribution Planning

Planning the distribution network during the energy transition requires the use of techniques capable of handling the intermittency of distributed renewable energy resources. The approaches used are detailed for both low- and medium-voltage networks.

For MV networks, the risk-oriented planning procedure proposed in [23], is adopted in the present paper, with the necessary amendments necessary to include the contribution of the qDTR approach. In this approach

suitable daily profiles are used for generation and demand; each profile is discretized in 24 hours, and the uncertainty in the power consumed or generated is modeled through Normal probability density functions. A linearized Probabilistic Load Flow (PLF) is solved for each of the 24 hours of the typical days, both in normal operating conditions and under N-1 contingencies. When the power in each node is known, it is possible to calculate nodal currents, $[I_{node}]^f$, in the f^{th} hour of the typical daily profile by using the nominal voltage. Thus, the voltage in every node can be determined directly, using nodal currents like random variables, with the Eq. (6).

$$[V_{node}] = [Z][I_{node}] \tag{6}$$

where $[\mathbf{Z}]$ denotes the impedance matrix.

The PLF analysis produces two key outputs: the nodal voltage matrix $[V_{node}]^f$ and the branch current matrix $[I_{branch}]^f$. These matrices are described using the mean (μ) and standard deviation (σ) of a normal distribution. Using these results, the probability (p_{tcv}) that the voltage will exceed its regulation limits [V_{min}, V_{max}] or that the current will surpass the conductor's maximum capacity [0, I_{max}] is estimated.

If X is a normally distributed variable with a mean (μ) and standard deviation (σ), representing a specific nodal voltage or line current, the probability that X will exceed a predefined maximum limit (X_{max_lim}) is calculated. First, X is transformed into a standard normal distribution (with μ=0 and σ=1) using the formula $Z=(X-\mu)/\sigma$. Then, the probability $P(Z>Z_{max\_lim})$ as the complement of the cumulative distribution function of the standard normal distribution is calculated, as shown in Eq. (7).

$$P\left(Z > Z_{\max\_lim}\right) = 1 - \frac{1}{\sqrt{2\pi}} \int_{-\infty}^{Z_{\max\_lim}} e^{-\frac{t^2}{2}} dt \tag{7}$$

In the paper, depending on the simulation executed, X_{max_lim} assumes the STR value of the component or its qDTR.

As discussed in [23], the final output is the total risk, R_{TOT}, of the network, expressed in hours of violation per year. R_{TOT} will be compared with the acceptable one, R_A, chosen by the planner. If $R_{TOT} > R_A$, planning options are implemented. When all the planning options have been examined, they are sorted in ascending order with the cost/benefit ratio, i.e., starting from the most effective; the procedure stops when the expected

risk, R_{TOT}, exceeds the maximum allowable risk, R_A. More details about the MV planning approach adopted are available in [23].

Optimizations are guided by the network investment cost, calculated as the Net Present Value of capital expenditures (CAPEX).

C. LV network evaluation

In the present paper, the LV networks will be used to evaluate the influence of local environmental conditions on grid criticalities to integrate EV and PV distributed generation penetration.

The procedure proposed in [24] is applied to identify critical events and estimate their occurrence, utilizing a Monte Carlo (MC) approach to simulate a wide range of network conditions. The MC simulation is performed on the network using unbalanced power flow calculations with the OpenDSS engine [25]. The process begins by randomly selecting an hour of the year, followed by performing unbalanced power flow calculations. These calculations derive values for load demand, PV production, and EV energy requirements based on predefined distributions. The power flow analysis evaluates the network state for the selected hour, specifically assessing the occurrence of technical violations such as excessive voltage drops, overvoltages, or thermal overloads.

Equation (8) expresses the constraints applied to identify these violations.

$$\begin{cases} S_{tr}(t) > S_{r,tr} \\ I_l(t) > I_{r,l} \\ V_i(t) > V_{max};\ V_i(t) < V_{min} \end{cases} \quad (8)$$

Where:

- $S_{tr}(t)$is the apparent power through the transformer (tr) at time t,
- $S_{r,tr}$is the rated capacity of the transformer,
- $I_l(t)$ is the current flowing through line l at time t,
- $I_{r,l}(t)$ is the rated current of line l,
- $V_i(t)$ is the voltage magnitude at bus i at time t,

- V_{max} and V_{min} are the maximum and minimum allowable voltage levels (± 5%).

The procedure is repeated iteratively until the MC stop criteria are satisfied: the maximum number of iterations or a given threshold ε to the convergence parameter β_n, calculated as in Eq. (9).

$$\beta_n = \frac{\sqrt{\sigma^2(h_v)}}{\mu(h_v)\cdot\sqrt{n}} \leq \varepsilon \qquad n = 1 \dots N \tag{9}$$

where n is the number of the current extraction, and $\sigma(h_v)$ $\mu(h_v)$ are the variance and the mean value of the h_v occurrence of violations (expressed in hours per year) calculated until the n^{th} extraction.

III. Energy Scenario and Weather Data

The increase in electricity load demand and production from RES derives from a previous study [5] carried out at regional and provincial bases to evaluate the potential to become a green model for the energy transition, thanks to the high electrification rate and the use of substantial renewable resources. Concerning demand, the load growth is guided by the Italian National Energy and Climate Plan. In the transport sector, the region is characterized by EVs' minimal spread (less than 0.01% of the total number of cars). However, thanks (also) to a greater spread of charging stations and the favourable costs of owning and operating vehicles, the share of EVs in 2050 is expected to be higher than 70%.

Charging facilities are typically located at two levels: 1) Home Charging Stations (HCS) at residential premises in LV networks and 2) Quick Charging Stations (QCS) in car parks or company facilities, and Fast Charging Stations (FCS) in refuelling stations or urban areas, both connected to the MV grid.

More details about the assumptions for the scenario adopted, including the load and generation growth, are reported in [16].

A. MV and LV networks profiles

Yearly customers' behaviour has been modelled through 12 daily curves (working day, Saturday, and Sunday for each season), discretized at a one-hour step resolution. These profiles have been derived from DSO's measurements or standard profiles differentiated by sector (e.g., residential, commercial…). Specific tools are used for charging station demand profiles, such as Fast Charging Stations (FCS) and Quick Charging

Stations (QCS) [27],[28]. These tools estimate daily charging profiles using random sampling, considering factors like driving distances, vehicle characteristics (battery capacity and consumption), charging rates, and driver habits. The coverage area and number of cars served also influence FCS and QCS profiles. For Home Charging Stations (HCS), the International Energy Agency's (IEA) online tool is used to generate various cases, building mean daily profiles based on EV model, charger power, and driver habits (e.g., travel distance, arrival and departure times) [26]. The planning period is 2024-2050, with an admissible voltage violation of ±5% and a maximum acceptable risk of 5 hours/year.

B. Climate and Weather Data

Historical meteorological data have been obtained from the ERA reanalysis. Mainly for the Sardinia region, covering the period from 1970 to 2023, with hourly resolution. Since the methodology for calculating thermal capacities requires more extensive information, a data description can be found in [22].

IV. RESULTS

This section explores how enhanced thermal rating affects network capacity planning under different load growth and DER penetration scenarios, considering the impact of local climate on network criticalities. Case studies will illustrate these contributions. The LV system is used to assess how local environmental conditions influence grid criticalities when integrating EVs and PV distributed generation. Conversely, the impact of qDTR is analysed on a representative portion of the MV distribution system, which includes distributed renewable energy sources (mainly PV) and high electrification of end-use energy.

A. qDTR results

Following a common practice in the industry, the STRs are normally calculated using historical values for the reference case. However, this approach may not fully account for the specific microclimate which has the potential to considerably alternate the effective component capacity. To counteract this, the qDTR is calculated for the PT, UGL and OHLs across the network, using representative MV/LV transformers and LV lines. It is crucial to maintain the load on power distribution equipment within acceptable risk margins to

ensure the safe operation of distribution networks and prevent overheating. To address this, a thermal fix probabilistic overload threshold of x_p = 1% to compute the qDTR is employed.

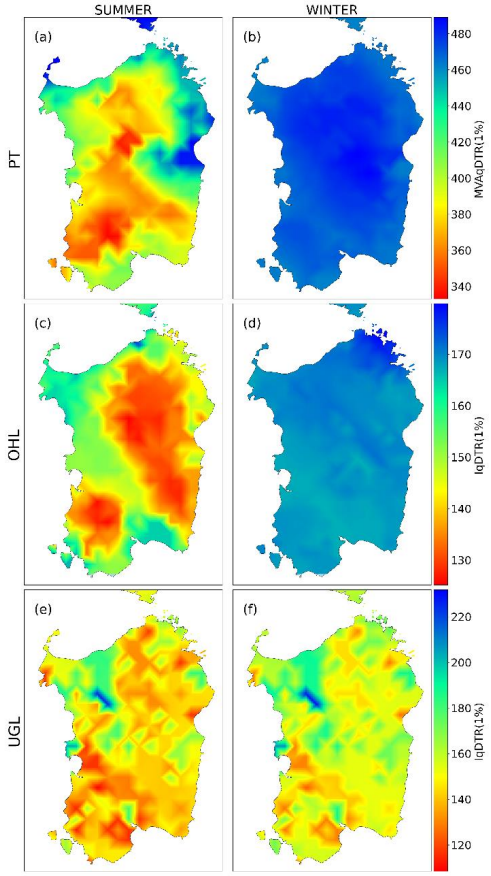

Fig 3 Geographical patterns of the qDTR difference over fifty years in historical reanalysis.

First, to understand the regional effect, a spatiotemporal analysis of the region is conducted to identify zones in the Sardinia region where climatic factors may have moderate, negligible, or extreme impacts. This can be seen in **Fig 3**, where geographical patterns of the qDTR difference over fifty years in historical reanalysis for PT (a, b), OHL (c, d) and UGL (e,f) are shown. The first column shows a typical summer day (h 14:00), and the second column a typical winter night (h 21:00). For instance, the southwest zone is anticipated to have a greater impact on PT than the north zone due to the consistent temperature increases

during summer. In contrast, the OHL must also account for wind as a critical factor, which could result in the creation of new impact zones. Concerning UGL, it does not reflect a certain pattern, given the preponderant influence of soil type.

Fig 4 illustrates how qDTR affects a distribution power component by showing the monthly variation of OHL thermal limits for the MV networks in the case study. The black dashed line represents the STR, while the other curves show qDTR for various conductor types and geographical areas. This highlights the seasonal influence of climate, with thermal limits increasing in autumn and winter, and qDTR converging closer to STR in summer.

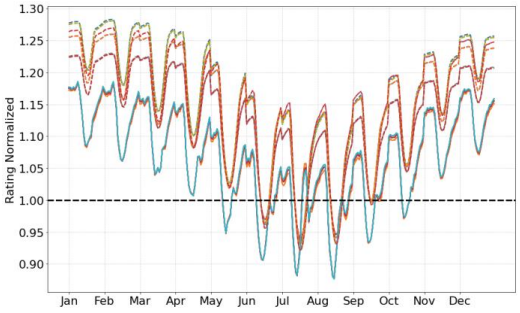

Fig 4 qDTR for the OHL types in the MV networks case study.

B. Influence of environmental conditions on LV criticalities

Here, the impact of local climate factors on the LV system is estimated. The network is analysed across three areas characterized by distinct climatic conditions based on historical data (1973–2023). To illustrate this, unfavourable conditions are defined as temperature > 35 °C, irradiation > 800 W/m², wind speed < 0.5 m/s, and precipitation < 0.2 mm. Area 1 experiences relatively low exposure to high temperatures—over 90% lower than Area 2, making it less affected by extreme climatic stress. In contrast, Area 3 shows the opposite pattern, with temperature exceedances 16 times higher than in Area 1. This trend also extends to precipitation, as Area 3 records values 1.8 times lower than Area 2, indicating drier conditions that intensify the thermal stress on the UGL.

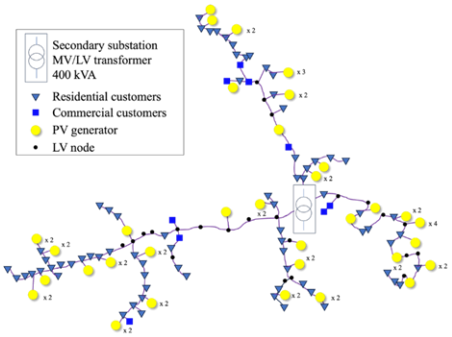

Fig 5 LV network adopted in the Case Study.

TABLE I - LV CASE STUDY DESCRIPTION

LV/MV Transformer	400 kVA - Indoor	
LV Users	350	
LV Feeders	3	
Lines	157	
Total lines length	0.76 km	
	Energy Scenarios	
	Existing (2024)	Future (2050)
PV (number/Pnom)	11 / 40 kW	57 / 226 kW
Number of HCS	20	44
Electricity demand	387 MWh/year	1362 MWh/year

The LV network used for the studies is shown in **Fig 5Error! Reference source not found.**. It represents an urban LV network characterized by high residential load penetration. The nodes are shape-coded based on the predominant user type (residential or commercial), highlighting PV plants. Table I reports the network's main characteristics and the existing (2024) and future (2050) scenarios, in terms of installed PV capacity, number of HCS, and load electrification stage. A common PV generation profile is adopted for all areas to ensure consistent comparisons and isolate the impact of QDTR across scenarios.

The procedure described in section II-C is applied to the network described above, using the standard methodology (STR approach). Simulation results in the three areas indicate a high frequency of overload violations, accounting for 97% of all observed violations in the network during the evening between 19:00 and 24:00. These overload violations are mainly concentrated on two lines: line 32 (the first branch of feeder F3) and line 121 (the first branch of feeder F2), which collectively contribute to 79% of the cases. In addition, PT overload cases occur mainly between 19:00 and 22:00.

Subsequently, the qDTR is implemented on the most affected components, specifically the PT and the first lines of feeder F2 and F3. As shown in **Fig *6***, qDTR enhances the STR, enabling up to a 35% increase over the fixed rating during the winter months (January in Area 2), making it an effective approach for alleviating network stress. However, during certain summer periods, particularly in the morning hours, a residual risk of overload remains due to unfavourable climatic conditions, as highlighted in light red.

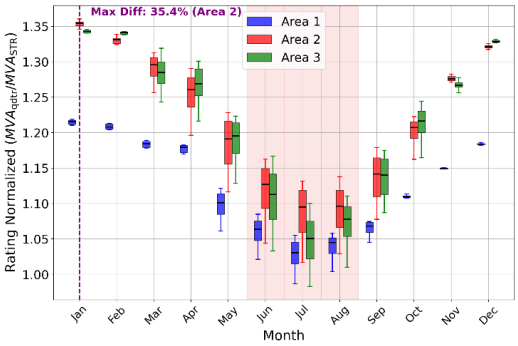

Fig 6 Monthly comparison of normalized ratings $(MVA_{\mathrm{qdtr}}/MVA_{\mathrm{STR}})$ for the PT in the LV network over selected Areas, during the night hours 18h-23h. Light red shading indicates months with overload risk, where qDTR falls below STR, while the purple dashed line indicates the month with the maximum deviation.

The LV network is reassessed using new dynamic ratings for three areas. **Fig 7** shows the hourly distribution of overload violations across all components, highlighting improvements with qDTR. Additionally, TABLE IV provides the percentage difference in monthly and hourly violations. Both representations mainly reflect the following aspects:

- The future scenario analysed requires a high penetration of HCS, but implementing qDTR across all regions mitigates the risk of violations, as shown in **Fig 7**. This approach is particularly effective during nighttime hours, achieving reductions from 24.6% to 100%. It addresses the limitations of conservative STR applications by guiding operators on areas with the most significant reductions, notably Area 1, where performance is best, primarily due to OHL.
- The regional impact of climatic factors, as shown in TABLE IV, aligns with the outcomes of applied capacity in reducing violations. Specifically, Area 3 has the lowest reduction in OHL overload violations, similar to Area 1 for PT. This is due to constant nighttime temperatures and weak wind speeds in Area 3, which minimize the difference between qDTR and STR. In contrast, Area 1 for PT shows a smaller qDTR/STR difference during nighttime in colder months compared to Area 2, as seen in **Fig *6***, highlighting the region's unique climate.

C. Influence of qDTR on MV distribution network planning

To examine the impact of qDTR on MV distribution network planning, two case studies address different issues. They vary by conductor type and technical violations on the existing network. High PV generation and low load density cause daytime overvoltage and power congestion during peak PV production. Conversely, evening peak demand leads to overcurrent or voltage drops due to load electrification and weak overhead lines. The two cases are described below:

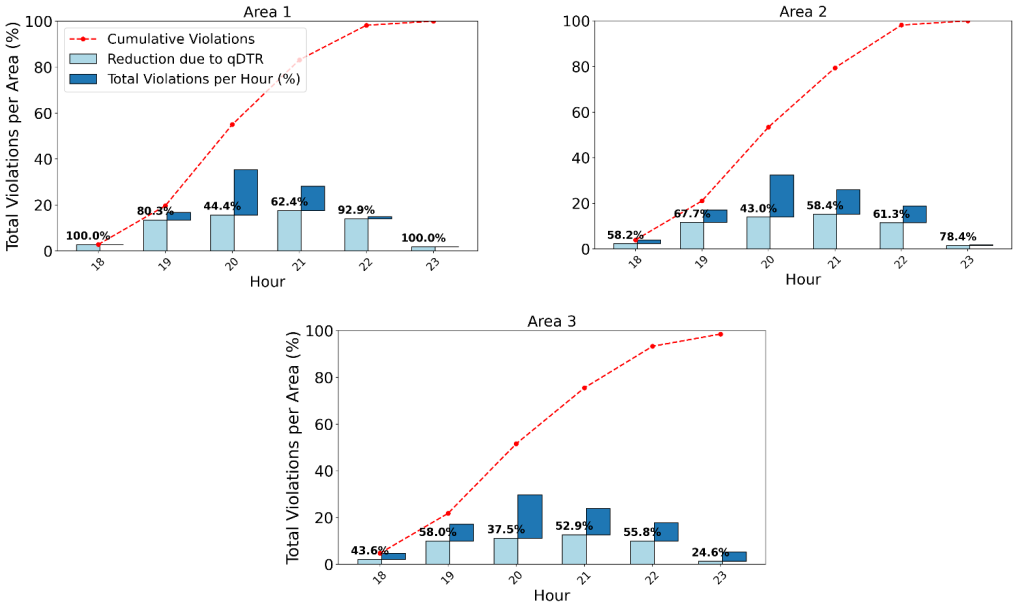

Fig 7 Impact of qDTR on Reducing Overload Across Areas

Case "A" (Fig. 8) is an urban MV network portion, consisting of overhead lines, that experiences only overcurrent violations. It has three feeders with 50 buses, supplying 5 MV loads and 37 LV networks via MV/LV substations. Key data, including the partition into UGL and OHL and the total electric demand (expressed as nominal power, Pnom), are summarized in Table II. The demand comprises a mix of agricultural, residential, and small industrial customers. The network characteristics (around 10-11 km length per feeder, around 500 kW per MV node) and the overhead distribution (OHL) make it a typical urban network of medium towns. For these cases, the most probable technical violation is the overcurrent, often

due to high load. These are the main aspects that make the qDTR effective.

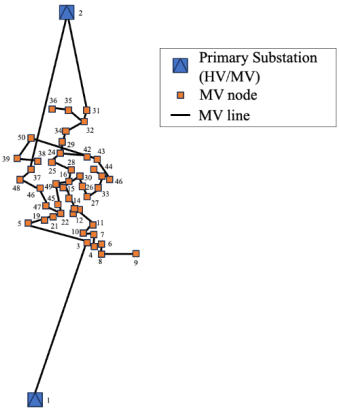

Fig 8 MV Networks adopted in the Case Study – Case A

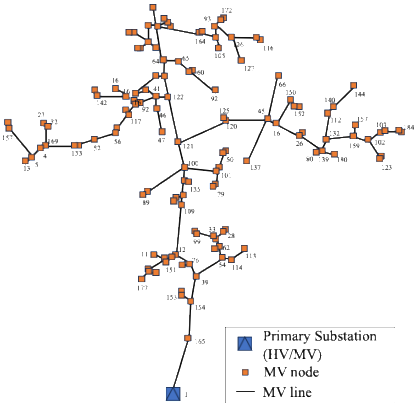

Fig 9 MV Networks adopted in the Case Study – Case B

In case "B," a rural MV feeder with some UGL branches (5% of lines) experiences simultaneous overcurrent and overvoltage issues due to overgeneration. Key feeder data is in TABLE II, and network details are shown in Fig 9. The typical technical violation of this kind of network is the overvoltage. Overcurrent may happen due to high penetration of generation (PV) plants. Being often exposed to high solar radiation (but also to wind), the adoption of DTR can bring out neglected overcurrent situations.

TABLE II - MV CASE STUDIES DESCRIPTION

	CASE A		**CASE B**	
MV Feeders	3		1	
UGL-OHL [%]	0%-100%		5%-95%	
MV/LV transformers (Pole Mounted)	37		60	
Total lines length	33.1 km		99.1 km	
	Energy Scenarios			
	2024	2050	2024	2050
PV (P_{nom})	2.3 MW	3.4 MW	0.3 MW	7.2 MW
P_{load}	20 MW	26.3 MW	5.2 MW	6.3 MW

The TABLE III presents the simulation results, showing yearly technical violations (h_{viol}) for the existing network and the CAPEX required to address these issues. The results align with the qDTR behaviour illustrated in **Fig 4**, quantifying the impact on technical violations and network investments.

TABLE III- RESULTS FOR THE MV CASE STUDIES

		Without qDTRcontribution	With qDTRcontribution
Case A	CAPEX [M€]	0.1	0 (-100.0%)
	hviol [hours/year]	199	0 (-100.0%)
Case B	CAPEX [M€]	13.4	13.7 (+2.2%)
	hviol [hours/year]	3,258	3,270 (+0.37%)

Case A focuses on overcurrent conditions, primarily occurring between 17:00 and 21:00 on working days. Network interventions are required to address these issues, with a CAPEX of 100 k€ over the planning period. Including qDTR in the planning eliminates technical violations by allowing higher thermal limits.

During PV production hours (10:00–18:00), Case B faces simultaneous overcurrent and overvoltage violations, amounting to 3,258 hours annually. Resolving these issues would require an estimated investment of 13 M€ over the planning period. Introducing qDTR leads to a slight rise in reported violations (+3.7%) and associated network costs. However, this increase actually represents a safety improvement: while the base case would overlook these thermal overloads, qDTR identifies them during planning, preventing unexpected flexibility or curtailment needs and reducing risks in passive networks. Although qDTR does not address overvoltage issues, its value lies in exposing previously undetected overcurrent occurrences.

D. Discussion

The examples demonstrate qDTR's contribution to distribution network planning. Properly integrating qDTR into planning models helps avoid overestimating or underestimating technical violations and network investments. The results show that qDTR, which considers extreme weather impacts, affects urban and rural networks differently. It can positively impact grids expecting increased mobility, as seen in LV violation analysis and MV Case A (TABLE III). However, it also highlights the risk of overloading during high-temperature seasons, particularly in grids with significant PV (TABLE III).

TABLE IV - PERCENTAGE DIFFERENCE IN MONTHLY/HOURLY VIOLATIONS WHEN USING $qDTR_H$ INSTEAD OF STR_H

		Area 1 -Hour						Area 2 -Hour						Area 3 -Hour					
	Typical	**18**	**19**	**20**	**21**	**22**	**23**	**18**	**19**	**20**	**21**	**22**	**23**	**18**	**19**	**20**	**21**	**22**	**23**
OHL	**1**	-100	-100	-39	-51	-100	-	-100	-100	-45	-51	-100	-100	-100	-100	-39	-51	-100	-100
	2	-100	-88	-64	-100	-	-	-100	-98	-84	-100	-100	-	-100	-94	-64	-100	-100	-
	3	-100	-82	-67	-100	-	-	-100	-96	-91	-100	-100	-	-100	-89	-81	-100	-100	-
	4	-100	-100	-84	-92	-100	-	-100	-100	-94	-96	-100	-100	-100	-100	-87	-90	-100	-100
	5	-100	-80	-3	-100	-100	-	-100	-89	-10	-100	-100	-	-100	-80	-9	-97	-100	-
	6	-	-100	-97	-100	-100	-	-	-100	-100	-100	-100	-	-100	-100	-98	-100	-100	-100
	7	-	-99	-15	-9	-65	-100	-100	-100	-25	-20	-78	-100	-100	-98	-10	-3	-43	-100
	8	-100	-86	-54	-100	-	-	-100	-89	-69	-100	-	-	-100	-82	-62	-100	-100	-
	9	-100	-97	-74	-100	-	-	-100	-97	-83	-100	-100	-	-100	-95	-54	-100	-100	-
	10	-100	-1	-19	-42	-90	-	-100	-36	-20	-42	-90	-100	-100	-44	-20	-42	-90	-100
	11	-100	0	-3	-18	-100	-	-100	-33	-31	-50	-100	-	-100	-40	-35	-24	-100	-
	12	-100	-18	-26	-100	-	-	-100	-62	-57	-100	-100	-	-100	-55	-53	-100	-100	-
	OVERALL	- 67.54%						-68.12%						-60.09%					
PT	**1**	-	-100	-100	-100	-100	-	-	-100	-100	-100	-100	-	-	-100	-100	-100	-100	-
	2	-	-100	-100	-100	-	-	-	-100	-100	-100	-	-	-	-100	-100	-100	-100	-
	3	-	-100	-100	-	-	-	-	-100	-100	-100	-	-	-	-100	-100	-100	-	-
	4	-	-	-100	-100	-	-	-	-100	-100	-100	-100	-	-	-100	-97	-98	-100	-
	5	-	-	-100	-	-	-	-	-100	-100	-100	-	-	-	-100	-97	-100	-	-
	6	-	-	-	-	-	-	-	-	-100	-100	-	-	-	-100	-100	-100	-	-
	7	-	-	-100	-100	-	-	-	-100	-100	-100	-100	-	-	-100	-99	-98	-100	-
	8	-	-	-	-	-	-	-	-	-100	-	-	-	-	-100	-100	-100	-	-
	9	-	-	-	-	-	-	-	-	-100	-	-	-	-	-100	-100	-	-	-
	10	-	-76	0	-34	-100	-	-100	-98	-3	-68	-100	-	-100	-76	0	-38	-100	-
	11	-	-100	-64	-100	-	-	-100	-100	-97.2	-100	-	-	-100	-100	-64	-100	-	-
	12	-	-100	-96	-	-	-	-	-100	-100	-100	-	-	-100	-100	-96	-100	-	-
	OVERALL	-82.83%						-92.43%						-89.19%					

Note: 1) The symbol "–" indicates that no violations were registered in that specific hour of the representative monthly day for the corresponding area and scenario.

2) The overall reduction is calculated based on the total number of violations between 18:00 and 23:00 over the representative days, using the following expression**:**

$$\frac{\sum_{Day=1}^{12}\sum_{Hour=18}^{23}\left(\text{Violation}_{STR,Day,Hour}\right)-\sum_{Day=1}^{12}\sum_{Hour=18}^{23}\left(\text{Violation}_{qDTR,Day,Hour}\right)}{\sum_{Day=1}^{12}\sum_{Hour=18}^{23}\left(\text{Violation}_{STR,Day,Hour}\right)}$$

However, far from concluding the studies on this topic, this work opens the path for future improvements, which include:

- A probabilistic framework should be developed to quantify the risk associated with DTR methodologies. This formulation aims to link the adopted DTR threshold risk level (e.g., 1%) to the probability of exceeding the actual thermal limit, expressed as $P(I_{max} > I_{DTR})$. Such an approach requires the characterization of the probability density functions for the flow and rating, which are partially correlated. For this, advanced statistical techniques, including convolution methods and Monte Carlo simulations, can be employed to establish a benchmark for evaluating and comparing different thermal rating strategies under uncertainty.
- This study uses historical weather values for qDTR calculation. It could be improved by creating unified scenarios for weather, demand, and renewable generation based on common climatic scenarios. This would also need the creation of localized climatic projections at finer resolution.
- This study considers losses, but not the aging due to potentially higher temperatures and potentially higher voltages that should be investigated.
- The PLF implemented in the MV planning approach includes only normal distribution functions. Further work can be undertaken to integrate different probabilistic functions.

V. CONCLUSION

This paper incorporates weather-dependent local grid capacity into distribution network planning during the energy transition, using qDTR as a long-term probabilistic solution with a specified risk tolerance.

When evaluating the same scenario across three geographically distinct areas for LV networks described in TABLE V, the results show that although there are generally positive effects on reducing violations, the use of long-duration ratings is more efficient in areas with low exposure to high temperatures and solar irradiation. This analysis of both the temporal and spatial dimensions provides a strategy for identifying future network criticalities, enabling the effective targeting of investments and prioritization of areas where they will have the greatest impact.

When different network types are used to examine the effect of long-term ratings on risk-oriented distribution

network planning, the qDTR relates network thermal risk to higher PV expansion, as in Case B, resulting in a slight increase in breaches (+3.7%) and network investments. However, under certain conditions, its application in planning eliminates technical violations—primarily occurring between 17:00 and 21:00 on weekdays and reduces the need for 100% of the necessary investments. Reflecting the trade-off characteristic of qDTR.

It can be concluded that adopting a long-term approach to increasing thermal capacity provides significant benefits, including deferred investments, support for HCS expansion in reclaimed areas, and enhanced safety and reliability of existing infrastructure, thereby improving overall system operational safety.

REFERENCES

[1] Draghi, M. (2024). The future of European competitiveness. Report Part A. A Competitiveness Strategy for Europe. September.

[2] H. Ramadan, A. Ali and C. Farkas, "Assessment of plug-in electric vehicles charging impacts on residential low voltage distribution grid in Hungary," 2018 6th International Istanbul Smart Grids and Cities Congress and Fair (ICSG), Istanbul, Turkey, 2018, pp. 105-109, doi: 10.1109/SGCF.2018.8408952.

[3] Csányi, G.M., Tamus, Z.Á., Varga, Á. (2017). Impact of Distributed Generation on the Thermal Ageing of Low Voltage Distribution Cables. In: Camarinha-Matos, L., Parreira-Rocha, M., Ramezani, J. (eds) Technological Innovation for Smart Systems. DoCEIS 2017. IFIP Advances in Information and Communication Technology, vol 499. Springer, Cham. 10.1007/978-3-319-56077-9_24

[4] F. D. Martín, M. Hable, R. Bessa, J. Lassila, C. Imboden and A. Krula, Final Report Flexibility in Active Distribution Systems, Jan. 2021, [online] Available: http://www.cired.net/cired-working-groups/flexibility-in-active-distribution-systems-wg-2019-3.

[5] G. Celli, G. Pisano, S. Ruggeri, G. G. Soma, F. Pilo, C. Papa, C. Pregagnoli, L. De Carolis, S. Ferrero, F. Cazzato, Distribution Systems as Catalysts for Energy Transition Embedding Flexibility in Large-Scale Applications, IEEE Access, vol. 12, pp. 92227-92240, 2024. DOI: 10.1109/ACCESS.2024.3421615

[6] D. Roberts, P. Taylor, and A. Michiorri, Dynamic thermal rating for increasing network capacity and delaying network reinforcements, in Proceedings of CIRED Seminar 2008: Smart Grids for Distribution, 2008.

[7] Y. Li, Y. Wang, and Q. Chen, Optimal Dispatch With Transformer Dynamic Thermal Rating in ADNs Incorporating High PV Penetration, IEEE Transactions on Smart Grid, vol. 12, no. 3, pp. 1989-1999, May 2021. DOI: 10.1109/TSG.2020.3037874

[8] J. Yang, X. Bai, D. Strickland, L. Jenkins, and A. M. Cross, Dynamic Network Rating for Low Carbon Distribution Network Operation—A U.K. Application, IEEE Transactions on Smart Grid, vol. 6, no. 2, pp. 988-998, March 2015. DOI: 10.1109/TSG.2015.2389711

[9] N. Viafora, K. Morozovska, S. H. H. Kazmi, T. Laneryd, P. Hilber, and J. Holbøll, Day-ahead dispatch optimization with dynamic thermal rating of transformers and overhead lines, Electric Power Systems Research, vol. 171, pp. 194-208, Jun. 2019.

[10]Y. Li, J. Teh, and B. Alharbi, Optimizing distributed generation and energy storage in distribution networks: Harnessing metaheuristic algorithms with dynamic thermal rating technology, Journal of Energy Storage, vol. 91, 111989, 2024. DOI: https://doi.org/10.1016/j.est.2024.111989

[11]Y. Li, Q. Chen, G. Strbac, K. Hur, and C. Kang, Active Distribution Network Expansion Planning With Dynamic Thermal Rating of Underground Cables and Transformers, IEEE Transactions on Smart Grid, vol. 15, no. 1, pp. 218-232, Jan. 2024. DOI: 10.1109/TSG.2023.3266782

[12]Y. Li, Y. Wang, C. Kang, J. Song, G. He, and Q. Chen, Improving distributed PV integration with dynamic thermal rating of power distribution equipment, iScience, vol. 25, no. 8, 104808, 2022. DOI: https://doi.org/10.1016/j.isci.2022.104808

[13]M. Rostamzadeh, M. H. Kapourchali, L. Zhao, and V. Aravinthan, Optimal Reconfiguration of Power Distribution Grids to Maintain Line Thermal Efficiency During Progressive Wildfires, IEEE Systems Journal, vol. 18, no. 1, pp. 632-643, March 2024. DOI: 10.1109/JSYST.2023.3339771

[14]S. Klyapovskiy, S. You, A. Michiorri, G. Kariniotakis, and H. W. Bindner, Incorporating flexibility options into distribution grid reinforcement planning: A techno-economic framework approach, Applied Energy, vol. 254, 113662, 2019. DOI: https://doi.org/10.1016/j.apenergy.2019.113662

[15]S. F. Hajeforosh, H. Bakhtiari, and M. Bollen, Risk assessment criteria for utilizing dynamic line rating in presence of electric vehicles uncertainty, Electric Power Systems Research, vol. 212, 108643, 2022. DOI: https://doi.org/10.1016/j.epsr.2022.108643

[16]S. Hadiwidjaja, S. D. Montana Salas, and A. Michiorri, Quasi-Dynamic Line Rating spatial and temporal analysis for network planning, HAL Archives Ouvertes, 2023. Retrieved from https://hal.archivesouvertes.fr/hal-03766110v2

[17]J. Iglesias, G. Watt, D. Douglass, V. Morgan, R. Stephen, M. Bertinat, D. Muftic, R. Puffer, D. Guery, S. Ueda, K. Bakic, and S. Hoffmann, Guide for thermal rating calculations of overhead lines (CIGRE 601), Paris: CIGRE, 2014.

[18]International Electrotechnical Commission, IEC 60287-1-1: Electric cables—Calculation of the current rating—Part 1-1: Current rating equations (100% load factor) and calculation of losses—General, Geneva, Switzerland: International Electrotechnical Commission, 2014.

[19]International Electrotechnical Commission (IEC), IEC 60076-7:2018, Power transformers - Part 7: Loading guide for mineral-oil-immersed power transformers, Geneva, Switzerland: International Electrotechnical Commission, 2018.

[20]J. Zhan, C. Y. Chung and E. Demeter, "Time Series Modeling for Dynamic Thermal Rating of Overhead Lines," in IEEE Transactions on Power Systems, vol. 32, no. 3, pp. 2172-2182, May 2017, doi: 10.1109/TPWRS.2016.2596285.

[21]A. Clauset, C. R. Shalizi, and M. E. J. Newman, Power-Law Distributions in Empirical Data, SIAM Review, vol. 51, no. 4, pp. 661–703, 2009. DOI: 10.1137/070710111

[22]Montana-Salas Sergio, Michiorri Andrea, Long term climate-driven underground cable thermal ratings for network planning, Electric Power Systems Research, Volume 241, 2025, 111401, ISSN 0378-7796, https://doi.org/10.1016/j.epsr.2024.111401.

[23]G. Celli, F. Pilo, G. Pisano, S. Ruggeri and G. G. Soma, "Risk-oriented planning for flexibility-based distribution system development", Sustain. Energy Grids Netw., vol. 30, Jun. 2022.

[24]S. Conti, A. Melis, G. Pisano, F. Pilo, S. Ruggeri, and G. G. Soma, Risk-oriented assessment of LV distribution network hosting capacity for electric vehicles, IET Conference Proceedings, vol. 2024, no. 5, pp. 665668, 2024. DOI: https://doi.org/10.1049/icp.2024.2125

[25]EPRI OpenDSS. Available online: https://www.epri.com/pages/sa/opendss (accessed on 30 October 2024).

[26]Electric Vehicle Charging and Grid Integration Tool Available online: https://www.iea.org/data-and-statistics/data-tools/electric-vehicle-charging-and-grid-integration-tool

[27]G. Celli, M. Galici and F. Pilo, "Definition of a Stochastic Charging model of EV Aggregation and Estimation of its Flexibility Amount," presented at 2022 2nd International Conference on Energy Transition in the Mediterranean Area (SyNERGY MED), Thessaloniki, Greece, 2022, pp. 1-5, 10.1109/SyNERGYMED55767.2022.9941468.

[28]G. Celli, G. G. Soma, F. Pilo, F. Lacu, S. Mocci and N. Natale, "Aggregated electric vehicles load profiles with fast charging stations," presented at 2014 Power Systems Computation Conference, Wroclaw, Poland, 2014, pp. 1-7, 10.1109/PSCC.2014.7038402.

B.7 Published Papers: Conference A

Weather-Based Quasi Dynamic Thermal Ratings for Power Transformers

Sergio-Daniel Montana-Salas
Centre PERSEE
Mines Paris - PSL
Sophia Antipolis, France
sergio-daniel.montana-salas@minesparis.psl.eu

Andrea Michiorri
Centre PERSEE
Mines Paris - PSL
Sophia Antipolis, France
andrea.michiorri@minesparis.psl.eu

2023 IEEE PES Innovative Smart Grid Technologies Europe (ISGT EUROPE) | 979-8-3503-9678-2/23/$31.00 ©2023 IEEE | DOI: 10.1109/ISGTEUROPE56780.2023.10408026

***Abstract*—This paper presents a preliminary study on climate change's impact on power transformers' ratings. This limit depends on the difference between air temperature and the maximum continuous allowable hot-spot oil temperature. On the other hand, atmospheric temperatures are expected to rise in the following years in Europe in a range between 0.52% and 8.18% Celsius degrees, according to the scenario. This will result in a rating reduction for existing and newly installed transformers.**

This study proposes a methodology to quantify this phenomenon and estimate its effect on several use cases. This is achieved by combining the transformers thermal model described in the IEC 60076-7 loading guide, historical meteorological reanalyses for 1970-2021, and climatic projections for 2022-2072 based on different greenhouse gas emissions hypotheses. Simulations are carried out using a quasi Dynamic Thermal Rating approach for HV transformers in the southeastern regions of France.

Results show how the methodology proposed allows for a 6% rating increase in the cooler hours of the day and that projected future ratings are expected to be 5.031% - 0.194% lower than the historical ones.

***Index Terms*—Power Transformers - Transformer Thermal - Dynamic Rating - Probabilistic forecasting**

I. Introduction

The climate change repercussions on the electric network have been analysed in [1], [2], showing transmission rating reductions from 5% to 15% over the long term and mainly influenced by ambient temperature. The effects of this rating reduction and new energy demand projections in [3], involve significant and costly network reinforcement or expansion to maintain the system's reliability.

In the transmission and distribution network, power transformers (PT) are critical assets connecting power plants and customers. Their failure could lead to outages, environmental risks, up to loss of life.

Therefore, with projections that anticipated a rise in the peak temperature range between 0.52% and 8.18% for the coming five decades in Europe [4] [5] observed in Fig. 1, the thermal stress increases the risk of premature failure and reduces the PT's rating.

According to the International Electrotechnical Commission (IEC) [6] and the Institute of Electrical Electronics Engineers (IEEE) loading guides [7], the rating of a PT is usually governed by the thermal limit or hot spot temperature (HST). Its accurate identification will provide essential information for life estimation, asset management strategies, and flexible scheduling. It can also be used to mitigate the risk of failure and to develop monitoring strategies. For this reason, transformers operating temperature has been investigated in the last three decades under the following strategies: The conventional Static Thermal Rating (STR), which international standards have extensively analysed [6] [7] using the thermal models investigated in [8] [9], and that is based on estimation of typical and conservative assumptions, together with safety and ageing criteria. However, despite its prolonged use, it only approximates the actual thermal values because it does not consider the instantaneous atmospheric conditions and the load profile [2]. The second is the Dynamic Thermal Rating (DTR) strategy, which determines the rating limits based on time-variable environmental conditions, such as air temperature. The third option, always within the concept of DTR, relies on direct temperature measurement, usually with a fibre optic sensor, [6], but this is often possible only for new transformers [10].

In this field, the application of the DTR approach is a proven concept and is presented as an alternative to improve the flexibility of the network in many scenarios. The main objectives are 1) increased transmission system efficiency and improvement reliability [2], and 2) Decreased or deferral of investments to reinforce or expand the existing network, where PT is often among the most expensive assets [10]. As this paper focuses on combining probabilistic thermal modelling and big data to determine the DTR of oil-immersed transformers, this section only reviews relevant works from the last decade.

Relevant literature addresses the evaluation of HST effect as the main parameter for determining the insulation ageing and its rating. In [11], the authors proposed a risk-based approach using a quantile Regression (QR) model to forecast the HST from the dynamic thermal model of the transformer. The results were developed in seasonal and hourly yield, and a fixed acceptable risk level validated the proposal from an energy and economic point of view. Another approach was developed in [12], [13] that employs thermal models from the IEC and IEEE guidelines to investigate the effect

979-8-3503-9678-2/23/$31.00 ©2023 IEEE

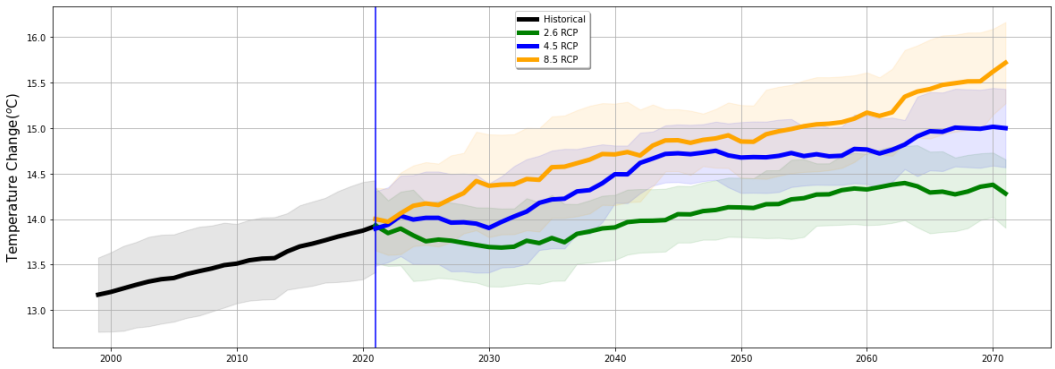

Fig. 1: Le Broc-Carros PT temperature change projection, evaluated rolling mean for 2.6, 4.5, 8.5 representative concentration pathways. Coloured shading represents one standard deviation

of DTR on a transformer's loss of life by calculating HST. The results reflect that the economic application of DTR could be financially beneficial while providing equal operating performance.

Data-driven thermal loading methodology for estimating annual continuous dynamic rating are presented in [14]. The analysis of the last five years of temperature ambient and load composition data is established, resulting in the continuous dynamic rating profiles under temperature scenarios for the planning region, introducing the concept of dynamic rating into the long-term planning process. The analysis of the existing literature above suggests that the topic of transformers rating is mostly faced with relatively short (i.e., five years) historical temperature records or short-term forecasts (i.e., a day ahead).

On the contrary, this research explores the behaviour of PT ratings considering both long-term historical reanalysis and climatic projections, with a perspective of 50 years in the past and the future. Thanks to the application to PT of the quasi Dynamic Thermal Rating (qDLR) approach presented in [15], it aims at identifying initial findings on the effect of climate change on the power systems.

In particular, this paper aims to provide the following contributions:

- The application of qDLR to power transformers.
- The estimation of the influence of climate change on transformers rating.

The paper is organised as follows: Section II illustrates the thermal model and methodology. Results are described in Section III, and conclusions are drawn in Section IV.

II. Methodology

The procedure developed to quantify the long-term effect of weather conditions on transformer power rating can be described as follows: 1) Air temperature time series for the past and future years are collected for the PT location. 2) For each hourly time step, The PT rating is calculated using the HST model described in [6]. 3) Results are grouped by month/hour. 4) A probability distribution is fit for the lower tail of each month/hour combination. 5) A rating is calculated from the probability distribution according to a chosen quantile corresponding to a tolerated risk level.

A. Thermal Model

Several models have been proposed for estimating the thermal state of loaded power oil-immersed transformers. Among the ones mentioned in Section I, the IEC 60076-7 loading guide [6] will be used due to its wide acceptance and simplicity. Other works propose more detailed models, including wind speed and solar radiations [16], [17]. Nevertheless, in this work, it was preferred to use the more recognised standard to give more general validity to the results.

PT rating is limited by the HST θ_h (°C), depending on ambient temperature θ_a (°C) and the hot-spot gradient rise of temperature within the transformer $\Delta\theta_h$ and it is calculated in (1). The Top-oil temperature θ_o (°C) with a cold start state assumptions can be calculated in (2).

$$\theta_o = \left[\frac{1+K^2R}{1+R}\right]^x (\Delta\theta_{or}) + \theta_a \tag{1}$$

$$\theta_h = \theta_o + \Delta\theta_h \tag{2}$$

Where the $\Delta\theta_{or}$ (°C) describes temperature rise in steady state at rated losses; x is the exponent related to oil temperature rise due to total losses; R is the ratio of load loses at rated current to no-load losses at rated voltage. The HST is used as the critical limiting parameter for the rating and to calculate load factor K (p. u) per iteration, defined as the ratio between load current and rated current.

B. Quasi Dynamic Thermal Rating

As proposed in [15], the DTR is determined by a two-step procedure: First, calculated ratings are grouped by month and hour to consider the yearly and daily weather periodicity. Secondly, a probability distribution is fit to each one of these subgroups; after an initial benchmark, the power law was chosen for this task. The model is shown in (3), where the constant parameter α is known as the exponent or scaling parameter and x represents the quantity in whose distribution is interested, for our case, the rating (I).

$$p(x) = Ax^{\alpha} \tag{3}$$

At this point, the rating is chosen from a predetermined distribution quantile. In this paper, the 0.1 % quantile is chosen. This corresponds to a temperature exceedance of roughly 8 hours per year.

C. Data

This study requires data from 1) the Transformer and 2) the Weather.

1) Transformer Data: At this stage, the transformer is evaluated based on the values of the typical guideline parameters [6], listed in Table I.

According to the given conditions, a population of five different transformers in the Provence region was analysed, listed in Table II. For these transformers, the rating is calculated from the available data.

TABLE I: Thermal Characteristic listed in IEC 60076-7 used in PT model equations

Parameter, Units	Symbol or Reference	Value
Oil exponent	x	0.8
Winding Exponent	y	1.3
Loss Ratio	R	6
Hot-Spot Temperature ($\circ C$)	θ_{h}	98
Hot-Spot to top-oil ($\circ C$)	$\Delta\theta_{\mathrm{hr}}$	26
Tap-Oil Temperature Raise ($\circ C$)	$\Delta\theta_{\mathrm{or}}$	52
Constant	K_{21}	2

TABLE II: Power transformer list with parameters for qDTR analysis

Unit	Name	Calculated Power (MVA)	Resistance R(Ω)	Reactance X(Ω)
T_1	Le Broc-Carros	1194	0.1	42.3
T_2	Biaçon	1168	0.24	43.1
T_3	Realtor	1210	0.12	41.7
T_4	Tamareau	1119	0.25	45
T_5	Tavel	1184	0.14	42.6

The static grid model in [18] provides the description, electrical parameters as voltage level, and seasonal ratings for the PT, and is complemented with the Enedis open data portal that contains the geographical reference for each transformer [19], illustrated in Fig. 2.

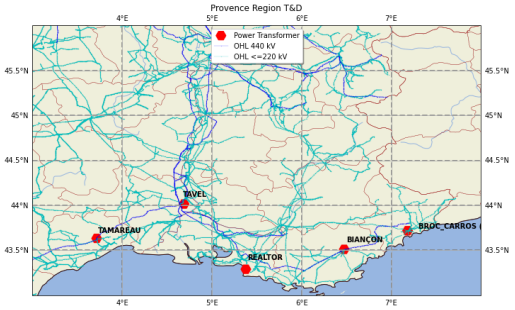

Fig. 2: Map of Provence transmission network with a location of PT highlighted in red dots

2) Weather: The ambient temperature data is retrieved from:

- ECMWF ERA5 dataset provides the historical weather reanalysis, with resolution of 0.25° x 0.25° (⁓24.5 km) and hourly time step. It is used in a 50-years period from January 01, 1970, to December 31, 2021 [4].
- Copernicus climate change service (C3S) - Climate and Energy indicators offers the Europe climate projections with a Representative Concentration Pathway (RCP) of 2.6, 4.5, and 8.5. The dataset has a resolution of 0.25°x. 0.25° (⁓24.5 km) and 3 hourly resolution [5]. The temperature ambient time series of the 50-year period from January 01, 2022, to December 31, 2072 were used.
- Climatic projections are linearly interpolated with a time resolution of 1 hour to match the frequency of the historical reanalysis.

III. Results

This section presents the results of the qDTR calculation, evaluated according to the methodology presented in Section II. The distribution fitting can be seen in Fig. 3 where green dots represent the calculated PT ratings using the thermal model represented in (1) and (2), and the dashed line represents the estimated probability distribution for the month of June at 2:00 pm. For each month/hour combination, the power law distribution fits the lowest 2% of the calculated ratings. For all the month/hour combinations, r^2 is greater than 0.94.

A set of hourly and monthly qDRTs for the analysed PT is shown in Fig. 4. Those are calculated considering an exceedance probability of 0.1% and compared with seasonal ratings calculated with the same exceedance probability, whose values were verified with the summer/winter ratings provided by the TSO in [16] for the same transformers. This resulted in an average error of 4.2%, considered acceptable.

From the analysis of this chart, it is possible to imply that: i) as expected, qDTRs allow us to better exploit the colder hours of the night, both in summer and winter. This has particular relevance to the integration of night winter load peaks. ii) This

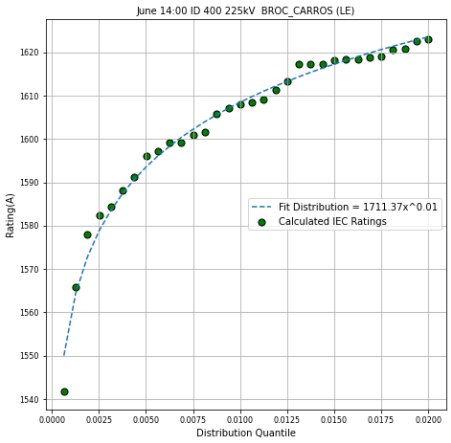

Fig. 3: Example of power law distribution fitting and calculating dots of the lower quantile

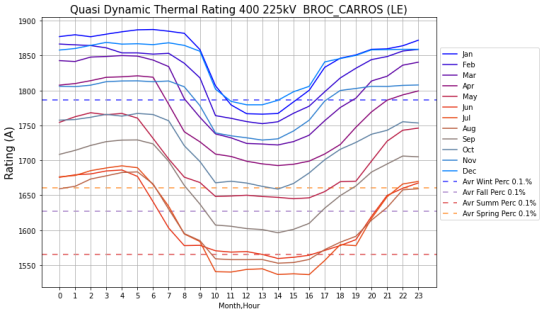

Fig. 4: qDTR for Broc-Carros PT with an exceedance probability of 0.1%

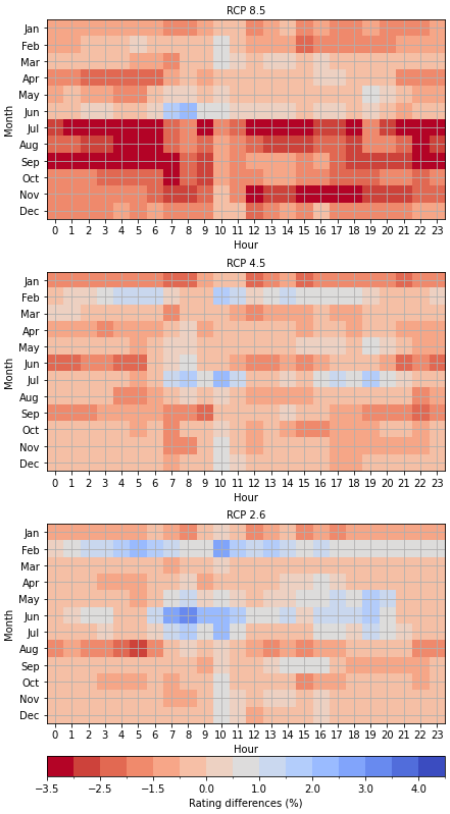

Fig. 5: Difference of the calculated qDTR month/hour between historical values and RCP projections 2.6, 4.5, 8.5

gap is also more significant in summer than in winter based on minimum and maximum values. This is a consequence of higher temperature differences in summer. iii) It must be noted that in the hottest daily hours, qDLRs tend to be lower than the seasonal rating.

The same procedure is applied to the three projected RCP scenarios. The effect of increased ambient temperature in the three RCP scenarios for the Broc-Carros PT, is shown in Fig. 5. The variations – albeit small – correspond, for example, to a maximal rating reduction of 4.1% in July for RCP 8.5 and 1.1% for RCP 4.5. This could be translated in terms of variation in the level of risk or the useful lifetime of the equipment for the network operator. On the other hand, it is possible to observe the opposite effect in specific months and hours, such as February or December and the late mornings.

Finally, Table III reports the average, minimum, and maximum values for the qDTRs calculated for the five transformers studied. This is done in absolute values for the historical reanalysis and percentage variations for the three climatic projections. It is possible to observe an average reduction in ratings in the order of 0.2%, 0.7%, and 1.5%, respectively, for the 2.6, 4.5, and 8.5 RCP.

IV. Conclusions

This paper presents a preliminary study on the influence of climate change on the rating of power transformers, using the qDTR approach. Its results can be summarised as follows:

- The qDTRs methodology introduced has the advantage of a higher average rating throughout the year in contrast to seasonal rating (an average uplift in the region of 7.7%). On the other hand, this rating is lower than that of DTRs.
- The hourly/month qDTR in PT yields rating improvements in specific periods, mainly at night. Network operators could use more straightforward approaches such as day/night in practical applications.

TABLE III: Average, minimum and maximum qDTR values compared to historical values

Description	Realtor	Biaçon	Broc-Carros	Tamareu	Tavel
Hist Avg (A)	1716	1652	1711	1575	1636
Hist Max (A)	1851	1787	1862	1706	1805
Hist Min (A)	1543	1455	1519	1363	1340
2.6 RCP Avg	-0.3%	-0.1%	-0.2%	-0.3%	-0.4%
2.6 RCP Max	0.2%	0.7%	0.0%	0.6%	0.31%
2.6 RCP Min	0.0%	-0.4%	-1.0%	-2.1%	-0.8%
4.5 RCP Avg	-0.9%	-0.6%	-0.7%	-0.5%	-0.8%
4.5 RCP Max	-0.5%	0.5%	-0.8%	0.3%	-0.08%
4.5 RCP Min	-0.7%	-0.9%	-0.5%	-1.7%	- 0.7%
8.5 RCP Avg	-1.7%	- 1.6%	-1.6%	-1.0%	-2.1%
8.5 RCP Max	-1.0%	-0.1%	-1.4%	-0.2%	-0.7%
8.5 RCP Min	-3.7%	-3.0%	-3.8%	-2.2%	-1.8%

- The qDTRs are not intended to be an alternative to DTRs, but a more straightforward solution that does not require telecommunications or controls and can be easily applied to network components. Leaving the application of DTRs to more critical assets.
- qDTRs, in contrast to DTRs, are known in advance and can be easily used in network expansion planning and operational scheduling.
- qDTRs are calculated in this work considering an exceedance probability level set at 0.1%. However, the impact of ageing needs to be taken into account. Network operators could use more or less stringent values depending on the specific load expected in each transformer or plan for slower or faster ageing.
- Future qDTRs are expected to be lower than past qDTRs due to projected temperature increases. In particular, 0.2%, 0.7%, and 1.5% on average, respectively, for the 2.6, 4.5, and 8.5 RCP.
- The availability of climate projections makes it possible to calculate time-dependent variables, such as qDTRs, under expected future conditions. Their use should be further explored for other transition and distribution network assets.
- The results of this work are influenced by the small size of the use case, limited to five transformers in a single region. Nevertheless, they reveal interesting patterns that deserve further study.

REFERENCES

[1] Schaeffer, R., Szklo, A. S., de Lucena, A. F. P., Borba, B. S. M. C., Nogueira, F. P. Fleming, A. Troccoli,M.Harrison, and M. S. Boulahya. Energy sector vulnerability to climate change: A review. Energy, 38(1):1–12, 2012.

[2] I. Daminov, A. Prokhorov, R. Caire, and M.-C. Alvarez-Herault, "Assessment of dynamic transformer rating, considering current and temperature limitations," International Journal of Electrical Power & Energy Systems, vol.129, p. 106886, Jul. 2021, doi: 10.1016/j.ijepes.2021.106886.

[3] DNV, World Meteorological Organization, 'ENERGY TRANSITION OUTLOOK 2022, A global and regional forecast to 2050' AS NO-1322 Høvik, Norway

[4] Copernicus Climate Change Service (2021): Climate and energy indicators for Europe from 2005 to 2100 derived from climate projections. Copernicus Climate Change Service (C3S) Climate Data Store (CDS). 10.24381/cds.f6951a62 (Accessed on 14-03-2023)

[5] Hersbach, H., Bell, B., Berrisford, P., Biavati, G., Horányi, A., Muñoz Sabater, J., Nicolas, J., Peubey, C., Radu, R., Rozum, I., Schepers, D., Simmons, A., Soci, C., Dee, D., Thépaut, J-N. (2023): ERA5 hourly data on single levels from 1940 to present. Copernicus Climate Change Service (C3S) Climate Data Store (CDS), 10.24381/cds.adbb2d47 (Accessed on 14-03-2023)

[6] IEC 60076-7:2018 - Power transformers - Part 7: Loading guide for mineral-oil-immersed power transformers,2018

[7] "IEEE Guide for Loading Mineral-Oil-Immersed Transformers and Step-Voltage Regulators," IEEE. doi:10.1109/IEEESTD.2012.6166928.

[8] D. Susa and M. Lehtonen, "Dynamic Thermal Modeling of Power Transformers: Further Development—Part I," IEEE Trans. Power Delivery, vol. 21, no. 4, pp. 1961–1970, Oct. 2006, doi: 10.1109/TPWRD.2005.864069.

[9] G. Swift, T. S. Molinski, and W. Lehn, "A fundamental approach to transformer thermal modeling. I. Theory and equivalent circuit," IEEE Trans. Power Delivery, vol. 16, no. 2, pp. 171–175, Apr. 2001, doi: 10.1109/61.915478.

[10] W. H. Tang and Q. H. Wu, Condition Monitoring and Assessment of Power Transformers Using Computational Intelligence. in Power Systems. London: Springer London, 2011. doi: 10.1007/978-0-85729-052-6.

[11] A. Bracale, G. Carpinelli, and P. De Falco, "Probabilistic risk-based management of distribution transformers by dynamic transformer rating," International Journal of Electrical Power & Energy Systems, vol. 113, pp. 229–243, Dec. 2019, doi: 10.1016/j.ijepes.2019.05.048.

[12] T. Zarei, K. Morozovska, T. Laneryd, P. Hilber, M. Wihlén, and O. Hansson, "Reliability considerations and economic benefits of dynamic transformer rating for wind energy integration," International Journal of Electrical Power & Energy Systems, vol. 106, pp. 598–606, Mar. 2019, doi: 10.1016/j.ijepes.2018.09.038.

[13] O. D. Ariza , K. Morozovska, T. Laneryd, O. Ivarsson, C. Ahlrot, and P. Hilber. Dynamic rating assists cost-effective expansion of wind farms by utilizing the hidden capacity of transformers. International Journal of Electrical Power & Energy Systems, 123:106188, 2020

[14] M. Dong, "A Data-driven Long-Term Dynamic Rating Estimating Method for Power Transformers," IEEE Trans. Power Delivery, vol. 36, no. 2, pp. 686–697, Apr. 2021, doi: 10.1109/TPWRD.2020.2988921.

[15] S. Hadiwidjaja, S. Montana-Salas, A.Michiorri 'Quasi-Dynamic Line Rating spatial and temporal analysis for network planning'. CIRED 2023

[16] Gorgan, B., Notingher, P. V., Wetzer, J. M., Verhaart, H. F. A., Wouters, P. A. A. F., Van Schijndel, A. (2012). Influence of solar irradiation on power transformer thermal balance. IEEE Transactions on Dielectrics and Electrical Insulation, 19(6), 1843-1850.

[17] Doolgindachbaporn, A., Callender, G., Lewin, P. L., Simonson, E., Wilson, G. (2021). A top-oil thermal model for power transformers that considers weather factors. IEEE Transactions on Power Delivery, 37(3), 2163-2171.

[18] RTE.France's Transmission System Operator, 'Electrical features of the network of RTE',Published. [Online]. Available:/https://www.services-rte.com/en/learn-more-about-our-services/static-grid-model.html.[Accessed: 05- Feb- 2023]

[19] Enedis. Enedis Open Data, 'Cartographie des réseaux exploités par Enedis', Published. [Online] Available:https://data.enedis.fr/pages/cartographie-des-reseaux-contenu/. [Accessed: 13- Mar- 2023]

B.8 Published Papers: Conference B

Assessing Regional Capacity Expansion: The Role of Quasi-Dynamic Thermal Ratings in a Changing Climate

Sergio-Daniel Montaña-Salas
Centre PERSEE
Mines Paris - PSL
Sophia Antipolis, France
sergio-daniel.montana-salas@minesparis.psl.eu

Andrea Michiorri
Centre PERSEE
Mines Paris - PSL
Sophia Antipolis, France
andrea.michiorri@minesparis.psl.eu

2024 IEEE PES Innovative Smart Grid Technologies Europe (ISGT EUROPE) | 979-8-3503-9042-1/24/$31.00 ©2024 IEEE | DOI: 10.1109/ISGTEUROPE62998.2024.10863802

***Abstract*—Proposing practical solutions to mitigate the effects of climate change on the electricity system requires thorough understanding and quantification. This paper introduces a new method of quantifying dynamic network capacity at the transmission level, using established thermal models and a set of regional expansion plan tools. The results suggest that this approach can increase component capacity by up to 21% during winter and up to 16% during the night for overhead lines. This method offers a viable option for electricity operators to address the challenge of balancing the need to reduce failure rates and capacity loss with the crucial demand for new investment in transmission assets, since it reduces more than 27% of system cost expansion by 2050.**

***Index Terms*—Climate Change, Dynamic Thermal Rating, Power Transmission, Meteorological Factors.**

I. Introduction

This paper presents the findings of research on regional network expansion planning, taking into account the impact of climate change on transmission network equipment. As emphasized by [1], a transmission network expansion of up to 80 million kilometers in Europe is possible, whilst a reduction of transmission capacity from 1.9% to 5.8% is expected in the United States [2]. These challenges underscore the importance of analyzing future investments and developing new flexibility strategies using established methods.

Regarding the transmission network, various solutions have been proposed to alleviate network congestion problems. One of them is the implementation of Dynamic Thermal Rating (DTR) on critical transmission lines. This technology aims to identify the real-time current-carrying capacity of network components , which is typically higher than their static nominal value or Static Thermal Rating (STR). By doing so, DTR enables the reduction of network congestion, associated curtailments, and delays, and the avoidance of network reinforcements, while simultaneously enhancing reliability. It can be integrated into power system expansion plans [3], [4], but its dependency on meteorological factors, such as ambient temperature, makes it particularly sensitive to climate change.

Climate scenario models and trajectories have been published for specific road maps. Among these, quantitative projections, such as Representative Concentration Pathways (RCPs) and Shared Socio-Economic Pathways (SSPs), provide valuable tools for assessing regional climate change and its specific impacts on the energy sector. Indeed, electricity demand is expected to increase by up to 21% [5], a key factor in determining capacity expansion planning.

In the academic literature, Long-Term Demand Forecasting Methods (LDFM) are often described as incorporating trend analysis, econometric modeling, or combined analysis, as discussed in [6], [7]. These methods explore linear and non-linear relationships among economic indicators, demographic factors, and weather variables such as Gross Domestic Product (GDP), ambient temperature, and population. Furthermore, statistical and machine-learning algorithms have been explored for this task.

As a main contribution, this research aims to quantify the impact of climate change on power system capacity as a part of strategic planning methodology for a regional utility by:

- Deriving a quasi-dynamic Thermal Ratings (qDTRs) algorithm; this is the first solution to recover lost transmission capacity for use in long-term analysis and reduce network costs.
- Quantifying the impact of climate change on regional capacity expansion planning considering future climatic projection datasets.

The paper is organized as follows: Section II illustrates the load demand forecast, thermal model, and methodology. The results are described in Section III, and conclusions are drawn in Section IV.

II. Methodology

A. Overview

We introduce a model to assess the long-term effects of climate conditions on regional capacity, employing qDTR as a critical metric in **II-B**. This model is delineated in Fig. 1. Initially, a regression machine learning model is trained using

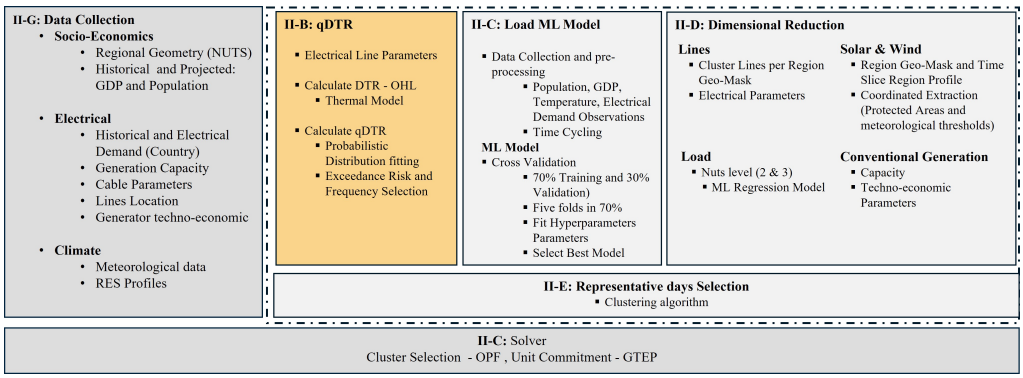

Fig. 1. Proposed block diagram: It is divided into three sections representing the estimation of network capacity using qDTR, the preparation of the network, and its economic analysis via G&TEP.

historical, techno-economic, regional and meteorological data to project demand by regions **II-C**. Subsequently, data describing the electrical grid configuration are gathered to cluster and construct the network **II-D**. The transmission information, including location details and meteorological time series, is then utilized in thermal models of the components to estimate the capacity **II-B**. These ratings are subsequently incorporated into a Generation, Transmission Expansion Planning (G&TEP), enabling the calculation of optimal investments and operating costs.

B. Quasi Dynamic Thermal Ratings

qDTR, as proposed in [8], are employed to quantify ratings for a long-term horizon. After gathering the time series and parameters outlined in Section II-G, the DTR is estimated using a component thermal model over its entire length. This model is based on the thermal balance between the heat generated by the Joule effect (I^2R) and the heat dissipated in the environment through convection or conductivity (Q_c), radiation (Q_r), and solar heat gain (Q_s), as described in (1) and applying the model outlined in [9]. These time series data are fitted with a probability distribution, as detailed in [10], focusing on the lower tail of the simulations for each month/day combination. A predetermined level of tolerance to the risk of thermal overload (0.1% in this case) is then selected.

$$I^2R + Q_s = Q_r + Q_c \tag{1}$$

C. Load Model

Long-term regional energy demand forecasting comprehensively assesses factors that drive future energy consumption patterns, such as economic parameters, seasonal variations, and spatial behaviors. With an hourly resolution, this module targets each sub-grid's load demand profile in MWh. The pre-selection of features was conducted using a combination of time series meteorological data, demographic factors, and demand observations, guided primarily by bibliographic analyses in [6]. This selection process adheres to the nonlinear relationship described in (2), where i represents the year, and a, b, and c are parameters derived from historical data. To ensure the spatiality of the system throughout the European region, we rely on the open sources described in section II-G. The profile and shape of the hourly demand result depend mainly on economic influences and the temperature condition of the region. Demand curves are calculated for the sub-grid by gathering the profile demand of the above region (country or region) from [11], GDP, population, and hourly temperatures.

$$D_i = a(\text{per capita income})b_i(\text{population})c_i \tag{2}$$

Due to the complexity of the problem, we implemented the following preprocessing and numerical transforms: a) minimum and maximum scaling, b) encoding of the cyclical day of the year, and c) hourly interpolation. During the initial phase, we assessed a range of regression machine-learning techniques to determine the most fitting approach for our method. This evaluation centered on key error metrics such as Root Mean Squared Error (RMSE) and Mean Absolute Error (MAE). The dataset is divided by geographical regions to train and test the models. The training set is initially randomly partitioned into 70%, with an additional 10% reserved for tuning the model hyperparameters, employing techniques outlined in [12]. The remaining 30% is designated as the validation set for model testing. N-fold cross-validation is employed to mitigate overfitting, and divides the test dataset into five folds. This ensures that all region sizes are represented in each fold, thus maintaining homogenous selection.

D. Dimensional Reduction

The objective is to analyze the electricity network of European regions, focusing on long-term generation and demand patterns. The process starts with the regions categorized at level zero of the Nomenclature of Territorial Units for Statistics (NUTS) (countries) and extends to the administrative

department level (NUTS 3 level). This analysis is based on geographic information about electricity transmission and generation networks as well as technical-economic data.

A regional strategic approach to the power system follows the same methodology, utilizing geographical boundaries from [13]. To account for the fluctuating nature of renewables, each region is analyzed using wind production density [14]. A coordinate is selected based on the criterion of reflecting an average speed of more than 4.5 m/s during the period analyzed, ensuring that it is not located more than 1000 m above sea level or within a protected natural area [15]. The production is extrapolated to form a defined curve. Similarly, a profile for the PV (photovoltaic) system is generated, with the distinction that coordinate selection is based on a statistical analysis of the 50th percentile. In addition to the demand model presented in section **II-C**, hydrogen demand is developed from 2020 and projected as an additional load to the regional energy profile until 2050, according to [16].

The geographic locations of the transmission lines and the electrical parameters are imported, analyzed, and established. A geographic mask is generated for each line based on its departure and arrival locations using its NUTS 2 and 3 regional codes. The lines are sorted by voltage and linearly aggregated in their bundles to maintain transmission capacity. In addition, a single transformer is configured between the high- and low-voltage buses at each regional location.

E. Selection Representative Days

In order to keep the problem computationally manageable, a representative set of days is chosen, applying a clustering algorithm per region described in (3). This set incorporates diverse input time series and is evaluated over the scenario horizon. A scaling method is selected to normalize all data points, and one representative day and one extreme day are chosen per month, region, and country. This ensures that critical points from each sub-region are included and maintains the representation of typical days for the entire system.

$$\arg \min_{\{\mu_1,\ldots,\mu_k\}} \sum_{j=1}^{k} \sum_{\mathbf{x}_i \in C_j} \|\mathbf{x}_i - \mu_j\|^2 \tag{3}$$

Where μ_k are the centroids of the k clusters, each representing a typical day for a specific region and month.

F. Generation, Transmission and Expansion Planning

Economic implications arising from reduced capacity due to climate change are evaluated through G&TEP [17], and carried out using qDTR_{RCP} based on three climatic projections. This comparison illuminates the errors incurred when the impact of climate change on transmission capacity is overlooked.

In generation, conventional power plants (CCGT, OCGT, Oil, and Hydro) include some technical constraints such as capacity constraints, $p_{nom_{max}}$, CO_2 emissions, and technology efficiency.

In addition, G&TEP utilizes STR alongside the year calculated from each RCP datum. This comparison highlights the advantages of qDTRs, which vary over time to recover lost transmission capacity.

G. Data Collection

The impact on qDTR capacity is quantified by organizing data into three primary categories:

- Socio-economic data: This includes national/regional account data such as GDP [18] and population [19]. Geographical boundaries are defined based on the Eurostat regional classification of territorial units for statistics (NUTS3 & NUTS2) [13].
- Electrical Data: Historical hourly time series of electricity demand profiles for each country and region [11], [20], combined with annual geolocated generation plants with physical characteristic [21], such as fuel type and capacity, and techno-economic assumptions such as fuel prices, VOM [22]–[24]. OHLs electrical parameters and locations are also considered [17].
- Climate datasets: Historical reanalysis and Representative Concentration Pathway (RCP)-based climate projections from ECMWF ERA5 and Copernicus C3S, with a high resolution of 0.25°, covering the period from January 01, 1970, to December 31, 2072 [20].

TABLE I
DATASETS AND PARAMETERS

Variable	Units	Process	Source
Socio-Economics			
GDP	MEuros	II-C	[18]
Population	M	II-C	[19]
Territorial Classification	^{o}	II-C,II-B,II-D	[13]
Electrical			
Load Profile	MW	II-C	[11], [20]
Power Plant Capacity	MW	II-F	[21]
Power Plant Techno-Economic	-	II-F	[22]–[24]
Electrical OHL and Location	-	II-B , II-F	[17]
Hydrogen Demand	TWh/year	II-D	[17]
Climate			
Air Temp. at 2 m	K	II-C,II-B	[20]
Net Surface Solar Radiation	Jm^{-2}	II-B, II-F	[20]
u - v - wind at 10 m and 100m	ms^{-1}	II-B, II-F	[20]

III. RESULTS

The hourly simulations were performed based on a selection of representative days over the projected horizon, delineating the electricity benefits attributable to the adoption of qDTR. The spatial distribution, comprising 69 pre-selected regions, is shown in Fig. 3. The data for each region were processed and assimilated as set out in II-G.

The model is designed to optimize the expansion and operation of the existing grid capacity, projected from 2020, to meet the anticipated growing demand by 2050. The simulation parameters, delineated in Table II, dictate the framework

within which these optimizations are performed. As mentioned in II-C, a LDFM leveraging regression-based methodologies at an hourly step was trained, validated, and selected. Although the results are not shown in this paper, the outcomes underscore the efficacy of linear regression and XG-Boost methodologies, manifesting an average deviation of 12% from observed values.

TABLE II
MODEL SPECIFICATIONS PARAMETERS

Variable	Units	Value
Socio-Economics		
Technology Financial	$\frac{\text{MEUR}}{\text{MW}_e}$	[22]–[24]
CO_2 Emissions	$\frac{\text{tCO}_2}{\text{MW}_h}$	[22]
Spatial Resolution	Km^2	25
Electrical		
Thermal Risk	%	0.1
PV Density	$\frac{\text{MW}}{\text{Km}^2}$	2.60 [25]
Wind Density	$\frac{\text{MW}}{\text{Km}^2}$	6.64 [26]
Hydro p_{max}	%	9
OHL Conductor	-	490-AL1/64-ST1A
Bus Voltage	kV	220 / 380
Scenarios Description		
Projection	RCP	2.6, 4.5, 8.5
Timeframe	Year	2021 - 2050
Resolution	Hour	24
Days Selection	Days	(2) Representative + (1) Extreme
Expansion Limit	-	1.5 to 4.5 times (220kV - 380kV)
Modeling tools		[17]

A. Benefits of qDTR vs STR

As described in II-B and detailed for a specific line in Fig. 2, qDTR is used to determine the maximum capacity of OHLs, considering future meteorological projections from 2020 to 2050 across different RCP scenarios ($\text{qDTR}_{\text{RCPx}}$, where x represents the RCP scenario evaluated). Table III illustrates the percentage mean variation of the average rating compared with the STR. In all three scenarios, qDTR_{RCP} consistently exceeds STR_{RCP} with increases of 16% and 20% specifically for the 2.6 scenario. In contrast, as a trade-off, using a risk probability of 0.1%, we ensure that during the high-temperature season, the rating operates within the safety zone, with an average decrease of 7% during the day and in summer. This trend persists across all seasons and projections. Consequently, enhancing the capacity increases loadability, relieving stress on the network and thus reducing load shedding events by 29% in the high emissions scenario and decreasing need for transmission expansion by 28% in the medium-emission scenario.

B. Impact on Network Costs

This section delves into investment decisions in the G&TEP, integrating climate-variant supply and qDTR for power system components. We apply STR_{RCP} and qDTR_{RCP} based on

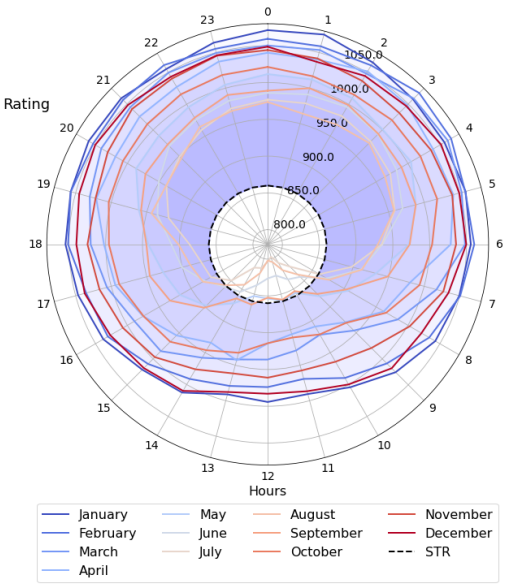

Fig. 2. qDTR for Line FRC1 - FRF2 with an exceedance probability of 0.1%

TABLE III
$\Delta_{\%}$ QDTR / STR MEAN CAPACITY DIFFERENCES OVER A FIFTY-YEAR PERIOD WITH $\text{RCP}_{2.6,\,4.5,\,8.5}$

Description	Summer	Winter	Autumn	Spring	Day	Night
$\text{qDTR}_{\text{RCP8.5}}$,STR						
Min	-7	12	-2	-1	-7	3
Max	13	21	18	20	20	21
Average	4	18	12	12	8	15
$\text{qDTR}_{\text{RCP4.5}}$,STR						
Min	-6	12	-2	-1	-7	3
Max	13	13	20	22	20	21
Average	5	21	13	12	8	15
$\text{qDTR}_{\text{RCP2.6}}$,STR						
Min	-7	12	-1	-1	-7	2
Max	13	23	20	21	23	23
Average	5	20	13	12	9	16
	$\text{RCP}_{8.5}$,STR		**$\text{RCP}_{4.5}$**,STR		**$\text{RCP}_{2.6}$**,STR	
L. Shedding	-29		-23		-27	

climate projections. The ensuing G&TEP estimates changes in CAPEX, OPEX, and renewable curtailment. The results in Table IV highlight: [1] enhancements with qDTR_{RCP} over STR_{RCP} with a maximum increase above 20% in winter and during the night. [2] significant reductions in curtailment over 14%, resulting in reductions of more than 27% in the total cost of the system.

IV. CONCLUSIONS

In summary, this study verifies that:

- Climate projections, marked by increased ambient temperatures, lead to a decline in transmission capacity in

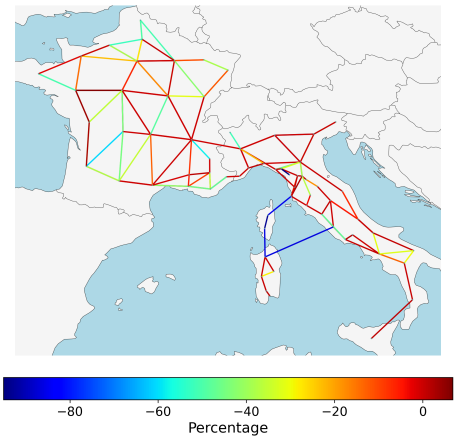

Fig. 3. Geographical representation highlights the analyzed regions, illustrating the variance in line expansion from STR to RCP 4.5.

TABLE IV
VARIATION (IN %) FOR THE THREE SCENARIOS CONCERNING YEARLY FIXED RATING AND COSTS

	RCP$_{8.5}$,STR	**RCP$_{4.5}$,STR**	**RCP$_{2.6}$,STR**
CAPEX			
Renewable	< 1	-7	-7
Fossil	13	9	-10
Nuclear	-9	-100	-100
Total	1	-9	-11
OPEX			
Renewable	-12	-9	-1
Fossil	-2	-2	-6
Nuclear	< 1	-4	-6
Total	-33	-26	-27
Curtailment	-2.6	-13	-14
System Cost	-27	-21	-24

the power system. Specifically, they lead to a reduction of approximately 7% in the worst-case scenario.

- qDTRs provide a straightforward, telecommunications or controls-free solution for long-term planning, easily applicable to network components while leaving critical assets for traditional DTRs. This approach enhances transmission capacities, counteracting rating reductions caused by climate change, and can increase average component capacity by up to 12%.
- Overall network costs demonstrate strong fluctuations, while a consistent decline is achieved in renewable production curtailment and Load Shedding, on average 10% and 26%.
- qDTR allows for higher transmission capacities, concluding in a 27% reduction in the system's total cost, potentially saving billions of Euros.
- Further work: There is a need, firstly, to work on methodologies to better integrate qDTR into OPF and G&TEP in order to better understand the limits of this approach, and secondly, to include the temporal and spatial correlation between RES and DTR.

V. ACKNOWLEDGEMENTS

This work was carried out with partial support from the 'H2MOVE' project under the Interreg Marittimo FR-IT programme, co-funded by the European Union.

REFERENCES

[1] International Energy Agency, "Electricity Grids and Secure Energy Transitions," Paris, 2023.
[2] M. Bartos, M. Chester, N. Johnson, B. Gorman, D. Eisenberg, I. Linkov, M. Bates "Impacts of rising air temperatures on electric transmission ampacity and peak electricity load in the United States," Environmental Research Letters, vol. 11, pp. 114008, 2016.
[3] P. Glaum and F. Hofmann, "Enhancing the German Transmission Grid Through Dynamic Line Rating," in 2022 18th International Conference on the European Energy Market (EEM), 2022, pp. 1-7.
[4] A. Trpovski and T. Hamacher, "A Comparative Analysis of Transmission System Planning for Overhead and Underground Power Systems using AC and DC Power Flow," in 2019 IEEE PES Innovative Smart Grid Technologies Europe (ISGT-Europe), 2019, pp. 1-5.
[5] J. Añel , M. Fernández-González , X. Labandeira , X. López-Otero, L. De la Torre, , "Impact of Cold Waves and Heat Waves on the Energy Production Sector" Atmosphere 8, no. 11: 209.
[6] Seifi, H., Sepasian, M.S. (2011). "Load Forecasting. In: Electric Power System Planning". Power Systems. Springer, Berlin, Heidelberg.
[7] K.B. Lindberg, P. Seljom, H. Madsen, D. Fischer, M. Korpås, "Long-term electricity load forecasting: Current and future trends," Utilities Policy, vol. 58, pp. 102-119, 2019.
[8] S. Hadiwidjaja , A. Michiorri , S. Montana , "Quasi-Dynamic Line Rating spatial and temporal analysis for network planning,"
[9] CIGRE, "Guide for Thermal Rating Calculations of Overhead Lines". Paris, France: December 2014, Technical brochure N° 601
[10] A. Clauset, C. Shalizi, M. E. J. Newman, "Power-Law Distributions in Empirical Data," SIAM Review, vol. 51, no. 4, pp. 661–703, Nov. 2009.
[11] ENTSO-E Transparency Platform, "ENTSO-E Transparency Platform".
[12] T. Akiba, "Optuna: A Next-generation Hyperparameter Optimization Framework," in Proceedings of the 25th ACM SIGKDD International Conference on Knowledge Discovery and Data Mining, 2019.
[13] Eurostat, "Statistical regions in the european union and partner countries— nuts and statistical regions 2021".
[14] N. Mortensen, N. Davis, J. Badger, A. Hahmann , "Global Wind Atlas version 3.0".
[15] "Natura 2000 protected areas network," European Environment Agency.
[16] ENTSO-E. Ten Year Network Development Plan 2022: Scenario Report. 2022
[17] T. Brown, J. Hörsch, D. Schlachtberger, "PyPSA: Python for Power System Analysis", 2018, Journal of Open Research Software.
[18] Eurostat, "Reference Metadata in Euro SDMX Metadata Structure (ESMS) for Regional Economic Accounts (reg_eco10)"
[19] Eurostat, "Population on January 01 by Age, Sex and NUTS 2 Region," 2021.
[20] Copernicus Climate Change Service, "Climate and energy indicators for Europe from 2005 to 2100 derived from climate projections," Climate Data Store (CDS), 2021.
[21] Global Energy Observatory, Google, KTH Royal Institute of Technology in Stockholm, Enipedia, World Resources Institute, "Global Power Plant Database," Published on Resource Watch, 2019.
[22] U.S. Energy Information Administration, data browser, "Annual Energy Outlook 2023."
[23] Danish Energy Agency, Energinet, "Technology Catalogues".
[24] Timilsina, Govinda R. "Demystifying the costs of electricity generation technologies." (2020).
[25] la Tour, Marie-Alix Dupré. "Photovoltaic and wind energy potential in Europe–A systematic review." Renewable and Sustainable Energy Reviews 179 (2023): 113189.
[26] Enevoldsen, Peter, and Mark Z. Jacobson. "Data investigation of installed and output power densities of onshore and offshore wind turbines worldwide." Energy for Sustainable Development 60 (2021): 40-51.

Bibliography

[1] David R. Maidment, ed. *Handbook of Hydrology*. New York: McGraw-Hill, 1993. URL: https://books.google.com/books/about/Handbook_of_Hydrology.html?id=6N7kTUv3dV4C (cit. on pp. xv, xvi, 21, 35).

[2] C.B. Field, V. Barros, T.F. Stocker, D. Qin, D.J. Dokken, K.L. Ebi, et al., eds. *Managing the Risks of Extreme Events and Disasters to Advance Climate Change Adaptation*. The Edinburgh Building, Shaftesbury Road, Cambridge CB2 8RU, England: Cambridge University Press, 2012, p. 582 (cit. on pp. xv, 129).

[3] CIGRÉ Working Group B1.35. *A Guide for Rating Calculations of Insulated Cables*. Tech. rep. Technical Brochure 640. Paris, France: CIGRÉ, 2015. URL: https://www.e-cigre.org/publication/640-a-guide-for-rating-calculations-of-insulated-cables (cit. on pp. xv, xvi, 10, 11, 21).

[4] Friedrich Kiessling, Peter Nefzger, João Felix Nolasco, and Ulf Kaintzyk. *Overhead Power Lines: Planning, Design, Construction*. Power Systems. Berlin, Heidelberg: Springer, 2003. URL: https://link.springer.com/book/10.1007/978-3-642-97879-1 (cit. on pp. xv, xvi, 2, 20, 21, 66).

[5] Hossein Seifi and Mohammad Sadegh Sepasian. *Electric Power System Planning: Issues, Algorithms and Solutions*. Power Systems. Springer, 2011. URL: https://link-springer-com.minesparis-psl.idm.oclc.org/book/10.1007/978-3-642-17989-1 (cit. on pp. xv, 66, 70).

[6] Joaquín Muñoz Sabater. *ERA5-Land hourly data from 1950 to present*. 2019. URL: https://doi.org/10.24381/cds.e2161bac (cit. on pp. xvi, 49, 87, 90, 112, 132).

[7] H. Wan, J.D. McCalley, and V. Vittal. "Increasing thermal rating by risk analysis". *IEEE Transactions on Power Systems* 14.3 (1999), pp. 815–828 (cit. on pp. xvi, 17, 21).

[8] CIGRÉ Working Group B1.41. *Long Term Performance of Soil and Backfill Systems*. Tech. rep. Technical Brochure 714. Paris, France: CIGRÉ, 2017. URL: https://www.e-cigre.org/publications/detail/714-long-term-performance-of-soil-and-backfill-systems.html (cit. on pp. xvi, 9, 10, 21, 36).

[9] Daniel S. Kirschen and Goran Strbac. *Fundamentals of Power System Economics*. John Wiley & Sons, Incorporated, 2004 (cit. on p. xvi).

[10] Federal Energy Regulatory Commission. *Managing Transmission Line Ratings*. Tech. rep. 2019. URL: https://www.ferc.gov/industries-data/resources/ferc-staff-reports-and-papers (cit. on pp. 2, 12, 13, 20, 21, 78).

[11] *Climate Change 2013: The Physical Science Basis. Contribution of Working Group I to the Fifth Assessment Report of the Intergovernmental Panel on Climate Change*. Tech. rep. Cambridge, United Kingdom and New York, NY, USA: Intergovernmental Panel on Climate Change (IPCC), 2013, p. 1535 (cit. on p. 2).

[12] Andrea K. Gerlak, Jaron Weston, Ben McMahan, Rachel L. Murray, and Megan Mills-Novoa. "Climate risk management and the electricity sector". *Climate Risk Management* 19 (2018), pp. 12–22. URL: https://www.sciencedirect.com/science/article/pii/S2212096317301572 (cit. on pp. 2, 21).

[13] Seleshi G Yalew, Michelle TH van Vliet, David EHJ Gernaat, Fulco Ludwig, Ariel Miara, Chan Park, et al. "Impacts of climate change on energy systems in global and regional scenarios". *Nature Energy* 5.10 (2020), pp. 794–802 (cit. on pp. 2, 20, 21).

[14] Omar Rafae Alomar, Bashar Mahmood Ali, Obed Majeed Ali, and Ahmed Nawfal Mustafa. "Impacts of environmental conditions on thermal, emissions and economic performance of gas turbine using different types of fuels: An experimental investigation". *Results in Engineering* 24 (2024), p. 103402 (cit. on p. 2).

[15] Y. Romitti and I. Sue Wing. "Heterogeneous climate change impacts on electricity demand in world cities circa mid-century". *Scientific Reports* 12 (2022), p. 4280. URL: https://doi.org/10.1038/s41598-022-07922-w (cit. on pp. 2, 21).

[16] Michelle Davis and Steve Clemmer. "Power Failure: How Climate Change Puts Our Electricity at Risk—and What We Can Do" (2014). URL: http://www.jstor.org/stable/resrep00019 (cit. on pp. 3, 19, 20).

[17] Margherita Bellanca. "What, how and where: an assessment of multi-level European climate mitigation policies". *npj Climate Action* 3 (2024), p. 119. URL: https://doi.org/10.1038/s44168-024-00200-7 (cit. on p. 3).

[18] Simon Montfort, Lukas Fesenfeld, Karin Ingold, et al. "Political enablers of ambitious climate policies: a framework and thematic review". *npj Climate Action* 4 (2025), p. 14. URL: https://doi.org/10.1038/s44168-024-00206-1 (cit. on p. 3).

[19] Joel Goop, Mikael Odenberger, and Filip Johnsson. "The effect of high levels of solar generation on congestion in the European electricity transmission grid". *Applied Energy* 205 (2017), pp. 1128–1140. URL: https://www.sciencedirect.com/science/article/pii/S0306261917311601 (cit. on p. 3).

[20] Hans Schermeyer, Claudio Vergara, and Wolf Fichtner. "Renewable energy curtailment: A case study on today's and tomorrow's congestion management". *Energy Policy* 112 (2018), pp. 427–436. URL: https://www.sciencedirect.com/science/article/pii/S0301421517307115 (cit. on p. 3).

[21] Organisation for Economic Co-operation and Development (OECD) and International Energy Agency (IEA). *Electricity Grids and Secure Energy Transitions: Enhancing the Foundations of Resilient, Sustainable and Affordable Power Systems*. Tech. rep. Paris, France: OECD/IEA, 2023. URL: https://www.oecd.org/publications/electricity-grids-and-secure-energy-transitions-9789264738487-en.htm (cit. on p. 3).

[22] Matthew Bartos, Mikhail Chester, Nathan Johnson, Brandon Gorman, Daniel Eisenberg, Igor Linkov, et al. "Impacts of rising air temperatures on electric transmission ampacity and peak electricity load in the United States". *Environmental Research Letters* (). URL: https://dx.doi.org/10.1088/1748-9326/11/11/114008 (cit. on pp. 3, 20, 21).

[23] Gary Brennan, Zibby Kieloch, and Jan Lundquist. "Uprating and Upgrading". *Overhead Lines*. Ed. by Konstantin O. Papailiou. Springer International Publishing, 2017, pp. 1227–1297. URL: https://link.springer.com/referenceworkentry/10.1007/978-3-319-31747-2_18 (cit. on pp. 3, 4, 11, 17).

[24] Nhlanhla Mbuli, Ronald Xezile, Lethoko Motsoeneng, Mavula Ntuli, and Jan-Harm Pretorius. "A literature review on capacity uprate of transmission lines: 2008 to 2018". *Electric Power Systems Research* 170 (2019), pp. 215–221. URL: https://www.sciencedirect.com/science/article/pii/S0378779619300124 (cit. on p. 3).

[25] U.S. Department of Energy. *Dynamic Line Rating Systems for Transmission Lines: Topical Report*. Tech. rep. Smart Grid Demonstration Program, Office of Electricity Delivery and Energy Reliability, U.S. Department of Energy, 2014. URL: https://www.energy.gov/sites/prod/files/2016/10/f34/SGDP_Transmission_DLR_Topical_Report_04-25-14.pdf (cit. on pp. 3, 9).

[26] *Climate Change 2013: The Physical Science Basis. Contribution of Working Group I to the Fifth Assessment Report of the Intergovernmental Panel on Climate Change*. Tech. rep. Cambridge, United Kingdom and New York, NY, USA: Intergovernmental Panel on Climate Change (IPCC), 2013, p. 1535 (cit. on p. 3).

[27] G.J. Anders. *Rating of Electric Power Cables in Unfavorable Thermal Environment*. Hoboken, NJ: John Wiley & Sons, 2005 (cit. on pp. 6, 9, 10, 21, 35–37, 170).

[28] Jonas Hörsch, Fabian Hofmann, David Schlachtberger, and Tom Brown. "PyPSA-Eur: An open optimisation model of the European transmission system". *Energy Strategy Reviews* 22 (2018), pp. 207–215 (cit. on pp. 7, 90, 92, 121, 123, 173).

[29] Javier Iglesias, George Watt, Dale Douglass, Vincent Morgan, Rob Stephen, Mark Bertinat, et al. *Guide for Thermal Rating Calculations of Overhead Lines*. Paris, France, 2014. URL: https://www.e-cigre.org/publication/601-guide-for-thermal-rating-calculations-of-overhead-lines (cit. on pp. 6, 7, 21, 32, 33, 81, 86, 166).

[30] Seyede Fatemeh Hajeforosh. "Multiple Aspects of Dynamic Rating in the Power System". PhD thesis. Luleå, Sweden: Luleå University of Technology, 2022 (cit. on pp. 6, 8, 21).

[31] V.T. Morgan. *The Thermal Behaviour of Electrical Conductors*. Somerset, England: Research Studies Press Ltd, 1997 (cit. on p. 6).

[32] G.J. Anders. *Rating of Electric Power Cables: Ampacity Computations for Transmission, Distribution, and Industrial Applications*. IEEE Press power engineering series. McGraw-Hill, 1997 (cit. on pp. 6, 9, 21, 35, 86).

[33] G. Swift, T.S. Molinski, and W. Lehn. "A fundamental approach to transformer thermal modeling. I. Theory and equivalent circuit". *IEEE Transactions on Power Delivery* 16.2 (2001), pp. 171–175 (cit. on pp. 6, 8, 21).

[34] D. Susa, M. Lehtonen, and H. Nordman. "Dynamic thermal modelling of power transformers". *IEEE Transactions on Power Delivery* 20.1 (2005), pp. 197–204 (cit. on pp. 6, 21).

[35] International Electrotechnical Commission. *Power Transformers – Part 7: Loading Guide for Mineral-Oil-Immersed Power Transformers*. Tech. rep. 2018 (cit. on pp. 6, 8, 9, 18, 21, 42).

[36] A. Michiorri, P. C. Taylor, and S. C.E. Jupe. "Investigation into the influence of environmental conditions on power system ratings". *Proceedings of the Institution of Mechanical Engineers Part M: Journal of Engineering for the Maritime Environment* 223.4 (2009), pp. 743–757 (cit. on pp. 7, 8, 21).

[37] IEEE Power and Energy Society. *IEEE Standard for Calculating the Current-Temperature Relationship of Bare Overhead Conductors*. Piscataway, NJ, USA: Institute of Electrical and Electronics Engineers, 2023. URL: https://standards.ieee.org/ieee/738/10207/ (cit. on pp. 7, 10, 21, 32).

[38] Alberto Arroyo, Pablo Castro, Raquel Martinez, Mario Manana, Alfredo Madrazo, Ramón Lecuna, et al. "Comparison between IEEE and CIGRE Thermal Behaviour Standards and Measured Temperature on a 132-kV Overhead Power Line". *Energies* 8.12 (2015), pp. 13660–13671. URL: https://www.mdpi.com/1996-1073/8/12/12391 (cit. on pp. 7, 21).

[39] Martin Kanálik, Anastázia Margitová, and Ľubomír Beňa. "Temperature calculation of overhead power line conductors based on CIGRE Technical Brochure 601 in Slovakia". *Electrical Engineering* 101.4 (2019), pp. 921–933. URL: https://doi.org/10.1007/s00202-019-00831-8 (cit. on p. 7).

[40] Andrea Michiorri, Huu-Minh Nguyen, Stefano Alessandrini, John Bjørnar Bremnes, Silke Dierer, Enrico Ferrero, et al. "Forecasting for dynamic line rating". *Renewable and Sustainable Energy Reviews* 52 (2015), pp. 1713–1730. URL: https://www.sciencedirect.com/science/article/pii/S1364032115007819 (cit. on pp. 7, 21).

[41] Zhengganzhe Chen, Bin Zhang, Anbo Meng, and Panshuo Li. "Prediction interval estimation of dynamic thermal rating considering weather uncertainty". *Electric Power Systems Research* 214 (2023), p. 108927. URL: https://www.sciencedirect.com/science/article/pii/S0378779622009786 (cit. on pp. 7, 21).

[42] Oisín Armstrong, Gary Southern, Alan Carroll, and Gerry O'Brien. "Low Wind Speed Occurrences and Aging Conductors: More Than Just a Sag Problem?" *2018 IEEE/PES Transmission and Distribution Conference and Exposition (T&D)*. 2018, pp. 1–5 (cit. on p. 8).

[43] Bishnu P. Bhattarai, Jake P. Gentle, Timothy McJunkin, Porter J. Hill, Kurt S. Myers, Alexander W. Abboud, et al. "Improvement of Transmission Line Ampacity Utilization by Weather-Based Dynamic Line Rating". *IEEE Transactions on Power Delivery* 33.4 (2018), pp. 1853–1863. URL: https://ieeexplore.ieee.org/document/8269366/ (visited on 05/02/2025) (cit. on pp. 8, 21).

[44] Peter J. Davison, Pádraig F. Lyons, and Philip C. Taylor. "Temperature sensitive load modelling for dynamic thermal ratings in distribution network overhead lines". *International Journal of Electrical Power & Energy Systems* 112 (2019), pp. 1–11. URL: https://www.sciencedirect.com/science/article/pii/S0142061518316089 (cit. on pp. 8, 21).

[45] Soheila Karimi, Petr Musilek, and Andrew M. Knight. "Dynamic thermal rating of transmission lines: A review". *Renewable and Sustainable Energy Reviews* 91 (2018), pp. 600–612. URL: https://www.sciencedirect.com/science/article/pii/S1364032118302119 (cit. on pp. 8, 13).

[46] D. Susa and M. Lehtonen. "Dynamic thermal modeling of power transformers: further Development-part I". *IEEE Transactions on Power Delivery* 21.4 (2006), pp. 1961–1970 (cit. on pp. 8, 21).

[47] Ildar Daminov, Anton Prokhorov, Raphael Caire, and Marie-Cécile Alvarez-Herault. "Assessment of dynamic transformer rating, considering current and temperature limitations". *International Journal of Electrical Power & Energy Systems* 129 (2021), p. 106886. URL: https://www.sciencedirect.com/science/article/pii/S0142061521001265 (cit. on pp. 8, 11, 21).

[48] Indera Arifianto, Fretz Josue, Robert Saers, Johanna Rosenlind, Patrik Hilber, and Suwarno. "Investigation of transformer top-oil temperature considering external factors". *2012 IEEE International Conference on Condition Monitoring and Diagnosis*. 2012, pp. 198–201 (cit. on pp. 9, 21).

[49] Jin Yang, Xuefeng Bai, Dani Strickland, Lee Jenkins, and Andrew M. Cross. "Dynamic Network Rating for Low Carbon Distribution Network Operation—A U.K. Application". *IEEE Transactions on Smart Grid* 6.2 (2015), pp. 988–998 (cit. on pp. 9, 21, 42).

[50] Ali Asghar Taheri, Ali Abdali, and Abbas Rabiee. "A Novel Model for Thermal Behavior Prediction of Oil-Immersed Distribution Transformers With Consideration of Solar Radiation". *IEEE Transactions on Power Delivery* 34.4 (2019), pp. 1634–1646 (cit. on pp. 9, 21).

[51] International Electrotechnical Commission. *Electric Cables – Calculation of the Current Rating – Part 1-1: Current Rating Equations (100% Load Factor) and Calculation of Losses*. IEC Standard 60287-1-1. 2018. URL: https://doi.org/10.1109/IEEESTD.2018.8353815 (cit. on pp. 9, 21, 36, 37, 81, 113, 170).

[52] Carson Bates, Keith Malmedal, and David Cain. "Cable Ampacity Calculations: A Comparison of Methods". *IEEE Transactions on Industry Applications* 52.1 (2016), pp. 112–118 (cit. on pp. 9, 21).

[53] Theofilos A. Papadopoulos, Andreas I. Chrysochos, and Michael Fotos. "Comparison of Power Cables Current Rating Calculation Methods". *2023 58th International Universities Power Engineering Conference (UPEC)*. 2023, pp. 1–6 (cit. on p. 9).

[54] Carson Bates. *Underground Cable Ampacity: A Fresh Look At Addressing The Future Electric Grid*. Colorado School of Mines, 2018 (cit. on p. 9).

[55] Devendra Narain Singh and Konchenapalli Devid. "Generalized relationships for estimating soil thermal resistivity". *Experimental Thermal and Fluid Science* 22.3 (2000), pp. 133–143. URL: https://www.sciencedirect.com/science/article/pii/S0894177700000200 (cit. on pp. 9, 21).

[56] B.J. Cosby, G.M. Hornberger, R.B. Clapp, and T.R. Ginn. "A Statistical Exploration of the Relationships of Soil Moisture Characteristics to the Physical Properties of Soils". *Water Resources Research* 20.6 (1984), pp. 682–690. URL: https://doi.org/10.1029/WR020i006p00682 (cit. on pp. 10, 21).

[57] Stephen D. Foss, Sheng H. Lin, and Roosevelt A. Fernandes. "Dynamic Thermal Line Ratings Part I Dynamic Ampacity Rating Algorithm". *IEEE Transactions on Power Apparatus and Systems* PAS-102.6 (1983), pp. 1858–1864 (cit. on pp. 10, 12, 13, 21).

[58] Ildar Daminov. "Dynamic Thermal Ratings of Power Transformers: Modelling, Concepts, and Application case" () (cit. on p. 11).

[59] Anjan K. Deb. *Powerline Ampacity System: Theory, Modeling and Applications*. Boca Raton, FL: CRC Press, 2000 (cit. on p. 11).

[60] Jana Heckenbergerova, Petr Musilek, and Konstantin Filimonenkov. "Assessment of seasonal static thermal ratings of overhead transmission conductors". *2011 IEEE Power and Energy Society General Meeting*. 2011, pp. 1–8 (cit. on pp. 12, 16, 21).

[61] M.W. Davis. "A new thermal rating approach: The real time thermal rating system for strategic overhead conductor transmission lines – Part I: General description and justification of the real time thermal rating system". *IEEE Transactions on Power Apparatus and Systems* 96.3 (1977), pp. 803–809 (cit. on p. 12).

[62] S. Foss, S. Lin, H. Stillwell, and R. Fernandes. "Dynamic Thermal Line Ratings Part II: Conductor Temperature Sensor and Laboratory Field Test Evaluation". *IEEE Transactions on Power Apparatus and Systems* PAS-102 (1983), pp. 1865–1876 (cit. on pp. 12, 21).

[63] Romain Dupin, George Kariniotakis, and Andrea Michiorri. "Overhead Lines Dynamic Line Rating Based on Probabilistic Day-Ahead Forecasting and Risk Assessment". *International Journal of Electrical Power & Energy Systems* 110 (2019), pp. 565–578. URL: https://www.sciencedirect.com/science/article/pii/S014206151831891X (cit. on pp. 12, 14, 21).

[64] Sudhakar Cherukupalli and George J. Anders. *Distributed Fiber Optic Sensing and Dynamic Rating of Power Cables*. Hoboken, NJ: Wiley-IEEE Press, 2019. URL: https://www.wiley.com/en-us/Distributed+Fiber+Optic+Sensing+and+Dynamic+Rating+of+Power+Cables-p-9781119487722 (cit. on p. 13).

[65] Philipp Glaum and Fabian Hofmann. "Leveraging the existing German transmission grid with dynamic line rating". *Applied Energy* 343 (2023), p. 121199. URL: https://www.sciencedirect.com/science/article/pii/S0306261923005639 (cit. on pp. 13, 21).

[66] Yinxiao Li, Qixin Chen, Goran Strbac, Kyeon Hur, and Chongqing Kang. "Active Distribution Network Expansion Planning With Dynamic Thermal Rating of Underground Cables and Transformers". *IEEE Transactions on Smart Grid* 15.1 (2024), pp. 218–232 (cit. on pp. 13, 17, 21).

[67] Yinxiao Li, Yi Wang, Chongqing Kang, Jie Song, Guannan He, and Qixin Chen. "Improving distributed PV integration with dynamic thermal rating of power distribution equipment". *iScience* 25.8 (2022), p. 104808. URL: https://www.sciencedirect.com/science/article/pii/S258900422201080X (cit. on pp. 13, 21).

[68] Shuran Liu and Konstantinos Kopsidas. "Risk-Based Underground Cable Circuit Ratings for Flexible Wind Power Integration". *IEEE Transactions on Power Delivery* 36.1 (2021), pp. 145–155 (cit. on pp. 13, 21).

[69] Susanne Sandell and Iver Bakken Sperstad. "Evaluating grid development strategies for a regional grid using dynamic line rating sensors". *2024 IEEE PES Innovative Smart Grid Technologies Europe (ISGT EUROPE)*. 2024, pp. 1–5 (cit. on p. 13).

[70] Dale Douglass, William Chisholm, Glenn Davidson, Ian Grant, Keith Lindsey, Mark Lancaster, et al. "Real-Time Overhead Transmission-Line Monitoring for Dynamic Rating". *IEEE Transactions on Power Delivery* 31.3 (2016), pp. 921–927 (cit. on pp. 13, 21).

[71] Kateryna Morozovska and Patrik Hilber. "Study of the Monitoring Systems for Dynamic Line Rating". *Energy Procedia* 105 (2017), pp. 2557–2562. URL: https://www.sciencedirect.com/science/article/pii/S1876610217307981 (cit. on p. 13).

[72] D. O. Koval and Roy Billinton. "Determination of Transmission Line Ampacities by Probability and Numerical Methods". *IEEE Transactions on Power Apparatus and Systems* PAS-89.7 (1970), pp. 1485–1492 (cit. on pp. 14, 21).

[73] J.L. Reding. "A method for determining probability based allowable current ratings for BPA's transmission lines". *IEEE Transactions on Power Delivery* 9.1 (1994), pp. 153–161 (cit. on pp. 14, 21).

[74] Antonio Bracale, Pierluigi Caramia, Pasquale De Falco, Andrea Michiorri, and Angela Russo. "Day-Ahead and Intraday Forecasts of the Dynamic Line Rating for Buried Cables". *IEEE Access* 7 (2019), pp. 4709–4725 (cit. on pp. 14, 21).

[75] Dale A. Douglass, Jake Gentle, Huu-Minh Nguyen, William Chisholm, Charles Xu, Tip Goodwin, et al. "A Review of Dynamic Thermal Line Rating Methods With Forecasting". *IEEE Transactions on Power Delivery* 34.6 (2019), pp. 2100–2109 (cit. on p. 14).

[76] Nicola Viafora, Stefanos Delikaraoglou, Pierre Pinson, and Joachim Holbøll. "Chance-constrained optimal power flow with non-parametric probability distributions of dynamic line ratings". *International Journal of Electrical Power & Energy Systems* 114 (2020), p. 105389. URL: https://www.sciencedirect.com/science/article/pii/S0142061519309317 (cit. on pp. 14, 17, 21).

[77] SeyedeFatemeh Hajeforosh and Math H.J. Bollen. "Uncertainty analysis of stochastic dynamic line rating". *Electric Power Systems Research* 194 (2021), p. 107043. URL: https://www.sciencedirect.com/science/article/pii/S0378779621000237 (cit. on pp. 14, 21).

[78] F.R. McElvain and S.S. Mulnix. "Statistically determined static thermal ratings of overhead high voltage transmission lines in the Rocky Mountain region". *IEEE Transactions on Power Systems* 15.2 (2000), pp. 899–902 (cit. on pp. 14, 21).

[79] B. Clairmont. *Increased Power Flow Through Transmission Circuits: Overhead Line Case Studies and Quasi-Dynamic Rating*. Tech. rep. 1012533. Palo Alto, CA: Electric Power Research Institute (EPRI), 2006. URL: https://www.epri.com/research/products/000000000001012533 (cit. on pp. 14, 15, 21).

[80] H. Shokouhandeh, M. A. Kamarposhti, G. Lorenzini, A. A. A. Solyman, and R. S. Agieb. "Increasing Power Transfer Capability of Transmission Lines Using the Quasi-Dynamic Operation and Monitoring System". *Mathematical Modelling of Engineering Problems* 9.2 (2022), pp. 291–297. URL: https://iieta.org/journals/mmep/paper/10.18280/mmep.090201 (cit. on pp. 15, 21).

[81] Fan Song, Yanling Wang, Hongbo Yan, Xiaofeng Zhou, and Zhiqiang Niu. "Increasing the Utilization of Transmission Lines Capacity by Quasi-Dynamic Thermal Ratings". *Energies* 12.5 (2019), p. 792. URL: https://www.mdpi.com/1996-1073/12/5/792 (cit. on pp. 15, 17, 21, 68).

[82] Mohammad Mahmoudian Esfahani and Gholam Reza Yousefi. "Real Time Congestion Management in Power Systems Considering Quasi-Dynamic Thermal Rating and Congestion Clearing Time". *IEEE Transactions on Industrial Informatics* 12.2 (2016), pp. 745–754 (cit. on pp. 15, 21).

[83] Yanling Wang, Zidan Sun, Zhijie Yan, Likai Liang, Fan Song, and Zhiqiang Niu. "Power Transmission Congestion Management Based on Quasi-Dynamic Thermal Rating". *Processes* 7.5 (2019), p. 244. URL: https://www.mdpi.com/2227-9717/7/5/244 (cit. on pp. 15, 21).

[84] Huanyue Liao and Wei Liu. "Weather-based dynamic line rating of overhead transmission lines over Europe interconnected network". *IOP Conference Series: Materials Science and Engineering* 382 (2018), p. 052035. URL: https://iopscience.iop.org/article/10.1088/1757-899X/382/5/052035 (visited on 04/20/2023) (cit. on pp. 15, 21).

[85] Jana Heckenbergerová, Petr Musilek, and Konstantin Filimonenkov. "Quantification of Gains and Risks of Static Thermal Rating Based on Typical Meteorological Year". *International Journal of Electrical Power & Energy Systems* 44.1 (2013), pp. 227–235. URL: https://www.sciencedirect.com/science/article/pii/S0142061512003651 (cit. on pp. 16, 21).

[86] Rafael Alberdi, Igor Albizu, Elvira Fernandez, Roberto Fernandez, and Miren Terese Bedialauneta. "Overhead Line Ampacity Forecasting With a Focus on Safety". *IEEE Transactions on Power Delivery* 37.1 (2022), pp. 329–337 (cit. on p. 16).

[87] CIGRE. *Guide for the selection of weather parameters for bare overhead conductor ratings*. Technical Brochure 299. CIGRE, 2006 (cit. on pp. 16, 21, 32).

[88] A. Kirilenko, M. Esmaili, and C. Y. Chung. "Risk-Averse Stochastic Dynamic Line Rating Models". *IEEE Transactions on Power Systems* 36.4 (2021), pp. 3070–3079. URL: https://doi.org/10.1109/TPWRS.2020.3045589 (cit. on pp. 16, 17).

[89] Jiashen Teh and Ching-Ming Lai. "Reliability impacts of the dynamic thermal rating and battery energy storage systems on wind-integrated power networks". *Sustainable Energy, Grids and Networks* 20 (2019), p. 100268. URL: https://www.sciencedirect.com/science/article/pii/S2352467719304680 (cit. on pp. 16, 21).

[90] Kateryna Morozovska, Miguel Heleno, Alan Valenzuela Meza, and Patrik Hilber. "Including Dynamic Line Rating Into the Optimal Planning of Distributed Energy Resources". *IEEE Transactions on Smart Grid* 12.6 (2021), pp. 5052–5059 (cit. on pp. 16, 17, 21).

[91] Mengxia Wang, Ming Yang, and Xueshan Han. "Optimal power flow considering transient thermal behavior of overhead transmission lines". *International Journal of Electrical Power & Energy Systems* 114 (2020), p. 105396. URL: https://linkinghub.elsevier.com/retrieve/pii/S0142061518320799 (visited on 05/16/2024) (cit. on pp. 17, 21).

[92] Matthias A. Bucher, Maria Vrakopoulou, and Goran Andersson. "Probabilistic N-1 security assessment incorporating dynamic line ratings". *2013 IEEE Power & Energy Society General Meeting*. Vancouver, BC: IEEE, 2013, pp. 1–5. URL: http://ieeexplore.ieee.org/document/6672679/ (visited on 01/15/2024) (cit. on pp. 17, 21).

[93] Antonio Bracale, Guido Carpinelli, and Pasquale De Falco. "Probabilistic Risk-Based Management of Distribution Transformers by Dynamic Transformer Rating". *International Journal of Electrical Power & Energy Systems* 113 (2019), pp. 229–243. URL: https://www.sciencedirect.com/science/article/pii/S0142061519308063 (cit. on pp. 17, 21).

[94] Daniel Bienstock, Michael Chertkov, and Sean Harnett. "Chance-Constrained Optimal Power Flow: Risk-Aware Network Control under Uncertainty". *SIAM Review* 56.3 (2014), pp. 461–495. URL: https://epubs.siam.org/doi/10.1137/130910312 (cit. on pp. 17, 21).

[95] Andrej Trpovski and Thomas Hamacher. "A Comparative Analysis of Transmission System Planning for Overhead and Underground Power Systems using AC and DC Power Flow". *2019 IEEE PES Innovative Smart Grid Technologies Europe (ISGT-Europe)*. 2019, pp. 1–5 (cit. on p. 17).

[96] Junpeng Zhan, Weijia Liu, and C. Y. Chung. "Stochastic Transmission Expansion Planning Considering Uncertain Dynamic Thermal Rating of Overhead Lines". *IEEE Transactions on Power Systems* 34.1 (2019), pp. 432–443 (cit. on pp. 17, 21).

[97] Cheng Wang, Rui Gao, Feng Qiu, Jianhui Wang, and Linwei Xin. "Risk-Based Distributionally Robust Optimal Power Flow With Dynamic Line Rating". *IEEE Transactions on Power Systems* 33.6 (2018), pp. 6074–6086 (cit. on p. 17).

[98] Matthias A. Bucher and Göran Andersson. "Robust Corrective Control Measures in Power Systems With Dynamic Line Rating". *IEEE Transactions on Power Systems* 31.3 (2016), pp. 2034–2043 (cit. on p. 17).

[99] H. Lee Willis and R. Roy Schrieber. *Aging Power Delivery Infrastructures*. 2nd. CRC Press, 2013. URL: https://doi.org/10.1201/b14559 (cit. on p. 18).

[100] PJM Interconnection. *Guide for Determination of Power Transformer Load Capability Ratings*. https://www.pjm.com/-/media/committees-groups/committees/pc/20180510/20180510-item-07-transformer-loading-guide.ashx. 2018 (cit. on p. 18).

[101] Jelena Lj. Klimenta, Marija V. Panić, Miodrag S. Stojanović, Dardan O. Klimenta, Miloš J. Milovanović, and Bojan D. Perović. "Thermal Aging Management for Electricity Distribution Networks: FEM-Based Qualification of Underground Power Cables". *Thermal Science* 26.5 Part B (2022), pp. 3937–3950. URL: https://doi.org/10.2298/TSCI2205937K (cit. on p. 18).

[102] Jiashen Teh and Ching-Ming Lai. "Risk-Based Management of Transmission Lines Enhanced With the Dynamic Thermal Rating System". *IEEE Access* 7 (2019), pp. 76562–76571. URL: https://doi.org/10.1109/ACCESS.2019.2921575 (cit. on p. 18).

[103] Z. Z. Bajbor. "Cable Life Expectancy Calculation - A Practical Approach". *IEEE Transactions on Electrical Insulation* EI-22.4 (1987), pp. 485–487 (cit. on p. 18).

[104] Ming Dong. "A Data-driven Long-Term Dynamic Rating Estimating Method for Power Transformers". *IEEE Transactions on Power Delivery* 36.2 (2021), pp. 686–697. URL: https://doi.org/10.1109/TPWRD.2020.2988921 (cit. on p. 18).

[105] IEEE Power and Energy Society. *IEEE Guide for Loading Mineral-Oil-Immersed Transformers*. 2011. URL: https://doi.org/10.1109/IEEESTD.2012.6138671 (cit. on pp. 18, 21).

[106] Tahereh Zarei, Kateryna Morozovska, Tor Laneryd, Patrik Hilber, Malin Wihlén, and Olle Hansson. "Reliability Considerations and Economic Benefits of Dynamic Transformer Rating for Wind Energy Integration". *International Journal of Electrical Power & Energy Systems* 106 (2019), pp. 598–606. URL: https://doi.org/10.1016/j.ijepes.2018.09.038 (cit. on p. 18).

[107] Md. Mafijul Islam Bhuiyan. "Spatial Analysis of Thermal Aging of Overhead Power Transmission Lines" (2011). URL: https://era.library.ualberta.ca/items/e1e4a69b-ee8b-4f78-9ab3-6512b9be1196 (cit. on p. 18).

[108] JL Reding. "Conductors, connectors, and hardware operating at high temperatures". *IEEE PES General Meeting*. 2010, pp. 1–6 (cit. on p. 18).

[109] Energy Research and Development Division. *Demonstration of Advanced Conductors for Overhead Transmission Lines*. Final Project Report. Sacramento, CA: Electric Power Research Institute, 2008 (cit. on p. 18).

[110] G. M. Beers, S. R. Gilligan, H. W. Lis, and J. M. Schamberger. "Transmission Conductor Ratings". *IEEE Transactions on Power Apparatus and Systems* 82.68 (1963), pp. 767–775 (cit. on pp. 18, 114).

[111] Richard H. Moss, James A. Edmonds, Kathy A. Hibbard, Martin R. Manning, Steven K. Rose, Detlef P. van Vuuren, et al. "The Next Generation of Scenarios for Climate Change Research and Assessment". *Nature* 463.7282 (2010), pp. 747–756. URL: https://www.nature.com/articles/nature08823 (cit. on pp. 19, 130).

[112] A. T. D. Perera, Vahid M. Nik, Deliang Chen, Jean-Louis Scartezzini, and Tianzhen Hong. "Quantifying the impacts of climate change and extreme climate events on energy systems". *Nature Energy* 5.2 (2020), pp. 150–159. URL: https://www.nature.com/articles/s41560-020-0558-0 (visited on 05/21/2025) (cit. on p. 20).

[113] B. Gorgan, P. V. Notingher, J. M. Wetzer, H. F.A. Verhaart, P. A.A.F. Wouters, and A. Van Schijndel. "Influence of solar irradiation on power transformer thermal balance". *IEEE Transactions on Dielectrics and Electrical Insulation* 19.6 (2012), pp. 1843–1850 (cit. on pp. 21, 43).

[114] Masood Jabarnejad and Jorge Valenzuela. "Optimal investment plan for dynamic thermal rating using benders decomposition". *European Journal of Operational Research* 248.3 (2016), pp. 917–929. URL: https://www.sciencedirect.com/science/article/pii/S0377221715007274 (cit. on p. 21).

[115] S. Hadiwidjaja, S. D. Montana Salas, and A. Michiorri. "Quasi-dynamic line rating spatial and temporal analysis for network planning". *27th International Conference on Electricity Distribution (CIRED 2023)*. Vol. 2023. 2023, pp. 276–280 (cit. on pp. 33, 34, 45, 47, 157).

[116] CIGRE Working Group B1.07. *Statistics of AC Underground Cables in Power Networks*. Technical Brochure 338. International Council on Large Electric Systems (CIGRE), 2007. URL: https://www.e-cigre.org/publication/338-statistics-of-ac-underground-cables-in-power-networks (cit. on p. 34).

[117] Christoph Emanuel Mueller, Silke Inga Keil, and Christian Bauer. "Underground cables vs. overhead lines: Quasi-experimental evidence for the effects on public risk expectations, attitudes, and protest behavior". *Energy Policy* 125 (2019), pp. 456–466. URL: https://linkinghub.elsevier.com/retrieve/pii/S0301421518307079 (visited on 05/12/2023) (cit. on p. 34).

[118] Nils May and Karsten Neuhoff. "Underground Cables versus Overhead Lines: Do Cables Increase Social Acceptance of Grid Development? Results of a Contingent Valuation Survey in Germany". *International Journal of Sustainable Energy Planning and Management* 3 (2016), pp. 29–46 (cit. on p. 34).

[119] Jie Ren, Lei Men, Wei Zhang, Yang Liu, and Shaopeng Wu. "A new empirical model for the estimation of soil thermal conductivity". *Environmental Earth Sciences* 78.11 (2019), p. 361. URL: https://doi.org/10.1007/s12665-019-8360-7 (cit. on p. 38).

[120] R. S. Olsen, G. J. Anders, J. Holboell, and U. S. Gudmundsdottir. "Modelling of Dynamic Transmission Cable Temperature Considering Soil-Specific Heat, Thermal Resistivity, and Precipitation". *IEEE Transactions on Power Delivery* 28.3 (2013), pp. 1909–1917. URL: https://doi.org/10.1109/TPWRD.2013.2263300 (cit. on p. 38).

[121] Oistein Johansen. "Thermal Conductivity of Soils". PhD thesis. University of Trondheim, Norway, 1977 (cit. on p. 38).

[122] Takuya Akiba, Shotaro Sano, Takeru Yanase, Toshihiko Ohta, and Masanori Koyama. "Optuna: A Next-generation Hyperparameter Optimization Framework". *Proceedings of the 25th ACM SIGKDD International Conference on Knowledge Discovery & Data Mining*. ACM, 2019, pp. 2623–2631. URL: https://doi.org/10.1145/3292500.3330701 (cit. on pp. 40, 97).

[123] Tianqi Chen and Carlos Guestrin. "XGBoost: A Scalable Tree Boosting System". *Proceedings of the 22nd ACM SIGKDD International Conference on Knowledge Discovery and Data Mining*. ACM, 2016, pp. 785–794. URL: https://doi.org/10.1145/2939672.2939785 (cit. on p. 40).

[124] Robert Tibshirani. "Regression Shrinkage and Selection Via the Lasso". *Journal of the Royal Statistical Society: Series B (Methodological)* 58.1 (1996), pp. 267–288. URL: https://doi.org/10.1111/j.2517-6161.1996.tb02080.x (cit. on p. 40).

[125] S.V. Kulkarni and S.A. Khaparde. *Transformer Engineering: Design, Technology, and Diagnostics*. 2nd. Boca Raton, FL: CRC Press, 2013 (cit. on p. 42).

[126] G. Swift, T.S. Molinski, and W. Lehn. "A fundamental approach to transformer thermal modeling. I. Theory and equivalent circuit". *IEEE Transactions on Power Delivery* 16.2 (2001), pp. 171–175 (cit. on p. 43).

[127] Wílerson Venceslau Calil, Kateryna Morozovska, Tor Laneryd, Eduardo Coelho Marques da Costa, and Maurício Barbosa de Camargo Salles. "Determining total cost of ownership and peak efficiency index of dynamically rated transformer at the PV-power plant". *Electric Power Systems Research* 229 (2024), p. 110061 (cit. on pp. 43, 48, 169).

[128] International Electrotechnical Commission (IEC). *Power transformers - Part 2: Temperature rise for liquid-immersed transformers*. Geneva, Switzerland, 2011 (cit. on pp. 43, 48, 168).

[129] Irina Lupandina, Wolfgang Gawlik, Michael Schrammel, et al. "Evaluation of dynamic loading capability for optimal loading strategies of power transformers". *Elektrotech. Inftech.* 137 (2020), pp. 515–522. URL: https://doi-org.minesparis-psl.idm.oclc.org/10.1007/s00502-020-00845-2 (cit. on pp. 43, 61).

[130] Rainer Hiederer. *Mapping Soil Properties for Europe: Spatial Representation of Soil Database Attributes*. Dataset. 2013. URL: https://data.europa.eu/doi/10.2788/94128 (cit. on p. 49).

[131] Wouter Dorigo, Ina Himmelbauer, Daniel Aberer, Lukas Schremmer, Ivana Petrakovic, Luca Zappa, et al. "The International Soil Moisture Network: Serving Earth System Science for Over a Decade". *Hydrology and Earth System Sciences* 25 (2021), pp. 5749–5804. URL: https://doi.org/10.5194/hess-25-5749-2021 (cit. on p. 49).

[132] Turan Gonen. *Electric Power Transmission System Engineering: Analysis and Design*. 3rd. Boca Raton, FL: CRC Press, 2014 (cit. on pp. 66–68).

[133] T Sum-Im, GA Taylor, MR Irving, and YH Song. "A comparative study of state-of-the-art transmission expansion planning tools". *Proceedings of the 41st International Universities Power Engineering Conference*. Vol. 1. IEEE. 2006, pp. 267–271 (cit. on p. 68).

[134] Sara Lumbreras and Andrés Ramos. "The new challenges to transmission expansion planning. Survey of recent practice and literature review". *Electric Power Systems Research* 134 (2016), pp. 19–29 (cit. on p. 69).

[135] Enrique Castillo, Antonio J Conejo, Pablo Pedregal, Ricardo Garcia, and Natalia Alguacil. *Building and solving mathematical programming models in engineering and science*. John Wiley & Sons, 2011 (cit. on p. 69).

[136] Antonio J Conejo, Luis Baringo, S Jalal Kazempour, and Afzal S Siddiqui. "Investment in electricity generation and transmission". *Cham Zug, Switzerland: Springer International Publishing* 119 (2016) (cit. on p. 69).

[137] Dimitris Bertsimas, David B. Brown, and Constantine Caramanis. "Theory and Applications of Robust Optimization". *SIAM Review* 53.3 (2011), pp. 464–501. URL: http://epubs.siam.org/doi/10.1137/080734510 (visited on 04/21/2023) (cit. on p. 69).

[138] Sonja Wogrin, D Tejada-Arango, Anthony Downward, and AB Philpott. "Welfare-maximizing transmission capacity expansion under uncertainty". *Philosophical Transactions of the Royal Society A* 379.2202 (2021), p. 20190436 (cit. on p. 69).

[139] Reza Hemmati, Rahmat-Allah Hooshmand, and Amin Khodabakhshian. "State-of-the-art of transmission expansion planning: Comprehensive review". *Renewable and Sustainable Energy Reviews* 23 (2013), pp. 312–319. URL: https://linkinghub.elsevier.com/retrieve/pii/S1364032113001743 (visited on 04/21/2023) (cit. on p. 70).

[140] Gurobi Optimization, LLC. *Gurobi Optimizer Reference Manual*. 2024. URL: https://www.gurobi.com (cit. on pp. 72, 73, 120).

[141] Á. García-Cerezo, R. García-Bertrand, and L. Baringo. "Computational Performance Enhancement Strategies for Risk-Averse Two-Stage Stochastic Generation and Transmission Network Expansion Planning". *IEEE Transactions on Power Systems* 39.1 (2024), pp. 273–286 (cit. on pp. 73, 104).

[142] Andrés Ramos, Erik Quispe, and Sara Lumbreras. "openTEPES: Open-source Transmission and Generation Expansion Planning". *SoftwareX* 18 (2022), p. 101070. URL: https://www.sciencedirect.com/science/article/pii/S235271102200053X (cit. on p. 74).

[143] Fabian Neumann, Veit Hagenmeyer, and Tom Brown. "Assessments of linear power flow and transmission loss approximations in coordinated capacity expansion problems". *Applied Energy* 314 (), p. 118859. URL: https://linkinghub.elsevier.com/retrieve/pii/S0306261922002938 (cit. on p. 74).

[144] PJM Interconnection. *Guide for Determination of Bare Overhead Transmission Conductors*. Technical guide, PJM Interconnection. 2022. URL: https://www.pjm.com/-/media/documents/manuals/m14c.ashx (cit. on pp. 76, 77).

[145] C. Grigg, P. Wong, P. Albrecht, R. Allan, M. Bhavaraju, R. Billinton, et al. "The IEEE Reliability Test System-1996. A report prepared by the Reliability Test System Task Force of the Application of Probability Methods Subcommittee". *IEEE Transactions on Power Systems* 14.3 (1999), pp. 1010–1020 (cit. on pp. 79, 87, 103, 104, 110, 114, 140, 142).

[146] Tommy Odland. *KDEpy: Kernel Density Estimation in Python*. https://doi.org/10.5281/zenodo.2392268. 2018 (cit. on pp. 81, 114, 116).

[147] Ivar Bjerkebæk and Håkon Toftaker. "Reliability assessment combining importance resampling and the cross entropy method". *Electric Power Systems Research* 234 (2024), p. 110722. URL: https://www.sciencedirect.com/science/article/pii/S0378779624006084 (cit. on p. 83).

[148] Adriano Arrigo, Christos Ordoudis, Jalal Kazempour, Zacharie de Grève, Jean-François Toubeau, and François Vallée. "Optimal Power Flow Under Uncertainty: An Extensive Out-of-Sample Analysis". *2019 IEEE PES Innovative Smart Grid Technologies Europe (ISGT-Europe)*. 2019, pp. 1–5 (cit. on pp. 83, 116).

[149] Svante Arrhenius. "Über die Dissociationswärme und den Einfluss der Temperatur auf den Dissociationsgrad der Elektrolyte". *Zeitschrift für physikalische Chemie* 4.1 (1889), pp. 96–116 (cit. on p. 85).

[150] Selma K. E. Awadallah, Jovica V. Milanović, and Paul N. Jarman. "The Influence of Modeling Transformer Age Related Failures on System Reliability". *IEEE Transactions on Power Systems* 30.2 (2015), pp. 970–979 (cit. on p. 85).

[151] PyPSA. *System Optimization*. URL: https://pypsa.readthedocs.io/en/latest/user-guide/optimal-power-flow.html (visited on 02/03/2025) (cit. on pp. 87, 93, 95, 100, 101).

[152] Hossein Seifi and Mohammad Sadegh Sepasian. "Load Forecasting". *Electric Power System Planning*. Power Systems. Berlin, Heidelberg: Springer, 2011, pp. 161–187. URL: https://doi.org/10.1007/978-3-642-17907-2_7 (cit. on pp. 87, 96).

[153] K. B. Lindberg, P. Seljom, H. Madsen, D. Fischer, and M. Korpås. "Long-term electricity load forecasting: Current and future trends". *Utilities Policy* 58 (2019), pp. 102–119. URL: https://doi.org/10.1016/j.jup.2019.04.002 (cit. on pp. 87, 96).

[154] U.S. Energy Information Administration. *Annual Energy Outlook 2023*. https://www.eia.gov/outlooks/aeo/. 2023 (cit. on pp. 87, 101).

[155] Govinda R. Timilsina. "Demystifying the Costs of Electricity Generation Technologies". *Energy Strategy Reviews* 30 (2020), p. 100512 (cit. on pp. 87, 101).

[156] S.J. Smith and T.M.L. Wigley. "Multi-Gas Forcing Stabilization with the MiniCAM". *Energy Journal (Special Issue #3)* (2006), pp. 373–391 (cit. on pp. 87, 92).

[157] D. van Vuuren, M. den Elzen, P. Lucas, B. Eickhout, B. Strengers, B. van Ruijven, et al. "Stabilizing greenhouse gas concentrations at low levels: an assessment of reduction strategies and costs". *Climatic Change* (2007) (cit. on pp. 87, 92).

[158] L. Clarke, J. Edmonds, H. Jacoby, H. Pitcher, J. Reilly, and R. Richels. *Scenarios of Greenhouse Gas Emissions and Atmospheric Concentrations*. Sub-report 2.1A of Synthesis and Assessment Product 2.1. Washington, DC, USA: U.S. Climate Change Science Program and the Subcommittee on Global Change Research, Department of Energy, Office of Biological & Environmental Research, 2007, p. 154 (cit. on pp. 87, 92).

[159] M.A. Wise, K.V. Calvin, A.M. Thomson, L.E. Clarke, B. Bond-Lamberty, R.D. Sands, et al. "Implications of Limiting CO2 Concentrations for Land Use and Energy". *Science* 324 (2009), pp. 1183–1186 (cit. on pp. 87, 92).

[160] RTE – Réseau de Transport d'Électricité. *éCOmix – All of France's electricity data in real time*. https://www.rte-france.com/eco2mix (cit. on pp. 87, 96, 111).

[161] ENTSO-E. *ENTSO-E Transparency Platform*. https://transparency.entsoe.eu/ (cit. on pp. 87, 96).

[162] Niels G. Mortensen, Neil Davis, Jake Badger, and Andrea N. Hahmann. *Global Wind Atlas version 3.0*. https://globalwindatlas.info/. 2023 (cit. on p. 87).

[163] Marie-Alix Dupré la Tour. "Photovoltaic and Wind Energy Potential in Europe–A Systematic Review". *Renewable and Sustainable Energy Reviews* 179 (2023), p. 113189 (cit. on pp. 87, 99, 101).

[164] Peter Enevoldsen and Mark Z. Jacobson. "Data Investigation of Installed and Output Power Densities of Onshore and Offshore Wind Turbines Worldwide". *Energy for Sustainable Development* 60 (2021), pp. 40–51 (cit. on pp. 87, 99, 101).

[165] Bokan Chen, Jianhui Wang, Lizhi Wang, Yanyi He, and Zhaoyu Wang. "Robust Optimization for Transmission Expansion Planning: Minimax Cost vs. Minimax Regret". *IEEE Transactions on Power Systems* 29.6 (2014), pp. 3069–3077 (cit. on pp. 87, 112, 143).

[166] Pantelis Capros, Leonidas Paroussos, Panagiotis Fragkos, Stella Tsani, Baptiste Boitier, Fabian Wagner, et al. "European decarbonisation pathways under alternative technological and policy choices: A multi-model analysis". *Energy Strategy Reviews* 2.3 (2014), pp. 231–245. URL: https://www.sciencedirect.com/science/article/pii/S2211467X13001053 (cit. on pp. 87, 112, 143).

[167] Mark Bolinger, Joachim Seel, Julie Mulvaney Kemp, Cody Warner, Anjali Katta, and Dana Robson. *Utility-Scale Solar, 2023 Edition: Empirical Trends in Deployment, Technology, Cost, Performance, PPA Pricing, and Value in the United States*. 2023 (cit. on pp. 87, 112, 132, 144).

[168] Tyler Stehly, Annika Eberle, Owen Roberts, and Daniel Mulas Hernando. *Land-Based Wind / Electricity / 2024*. 2024. URL: https://atb.nrel.gov/electricity/2024/land-based_wind (cit. on pp. 87, 112, 132, 144).

[169] Danish Energy Agency. *Technology Data for Transport of Energy*. Version 7. 2024. URL: https://ens.dk/en/analyses-and-statistics/technology-data-transport-energy (cit. on pp. 87, 112, 132, 144).

[170] Edmund Widl, Dennis Cronbach, Peter Sorknæs, Jaume Fitó, Daniel Muschick, Maurizio Repetto, et al. "Expert survey and classification of tools for modeling and simulating hybrid energy networks". *Sustainable Energy, Grids and Networks* 32 (2022), p. 100913. URL: https://www.sciencedirect.com/science/article/pii/S2352467722001606 (cit. on p. 89).

[171] Philipp Glaum and Fabian Hofmann. "Leveraging the existing German transmission grid with dynamic line rating". *Applied Energy* 343 (2023), p. 121199. URL: https://www.sciencedirect.com/science/article/pii/S0306261923005639 (cit. on p. 91).

[172] B. Xiong, D. Fioriti, F. Neumann, I. Riepin, and T. Brown. "Modelling the high-voltage grid using open data for Europe and beyond". *Scientific Data* 12 (2025), p. 277. URL: https://doi.org/10.1038/s41597-025-04550-7 (cit. on pp. 91, 100, 139).

[173] Fabian Neumann, Elisabeth Zeyen, Marta Victoria, and Tom Brown. "The potential role of a hydrogen network in Europe". *Joule* 7.8 (2023), pp. 1793–1817. URL: https://www.sciencedirect.com/science/article/pii/S2542435123002660 (cit. on p. 92).

[174] Eurostat. *Statistical Regions in the European Union and Partner Countries—NUTS and Statistical Regions 2021*. https://ec.europa.eu/eurostat/web/nuts/background. 2021 (cit. on p. 99).

[175] European Environment Agency. *Natura 2000 Protected Areas Network*. https://www.eea.europa.eu/themes/biodiversity/natura-2000 (cit. on p. 99).

[176] The Wind Power EI. *The Wind Power Database*. http://www.thewindpower.net. 19, rue du Limousin, 31170 Tournefeuille, France, 2023 (cit. on p. 99).

[177] Danish Energy Agency and Energinet. *Technology Catalogues* (cit. on p. 101).

[178] C. Barrows, E. Hale, D. Helms, W. Jones, J. Katz, J. King, et al. "The IEEE Reliability Test System: A Proposed 2019 Update". *IEEE Transactions on Power Systems* (2019) (cit. on p. 103).

[179] Jiashen Teh and Ian Cotton. "Critical span identification model for dynamic thermal rating system placement". *IET Generation, Transmission & Distribution* 10.2 (2015), pp. 1–8. URL: https://doi.org/10.1049/iet-gtd.2015.0601 (cit. on p. 110).

[180] RTE – Réseau de Transport d'Électricité. *Futurs énergétiques 2050 – Rapport complet*. 2022. URL: https://rte-futursenergetiques2050.com/documents (cit. on pp. 112, 132, 143, 144, 174).

[181] Coastal Climate Change Infographic Series (NCCARF). *What are the RCPs?* Infographic, CoastAdapt / NCCARF. 2017. URL: https://coastadapt.com.au/sites/default/files/infographics/15-117-NCCARFINFOGRAPHICS-01-UPLOADED-WEB%5C%2827Feb%5C%29.pdf (cit. on p. 127).

[182] *Climate and energy indicators for Europe from 2005 to 2100 derived from climate projections [dataset]*. Copernicus Climate Change Service (C3S) Climate Data Store (CDS). 2021 (cit. on pp. 132, 140, 143).

[183] Copernicus Climate Change Service. *Climate and energy related variables from the Pan-European Climate Database derived from reanalysis and climate projections*. https://cds.climate.copernicus.eu. 2024 (cit. on p. 164).

[184] TELE-FONIKA Kable S.A. *High and Extra High Voltage Cables*. 1st edition. Kraków, Poland: TELE-FONIKA Kable S.A., 2019. URL: https://www.tfkable.com (cit. on pp. 173, 174).

[185] CIGRÉ Working Group A2.36. *Guidelines for Conducting Design Reviews for Power Transformers*. Technical Report 529. CIGRÉ, 2013 (cit. on p. 174).

[186] D. Cable. *66–500 kV XLPE Cable: High and Extra High Voltage Cable System*. Barbaros Bulvarı 59, Beşiktaş, Istanbul, Turkey: Demirer Cable, 2018 (cit. on p. 174).

RÉSUMÉ

Cette thèse examine les impacts du changement climatique sur les capacités thermiques des composants des réseaux de transport d'électricité et propose une méthodologie intégrée pour leur prise en compte dans la planification à long terme des réseaux électriques. La recherche s'articule autour de l'interaction de trois domaines clés : **modélisation thermique des composants de réseau de transport**, **planification à long terme du réseau** et **changement climatique**, réduisant ainsi la lacune méthodologique inhérente aux approches statiques traditionnelles, qui souvent n'intègrent pas la variabilité climatique et manquent de spécificité temporelle ou spatiale. Pour combler cette lacune, une méthodologie quasi-Dynamic Thermal Rating (qDTR) est développée, permettant de capturer l'influence dynamique des conditions environnementales sur la capacité des composants. Les résultats indiquent que, dans des études de cas européennes, les projections climatiques futures devraient entraîner une diminution de la capacité de réseau de transport, avec des réductions moyennes sous le scénario à fortes émissions $RCP_{8.5}$ (2070) de 1,53% pour les lignes aériennes, 2,1% pour les transformateurs de puissance et 0,2% pour les câbles souterrains par rapport aux références historiques. Néanmoins, comparée aux capacités fixes conventionnels, l'approche proposée offre des avantages économiques, réduisant les besoins totaux en investissements jusqu'à 68,1% et les coûts opérationnels de 0,36%. De plus, des résolutions temporelles plus fines (mois/heure) permettent de capturer efficacement la variabilité intra-annuelle et intra-quotidienne, entraînant une réduction de 20,14% de pertes électriques du réseau, l'élimination des renforts liés aux réductions de production et le report complet des dépenses d'investissement dans plusieurs cas. Dans l'ensemble, ces résultats démontrent que les probabiliste, basé sur les informations climatiques thermal ratings sont à la fois techniquement réalisables et économiquement avantageux. En reliant explicitement les variations temporelles et spatiales de capacité et de flexibilité à la planification des investissements à long terme, la méthodologie proposée améliore la résilience, la fiabilité et l'efficacité économique des systèmes électriques futurs dans un contexte d'incertitude climatique croissante.

MOTS CLÉS

Capacités thermiques dynamiques, Changement climatique, Modèles thermiques, Planification de l'expansion des réseaux

ABSTRACT

This thesis investigates the impacts of climate change on the thermal ratings of transmission system components and proposes an integrated methodology for their inclusion in long-term grid planning. The research is framed around the interaction of three key domains: **transmission component thermal modelling**, **long-term network planning**, and **climate change**, addressing the methodological gap in traditional static approaches, which often neglect climatic variability and lack temporal or spatial integration. To bridge this gap, a quasi-Dynamic Thermal Rating (qDTR) methodology is developed, which captures the dynamic influence of environmental conditions on component capacity. Results indicate that, in European case studies, future climate projections are expected to reduce transmission capacity, with average declines under the high-emission $RCP_{8.5}$ scenario (2070) of 1.53% for overhead lines, 2.1% for power transformers, and 0.2% for underground cables relative to historical baselines. Nevertheless, compared with conventional static ratings, the proposed approach yields substantial economic benefits, reducing total investment needs by up to 68.1% and operating costs by 0.36%. Furthermore, higher temporal resolutions (month/hour) effectively capture intra-annual and intra-day variability, leading to a 20.14% reduction in network losses, the elimination of curtailment-related reinforcements, and the complete deferral of capital expenditures in several cases. Overall, the results demonstrate that probabilistic, climate-informed thermal ratings are both technically feasible and economically advantageous. By explicitly linking temporal and spatial variations in capacity and flexibility with long-term investment planning, the proposed framework enhances the resilience, reliability, and cost efficiency of future power systems under increasing climatic uncertainty.

KEYWORDS

Dynamic Thermal Ratings, Climate change, Thermal models, Network Expansion Planning